# MD Thesis

# CORRELATION OF STRUCTURAL AND FUNCTIONAL MEASUREMENTS IN PRIMARY OPEN ANGLE GLAUCOMA (OPTIC DISC MORPHOLOGY AND PSYCHOPHYSICS)


## David F. Garway-Heath, FRCOphth

### Supervisors

Professor F W Fitzke PhD

Professor R A Hitchings FRCS FRCOphth.

### Institutions:

Institute of Ophthalmology, Bath Street London EC1

Moorfields Eye Hospital, City Road, London EC1

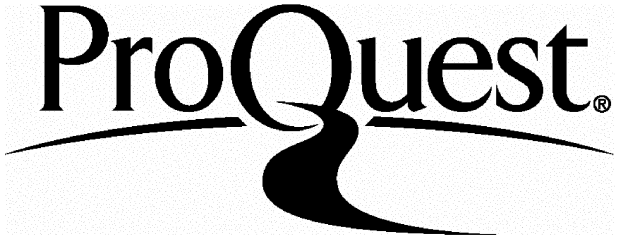

# 1 SECTION I: Overview

"No one who has studied the congeries of conditions which we classify under the term "glaucoma" can fail to be convinced of the depth of our ignorance on the subject we are discussing." (Elliot, 1921)

## 1.1 Abstract

**Background:** Primary open angle glaucoma (POAG) is the term given to a progressive optic neuropathy for which the major risk factors are raised intraocular pressure and older age. The presence of glaucoma is defined by functional (visual field) defects that are associated with loss of retinal ganglion cells and neuroretinal tissue at the optic nerve head (ONH). The relationship between the functional and structural changes is, therefore, of great importance to the understanding of the disease process, and to the clinician's interpretation of the state of the disease. This thesis sets out to define the relationship between retinal function, as measured by conventional white-on-white perimetry, and optic nerve head structure, as measured by scanning laser ophthalmoscopy.

**Plan of research:** The investigations are divided into four parts. Firstly, the ONH structural measurements that best distinguish glaucomatous from normal eyes are determined. This includes an analysis of the relationship between the optical components of the eye and image magnification. Secondly, an analysis of the physiological relationship between ganglion cell numbers and retinal function. Thirdly, the establishment of the anatomical relationship between visual field locations and the ONH (a map relating the visual field to the ONH). And fourthly, the investigation of the correlation between structural and functional measurements in POAG.

**Results:** Neuroretinal rim area in relation to optic disc size is the best parameter to distinguish glaucomatous from normal eyes. The physiological relationship of ganglion cell numbers to decibel light sensitivity (10*log[1/light intensity]) is curvilinear and to light sensitivity (1/light intensity) is linear. The visual field/ONH map allows a correlation of sectoral ONH and regional visual field sensitivity. Analyses demonstrate that the relationship of neuroretinal rim area to decibel light sensitivity is curvilinear in glaucoma.

**Clinical significance:** The curvilinear relationship between decibel light sensitivity and neuroretinal rim area indicates that staging of glaucoma by decibel summary indices may underestimate the amount of structural damage in early disease. In addition, the analysis of disease progression by linear modelling of decibel light sensitivity over time may need re-evaluation.

## 1.2 Table of contents

## 1.3 List of Tables

## 1.4 List of Figures

## 1.5 Acknowledgements

I would like to acknowledge the guidance and support of my supervisors Professor Fitzke (Institute of Ophthalmology) and Professor Hitchings (Moorfields Eye Hospital), and thank them for their invaluable advice regarding potentially fruitful avenues of research at the same time as allowing freedom to address subjects of particular interest to me.
I would also like to acknowledge the contributions to my general scientific training, and to my clinical understanding of glaucoma, from the consultants in the Glaucoma Service at Moorfields Eye Hospital (Professor Roger Hitchings, Professor Peng Khaw, Mr Michael Miller, Mr Richard Wormald, Miss Wendy Franks, Mr Ian Murdoch and Mr Keith Barton).
I would like to thank my co-investigators:
Alicja Rudnicka for work on ocular and camera magnification corrections (sections 3.2.1.1 and 3.2.1.2)
Anuja Bhandari for work on the magnification effects in fundus imaging (section 3.2.1.2).
Gadi Wollstein for his contributions to the work evaluating the optimal parameters to distinguish normal and glaucomatous optic nerves with the scanning laser ophthalmoscope (section 3.2.2)
Darmalingham Poinoosawmy who provided the nerve fibre layer images used in section 3.4

I would also like to thank the colleagues with whom I have worked during the period of research for the thesis: Simon Ruben, Mark Westcott, Ananth Viswanathan, Debbie Kamal, Aachal Kotecha and Dave Crabb. Discussion around the topics of psychophysics and imaging in glaucoma with these colleagues has helped form ideas and develop an understanding of the field of study.

I would like to thank the technical staff, without whom it would not have been possible to record the high-quality patient data that was required for the investigations: Grace Wu, Isabelle Antunes, Sinyu Zyang, and Ian Tresher.

I gratefully acknowledge the generous support of the *Guide Dogs for the Blind Association* that provided the main project grant for the Ocular Hypertension Treatment Study, which was the context in which the patient data was collected.

# 2 SECTION II: Introduction

## 2.1 Glaucoma

### 2.1.1 Definition and Classification

Glaucoma is the name given to a group of diseases ('the glaucomas') that have certain features in common: 'characteristic deformations' of the optic nerve head (glaucomatous cupping) and visual field loss ('nerve fibre bundle' type) (Hitchings, 1996).

Traditionally 'glaucoma' was regarded as a triad of raised intra-ocular pressure (IOP), enlargement of the optic cup and visual field loss. Visual field loss was a *sine qua non* for the diagnosis of glaucoma, although there is now much evidence that anatomical changes frequently occur before detectable functional changes (Motolko and Drance, 1981; Pederson and Anderson, 1980; Sommer et al., 1979b; Sommer et al., 1991a; Quigley et al., 1982; Quigley et al., 1992; Airaksinen et al., 1992).

'Glaucomatous cupping' is usually required to establish a definite diagnosis, yet its presence only becomes clinically obvious when advanced. Early changes are difficult to define clinically. The 'characteristic' appearance of the neuropathy is rarely described, but "we presume to know it when we see it" (Sommer, 1996). Historically an elevated IOP above 21mmHg was essential for the diagnosis. However, there is epidemiological evidence that 24% to 32% (Klein et al., 1992) or more (Sponsel, 1989) of patients with optic disc cupping and visual field loss have intra-ocular pressures within the normal range. Raised IOP is now regarded as a risk factor rather than a requirement for diagnosis.

The glaucomas are divided into those with an open drainage angle (open angle glaucoma) and those with an occluded angle (angle closure glaucoma).

Those with an open angle are further divided into those with an identifiable cause for raised intra-ocular pressure (secondary open angle glaucoma) and those without (primary open angle glaucoma). Examples of secondary causes for raised IOP are pseudoexfoliation, pigment dispersion, and uveitis. Primary open angle glaucoma (POAG) is, therefore, a diagnosis of exclusion (Murdoch, 1996).

POAG, although regarded as a 'diagnosis', may be the result of more than one disease process.

The following definition of POAG may be given: a chronic progressive optic neuropathy, occurring in the absence of any other discernible ocular or extra-ocular disease, with functional deficits, measurable as visual field loss, associated with optic nerve head and retinal nerve fibre layer structural changes.

### 2.1.2 Epidemiology

#### 2.1.2.1 Prevalence of POAG

The commonest form of glaucoma in the Western world is POAG.

Prevalence estimates vary:

0.43% in white subjects aged 40-75 years in the Rhondda valley (Hollows and Graham, 1966)

0.71% in white subjects aged ≥40 years in Bedford (Bankes et al., 1968)

0.9% in white subjects aged 49-63 years in Dalby (Bengtsson, 1981a)

2.1% in white subjects aged 43-84 years in Beaver Dam (Klein et al., 1992)

8.8% in black subjects aged 30-86 years in St Lucia (Mason et al., 1989)

1.3% in black and white subjects aged ≥40 years in Baltimore (Tielsch et al., 1990; Tielsch et al., 1991)

2.6% in oriental subjects aged ≥40 years in Japan (Shiose et al., 1991)

1.9% in white subjects aged ≥50 years in County Roscommon (Coffey et al., 1993)

6.6% in black subjects aged 40-84 years in Barbados (Leske et al., 1994)

1.1% in white subjects aged ≥55 years in Rotterdam (Dielemans et al., 1994)

2.4% in white subjects aged ≥49 years in the Blue Mountains (Mitchell et al., 1996)

The wide variation in prevalence estimates results from differences in study population characteristics (especially age and ethnic composition) and differences in criteria used to define glaucoma cases.

A median age-adjusted prevalence, taken from a number of population surveys, is 1.55% for a white population >40 years and 4.62% for a black population >40 years (Quigley and Vitale, 1997).

### 2.1.2.2 Prevalence of POAG blindness

By the end of the 20th Century, it was estimated by the World Health Organization that the glaucomas will be the most common cause of irreversible blindness in the world (Thylefors et al., 1995).

The prevalence of glaucoma blindness varies enormously from population to population. In Baltimore, glaucoma blindness in the over 40's is estimated at 0.03% for whites and 0.5% in blacks. In Sierra Leone the estimate is 0.6% (Murdoch, 1996).

Quigley and Vitale (1997) estimated that approximately 4% of white subjects with glaucoma and 8% of black subjects are bilaterally blind.

In the UK, almost a million people are blind or partially sighted. And as many as one in seven people over 75 years old are blind or partially sighted. Glaucoma is responsible wholly or in part for 13% of those on the blind register in England and Wales.

It is unlikely that the blind register fully reflects all those that are eligible for blind or partial sight registration. A survey of patients attending ophthalmology outpatients found that fewer than half those eligible were in fact on the register (Robinson et al., 1994; Bunce et al., 1998). A patient whose visual impairment is due to abnormal visual fields (the predominant cause being POAG) has been estimated to be greater than three times more likely to be non-certified than one with low visual acuity of similar severity (Bunce et al., 1998). These surveys are of patients in the health care system, and do not necessarily reflect the actual burden of visual impairment in the community. A recent

community survey of subjects over 65 years of age found that the prevalence of vision-impairing age related macular degeneration was 8% and of glaucoma (definite cases) was 3%. Three quarters of the people with definite glaucoma were not known to the eye services (Reidy et al., 1998).
Population surveys have consistently found that around 50% of those found to have glaucoma were previously undiagnosed (Quigley and Vitale, 1997; Wormald et al., 1992; Sheldrick and Sharp, 1994).
POAG is asymptomatic early in the course of the disease, and the disease therefore progresses to an advanced stage before the patient is aware of a problem ('the silent thief of sight'). Up to 20% of new cases have advanced visual loss at the time of disease detection (Sheldrick et al., 1994; Coffey et al., 1993).

### 2.1.2.3 Incidence of POAG

Five-year incidence rates for POAG have been estimated to increase from 0.2% to 1.0% with an increase of age from 55 to 75 years (Podgor et al., 1983). A high estimate of 0.24% per year was found in a follow-up study in Sweden (Bengtsson, 1989).
Lundberg followed 38 normotensive and 41 ocular hypertensive subjects for 20 years (Lundberg et al., 1987). The incidence of glaucoma in the two groups was 5% and 34%, respectively.
Perkins (1973a; 1973b)determined an incidence of 0.6% and 3.23% in normotensives and ocular hypertensives, respectively, over a 5-7 year follow-up period.
Kitazawa reported a 10% incidence in 9 years' follow-up in untreated ocular hypertension (Kitazawa et al., 1977).
Georgopoulos (1997) found that about 20% of patients with ocular hypertension (IOP >21mmHg) developed glaucoma over a period of seven years.
Linner re-examined 408 (of a planned 1076) normotensive subjects after 15.8 to 18.3 years. 24 had developed ocular hypertension, one of whom had glaucoma. The incidence was, therefore, 0.25% in 16 years (Jensen, 1984).

### 2.1.3 Risk factors for POAG

The risk factors for POAG can be divided into major, moderate and possible risk factors.

#### 2.1.3.1 Major risk factors:

##### 2.1.3.1.1 Raised Intraocular pressure (IOP)

The level beyond which IOP is considered raised is usually given as 21mmHg. This figure arose from a study by Leydhecker (1959) in which the IOP was measured in 20 000 eyes with Schiotz tonometry. The mean IOP was 15.5mmHg, with a standard deviation of 2.57mmHg. Assuming a normal distribution, only 2.5% of the population would be expected to have an IOP above 20.5mmHg. However, IOP is not normally distributed, it is skewed to the right, and as a result up to 8% of the population has an IOP > 21mmHg (Sommer et al., 1991b). In addition, population studies have demonstrated that 24% to 32% (Klein et al., 1992) or more (Sponsel, 1989) of patients with glaucoma may have intra-ocular pressures within the normal range ('normal tension glaucoma' (NTG)). As a result, an IOP > 21mmHg is a poor predictor of the presence of POAG. Tonometry has been shown to have a sensitivity of 47 % and a specificity of 92% for identifying individuals with glaucomatous optic nerve damage (Katz et al., 1993).

The role of raised IOP as a risk factor for POAG is well established. In the Baltimore survey 1.2% of the population with an IOP ≤ 21mmHg were found to have glaucoma and 10.3% of the population with IOP ≥ 22mmHg were found to have glaucoma. The relative risk of the higher pressures is, therefore, 8.6 times that of the lower pressures (Sommer et al., 1991b). Data from the Collaborative Glaucoma Study (Armaly et al., 1980) also support the concept of IOP as a risk factor for developing glaucoma. At follow-up 5 years from the initial screening, 98.5% of subjects with an IOP < 20mmHg were glaucoma free, whereas only 93.3% with an IOP ≥ 20mmHg were glaucoma free.

The height of the IOP is positively correlated with the relative risk for glaucoma (Sommer et al., 1991b), and there is a positive relationship between the height of the IOP and the severity of field damage at presentation (Jay and Murdoch, 1993; Quigley et al., 1996b).

The high numbers in the population with 'NTG' can be predicted from the IOP-related glaucoma prevalence and the prevalence of raised IOP. 92% of the population has an IOP ≤ 21mmHg, and 1.2% of that population has glaucoma (1.2 * 0.92 = 1.1%). 8% of the population has an IOP≥ 22mmHg, and 10.3% of that population has glaucoma (10.3 * 0.08 = 0.8%). So the numbers with glaucoma and 'normal pressure' are predicted to be greater than those with 'high pressure'.

Even in patients with NTG, there is evidence that the level of IOP plays a role. The eye with the higher IOP has more severe field loss (Cartwright and Anderson, 1988; Crichton et al., 1989), and the level of IOP is a risk factor for progression (Sekine et al., 1994).

#### 2.1.3.1.2 Greater age

The prevalence of POAG increases with age (Tielsch et al., 1991; Klein et al., 1992; Coffey et al., 1993; Mitchell et al., 1996).

Age-specific prevalence varies with ethnic origin and estimates have been calculated in a recent review of the literature (Quigley and Vitale, 1997):

> around 1% of white subjects have POAG at the age of 50 years, rising to around 4% at the age of 80 years.
>
> around 3% of black subjects have POAG at the age of 50 years, rising to around 13% at the age of 80 years.

In the Collaborative Glaucoma Study (Armaly et al., 1980), after 13 years follow-up, visual field defects occurred in 4.8% of subjects aged >60 years at baseline, and in 0.7% of those aged <40 years.

#### 2.1.3.1.3 Ethnic origin

Population studies have consistently found higher prevalences of POAG in black populations when compared with white populations (Mason et al., 1989; Coffey et al., 1993; Leske et al., 1994; Mitchell et al., 1996).

In the Baltimore Eye Survey (Tielsch et al., 1991), age-adjusted prevalence rates for primary open-angle glaucoma were four to five times higher in blacks as compared with whites.

In the African Caribbean Eye Survey (Wormald et al., 1994), an age-standardised comparison with the findings of the Roscommon survey revealed a relative risk for glaucoma for Haringey blacks compared with Irish whites of 3.7. Significant risk factors for glaucoma included age, African birthplace and darker skin colour.

### 2.1.3.2 Moderate risk factors:

#### 2.1.3.2.1 Heredity

##### 2.1.3.2.1.1 Family history

Accurate estimates of the risk of a positive family history for POAG are difficult to obtain in population studies, because of recall biases. And in case-control studies, patients are more likely to enquire of relatives than controls. However, a positive association has been reported (Tielsch et al., 1994; Leske et al., 1995). In a case-control study, Charliat et al. (1994) found a positive family history to be a major risk factor (OR = 7.67; 95% CI: [3.25-18.1]; $p < 10^{-5}$). In the Baltimore Eye Survey (Tielsch et al., 1994), age-adjusted associations of primary open angle glaucoma with a family history of glaucoma were higher in siblings (odds ratio = 3.69) than in parents (OR = 2.17) or children (OR = 1.12). Odds ratios were slightly higher in blacks than in whites, and there was evidence of selection bias, with ORs between two and three times higher for those who had prior knowledge of their

glaucoma diagnosis than for those who first received their diagnosis by the study examination (history in siblings OR = 4.72 for those with prior knowledge versus 2.77 for those without).
Twin studies provide reliable data on heritability of many conditions. A Finnish twin study estimated the heritability of POAG to be 13% (Teikari, 1987).

#### 2.1.3.2.1.2 Genetics

A single-gene hypothesis for POAG is not consistent with the low prevalence of POAG in first-degree relatives of those with the disease. With advances in molecular genetics, it is now becoming possible to screen individuals and families for known mutations. However, one of the great challenges facing glaucoma researchers is to be able to reliably phenotype 'the glaucomas', so that phenotypes can be related to the many genetic mutations that are likely to be found. Accurate quantification of the morphology of the optic nerve, and other ocular structures, will be necessary, as well as careful documentation of known and likely (environmental and systemic) concomitant risk factors.
A gene has been identified, located on chromosome 1 (1q23-25), that is involved with aqueous outflow from the trabecular meshwork (Lutjen-Drecoll, 1999), and mutations in the gene are associated with juvenile glaucoma and POAG (Allingham et al., 1998). The gene, TIGR (trabecular meshwork inducible glucocorticoid response) or myocilin modulates the deposition of extracellular material in the trabecular meshwork in response to dexamethasone and oxidative damage (Lutjen-Drecoll, 1999). To date, 26 mutations have been described in this gene (Johnson, 2000). In recent years, other genetic locations for POAG have been identified (Craig and Mackey, 1999).

#### 2.1.3.2.2 Myopia

Most evidence is from observation of increased prevalence of myopia in glaucoma clinics (Daubs and Crick, 1981; Perkins and Phelps, 1982; Chen et al., 1997), and as such is open to considerable selection biases. However, myopia has been found to be a risk factor for the development of visual field defects in patients with ocular (Georgopoulos et al., 1997).

### 2.1.3.3 Possible risk factors

#### 2.1.3.3.1 Diabetes

The association between diabetes and POAG found in case-control studies (Wilson et al., 1987) has not generally been supported by epidemiological studies (Kahn et al., 1977; Bengtsson, 1981a; Leske et al., 1995). Diabetes was highly prevalent in the Baltimore Eye Survey population, with 10.6% of white subjects and 17.2% of black subjects reporting a positive history (Tielsch et al., 1995a). Diabetes was associated with higher IOP, but the differences were not large (means, 17.4, 18.0, and 17.8mmHg for subjects without diabetes, those with diabetes not using insulin, and those with

diabetes using insulin, respectively). Diabetes was not associated with POAG (age-race-adjusted odds ratio, 1.03; 95% confidence interval, 0.85, 1.25). Those with POAG diagnosed before the study examination showed a positive association with diabetes (odds ratio, 1.7, 95% confidence interval, 1.03, 2.86), indicating that selection bias could explain the positive results of previous clinic-based investigations.

More recent epidemiological studies have found an association of diabetes with both raised IOP (Dielemans et al., 1996; Mitchell et al., 1997) and glaucoma (Klein et al., 1994; Dielemans et al., 1996; Mitchell et al., 1997). In the Blue Mountains Study (Mitchell et al., 1997), ocular hypertension was more common in people with diabetes (6.7%), compared with those without diabetes (3.5%; odds ratio 1.86, CI 1.09-3.20), and in the Rotterdam study (Dielemans et al., 1996), diabetes was associated with higher IOP of 0.31mmHg (95% confidence interval, 0.12-0.50). In the Beaver Dam Eye Study (Klein et al., 1994) the rates of persons meeting the criteria for definite glaucoma were more common in those with older-onset diabetes than in those without (4.2% versus 2.0%; P = 0.004). In the Blue Mountains eye study glaucoma prevalence was increased in people with diabetes (5.5%), compared with those without diabetes (2.8%; age-gender adjusted odds ratio 2.12, 95% confidence intervals 1.18-3.79), and the effect was independent of the effect of diabetes on IOP. In the Rotterdam Study diabetes was associated with a threefold increased in high-tension glaucoma (odds ratio, 3.11; 95% confidence interval, 1.12-8.66).

#### 2.1.3.3.2 Vascular factors

##### 2.1.3.3.2.1 Systemic hypertension

The role of blood pressure as a risk factor in POAG is unclear and probably complex. The effects of various levels of blood pressure will be difficult to disentangle from the effects of treatment for systemic hypertension, and also the effects of glaucoma treatments on blood pressure.

An analysis of data from the Framingham study demonstrated a positive relationship between blood pressure and IOP in subjects without visual field defects, and a low blood pressure/IOP ratio in those with field defects (Leske and Podgor, 1983).

In the Baltimore Eye Survey (Tielsch et al., 1995b) systemic blood pressure and IOP were significantly correlated. A systolic or diastolic blood pressure that was 10 mmHg higher was associated with an IOP that was 0.25mmHg or 0.19mmHg higher, respectively ($p<0.001$). In the Rotterdam Study (Dielemans et al., 1995) a systolic or diastolic blood pressure that was 10mmHg higher was associated with an IOP that was 0.23mmHg or 0.24 mmHg higher, respectively.

Systolic and diastolic blood pressure show a modest, positive association with POAG (Tielsch et al., 1995b). The effect of blood pressure on POAG is modified by age, with a stronger association among older subjects. There is a suggestion (not statistically significant) that raised blood pressure in younger (<60yrs) subjects was protective, and in the older (>70yrs) subjects was a risk factor. This has not been supported by other studies (Leske and Wu, 1996).

In the Rotterdam study, there was an association between higher systolic blood pressure and high-tension POAG, but not NTG (Dielemans et al., 1995).
Lower perfusion pressure (blood pressure minus IOP) has been associated with an increased prevalence of POAG (Tielsch et al., 1995b; Leske et al., 1995). However, this effect may be explained by the strong association between raised IOP and POAG (Leske et al., 1995).
In a follow-up study of patients with ocular hypertension, arterial hypertension was found to be a significant risk factor for the development of glaucomatous field defects (Georgopoulos et al., 1997).

#### 2.1.3.3.2.2 Vasospasm

There is some evidence that vasospasm may be related to certain patterns of tissue loss at the optic nerve head (ONH) in glaucoma (Broadway and Drance, 1998). Patients with focal ischaemic discs are more frequently women (66%) and have a higher prevalence of vasospasm (63% versus 25%-49%; $p = 0.01$), migraine (32% versus 8%-19%; $p = 0.02$), and cold extremities (66% versus 17%-30%; $p = 0.00003$) than other optic disc types.
Migraine has been reported to be more frequent in patients with NTG than controls, ocular hypertensives and patients with high-tension POAG (Phelps and Corbett, 1985). Although other studies have found no association (Usui et al., 1991).
Population studies have been inconclusive, one report finding a possible association between history of typical migraine headache and OAG, which could be modified by age (Wang et al., 1997a).
Cold induced vasospasm is more frequent in patients with NTG compared to age-matched non-glaucomatous controls (Drance et al., 1988).

#### 2.1.3.3.3 Gender

Most studies have found no sex association in POAG (Hollows and Graham, 1966; Tielsch et al., 1991; Coffey et al., 1993; Klein et al., 1994). Some studies have found male sex to be a risk factor (Kahn et al., 1977; Leske et al., 1995; Dielemans et al., 1995), and others female sex (Bengtsson, 1981b; Mitchell et al., 1997).
NTG is more common amongst women (Levene, 1980).

### 2.1.4 Aetiology

The pathogenesis of POAG is almost certainly multifactorial. The two major mechanisms, which are given different weight by different researchers, are 'mechanical' and 'vascular'.

#### 2.1.4.1 Mechanical (IOP-related) mechanisms

These propose that raised IOP can induce optic nerve damage through biomechanical means. However, not all eyes with raised IOP develop glaucoma, so there must be modulating factors. Histological and experimental evidence suggests that the damage to ganglion cell axons occurs at the lamina cribrosa:

a. There are regional structural differences in the lamina. The pores in the lamina are larger, and connective tissue supports thinner, in the superior and inferior quadrants (Radius and Gonzales, 1981), and there may be preferential loss of neuroretinal tissue in these parts of the ONH in glaucoma.

b. Changes in the lamina in POAG. There is compression and bowing of the lamina plates, resulting from posterior rotation of the peripheral lamina (Quigley et al., 1983).

c. There are axonal transport disturbances at the lamina in subjects with elevated IOP (Quigley et al., 1981; Sakugawa and Chihara, 1985). Orthograde (away from the cell body) and retrograde axonal transport has been studied in primate models of glaucoma, in which the intraocular pressure has been raised. Flow in both directions is impaired (Lampert et al., 1968; Minckler et al., 1976; Quigley and Anderson, 1976; Minckler et al., 1978; Radius, 1981b). The location of impaired flow is greater in the superior, temporal and inferior parts of the nerve than in the nasal part (Radius, 1981b). Retrograde axonal transport includes the movement of neurotrophic factors, required for normal cellular maintenance. Deprivation of these factors may be a mechanism triggering the death of ganglion cells by apoptosis (Quigley et al., 1995; Quigley, 1995; Nickells, 1996; Kerrigan et al., 1997).

d. Changes to the extracellular matrix. Ageing changes have been described, which may lead to a less flexible lamina. Changes to elastin have been demonstrated in the lamina cribrosa of glaucomatous eyes

#### 2.1.4.2 Vascular mechanisms

Interest in a vascular aetiology stems from the findings in population studies that up to half POAG cases have an IOP that is within the 'normal range' (<21mmHg). However, the relevance of abnormal ocular vasculature in POAG is difficult to establish, as it could be either cause or result of the disease process. In addition, the effects of ocular hypotensive medication have to be considered, as studies are frequently performed on treated individuals.

Blood flow in the optic nerve head may be represented by the following equation (Hayreh, 1996b):

flow = perfusion pressure / resistance to flow

and

perfusion pressure = mean blood pressure (BP) minus IOP

The blood flow in the nerve head therefore depends on

- arterial BP
- IOP
- resistance to flow

The resistance to flow is proportional to blood viscosity, the length of the vessel and inversely proportional to the 4th power of the radius of the vessel. The calibre of the vessels is governed by autoregulation and the presence, or not, of hypertensive arterial changes. The mechanisms of autoregulation are not fully understood, but various factors produced by the vascular endothelium (endothelin-1, thromboxane $A_2$, prostoglandin $H_2$ and nitric oxide) are known to be powerful modulators of vascular tone (Haeffliger et al., 1994). High levels of endothelin-1 have been found in the plasma and aqueous humour of patients with POAG (Tezel et al., 1997), and the normal response of endothelin-1 to postural changes has been found to be absent in patients with NTG (Kaiser et al., 1995).

Defective autoregulation can arise in a number of circumstances (Hayreh, 1996b): the perfusion pressure can rise or fall outside the autoregulatory range, arterial hypertension resets the gain on the autoregulatory range (making the tissue susceptible to drops in perfusion pressure), changes in the size of the lumen of the precapillary arteriole (as in systemic hypertension), and changes in vascular endothelial function.

Ischaemic episodes in the ONH may be precipitated by drops in blood pressure (in the presence of defective autoregulation). Blood pressure falls at night (Richardson et al., 1964) and Hayreh (1974) postulated 'nocturnal dips' as a precipitating factor in ischaemic optic neuropathy. In addition, IOP rises in subjects in the supine position, with a consequent reduction in pulsatile ocular blood flow (Trew and Smith, 1991b; Trew and Smith, 1991a). Low blood pressure has been reported as a contributory factor in NTG (Goldberg et al., 1981; Hayreh et al., 1994) and in progressive POAG despite normalised IOP (Kaiser et al., 1993).

Increased blood viscosity, which may cause increased vascular resistance, has been found in some patients with POAG, especially those with 'focal ischaemic' NTG (Klaver et al., 1985). Abnormalities in coagulation and fibrinolytic parameters have also been found in glaucoma patients not receiving either systemic or ocular hypotensive treatment (O' Brien et al., 1997).

Colour Doppler ultrasound may be used to image retrobulbar vessels. Only blood velocity measurements are possible, and calculation of volume flow and resistance is theoretical. Reduced (Kaiser et al., 1997) and increased (Butt et al., 1997) blood velocity has been demonstrated in patients with POAG. One study has found that the blood velocity was decreased the eyes with a normal visual field in patients with asymmetric glaucoma, perhaps suggesting that the vascular abnormalities precede detectable damage (Nicolela et al., 1996a). Increased resistance to flow has been found in high tension POAG and NTG (Butt et al., 1995; Butt et al., 1997).

Scanning laser Doppler flowmeters have also been used to assess ocular tissue blood flow. Reduced flow in the lamina cribrosa has been demonstrated in POAG (Nicolela et al., 1996b). Contradictory results have been reported for blood flow in the neuroretinal rim, by this method, showing either reduced (Michelson et al., 1996) or normal (Nicolela et al., 1996b) flow.

The choroidal vasculature has also been found to be abnormal in POAG, with a generalised (diffuse) loss of the innermost choroidal vessels (Yin et al., 1997). In the peripapillary region, a zone of non-fluorescence is seen in most eyes (Yamazaki et al., 1996). Zone width had some correlation with visual field defect. Visible ciliary vessels suggested the absence of choriocapillaris in this zone. Although peripapillary choroidal vessels make little contribution to the optic nerve vasculature, they have the same posterior ciliary supply, so that there may be a common pathogenesis (Wang et al., 1998).

Pulsatile ocular blood flow (POBF), a measure that reflects choroidal flow, has been found to be reduced in NTG (James and Smith, 1991) and POAG (Trew and Smith, 1991a). POBF has also been found to be reduced in both the normal-field and glaucomatous eyes of patients with NTG, and in the glaucomatous eye compared with the normal-field eye (Fontana et al., 1998b).

## 2.2 Anatomy and functional organisation of the visual pathway

At photopic adaptation levels, light detection is mediated by a number of retinal elements, from the cone photoreceptors, through bipolar cells, to ganglion cells, and ultimately the visual cortex.

### 2.2.1 Cone photoreceptors

In the human retina, the cones form a regular hexagonal mosaic with a peak density at the fovea of 162,000/mm$^2$ (Curcio et al., 1987) to 208,300/mm$^2$ (Curcio and Allen, 1990). There is a high inter-individual variation in foveal cone density: 1.6 (Curcio and Allen, 1990) to 2.9-fold (Curcio et al., 1987) although artefacts resulting from histological fixation may account for some of the variability. Cone density outside the central 1 to 2 degrees varies much less (Curcio et al., 1987).

There is radial asymmetry, with isodensity contours forming a horizontal ellipse centred on the fovea. Cone density is also higher in the nasal than in the temporal retina. This latter finding is inconsistent within the central 15 degrees, but consistent peripherally (Curcio et al., 1987).

Blue (S-) cones form about 7% of the retinal cones in the central 4mm. They are sparse in the fovea, and absent from the central 100μ. The highest density is found at 0.1 to 0.3mm eccentricity, where their arrangement is irregular (Curcio et al., 1991). More peripherally, they are organised in a moderately regular lattice, which is independent of the red/green mosaic. The ratio of red cones to green cones is uncertain, and they distributed in a common, highly regular, mosaic (Curcio et al., 1991; Wassle and Boycott, 1991; Kouyama and Marshak, 1997).

### 2.2.2 Retinal horizontal cells

Horizontal cell bodies are located at the outer margin of the inner nuclear layer (INL), and their dendrites and axons ramify in the outer plexiform layer (OPL). There are two morphological and physiological types (Wassle and Boycott, 1991; Lee, 1996; Dacey, 1996). Type I cells are achromatic, but avoid S-cones, and type II cells, which contact all cone types, but which selectively seek out S-cones (Lee, 1996; Dacey, 1996). Their precise physiological role is still uncertain.

### 2.2.3 Retinal bipolar cells

Bipolar cell bodies are located in the inner nuclear layer. Their dendritic tree is in the OPL and their axon makes contact with amacrine or ganglion cells, or both, in the inner plexiform layer (IPL) (Wassle and Boycott, 1991).

There are two broad anatomical categories of cone bipolar cells: midget bipolar cells, which have a 1 to 1 connectivity with midget ganglion cells, and diffuse bipolar cells some of which are likely to provide input to the parasol ganglion cells (Wassle and Boycott, 1991) and blue ON- cells (Ghosh et al., 1997). Cone bipolar cells are of two physiological types, distinguished by their response to a light stimulus at the centre of their receptive field: ON-cells are depolarised by a light spot (dark surround), and OFF-cells are depolarised by a dark spot (light surround). The axons of OFF-cells probably branch in the outer part of the IPL, and those of ON-cells in the inner part of the IPL.

ON-bipolar cells are excitatory to ON-ganglion cells and OFF-bipolar cells are excitatory to OFF-ganglion cells. There is also some inhibitory input, either direct or through amacrine cells, from bipolar cells to the opposite type of ganglion cell.

In the receptive field centre there is input from one type of cone only, and the surround has been reported to be colour antagonistic. 'Red' and 'green' cones in the centre of the retina make synapses with at least four different bipolar cells: an ON- and an OFF- midget bipolar cell and an ON- and an OFF-diffuse bipolar cell. Midget bipolar cells are connected to only one cone, and therefore carry chromatic information. Diffuse bipolar cells, even in the region of the fovea, are connected to all cones within their dendritic field, and presumably carry mixed information (a luminosity signal) (Wassle et al., 1994). Thus colour and luminosity information may be transmitted by different types of bipolar cell (Wassle and Boycott, 1991).

### 2.2.4 Amacrine cells

Amacrine cells are interneurones making synapses with processes of bipolar, ganglion, and other amacrine cells. They have cell bodies in the INL or ganglion cell layer ('displaced amacrine cells'). Displaced amacrine cells account for fewer than 3% of cells in the ganglion cell layer at 3.5° (1mm) eccentricity, rising to 70% at the ora serrata (Curcio and Allen, 1990).

### 2.2.5 Retinal ganglion cells

#### 2.2.5.1 Cone/ganglion cell ratios

Both cones and ganglion cells are present at a higher density towards the fovea, in a horizontally oriented streak. The density is higher in the nasal compared to the temporal retina (Curcio et al., 1987; Curcio and Allen, 1990), and the naso-temporal asymmetry is greater for ganglion cells than for cones. Ganglion cell density is higher in the superior retina, whereas cone density is slightly higher in the inferior retina. The overall cone/ganglion cell ratio varies from 2.9 to 7.5 between eyes (Curcio and Allen, 1990).

The central-peripheral gradient is steeper for ganglion cells than for cones, reflecting the differences in cone-ganglion cell convergence across the retina.

Calculation of ratios in the fovea is complicated by the peripheral displacement of ganglion cells away from the foveal centre, indicated histologically by the oblique fibres of Henle. At eccentricities where oblique fibres of Henle are just no longer visible, the cone/ganglion cell ratio is 1.04 (9°/2.6 mm nasal) and 1.80 (12°/3.4 mm inferior). Beyond these eccentricities, there is substantial meridional variability in the cone/ganglion cell ratio (Curcio and Allen, 1990).

The numbers of central cones and laterally displaced ganglion cells is consistent with a central cone/ganglion cell ratio of 1/3 (Sjostrand et al., 1994; Curcio and Allen, 1990), and rising smoothly with eccentricity (Curcio and Allen, 1990).

A cone/ganglion cell of ratio of 1/4.2 has been demonstrated in the marmoset New World monkey (Callithrix jacchus). The peak sampling density of ganglion cells was calculated to be a 550,000 cells/mm$^2$, allowing for lateral displacement of cells from the fovea (Wilder et al., 1996). In the macaque retina, the ratio of cones to ganglion cells is 0.3 at the fovea and rises to 0.5 at 1.0mm, to 1.0 at 3.5mm, and to 16 at about 10mm eccentricity (Wassle et al., 1989; Wassle and Boycott, 1991). At 10mm eccentricity, there is still one ON- and one OFF- midget bipolar for each cone. This suggests that convergence is between the bipolar and ganglion cells, and may be as high as 22 to 1 at 10mm eccentricity (Wassle et al., 1994).

The change in the cone/ganglion cells ratio with eccentricity is less marked for parasol ganglion cells than for midget ganglion cells. For parasol cells, the ratio is about 70/1 at 1° eccentricity, rising to about 300/1 at 30° (Goodchild et al., 1996).

### 2.2.5.2 Ganglion cell numbers and densities

The topography of ganglion cell density has been described from histopathological examination of 6 retinas of 5 individuals aged between 27 and 37 years (Curcio and Allen, 1990). The highest densities are found in a horizontal ellipse that, at half-height, extends 0.4 to 2.0 mm from the centre of the fovea. The ganglion cell-free zone extends 63 to 234 microns from the foveal centre. A mean peak ganglion cell density of around 35,100 cells/mm$^2$ (range 31,600 to 37,800) occurs at about 1mm from the foveal centre. The average retina contains 1.07 million ganglion cells (range 710,000 to 1,540,000), 50% of which are within the central 16 degrees. The two-fold variation in ganglion cell numbers cannot be explained by differences in retinal area, which varied by only 1.17 times.

### 2.2.5.3 Inter-individual variability in ganglion cell density

Different eyes have a similar ganglion cell density from 0.7 to 4.2° (0.2 to 1.2mm) with a coefficient of variation of <15%. Variability tends to increase with eccentricity, being greater in the temporal retina (nasal field). As ganglion cell density is greatest centrally, most of the inter-individual variability in overall ganglion cell numbers occurs between about 4.2 and 18° (1.2 to 5mm) (Curcio and Allen, 1990).

### 2.2.5.4 Physiological types of ganglion cell

Different aspects of a visual scene, such as colour and motion, are processed by the visual system in parallel. That is, there are parallel, function-specific pathways, which are structurally discrete, although the extent of their independence is controversial (Casagrande, 1994).

Ganglion cell response properties have been described as broadband (non-opponent) and chromatic (opponent) (Shapley, 1990; Harwerth et al., 1993). Spectral opponency describes cells that are excited by some wavelengths and inhibited by others. Two types (1 and 2) of opponent cell are described. Type 1 cells have a colour-specific centre, and an opposing surround (which may or may not be

colour specific (Dacey, 1996)). Red/green cells are typically Type 1. Type 2 cells are excited by one colour, and inhibited by another, across the whole receptive field. Blue ON- cells are of this type (Dacey, 1996).

The different response properties are thought to arise from different neural combinations of the three cone types. There are generally considered to be three photopic mechanisms underlying spectral sensitivity (Harwerth et al., 1993): an independent short-wavelength-sensitive (SWS) mechanism (reflecting the sensitivity of the SWS cones); a colour-opponent (chromatic) mechanism derived from differential inputs of the middle-wavelength-sensitive (MWS) and long-wavelength-sensitive (LWS) cones; and a colour non-opponent (luminance) mechanism derived from undifferentiated MWS and LWS cone inputs. A small contribution of the blue cones to the luminance channel has been demonstrated in extreme conditions.

There are probably around 20 ganglion cell types in the primate retina (Dacey, 1994), although only a few have been well characterised. These have been classified according to various functional specialisations (Lee, 1996):

| Physiological type | Anatomical type |
|---|---|
| Magnocellular pathway | |
| ON-centre | inner parasol |
| OFF-centre | outer parasol |
| Parvocellular pathway | |
| blue on, yellow off | small bistratified |
| blue off, yellow on | large-field inner cell? |
| green and red ON-centre | inner midget |
| green and red OFF-centre | outer midget |
| Other pathways | |
| various transient, non-opponent cells | unknown |

The pattern by which a ganglion cell type tiles the retina is given the term 'mosaic', and the dendritic field size and degree of overlap of dendritic fields (coverage) is characteristic for any given mosaic. In addition, each mosaic has a specific central projection (parallel pathway).

#### 2.2.5.5 Parasol cell mosaics

Two populations of parasol (Pα) cell (Wassle and Boycott, 1991), that project to the magnocellular layer of the lateral geniculate nucleus (LGN) (Leventhal et al., 1981), have been identified. The populations differ by the depth of their dendritic tree in the IPL. Those forming a lamina in the outer IPL probably correspond to OFF-centre cells, and those forming a lamina in the inner IPL to the ON-centre cells (Wassle and Boycott, 1991; Lee, 1996). The 'inner' parasol ganglion cell dendritic

fields have been found to be larger in diameter than their 'outer' counterparts (Dacey and Petersen, 1992).

#### 2.2.5.5.1 Physiology

The magnocellular projection of the parasol cells to the LGN indicates that these cells are characterised by an ON- or OFF- centre phasic response and a non-opponent receptive field organisation. They have large receptive fields, and convey a luminance signal to the magnocellular system (Dacey, 1994). The spectral sensitivity of the receptive field centre represents the sum of M- and L-cone inputs, with no evidence for S-cone input. Parasol cell dendritic tree size appears to correlate with the receptive field centre diameter (Lee, 1996), although the correlate of the parasol cell, the alpha ganglion cell, in the cat have been shown to have to a receptive field twice the area of the dendritic tree. Coupling between parasol cells in the Primate retina, probably through intermediary amacrine cells, has been demonstrated. The functional significance of this coupling is not fully understood (Dacey and Brace, 1992).
Achromatic contrast sensitivity of the magnocellular cells is a factor of 8 to 10 times higher than that of parvocellular cells. Achromatic spatial summation within the receptive field centre is linear (Lee, 1996).

### 2.2.5.6 Small bistratified cell mosaic

The small bistratified ganglion cells are stratified close to the inner and outer margins off the IPL (Dacey and Lee, 1994; Martin et al., 1997; Calkins et al., 1998; Ghosh et al., 1997). The dendritic field diameter falls within and above the size range of the parasol cells at any eccentricity (Ghosh et al., 1997), and a coverage factor of about 1.8 has been calculated (Dacey, 1993a). If the coverage factor is constant across retina, these cells form about 1% of the ganglion cell population in the central retina, increasing to about 6 to 10 % in the far periphery. The outer dendritic tree is larger than the inner in the ratio 1.3/1 (Dacey, 1993a). The inner dendritic tree (ON-stratum) makes synapses with a bipolar cell that makes exclusive contact with blue cones (Kouyama and Marshak, 1997; Calkins et al., 1998). The outer dendritic tree (OFF-stratum) makes synapses with diffuse bipolar cells that contact red and green cones (Calkins et al., 1998).
Blue ON- cells have been localised to the interlaminar layer and the border of the parvocellular/interlaminar layer of the LGN in the marmoset (Martin et al., 1997). Cells in the interlaminar layer project to the colour-selective 'blobs' in the primary visual cortex (Casagrande, 1994).

#### 2.2.5.6.1 Physiology

These cells are blue-ON yellow-OFF colour opponent cells (Dacey and Lee, 1994). Both excitatory and inhibitory inputs have similar physiological extents, and match dendritic tree diameter (Lee, 1996; Calkins et al., 1998).

### 2.2.5.7 Midget cell mosaics

There are two populations of midget (Pβ) ganglion cells whose dendrites stratify in the inner and outer part off the IPL, forming two (inner- and outer-midget cell) mosaics. These are likely to correspond to (green and red) ON- and (green and red) OFF- centre ganglion cells, respectively (Dacey, 1993b). Midget ganglion cells project to the parvocellular layers of the LGN.
The dendritic field size of midget cells is related to their eccentricity, with the size increasing with greater distance from the fovea. The relationship between size and eccentricity is not linear. From between about 0° and 6° eccentricity (0.25 to 2 millimetres) the dendritic field diameter is 5 to 10 at microns. Between 6° and 25° (2 and 7 millimetres) the dendritic tree shows a tenfold increase in size. From 25° to 75° (7 and 20 millimetres) the increase is two to threefold. The range in field size at any given retinal location is large. Between 5 and 10 millimetres from the fovea, there is a 2.8-fold range (Dacey, 1993b). Dacey (1993b) has suggested that the dendritic field diameter of the inner midget cells is, on average, about 30 % larger than that of the outer midgets, and the ratio of the density of outer to inner midget cells is about 1.7 to 1.
At 5mm eccentricity (peripheral to the zone of laterally displaced foveal ganglion cells) the midget cells (ON- and OFF-) have a dendritic field of about 40 microns and their density is about 2,300/mm2 (Wassle et al., 1990), so that the resulting coverage factor is 2.9 (both types included). At this eccentricity, midget bipolar cells provide contacts with individual cone pedicles.

#### 2.2.5.7.1 Physiology

In the primate retina, midget cells represent red-green opponent (colour-antagonistic), tonic ganglion cells with small receptive fields, subserving high spatial resolution and colour vision (Wassle and Boycott, 1991; Dacey, 1994). In the periphery, midget ganglion cells lose their colour opponency. They exhibit a summed input from red and green cones, although weak on- off- chromatic responses may remain (Dacey, 1996).
The maximum theoretical spatial resolution in the central retina is limited by cone spacing, and peripheral to about 10° to 15°, resolution is limited by midget ganglion cells density. Actual spatial resolution in the fovea is limited by the optics of the eye (Thibos, 1998).
The receptive field centre diameters of midget cells are about 1.5 times the dendritic field diameters (Wassle and Boycott, 1991; Lee, 1996).

## 2.2.6 Anatomical pathways subserving differential light sensitivity

The density of retinal elements, such as the rods, cones and ganglion cells varies with retinal location. The question arises whether the mechanisms of light detection vary with retinal location in a qualitative way, or only a quantitative manner resulting from scaling (density of neural elements).

It has been demonstrated that both opponent and non-opponent channels may be responsible for the detection of white-on-white stimuli (Schiller et al., 1990). Factors affecting the balance of sensitivities between opponent and non-opponent channels include intensity of background illumination, size of the test field, exposure duration and retinal location.

Which stimulus detection mechanism (short-wave-length sensitive, colour opponent or non-opponent) is involved in standard white-on-white perimetry is not known. The conditions of white-on-white perimetry may favour any one mechanism or a combination. A study in monkey eyes found that, under the standard testing conditions (Goldmann size III target and 31.5 apostilb background) of the Humphrey field analyser (HFA) the three detection mechanisms had approximately equal sensitivity (Harwerth et al., 1993). Some of the stimulus conditions of the HFA (background illumination and stimulus duration) favour opponent mechanisms, while other (small test spot size and wide adaptation field) favour non-opponent mechanisms (Harwerth et al., 1993). The balance of these factors varies across the field. The Goldmann size II target favoured the nonopponent system, and the size V target favoured the opponent mechanism. The nonopponent became more predominant at greater eccentricities. Larger test spot sizes also favoured the SWS system. However, under HFA test conditions, specific detection mechanisms could not be specified because the sensitivity of each detection mechanism was approximately equal.

In the conditions of blue-on-yellow perimetry, threshold values reflect the SWS system. Only in parts of the field with reduced sensitivity (where brighter stimuli are required for threshold) may the blue cone input to the luminance channel contribute to detection thresholds (Felius et al., 1995).

### 2.2.7 Lateral geniculate nucleus

Axons arising from ganglion cells in the retina synapse in the LGN. The axons project to cells that are segregated into layers according to functional specialisation: parvocellular, magnocellular, and an 'interlaminar' (koniocellular) layer (Leventhal et al., 1981; Casagrande, 1994).

### 2.2.8 Cortical magnification

The likelihood of a response to a light stimulus on the retina also depends on the cortical representation of the retina, specifically whether the same cortical 'weight' is given to stimuli throughout the retina. Foveal vision occupies a much larger cortical area than does peripheral vision, so that $1^{o2}$ in the fovea has a larger cortical representation than $1^{o2}$ in the periphery. This may result from either a cortical magnification of the neural elements of the retina, or it may simply result from the greater ganglion cell density at the fovea. Available data indicates that the latter is the case (Drasdo, 1977; Wassle et al., 1989; Curcio and Allen, 1990).

## 2.3 Anatomy of the retinal nerve fibre layer and optic nerve head

### 2.3.1 The retinal nerve fibre layer

The retinal nerve fibre layer (RNFL) forms the innermost layer of the retina. Ganglion cell axons gather together in bundles (fascicles) surrounded by glial tunnels formed by astrocytes and Müller cell processes (Radius and Anderson, 1979a; Ogden, 1984; Fine and Yanoff, 1979). Not all axons within a bundle are surrounded by glial tissue, and some are joined to each other by junctions (Hogan et al., 1971). In the primate, about 18% of the cross-sectional area of a nerve fibre bundle is glia. 14% is of Müller cell origin and 4% astrocytic (Ogden, 1983c). The astrocytes in the RNFL, rather than being star-shaped, are generally bipolar with their axis parallel to the axons (Hogan et al., 1971). The bundles are the striations that are visible ophthalmoscopically (Radius and Anderson, 1979a). The Müller cell processes ultimately arborise to contribute to the inner limiting membrane. The axons are unmyelinated in the retina, and vary in size between about 0.6 and 2.0μm.

The organisation of the ganglion cell axons in the RNFL and ONH is controversial (Caprioli, 1989). There are two aspects that need consideration:

1. the organisation of nerve fibres within the RNFL and ONH with respect to the circumferential origin of the axon
2. the organisation of nerve fibres within the RNFL and ONH with respect to the eccentricity of the origin of the axon

Studies of the nerve fibre layer organisation have been made in different species of the macaque monkey by injection of horseradish peroxidase or radioactive amino acid into the ONH or retina, or by making photocoagulation burns to the retina (Ogden, 1974; Ogden, 1983b; Radius and Anderson, 1979b; Minckler, 1980). These studies have determined that there is a level of organisation within the RNFL with respect to the eccentricity of the origin of the axons, although the studies do not agree on the detail. Some studies have concluded that the longer axons, from more peripheral ganglion cells, tend to lie deeper (scleral) to shorter axons axons (Radius and Anderson, 1979b; Minckler, 1980), with some intermixing (Radius and Anderson, 1979b). Others have concluded that the axons from peripheral ganglion cells are scattered throughout the thickness of RNFL (Ogden, 1974), or lie in the superficial (vitreal) part of the RNFL (Ogden, 1983b). The latter study found a degree of organisation within the RNFL, with respect to eccentricity of origin, but extensive intermingling of fibres as they crossed the ONH margin. The contrasting findings in some of these studies may relate in part to species variation in RNFL organisation. Stratification in the rhesus monkey has been found to be less prominent than in the owl monkey (Radius and Anderson, 1979b), and differences between the owl monkey and macaques have been noted (Ogden, 1983b; Ogden, 1983a), as well as differences between different species of macaque (Radius and Anderson, 1979a; Ogden, 1983b).

These experimental studies agree that there is a clear organisation with respect to the circumferential origin of axons (Radius and Anderson, 1979b; Ogden, 1983b). Injections of horseradish peroxidase at the ONH margin result in labelling of ganglion cells in a wedge shaped sector of retina extending into the periphery, with a few labelled ganglion cells scattered outside this wedge shape sector in a larger area. The latter are estimated to comprise fewer than a 2% of the total number labelled (Ogden, 1983b). The axons of these scattered cells may correspond to the accessory fascicles described by Vrabeč (1966). Axons with an aberrant intra-retinal course have been identified as belonging to giant parasol-like ganglion cells (Thanos et al., 1991).

The course of ganglion cell axons has been traced in the human retina (Fitzgibbon and Taylor, 1996; Fitzgibbon, 1997). Some lateral movement of fibres within a fascicle was observed, but axons generally remain parallel as they approach the disc. This circumferential organisation is maintained in the superficial ONH, with adjacent axons remaining in the same sector of the ONH. However, the fibres do not appear to be organised through the depth of the RNFL. Axons from most points in the retina were scattered throughout the thickness of the RNFL. Exceptions were fibres from the temporal raphé and arcuate bundles, which tended to remain deep (scleral), and a minority of fibres from the arcuate areas, which remain deep, and take a more direct course to the ONH than the bulk of the fibres. A few fibres in the region of the temporal raphé may cross to the opposite hemisphere, and enter the opposite side of the ONH. As the fibres enter the ONH, more superficial fibres pass to more central parts of the disc, and deeper fibres (such as those from the temporal raphé and arcuate areas) pass to more peripheral parts of the disc.

#### 2.3.1.1 Retinal nerve fibre layer thickness

At the region of the fovea, there is a central zone devoid of bipolar cells (350μm diameter), ganglion cells (400μm diameter), and capillaries (500μm diameter). The RNFL is first detectable at about 500μm from the foveola centre (Fine and Yanoff, 1979). Varma et al. (1996) measured the RNFL thickness at 27, 34, 26, and 12μm just superiorly, inferiorly, nasally and temporally, at an unspecified distance close to the foveola.

The RNFL thickness at the ONH margin (defined as the termination of Bruch's membrane) has been measured at 405 ± 28, 376 ± 40, 372 ± 43, and 316 ± 24μm at the superior, inferior, nasal and temporal poles respectively (Varma et al., 1996). The RNFL thickness decreases with increasing distance from the ONH margin, fitting a cubic regression model. However, calculations of the cross-sectional area of the RNFL at different distances from the ONH margin, using data derived from Varma's paper, demonstrate that the RNFL cross-sectional area halves at a distance of 1.5 disc diameters from the centre of the ONH (400μm from the disc edge). Only a small drop in cross-sectional area would be expected if the difference were only due to decreased numbers of axons. Dichtl et al. (1999) found the RNFL thickness at the ONH margin to be 313 ± 38, 397 ± 58, 165 ± 19, and 131 ± 15μm at the superior, inferior, nasal and temporal poles respectively. The differences

with Varma's findings are not fully explained. A larger disc size (a feature of Jonas's populations) might explain the thinner RNFL as a whole, but not the greater difference between the temporal and nasal thicknesses compared to the superior and inferior that was found in the latter study.

### 2.3.2 The internal limiting membrane

The internal limiting membrane (ILM) is 1 - 3μm thick, with a smooth inner surface and an irregular outer surface that is tiled by irregular polygonal processes of Müller cells (Hogan et al., 1971; Heegaard, 1997). The ILM is comprised of Müller cell and glial cell basement membrane (about 0.5μm thick) and a contribution from vitreous collagen fibrils.

### 2.3.3 Anatomy of the optic nerve head

There are three types of tissue that make up the ONH: neural (ganglion cell axons and glia), vascular, and connective tissues. Each varies in form and distribution according to the anatomical level within the ONH. The ONH can be divided into several layers: prelaminar, scleral (laminar), and retrobulbar (postlaminar).

#### 2.3.3.1 Histology

##### 2.3.3.1.1 Prelaminar (retinal and choroidal) part

At the optic disc, there is no internal limiting membrane like that covering the surface of the retina. Instead there is a thin layer of astrocytes (inner limiting membrane of Elschnig). The connective tissue collagen of the branches of the central retinal vessels is covered by processes of the glia, which frequently splits to form a sheath around the vessels (Hogan et al., 1971). There is a ring of transition between the thin basement membrane overlying the disc and that of the sensory retina. At this transition zone, there is a strong attachment to the (secondary) (Fine and Yanoff, 1979).
The ganglion cell axons and their astrocytes are separated by neuroglia from the retina (intermediary tissue of Kuhnt) and choroid (layer of Jacoby) (Hogan et al., 1971). Adjacent to this glia is a layer of connective tissue that is continuous with the framework of the choroid. The retinal layers terminate as they approach the disc. The nuclear and plexiform layers cease first, as the RNFL thickens. The retinal pigment epithelium extends furthest, but usually ends short of the termination of Bruch's membrane.
The surface topography of the ONH varies around the circumference, so that the nasal part of the nerve and the superior edge are more raised than the inferior edge, which, in turn, is more raised than the temporal part. The angle of insertion of the nerve into the globe affects its superficial morphology (Hogan et al., 1971). If the axis of the nerve is tilted temporally, then disc will show a 'temporal tilt', with the temporal side of the disc being flatter, and the nasal part raised. Temporal tilting is frequent in myopic eyes.

If the retinal pigment epithelium does not reach the edge of the disc, typically at the temporal margin of the disc, the choroidal edge is visible as a choroidal crescent. If the choroid doesn't reach the edge of the disc, then a scleral crescent is present. Occasionally, there is a pigment crescent at the nasal margin of the disc, which results from a thickening or folding of the pigment epithelium.
The anatomy of the anterior ONH is similar to that of the retinal nerve fibre layer, except that the Müller cell processes are replaced by processes of glial cell astrocytes (Radius, 1987). Near the disc edge, as the Müller cells disappear, the axons become segregated into bundles, or fascicles, by neuroglial cells oriented at right angles to the fascicles. The columns supporting the axon bundles are entirely of glial cell origin (specialised astrocytes called 'spider cells'), and are less well defined than in the scleral lamina. The astrocytes form a three-dimensional basket-like network, continuous through the disc from the retinal surface, through the scleral lamina, to the orbital part of the nerve. The astrocyte processes surround the fascicles, and extend into them (Hogan et al., 1971). The capillaries of this part of the ONH are enclosed within the glial framework (Anderson, 1969; Radius, 1987). At the level of the choroidal and anterior ONH, the only connective tissue elements in the trabeculae dividing axon bundles is that associated with the capillaries. The cribriform area at this level has been measured at 1.62 to 3.25 $mm^2$ (mean 2.35 $mm^2$) (Ogden et al., 1988).

The term lamina cribrosa is applied to the 'striated' portions of the bulbar optic nerve, and includes the choroidal part, where the fascicular columns are divided by astrocytes only, and the scleral part, where the trabecular beams divide the columns (Fine and Yanoff, 1979).

#### 2.3.3.1.2 Scleral lamina cribrosa

The scleral portion of the ONH is comprised of the lamina cribrosa and axon bundles passing through the lamina. The lamina is constructed of a series of about 11 collagenous sheets covered by astrocyte basement membrane. There is considerable inter-individual variability in the number of lamellae, and the position of attachment to the sclera. The lamina may lie in the anterior part of the scleral canal, the posterior part, or occupy the whole length of the canal (Elliot, 1921).
Astrocytes fill the spaces between the lamina sheets and nerve fibre bundles and line the rim of the lamina fenestrations. A few are found within the bundles of nerve fibres. The most posterior lamina sheet merges with the anterior end of the longitudinal connective tissue septa of the intraorbital part of the optic nerve, and beyond this level the ganglion cell axons become myelinated (Anderson, 1969). Capillaries of the scleral lamina cribrosa are imbedded in the lamina sheets (Anderson, 1969; Quigley and Addicks, 1981).
The beams of the lamina are formed by an extension of collagen bundles and elastic fibres from the inner two thirds of the sclera. The bundles extend from one side of the canal to the other, intersecting at various angles to form a sieve. Not all the bundles traverse the canal completely, with some joining the connective tissue of the central retinal vessels (Hogan et al., 1971).
The inner surface of the lamina is saddle-shaped, with the horizontal axis higher than the superior and inferior parts. The peripheral part of the lamina is thicker than the central part (Dichtl et al.,

1996). The sheets are perforated by pores ranging in diameter from 10μ to 100μ (Emery et al., 1974; Quigley and Addicks, 1981) and in area from 500 to 22500 $\mu m^2$ (Ogden et al., 1988), with a mean of about 4000 $\mu m^2$ (Jonas et al., 1991). The number of lamina pores depends on the size of the ONH, and ranges from 168 to 292 (mean 227) (Jonas et al., 1991). Ogden et al. (1988) reported an average of 392 linear channels through the lamina plates at the choroidal level and increasing to 540 posteriorly. Some channels pass directly posteriorly and other obliquely to the axis of the optic nerve (Emery et al., 1974; Quigley and Addicks, 1981). The course of peripheral channels tends to be curvilinear, and longer than central channels (Dichtl et al., 1996). The increase in number of channels correlates with branching and division of axonal bundles through the lamina (Quigley and Addicks, 1981; Ogden et al., 1988). Most axons take a relatively straight course through the lamina, although a significant minority (8-12%) take a more convoluted path, passing between cribrosal plates in both central and peripheral parts of the lamina (Morgan et al., 1998).

Studies have found that the pores at the superior and inferior poles are larger (diameter up to 100μm) than those at the nasal, temporal and central parts of the ONH (rarely larger than 50μm) (Quigley and Addicks, 1981; Dandona et al., 1990; Jonas et al., 1991), and pore area is consequently greater at the poles (Jonas et al., 1991). Another study found a higher proportion of small pores in the temporal part of the disc, roughly equal pore sizes in the superior and nasal parts, and the largest pores in the inferior part of the ONH (Ogden et al., 1988). The connective tissue sheets are also thinner at the poles, markedly so in a minority of eyes (Quigley and Addicks, 1981; Radius and Gonzales, 1981; Radius, 1981a), although nearly half the eyes in one study had no particular pattern of tissue density (Radius and Gonzales, 1981). Racial differences in lamina morphology has been investigated (Dandona et al., 1990). The total lamina area is greater in blacks than whites, reflecting larger ONH size, with a higher number of pores. The tissue/pore ratio is the same in the two groups.

The size and shape of visible pores (those not covered by neuroretinal tissue) have been measured in vivo using a confocal scanning laser ophthalmoscope and image processing techniques (Bhandari et al., 1997). Pores in normal eyes tend to be round (Fontana et al., 1998a).

The connective tissue of the ONH consists of cells and extracellular matrix (ECM), the cells being responsible for the maintenance and architecture of the ECM. The ECM is made up of an orderly array of collagens, proteoglycans, glycoproteins and elastin. The core of the cribriform plates contains fibres of elastin and fibrillin (a network of filamentous basement membrane and fibrillar collagen of types I and III). The elastin fibres characteristically have a round central amorphous component surrounded by a microfibrillar sheath, and are embedded in a dense collagen matrix (Pena et al., 1998). Covering the core, there is a continuous layer composed of type IV collagen, laminin and heparin sulphate proteoglycan (Hernandez et al., 1986; Hernandez et al., 1987; Hernandez and Ye, 1993). There is no collagen type IV in sclera (Hernandez et al., 1987). At the border between lamina and sclera, scleral projections interdigitate with glia (Anderson, 1969). This border region is rich in elastin fibres that are oriented circumferentially (Quigley et al., 1994). The

fibres in the border zone are larger, but less numerous, than in the lamina itself, and comprise about the same proportion of matrix (Quigley et al., 1996a).
The area of connective tissue has been found to be greater in young whites compared to young blacks, although no difference was found in older individuals (Hernandez and Neufeld, 1991). In young blacks, there is less collagen type I and IV and elastin, with a marked increase in type I with ageing. The relative excess of type I collagen in blacks compared to age-matched whites may indicate a less compliant lamina.

### 2.3.3.2 Vascular anatomy

The blood supply to the eye is from the orbital ophthalmic artery via the central retinal and ciliary branches. There are usually 2 to 3 ciliary trunks that give off the medial and lateral long posterior ciliary arteries and the short posterior ciliary arteries. Each main posterior ciliary artery divides into 10 to 20 short posterior ciliary arteries (Wang et al., 1998).
The anterior optic nerve may be divided into 4 parts:

- superficial
- prelaminar
- laminar
- retrolaminar

The blood supply to the superficial part is from adjacent retinal arterioles. The prelaminar part of the nerve receives arteriolar branches directly from the short posterior ciliary arteries and from the circle of Zinn-Haller (itself supplied from medial and lateral short posterior ciliary arteries (Olver et al., 1994)). The circle of Zinn-Haller is complete in about 75% of eyes (Olver et al., 1994). Although these branches may traverse the choroid, the choroidal circulation does not contribute to the blood supply (Hayreh, 1995; Wang et al., 1998). The supply to the laminar portion of the nerve is similar to the prelaminar part. The arterioles perforate the outer aspect of the lamina cribrosa before branching into an intraseptal capillary network. The retrolaminar part of the nerve is supplied by branches of the pial circulation and by branches of the posterior ciliary arteries. Although the capillaries of the peripapillary retina, the anterior optic nerve and the retrolaminar region are anatomically confluent, it is not known whether they are functionally confluent. The overall pattern of the blood supply is sectoral (Hayreh, 1996a).
There is much inter-individual variability. Hayreh has emphasised the importance of watershed zones in the blood supply from the posterior ciliary arteries. The optic disc often lies in the region of these zones. Areas within watershed zones are vulnerable to ischaemia if perfusion pressure drops.

### 2.3.3.3 Optic Disc Morphology and morphometry

In 1901, Elschnig published a classification of normal disc types which was later modified by Kronfeld (1967). The intention was to highlight features in a continuous spectrum rather than imply discrete entities. These initial descriptions were qualitative in nature, based on empirical observation. The subsequent technological advances of planimetry and photogrammetry have allowed observers such as Portney (1973; 1974; 1976) and Jonas et al. (1988g) to add quantitative information that may be applied to the original descriptions to give a more complete picture. The following, based on descriptions made by these observers, describes the forms of the optic nerve head and relate it to the size of the optic disc:

Type I disc: either there is no cup or a small, shallow, funnel-shaped excavation, pointed or rounded at the base and which does not usually extend to the level of the lamina cribrosa. These discs are small and the horizontal cup/disc ratio is usually 0.3 or less.

Type II disc: the cup is almost cylindrical and centred on the temporal side of the disc. The nasal wall is steep and coincides with the centre of the disc and the temporal wall may be flatter. These discs are small/moderate in size, with a horizontal cup/disc ratio of 0.3 or less. The lamina cribrosa is usually visible at the base of the cup.

Type III: the cup in these discs is central and symmetrical, with the lamina cribrosa clearly visible. The base is wide and flat and may be quite deep and the cup is occasionally ampulliform (Kirsch and Anderson, 1973b). The insertion of the nerve may be oblique (Kirsch and Anderson, 1973b), giving rise to a rim that is steep or overhanging on one side in about half the discs of this type (Portney, 1973). The steep or overhanging rim is most frequently in the superior and supero-nasal part of the disc with a sloping rim opposite. These discs are large and most have a horizontal cup/disc ratio of greater than 0.3 and some up to 0.65 (Portney, 1973).

Type IV: the cup in these discs has a steep nasal wall and a very gently sloping temporal wall, so that the cup may reach the temporal edge of the disc. The disc may otherwise look like a Type II or Type III disc and the horizontal cup/disc ratio is always greater than 0.3.

Type V: this 'type' represents a range of developmental abnormalities with atypical cupping.

There is a wide distribution of optic disc size in the normal population, which is not related to refractive error (Britton et al., 1987; Jonas et al., 1988g; Chi et al., 1989) except in high myopia (Jonas et al., 1988e). The largest discs may be 2.5 (Bengtsson, 1976) to 6.9 (Jonas et al., 1988g) times the size of the smallest and discs that are greater than or less than 2 standard deviations from the mean have been termed 'macrodiscs' and 'microdiscs' (Jonas et al., 1988g). Macrodiscs have a normal neuroretinal rim area and form, despite very large cups, and often have cilioretinal arteries (Jonas et al., 1989c), the number being greater as disc size increases (Jonas et al., 1988a). ONH drusen (Mullie

and Sanders, 1985; Jonas et al., 1987) and anterior ischaemic optic neuropathy (Mansour et al., 1988) are more common in small optic discs.

The actual size of the optic disc varies with measuring (instrument and magnification correction) technique and population studied, from a mean area of 1.57 $mm^2$ with the Rodenstock analyser (Caprioli et al., 1986) to 3.18$mm^2$ using the indirect ophthalmoscope (Montgomery, 1993). Histological measurements have estimated mean disc areas at about 2.6 $mm^2$ (Jonas et al., 1988c; Quigley et al., 1990), although measurement technique and the definition of the optic disc margin influence the results. In the former, measurements were made from photographs, and in the latter, termination of Bruch's membrane was taken as the disc margin. Similarly, mean vertical disc diameter measurements vary from 1.53 mm (Caprioli et al., 1986) to about 2.1 mm (Montgomery, 1993) (derived from the stated disc area), with most estimates between 1.66 mm (Britton et al., 1987) and 1.92 mm (Jonas et al., 1988g).

The shape of the disc is usually vertically oval (Gloster, 1975; Britton et al., 1987; Jonas et al., 1988g; Quigley et al., 1990), the vertical diameter being on average 9% greater than the horizontal (Jonas et al., 1988g). Racial differences in disc size have been reported (Maisel et al., 1989; Chi et al., 1989; Quigley et al., 1990), with black subjects having larger discs as a result of a greater vertical disc diameter (Quigley et al., 1990).

The area of the neuroretinal rim varies with optic disc size, so that larger discs have larger neuroretinal rim areas (Betz et al., 1981; Britton et al., 1987; Caprioli and Miller, 1987; Jonas et al., 1988g; Jonas et al., 1989c). Histological examination has demonstrated that this is, at least in part, due to a greater number of ganglion cell axons (Quigley et al., 1990; Jonas et al., 1992). The relationship between disc size and neuroretinal rim area is not straight forward as the measured rim area is influenced by the slope of the cup/rim edge. Given discs of equal size, those with sloping rim edges have larger measured rim areas than discs with steep rim edges (Jonas et al., 1988g).

The neuroretinal rim has a characteristic form, subject to the size and shape of the disc. In discs with cups the neuroretinal rim is at least as thick at the 12 and 6 o'clock positions as elsewhere (Kirsch and Anderson, 1973a) and usually thickest (83% of eyes) in the inferotemporal sector, followed by the superotemporal, nasal and then temporal sectors (the Werner/Jonas 'ISNT' rule) (Jonas et al., 1988g). This pattern is less marked in larger discs, in which the rim is distributed more evenly around the edge of the disc. The increased width of the inferotemporal with regard to the superotemporal rim may result from the anatomical position of the fovea, below the retinal horizontal midline (Sanchez et al., 1986; Jonas et al., 1989a), and the common inferotemporal disc tilt.

The characteristics of the optic cup are also determined by the size and shape of the disc in normal eyes. The area of the cup is positively correlated with disc size (Teal et al., 1972; Bengtsson, 1976; Caprioli and Miller, 1987; Britton et al., 1987; Jonas et al., 1988g) so that large cups may be normal if the disc is also large. As a result, expressing the size of a cup as a cup/disc ratio (CDR) is of limited value unless the size of the disc is known. In the normal population the CDR varies from 0.0 to 0.87

(Jonas et al., 1988g), though a CDR > 0.65 is found in less than 5% of the normal population (Snydacker, 1964; Carpel and Engstrom, 1981; Sommer et al., 1979a).
The shape of the cup may be more useful. Cups are on average horizontally oval (Portney, 1973; Gloster, 1975; Carpel and Engstrom, 1981; Jonas et al., 1988g) and when the shape of the cup is expressed in terms of a CDR, the horizontal CDR is larger than the vertical in 75% (Portney, 1973) to over 90% (Carpel and Engstrom, 1981; Jonas et al., 1988g) of normal eyes. However, large physiological cups in large discs tend to be more round than horizontally oval (Kirsch and Anderson, 1973a; Jonas et al., 1988g) and the more vertically oval discs tend toward having a more vertically oval cup (Tomlinson and Phillips, 1974).
Cupping tends to be symmetrical between the two eyes (Snydacker, 1964; Armaly, 1969a; Fishman, 1970; Carpel and Engstrom, 1981; Jonas et al., 1988g), the vertical CDR being within 0.2 in over 96% of normal subjects (Carpel and Engstrom, 1981; Jonas et al., 1988g).

### 2.3.4 Ageing changes of the optic nerve head

#### 2.3.4.1 Histology

##### 2.3.4.1.1 Lamina cribrosa

One study found a reduction in the number of axonal channels through the lamina of about 5% per decade after the age of 50 years (Minckler, 1989). Other studies have found no change in the number of pores (Ogden et al., 1988; Jonas et al., 1991), but a reduction in pore area of about 5% per decade after the age of 30 years (Ogden et al., 1988).
In young adults, the lamina ECM is a compliant tissue. As the lamina ages, there is an increase in connective tissue area (collagen types I, III, and IV) and in the density of the ECM in the core of the plates. There is also an increase in the density of elastin (Hernandez et al., 1989). The elastin fibres increase in thickness to form long tubular structures (Hernandez, 1992). These increases in fibrillar forms of collagen may make the lamina more rigid and less distensible to fluctuating IOP.

##### 2.3.4.1.2 Axon numbers

A decreasing axon count with age has been reported by a number of authors (Balazsi et al., 1984b; Johnson et al., 1987; Mikelberg et al., 1989; Jonas et al., 1990; Jonas et al., 1992), the reduction ranging between 4000 and 6723 per year (around 0.36% to 0.62% per year) (Jonas et al., 1992; Johnson et al., 1987).

#### 2.3.4.2 Morphology and morphometry

There is conflicting evidence in the literature with respect to ageing changes in optic disc cupping, with some authors reporting an increase (Pickard, 1948; Colenbrander, 1960; Ford and Sarwar, 1963; Schwartz et al., 1975; Schwartz, 1980; Carpel and Engstrom, 1981), and others finding none (Snydacker, 1964; Hollows and McGuiness, 1966; Armaly and Sayegh, 1969). Authors of early papers

relied on optic disc drawings (Pickard, 1948), clinical or stereo-photograph comparison with diagrammatic charts (Colenbrander, 1960; Schwartz, 1980), clinical estimation of the CDR (Ford and Sarwar, 1963; Schwartz et al., 1975; Carpel and Engstrom, 1981; Hollows and McGuiness, 1966), or comparison of non-stereoscopic photographs with diagrammatic charts (Snydacker, 1964; Hollows and McGuiness, 1966). Both clinical and non-stereoscopic evaluation of the optic disc are notoriously subject to high variability between different observers (Varma et al., 1992b; Lichter, 1976).

More recently, techniques that allow magnification-corrected measurements of optic disc images have been used. These include manual planimetry of non-stereoscopic photographs (Bengtsson, 1980), computer assisted planimetry of stereoscopic photographs (Jonas et al., 1988g; Balazsi et al., 1984a; Airaksinen et al., 1992; Caprioli, 1994; Garway-Heath et al., 1997; Healey et al., 1997; Moya et al., 1999), computerised digital stereo photogrammetry (Varma et al., 1994; Tsai et al., 1992; Funk et al., 1989) and confocal scanning laser ophthalmoscopy (Garway-Heath et al., 1997). These studies again have conflicting results, with some demonstrating age-related changes (Bengtsson, 1980; Balazsi et al., 1984a; Tsai et al., 1992; Airaksinen et al., 1992; Garway-Heath et al., 1997; Healey et al., 1997) and some showing none (Jonas et al., 1988g; Funk et al., 1989; Caprioli, 1994; Varma et al., 1994; Moya et al., 1999)

### 2.3.5 Glaucomatous changes of the optic nerve head

#### 2.3.5.1 Histology

In moderately advanced glaucoma, there is generalised disorganisation and compression of the fibres in the lamina plates, and fewer pores visible on the inner surface (Emery et al., 1974). The pores also lose their round shape, and become more elongated as field loss advances (Emery et al., 1974; Fontana et al., 1998a). The linear arrangement of pores longitudinally through the plates also becomes lost (Emery et al., 1974).

Recent histological studies of the ONH in glaucoma suggest the amount of glial tissue in the ONH in glaucoma is little altered and there may be glial hyperplasia (Quigley and Green, 1979; Quigley et al., 1982; Minckler and Spaeth, 1981). Early observations had suggested glial loss (Elliot, 1921). Studies also suggest that, in general, posterior displacement of the lamina is a relatively late occurrence (Elliot, 1921; Quigley and Green, 1979; Quigley et al., 1983). Compression of laminar plates, as measured by reduced overall lamina thickness, has been described as an early sign, occurring in some eyes before visual field loss (Quigley et al., 1983). The amount of compression was associated with the degree of glaucomatous visual field damage, and in advanced cases there was fusion, or loss in the number, of lamina plates. In advanced disease the lamina becomes displaced posteriorly, especially in the mid-peripheral parts, and the walls of the canal are displaced laterally posterior to Bruch's membrane (Quigley and Green, 1979; Quigley et al., 1983). The posterior bowing affects the upper and lower poles of the ONH more than the mid-nerve (Quigley et al., 1983).

There are marked changes in the ECM of the lamina cribrosa in glaucoma. There is an increase in the density of the basement membranes (collagen type IV) in the pre-laminar region and in the lamina (Hernandez et al., 1990). There is disorganisation of elastin fibres and granular masses of elastin appear (elastosis) in the lamina cribrosa and insertion region. The collagen matrix around the elastotic fibres is sparse (Pena et al., 1998). The area of elastin, defined by immunogold labelling, is increased in glaucoma (Pena et al., 1998), although, in severe disease, Hernandez found a loss of elastin from the anterior lamina plates (Hernandez et al., 1990). Quigley et al. (1996a) has reported an unchanged amount of elastin in glaucoma. Ultrastructurally, there is fragmentation of elastic fibres, accumulation of non-fibrillar elastic-like material and bundles of microfibrils are found in the core and insertion region of the plates (Hernandez, 1992). Quigley et al. (1991; 1994) have described a curled appearance of elastin fibres in glaucoma, which may result from a dissociation of elastin from the other components of the ECM . The appearance of elastin fibres in the lamina itself and in the border zone with the sclera tend to be the same (Quigley et al., 1996a).

There is also an increase in collagen type VI in glaucoma, not found in normal ageing (Hernandez and Neufeld, 1991). Collagen type VI links bundles of collagen fibres, and increases in amount in stressed tissues.

Axons are lost in all parts of the optic disc, but preferentially (in eyes with visual field loss) in the superior and inferior nerve sectors, giving an hourglass-like pattern to the atrophy (Quigley et al., 1982; Quigley et al., 1983). Regional variations in the structure of the lamina cribrosa may give rise to differences in the susceptibility of ganglion cell axons to damage in glaucoma according to their position within the disc.

### 2.3.5.2 Morphology and morphometry

A number of classifications have been proposed to describe the range of appearances of the glaucomatous disc (Kronfeld, 1967; Read and Spaeth, 1974; Hitchings and Spaeth, 1977; Geijssen and Greve, 1987; Geijssen and Greve, 1990; Spaeth, 1994; Nicolela and Drance, 1996; Broadway et al., 1999) and they serve to highlight important aspects of the changes that take place. The various terms that have been coined to describe patterns of rim loss seen in glaucoma refer to the appearances that result from different patterns of rim loss superimposed on the wide range of pre-existing normal disc morphology. These terms highlight the most prominent features in a continuous spectrum and should not be taken as discrete entities.

#### 2.3.5.2.1 Changes in the neuroretinal rim and optic cup

Progressive thinning of the neuroretinal rim has been documented in discs of patients who subsequently develop glaucomatous visual field defects (Sommer et al., 1979b; Pederson and Anderson, 1980; Motolko and Drance, 1981; Odberg and Riise, 1985; Quigley et al., 1992; Airaksinen et al., 1992). The pattern of loss of rim varies and may take the form of diffuse thinning, localised

notching, or both in combination (Jonas et al., 1988f; Tuulonen and Airaksinen, 1991). The result is a number of 'types' of glaucomatous cupping:

1. *Overpass cupping* (Read and Spaeth, 1974; Spaeth et al., 1976; Hitchings and Spaeth, 1976) or *central deep atrophy* (Kronfeld, 1967; Portney, 1976). This describes the initial change that occurs in small (Type I) optic discs that physiologically have no cupping or a shallow cup that does not reach the level of the lamina. It is characterised by the development of a central, deep pallor or translucency, giving the appearance of a hollow beneath the disc surface. At this stage many eyes will have a normal visual field (Hitchings and Spaeth, 1977).
2. As the disease process progresses, the surface may collapse, leading to a uniform sloping down to the central white area or *saucerization* (Chandler and Grant, 1965). Saucerization that produces concavity of the rim at the disc edge results in *sharpening of the rim* (Read and Spaeth, 1974) and is regarded as a sign suggestive of a field defect. *Focal saucerization* (Spaeth et al., 1976) describes a shallow sloping cup, usually inferotemporally, and associated with a paracentral scotoma.
3. The central deep atrophy may proceed to a central, cylindrical excavation (Portney, 1976), with the physiological cup deepened and the sides steepened. The cup mimics the physiological cupping in a larger disc. Photogrammetric measurements (Portney, 1976) show that the deepening of the cup (to the lamina) is also accompanied by an enlargement of the cup area, more so in the vertical than the horizontal direction. The excavation enlarges centrifugally, as an expanding vertically oriented ellipse, baring increasing amounts of lamina. That the enlargement of the cup occurs predominantly in the vertical direction has been emphasised by several authors (Chandler and Grant, 1965; Kirsch and Anderson, 1973a; Gloster, 1975). The vertical extension of the cup is often asymmetric (Portney, 1976) and most frequently downward (Read and Spaeth, 1974). Vertical expansion of the cup is usually accompanied by concurrent horizontal expansion that is of a smaller magnitude (Portney, 1976; Weismann et al., 1973), and results in a greater frequency of vertically oval cups amongst eyes with ocular hypertension and glaucoma (Weismann et al., 1973; Gloster, 1975; Jonas et al., 1988f).
4. The nature of rim loss in discs with larger physiological cups (Type III) may take several forms. The expansion of the cup may appear even (Pederson and Anderson, 1980) and has been termed *concentric enlargement* (Spaeth et al., 1976). This results in a rim that looks physiological, though too large for the size of the disc in which it occurs. Visual field loss usually occurs late in this case (Spaeth et al., 1976; Pederson and Anderson, 1980). *Temporal unfolding* refers to expansion of the cup more on the temporal side (Read and Spaeth, 1974; Spaeth et al., 1976) and *nasal cupping* refers to cupping on the nasal side of the retinal vessels as they emerge from the disc. This probably represents a form of concentric enlargement, though focal loss of tissue occasionally occurs on the nasal side.

5. Rim loss may appear less even and has been termed *broad sector atrophy* (Kronfeld, 1967; Portney, 1976). Often the expansion is greater in the infero-temporal or supero-temporal direction (Spaeth et al., 1976), giving a pattern of *vertical extension* of the cup. Marked asymmetry of expansion toward one of the poles results in *notching* (Kirsch and Anderson, 1973a; Read and Spaeth, 1974; Spaeth et al., 1976; Hitchings and Spaeth, 1976) of the rim, and occurs most frequently in the inferotemporal, followed by supero-temporal, region of the disc (Jonas et al., 1988f; Geijssen and Greve, 1990; Spaeth, 1994). Notching occurring in smaller discs was called *the phase of downward extension* of the deep central atrophy by Kronfeld (1967) and is often associated with an upper (arcuate) Bjerrum scotoma. If the notching is deep, the exposed lamina has been termed the *laminar dots sign* (Read and Spaeth, 1974), a proximal arcuate scotoma is frequently found. If there is still good colour and a sharpened rim, a distal arcuate scotoma is more likely (Read and Spaeth, 1974).
6. Highly localised loss of rim tissue is seen in glaucoma as an *acquired pit of the optic nerve* (Radius et al., 1978). These occur most frequently at the disc edge in the inferotemporal, and less frequently, supero-temporal part of the disc in rim that is already thinned. Initially there is a focal depression on the rim surface that gradually deepens. Eventually all that remains is a pit with lamina at the base, often with adjacent peripapillary atrophy. It has been suggested that acquired pit may be more common in normal tension glaucoma (Javitt et al., 1990), although biases in case selection make firm conclusions difficult.
7. *Myopic cupping* is a term given to glaucomatous cupping in a tilted myopic disc (Geijssen, 1991; Nicolela and Drance, 1996; Broadway et al., 1999). These have a temporal myopic crescent and additional signs of glaucomatous cupping. It is doubtful whether this represents a 'form' of glaucoma, rather than glaucoma occurring in a specific type of optic disc.
8. *Senile sclerotic cupping* is a term given to diffuse, shallow neuroretinal rim loss, giving rise to a 'moth-eaten' appearance (Geijssen and Greve, 1987). It is sometimes described as the development of pallor and a spongy appearance of the neuroretinal rim, without the loss of neuroretinal rim area or volume (Broadway et al., 1999). There is usually a complete ring of peripapillary atrophy and choroidal sclerosis (fundus tesselation).
9. The classic description of the final stages of a deeply excavated disc is *bean pot cupping* (Spaeth et al., 1976; Hitchings and Spaeth, 1976), in which the cup forms a bowl behind the scleral opening of the nerve head.

Planimetric measurements have confirmed that the thinning of the rim, while occurring in all disc sectors, is greatest at the inferior and superior poles (Tuulonen and Airaksinen, 1991; Jonas et al., 1993) leading to a loss of the physiological rim shape so that the inferotemporal rim is no longer the thickest (Jonas et al., 1988f; Jonas and Konigsreuther, 1994). If either the inferotemporal or

superotemporal rim is narrower than the nasal or temporal rim, it is considered almost pathognomonic for glaucoma (Jonas et al., 1988f).
The relative rates of vertical and horizontal expansion, as well as the disc size and physiological rim shape, affect the impression of the predominant pattern gained. Tuulonen and Airaksinen (1991) described the patterns of rim loss in a group of ocular hypertensive patients followed over 5 to 15 years. The initial pattern of loss in 23 eyes was diffuse in 10, diffuse with local notching in 4, local notching alone in 6 and pallor without rim loss in 3. The optic discs exhibiting diffuse loss were larger than those with more localised loss.
As cupping of the disc progresses, the various patterns seen in earlier disease tend to converge. Rim is lost so that the last remaining tissue is found at the temporal and nasal parts of the disc, and finally only thinned tissue at the nasal edge of the disc is seen.

The *pallor* of the disc (Schwartz et al., 1973) refers to the central yellow-white portion of the disc overlying the lamina cribrosa, contrasting with the reddish pink of the healthy neuroretinal rim tissue. In normal eyes the central pallor generally coincides with the cup as defined by the contour change of the rim (Schwartz et al., 1973). In glaucoma there may be loss of rim as defined by contour with relative preservation of the colour, so that the area of pallor is smaller than that of the cup. This particularly occurs in eyes with a shallow, gently sloping cup (Tuulonen et al., 1992). The loss of rim with preservation of the colour gives rise to the *tinted hollow* of Read and Spaeth (1974). Both cupping and pallor may progress at different rates. Where the rim maintains colour, the cupping may be termed *cupping without pallor* (Hitchings and Spaeth, 1976; Hitchings and Spaeth, 1977). The visual field is often intact at this stage (Schwartz et al., 1973; Read and Spaeth, 1974; Hitchings and Spaeth, 1977). Pallor affecting the rim and progressing to the disc edge results in *cupping with neuroretinal rim pallor* and is more often associated with a visual field defect (Read and Spaeth, 1974; Hitchings and Spaeth, 1977). Pallor in a small sector may be missed if the disc is not examined with a narrow beam on the slit lamp (Hitchings and Spaeth, 1977) as the rim may be coloured by scattered light from adjacent tissue.
Asymmetry of cupping occurs infrequently in normal eyes and more often in ocular hypertensive and glaucomatous eyes (Fishman, 1970). A study following 44 ocular hypertensive patients for a mean of 4.5 years found a that a CDR difference of 0.2 or greater occurred in 44% of those progressing to glaucoma and 24% of those remaining stable (Motolko and Drance, 1981).

#### 2.3.5.2.2 Cup/disc ratio

The CDR is of little value without knowledge of the size of the disc and as a result its use for glaucoma diagnosis is limited. A cut-off CDR of 0.6 to identify discs as glaucomatous has been reported to have a sensitivity of 92% and specificity of 65% (Sommer et al., 1979a) and sensitivity of 85% and specificity of 91% (Garway-Heath et al., 1998a).
Any loss of neuroretinal rim tissue causes a greater change in the cup/disc ratio when the CDR is initially small. When the CDR is large, in either glaucomatous or physiologically cupped discs, a

larger proportion of tissue has to be lost before much impact is made on the CDR (Montgomery, 1993).

#### 2.3.5.2.3 Vessels

As the cup enlarges in glaucoma, *nasal displacement* of the main disc vessels may occur. However, nasal exit is a feature of physiologically cupped discs (Armaly, 1969b; Tomlinson and Phillips, 1971; Kirsch and Anderson, 1973a) and should not be regarded as acquired unless change is observed. A more specific, and early, sign of acquired cup enlargement is the *bared circumlinear vessel* (Herschler and Osler, 1980). A circumlinear vessel is a small arteriole or vein that lies superficially on the neuroretinal rim at the edge of the cup and leaves the disc for the macula. At least one is present in 44% to 66% of eyes. As the cup enlarges in ocular hypertension and glaucoma the loss of rim tissue leaves the vessel isolated, or 'bared'. It may remain superficial or come to lie on the inner slope of the rim or on the cup floor. *Bayonetting* refers to the course of disc vessels up a steep cup slope, or undermined rim.

#### 2.3.5.2.4 Parapapillary Atrophy

The increased frequency of a peripapillary halo or ring in glaucoma was reported by Primrose (1971) and the frequency and magnitude of this feature adjacent to the disc have been quantified more recently by Jonas (Jonas et al., 1989b; Jonas and Naumann, 1989). The atrophy may take two forms, termed zone alpha and zone beta. Zone alpha is an area of irregular hypo- and hyper-pigmentation that lies next to normal retina on its outer side and the optic disc, or zone beta when present, on its inner side. Zone beta, immediately adjacent to the disc, is an area of marked atrophy of the retinal pigment epithelium, so that large choroidal vessels and sclera are visible. A temporal crescent of parapapillary atrophy is not uncommon in the normal population, with zone alpha in over 80% and zone beta in 15% . However, the frequency and area covered increases in glaucoma. Atrophy of either form is least frequent in normal eyes in the nasal disc sector, occurring in 9.2%. The prevalence increases to 43.7% in glaucomatous eyes. Likewise, circumferential atrophy is present in only 8.2% of the normal population and in 27.7% of the glaucomatous. Zone beta, when present, is widest outside the temporal horizontal sector in only 2.2% in normal eyes and 19% of glaucomatous eyes. The site of the largest area of zone beta atrophy tends to correspond with the part of the disc with most neuroretinal rim loss. Parapapillary atrophy is a prominent feature of 'senile sclerotic glaucoma' (Geijssen and Greve, 1987) in which the cupping is broad and shallow with marked pallor.

#### 2.3.5.2.5 Optic Disc Haemorrhage

Small haemorrhages related to the optic disc are an important feature of glaucoma. They are usually dot-shaped when in the neuroretinal rim and flame-shaped when on, or adjacent to, the disc margin, and are most frequent at the inferotemporal, then supero-temporal, parts of the disc (Airaksinen et al., 1981; Diehl et al., 1990; Jonas and Xu, 1994). The incidence in normal and glaucomatous patients

is unknown as a haemorrhage lasts an average about 10 weeks (range 2 to 35 weeks) (Kitazawa et al., 1986). The prevalence has been estimated at 0 to 1.0% in the normal population and 2.2 to 13.8% in glaucomatous patients (Kitazawa et al., 1986; Diehl et al., 1990; Jonas and Xu, 1994; Healey et al., 1998), and they may be slightly more common in normal-tension glaucoma (Kitazawa et al., 1986; Jonas and Xu, 1994; Healey et al., 1998). They may indicate progressive glaucomatous damage (Drance et al., 1977; Diehl et al., 1990) and have been seen to precede nerve fibre layer defects (Airaksinen et al., 1981).

#### 2.3.5.2.6 The Retinal Nerve Fibre Layer

Hoyt (Hoyt and Newman, 1972; Hoyt et al., 1973) reported slit-like defects, wedge-shaped defects, and diffuse loss of the NFL in glaucoma. Sommer et al (1991a) described NFL defects up to 6 years before the onset of visual field loss in ocular hypertensive patients. The prevalence of NFL defects in the normal population is very low, at less than 3% (Quigley et al., 1980; Jonas and Schiro, 1994). The initial abnormality in glaucoma may be either diffuse thinning or localised defects (Quigley et al., 1980; Tuulonen and Airaksinen, 1991). Glaucoma suspects are more likely to have localised defects (Quigley et al., 1980; Airaksinen et al., 1984) and patients with field defects diffuse loss, with or without localised loss (Airaksinen et al., 1984; Tuulonen and Airaksinen, 1991).

## 2.4 Measurement of retinal nerve fibre layer and optic nerve head structure

Images may be acquired of the fundus and ONH with instruments of varying degrees of sophistication. The principles of the scanning laser ophthalmoscope, used in the studies reported in this thesis, are outlined below.

### 2.4.1 Confocal scanning laser ophthalmoscopy

The confocal scanning laser ophthalmoscope (cSLO) is a method of imaging that utilises the confocal principle: a laser beam is brought to a focus in a given plane at the fundus and reflected light is received at a photodetector unit through an aperture that is confocal with the light source. In this way only light from the plane of focus is imaged, with resolution subject to the optics of the human eye. Stray light, from corneal, lenticular or vitreous reflections, or diffuse fundal reflection, does not enter the imaging aperture, so that the signal-to-noise ratio is increased. As the laser is monochromatic, images are not degraded by chromatic aberration. The laser beam is scanned across the fundus in a raster fashion. Light returning from the eye (3-5% of the incident light (Plesch et al., 1987)) travels back through the same scanning mirrors to a beam separator at a pupil-conjugate plane, where it is directed to the detector unit. This means that the illumination and detection pathways move synchronously. As the illumination beam is moving continuously, only one retinal location at a time is illuminated. Light returning to the detector is temporally, not spatially, separated, so that light returning when a given point is illuminated is coded as from that point (Knighton, 1995; Elsner et al., 1992; Woon et al., 1992).

The confocal aperture modifies the nature of the sampled returning light. For a small aperture, only light from structures near the plane of focus reach the detector. The volume around the point of focus (voxel) is small. This emphasises specular reflections (a diffusely scattering structure, such as the optic disc, appears dark). The voxel dimensions in a commercial cSLO, the Heidelberg retina tomograph (HRT), are between 11 and 23μm in the x and y directions, and 300 to 500μm in the z direction (Bartsch and Freeman, 1993). A larger aperture allows more widely scattered light from deeper layers to reach the detector. An 'indirect mode' aperture, with a central stop, blocks directly reflected light from structures close to the focal volume of the illuminating beam and only allows more diffusely scattered light to reach the detector (including some from corneal, lenticular and vitreous sources) (Knighton, 1995; Elsner et al., 1992; Woon et al., 1992).

#### 2.4.1.1 Tomography

The HRT records a series of 'optical sections' of the fundus by changing the plane of focus in an axial manner, beginning in the vitreous in front of the optic disc and ending behind the lamina cribrosa. Images are stored in a digital format of 256 by 256 pixels for each 'optical section'.

In order to construct a topographic representation of the optic disc, the HRT takes a series of 32 consecutive 'optical sections'. For any point at the retina or optic disc, a graph can be constructed of the intensity of light reflected at that point in each of the 32 sections (the axial intensity distribution or 'z-profile'). In order to be able to do this, each of the optical sections needs to be aligned, to compensate for small, or large, eye movements occurring between each section. The peak in the z-profile (optical section giving the most reflected light at that point) approximates to the surface in structures with a single reflecting surface. The determination of the origin of a point of light in the retina is limited by the optics of the eye (line or point spread function). The focal length of the eye, in combination with the imaging aperture (pupil) of 2.5mm, limits the axial resolution of a cSLO is about 300μm. Increasing the imaging aperture to 8mm would improve the axial resolution to 29μm were it not for the spherical aberrations of the eye. The axial resolution with an 8mm pupil is, in fact 472μm (Bartsch and Freeman, 1993). However, it is possible to localise the peak in the z-profile to within 30 to 50μm, which corresponds to the surface if the reflector is a single thin surface (Knighton, 1995).

The origin of most of the reflected light in a z-profile may vary with location in the retina. The tomographically-defined surface is often assigned to the ILM (Knighton, 1995). This is unlikely, as the specular reflection from the ILM is highly position sensitive. At angles away from normal, light from the ILM is not reflected back through the pupil. In addition, in older individuals, the ILM reflection is much diminished.

In a multi-layered structure, such as the retina, the shape of the z-profile is influenced by light reflected from all optical interfaces present in the retina as well as the principal (retinal surface) reflecting interface (Bartsch and Freeman, 1994). Each reflecting surface would, in theory, give rise to a discrete peak. However, as the eye is not a perfect optical system, the peaks are spread out and merge: the reflectance pattern of the retina is 'convolved' by the point spread function, giving rise to the measured z-profile. The contribution of several reflecting surfaces results in an asymmetric z-profile, with an extended tail (Bartsch and Freeman, 1993). In the HRT software, 'surface' determination is performed by identification of the centre of gravity of the z-profile (which is usually close to the peak). This is performed for each location (256*256 = 65,536) in the image to generate a surface topography.

Reflected light from a multi-layered surface and/or deeper structures will tend to broaden the z-profile (Bartsch and Freeman, 1993) and shift the peak to the right (deeper) and the tomographically identified surface will be deeper than the true surface (Bartsch and Freeman, 1994).

### 2.4.1.2 Topographic parameters

In order to produce conventional topographic parameters, such as the optic disc, cup and neuroretinal rim areas and optic cup and neuroretinal rim volumes, it is necessary to define the area of interest. This is done interactively, with the examiner outlining the margin of the ONH on the

computer screen. The software then defines a 'reference plane', which is a plane parallel to, and depressed below, the surface of the retina. All structures lying above the reference plane and inside the ONH margin (including blood vessels) are defined as neuroretinal rim, and space below the reference plane is defined as optic cup. There are 2 principle reference plane options: the '320μ reference plane', which is set 320μ below the mean height of the retinal surface at the reference ring (in the peripheral part of the image) and the 'standard reference plane', which is set 50μ below the height of the retina at the disc margin between 350° and 356° (just inferior to the temporal horizontal meridian). In addition to the conventional topographic parameters, the software provides an estimate of RNFL thickness (difference between retinal surface and reference plane), RNFL cross-sectional area (RNFL height times ONH circumference), height variation contour (surface height modulation around ONH margin) and cup shape measure (a description of the distribution of depth values within the ONH margin (Brigatti and Caprioli, 1995)).

### 2.4.2 Magnification corrections to images

It is possible to calculate the true size of a structure in the fundus from the size of the cSLO or photographic image. For features close to the optical axis, the linear size of an image (s) is related to the size of the retinal feature (t) by a camera correction factor (p) and an ocular correction factor (q), so that t = p.q.s (Bennett et al., 1994; Littmann, 1982). The camera constant ('p', in °/mm) relates the angle of the emergent ray (U °), at the first principal point (P), to the size of the image on the camera film ('s' mm), so that p = U°/s (Figure 2-1). The magnification of the camera varies with each model, and therefore needs to be established for the particular camera used for a study (Bengtsson and Krakau, 1992; Rudnicka et al., 1992a; Rudnicka et al., 1998). A telecentric camera (such as the HRT) is one in which the value of p is independent of the refractive error of the eye. A non-telecentric camera is one in which p varies with the refractive error, usually in a linear fashion. The ocular factor ('q', in mm/°) relates the size of the retinal feature ('t' mm) to the angle (U' °) subtended by the retinal feature at the second principal point (P') (Figure 2-1).

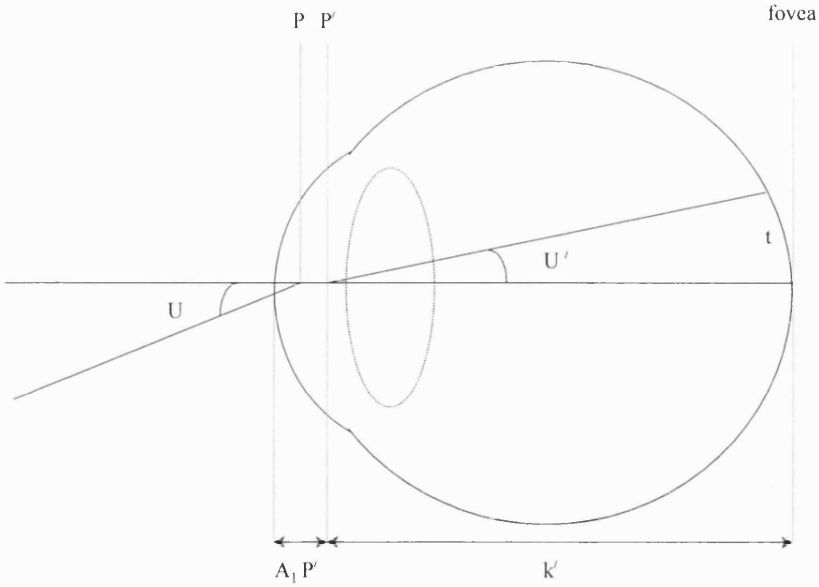


**Figure 2-1. Chief rays from a parafoveal retinal feature**

Chief rays from a parafoveal retinal feature forming the external angular difference (U)

U′ = angle subtended at second principal point (P′) by retinal feature with height 't'

k′ = distance from second principal point (P′) to fovea

$A_1P'$ = distance from apex of cornea to second principal point

U = external angular difference (= U′.(1.336))

It is assumed that the angle subtended at the second principal point by the retinal feature, U′, equals the angle of the emerging ray, subtended at the first principal point, divided by the refractive index of the final ocular medium (1.336) (Bennett et al., 1994), i.e. U′ = U/1.336.

Ocular magnification is entirely dependent on the vergence of the internal axis of the eye (K′) (Bengtsson and Krakau, 1977). K′ (measured in dioptres) represents the reduced and inverted distance between the second principal point and the fovea (k′) (Figure 2-1), i.e. K′ = 1.336/ k′.

The retinal feature height (t) may be expressed as (Bennett et al., 1994):

$$t = k' U' \qquad \text{('U' in radians, t in metres)}$$

k′ = 1.336/K′ and U′ = U/1.336 (above), therefore

$$t = U/ K'$$

or $$t = (17.455).U°/K' \qquad \text{(with 'U' in degrees and 't' in millimetres)}$$

p = U°/s (above), therefore

$U° = p\ s$

$t = (17.455).U°/K'$ and $U° = p\ s$, therefore

$t = (17.455/\ K').p.s$

$t = p.q.s$, therefore

$$q = 17.455/\ K'$$

Several methods have been described to calculate 'q'. The objective of these methods is to estimate K'. As information about the optical dimensions of the eye is usually incomplete, certain assumptions have to be made about missing data.

### 2.4.2.1 Description of methods to derive 'q'

The most accurate method to determine K' is by ray-tracing. This is possible with a knowledge of parameters such as the anterior and posterior radii of curvature of the cornea and crystalline lens, the asphericity of these surfaces, the thickness of cornea and lens, the anterior chamber depth, the axial length, the refractive indices of the ocular media (including layers of the crystalline lens) and the eccentricity of the retinal feature. It is not possible to collect this amount of data in clinical practice, and so K' has to be estimated on the basis of fewer, easily obtained parameters.

The most accurate estimation of K' is possible if the distance k' is known. k' can be calculated with knowledge of the axial length of the eye and the distance ($A_1P'$) from the apex of the cornea to the second principal point (Figure 2-1) (Bennett et al., 1994). The axial length is typically measured by ultrasound. The distance $A_1P'$ can be estimated from the effective power of the cornea (derived from the keratometry), the axial length, anterior chamber depth, crystalline lens thickness and the ametropia (Bennett, 1988; Bennett and Rabbetts, 1989).

When axial length is known, but anterior chamber depth and crystalline lens thickness are not, the distance $A_1P'$ cannot be estimated, and a constant value can be assumed. Bengtsson and Krakau (1992) took a value of 1.60 mm for $A_1P'$ from Gullstrand's exact schematic eye and Bennett et al. (1994) took 1.82 mm from the Bennett-Rabbetts' (1989) schematic eye.

When the keratometry and ametropia are known, but the axial length is not, more assumptions have to be made about the optical dimensions of the eye. Littmann (1982; 1992) published his much-used method in 1982. A value for 'q' was derived by tracing the chief ray from an extrafoveal point through the Gullstrand No. 1 schematic eye, using the constants of that eye and varying the corneal radius of curvature according to the measured value (Barr, 1995). Ametropia was generated by varying the axial length in the model. Littmann provided a nomogram from which it is possible to read off a value of 'q' from a series of curves if the keratometry and ametropia are known. This method was not easily accessible until equations were published to enable computerisation (Bennett et al., 1994). The constants assumed include 'normal' values for the effective power of the crystalline lens (19.11 D) and an axial length for emmetropia of 24.18 mm. A similar approach was taken by

Bengtsson and Krakau (1992). Gullstrand's 'normal' value for the refractive power of the eye (58.64 D) was taken, and variations from this were calculated from the observed ametropia and keratometry. Wilms (1986) also took a similar approach, assuming a 'normal' value for the lens power of 20.112 D. The HRT method uses a gradient index model for the optical properties of the crystal lens, with constants for the focal length of the crystalline lens and for the anterior chamber depth.

Finally, Littmann (1982; 1988) published curves for use when the axial length is known. The Gullstrand No. 1 schematic eye again was the model. The axial length measurement is used to derive a notional radius of corneal curvature for the observed refractive error of the eye. This notional radius of corneal curvature is then used to derive 'q' using the original published curves. Wilms' axial length method similarly derives a notional radius of corneal curvature for use in his original equation.

## 2.5 Measurement of visual function

### 2.5.1 Differential light sense perimetry

In the clinical setting, visual function is tested by automated static perimetry.
The two most frequently used automated perimeters are the Octopus Perimeter (OP) and the Humphrey Field Analyzer (HFA). The characteristics of the HFA will be detailed here.
The perimeter has a 330 mm bowl, with a 'white light' background illumination. Background illumination intensity is 31.5 apostilbs (10 candela/m2). This background ensures that the 'photopic' function of the retina is measured. That is, the background illumination is above the dynamic range of light sensitivity of the rod photoreceptors, and, therefore, only cone photoreceptor function is measured. Test stimuli of 'white light' are presented for 0.2 seconds. The stimuli are presented at a variety of retinal locations, covering the central 24 to 30 degrees in a regular grid pattern. Points are spaced 6 degrees apart, with points either on the horizontal and vertical meridia (24-1 or 30-1 programs) or 3 degrees each side (24-2 or 30-2 programs). The default test spot size is the Goldmann size III.
A primary point in each quadrant is tested twice at the start of each field test. The sensitivity at these points is used to establish the expected values for neighbouring points, which are assumed to drop by 0.3 dB per degree of eccentricity. Threshold values are obtained by a 'staircase' procedure. Light intensity decreases in 4 dB steps until the stimulus is no longer seen, and then increases in 2 dB steps until the stimulus is seen. Threshold determinations are performed twice at ten, fixed, test points to determine the fluctuation in the patient's responses during the test (short-term fluctuation). In addition, threshold determinations are performed twice at all points at which the first determination is out of line with the expected value (derived from neighbouring points).
The visual function at each tested retinal location is given by the differential light threshold. This is the intensity of the test spot that can be seen above the background illumination (light-difference or $\Delta L$) with a probability of 50%. The differential light threshold can be expressed as $\Delta L/L$, and the differential light sensitivity (DLS) as $L/\Delta L$.
The retina exhibits a very large dynamic range with respect to light sensitivity, being able to 'see' very dim and very bright stimuli. For this reason a scale for light sensitivity has to be selected so that the full range can be appreciated in a single plot. By convention, the scale used is logarithmic, and the units of sensitivity are decibels (dB). The dB is log(intensity)/-10. Very dim test spots therefore have a high dB value, denoting high retinal sensitivity. A decrease of 3dB represents a doubling of the test spot intensity. A change in spot illumination from 13dB to 10dB equates to a change in illumination from 500 to 1000 apostilbs (a difference of 500), whereas a change from 33dB to 30dB equates to a change from 5 to 10 apostilbs (a difference of 5).

### 2.5.2 Factors determining the differential light threshold in automated perimetry

There are a number of factors that affect the visibility of a white light stimulus, and include local retinal, optical and patient factors.

#### 2.5.2.1 Retinal factors:

##### 2.5.2.1.1 Background illumination

The differential light threshold is $\Delta L/L$. For detection at threshold in the photopic range (100 apostilb – 1000 apostilb, 31.5 – 315 candela/$m^2$), as in the Humphrey perimeter, the luminance difference ($\Delta L$) increases linearly with the luminance of the surroundings. Weber's law states that

$\Delta L/L$ = constant

The illumination at the perimeter bowl should not be taken as necessarily equivalent to the retinal illumination, as optical factors affect the intensity (and chromacity) of the light incident on the retina. In general, a photopic state of adaptation results in a steeper peripheral-central threshold detection gradient. In the mesopic range ($10^{-12}$ apostilb – 100 apostilb), the balance of sensitivity shifts from that of the rods to the cones, and in the mid-mesopic range the overall sensitivity gradient is flatter. In the scotopic range, there is decreased sensitivity in the central retina. The dynamic range over which thresholds may be determined is about 0.5 log units (5dB) greater at the mesopic level (4 apostilbs background/Octopus perimeter) compared with the photopic level (31.5 apostilbs/Humphrey perimeter) (Bedwell, 1982).

##### 2.5.2.1.2 Stimulus duration

The duration of a stimulus should be short enough not to influence the existing state of retinal adaptation and long enough to allow retinal summation effects to come in to play (integration of the light flux imaged on the retina) (Bedwell, 1982).

Within short time intervals (<100ms), the visual system summates brightness information (temporal summation), so that the brightness and duration of a stimulus are reciprocally related. For threshold detection, the Bunsen-Roscoe (or Bloch) law states that

$T * I$ = constant (T = stimulus duration and I = stimulus intensity)

when $T < 100$ms.

Beyond this time, summation is still evident, but incomplete, up to 0.5 to 1.0 seconds (Aulhorn and Harms, 1972).

Stimulus presentation time in the HFA is 200ms.

Temporal summation varies with retinal location and state of adaptation of the eye (Tate and Lynn, c1977).

#### 2.5.2.1.3 Stimulus size

Practical considerations dictate the size of stimulus employed in static perimetry. Very small stimuli are subject to degradation by refractive errors and may not be seen if they fall on blood vessels. Very large stimuli may cover areas of normal and abnormal retina, and sensitivity to small defects may be lost.

Within small retinal areas, the visual system summates brightness information (spatial summation), so that the brightness and area of a stimulus are reciprocally related (Glezer, 1965; Wilson, 1970; Matin, 1975; Scholtes and Bouman, 1977). For threshold detection, Ricco's law may be expressed as

$L * A^k = C$

(L = threshold stimulus intensity, A = stimulus area, k = summation co-efficient, and C = constant)

Ricco's law holds when k = 1. Piper's law is said to hold when k = 0.5, and Pieron's (or Elsberg-Spotnitz') law when k = 0.3 (Greve, 1973; Tate and Lynn, c1977).

The area within which complete summation holds (where k = 1) is termed 'Ricco's area'. As the stimulus size increases beyond 'Ricco's area', the simple reciprocal relationship no longer holds. The relationship has also been found to break down in peripheral (beyond 15°) retina if the target is very small (Scholtes and Bouman, 1977).

In areas larger than Ricco's area there is 'partial summation' (Wilson, 1970) or 'probability summation' ($1 > k > 0$), which tends towards k = 0 as the area enlarges (Sloan, 1961). In other words, the value of k itself changes over the range of target sizes used to measure it (Dannheim and Drance, 1971).

The detection threshold ($\Delta L/L$) for Ricco's area is constant over a wide range of photopic background luminance and retinal eccentricity (Glezer, 1965; Wilson, 1970; Lie, 1980).

##### 2.5.2.1.3.1 Measurement of Ricco's area

Ricco's area increases in size with more peripheral retinal location (Hallett, 1963; Wilson, 1970; Dannheim and Drance, 1971; Lie, 1980; Inui et al., 1981; Kasai et al., 1992), and gets smaller (in proportion to the square root of the background luminance) as background luminance increases in the scotopic/mesopic range (Glezer, 1965; Wilson, 1970).

Comparison of studies investigating spatial summation and the size of Ricco's area is complicated by the different experimental conditions used, particularly background illumination intensity.

Wilson found that the diameter of Ricco's area increased from about 8′ (38μm) at 5° eccentricity to 45′ (215μm) at 55° eccentricity (with a background illumination of 212 candela/m², 666 apostilbs).

Inui (Inui et al., 1981) used projection perimetry to precisely position test spots in the fovea and parafoveal retina in order to measure Ricco's area. Background illumination was 3.2 candela/m² (10 apostilbs). Estimates of Ricco's area were made at 0, 1, 2, 4, 5, and 10° on the temporal horizontal meridian. Ricco's area was estimated at about 4′ (20μm) at the fovea, 7′ (33μm) at 5° from the fovea, and 10′ (48μm) at 10° from the fovea.

Felius (1996) obtained a diameter for Ricco's area at 17° eccentricity (background illumination 31.5 apostilb) of 0.56° (160μm).

#### 2.5.2.1.3.2 Coefficient of summation

Kasai (1992) tested the central 60° with the 60-2 and 30-2 programs of the Humphrey Field Analyzer (background illumination of 31.5 apostilbs) with the Goldmann I to V spot sizes in 5 normal subjects. Straight lines were fitted to plots of log light intensity against log target area and the slope of the line used to determine the co-efficient of summation. Average k values were calculated for 10° intervals. The coefficients calculated are given in Table 2-1.

| Eccentricity | Coefficient of summation |
|---|---|
| Fovea | 0.36 |
| 0 - 10° | 0.54 |
| 10 - 20° | 0.59 |
| 20 - 30° | 0.71 |
| 30 - 40° | 0.79 |
| 40 - 50° | 0.87 |
| 50 - 60° | 0.79 |

**Table 2-1. Mean coefficients of summation with eccentricity (Kasai et al., 1992)**

Sloan (1961), used a modified Goldmann perimeter and tested 6 spot sizes (Goldmann 0 to V) at 6 retinal locations from 0 to 50° in the nasal field, and a background illumination of 31.6 apostilbs. She was not able to demonstrate a linear relationship between log light intensity and log target area, which would have indicted a single value of k for each location. Straight lines were fitted to the Goldmann size 0 to III spots, and values of k calculated from these (Table 2-2).

| Eccentricity | Co-efficient of summation |
|---|---|
| Fovea | 0.55 |
| 15° | 0.75 |
| 30° | 0.88 |
| 45° | 0.90 |

**Table 2-2. Coefficients of summation with eccentricity (Sloan, 1961)**

Wilson (1970) used 12 target sizes at 11 retinal locations in the nasal horizontal field (background illumination of 212 candela/m$^2$, 666 apostilbs). He observed that, on a plot of log light intensity and log target area, there appeared to be two parts to the curve, an initial part with a slope of -1 (representing complete spatial summation) and a second part with a shallower slope. Data from Wilson's paper (1970) are re-plotted in Figure 2-2.

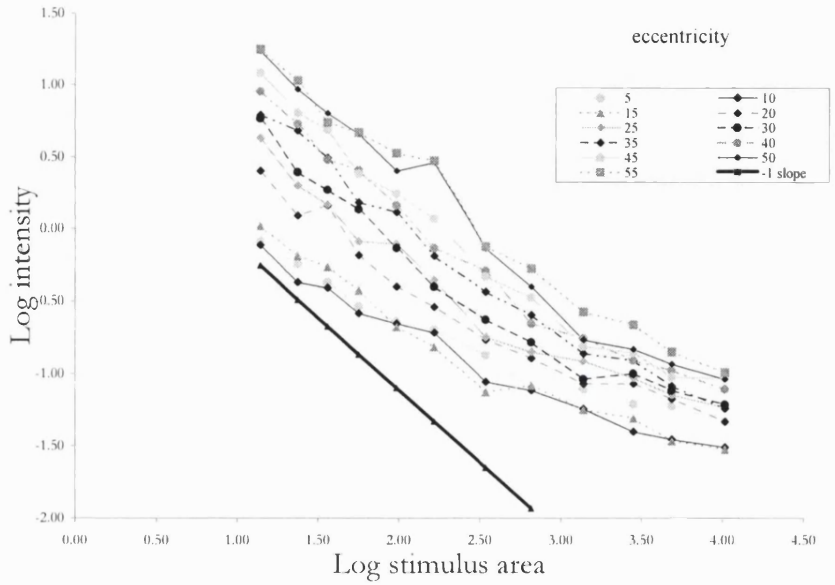


**Figure 2-2. Plot of log light intensity against log stimulus area at various retinal eccentricities (Wilson, 1970)**

He also observed that if the slopes were displaced laterally, along the log stimulus area axis, the lines could be made to overlap, and there appeared to be an initial part of the curve, with a slope of –1, and a second part of the curve, which was either a curve with a decreasing gradient or a straight line. Data from Wilson's paper (1970) are re-plotted in Figure 2-3.

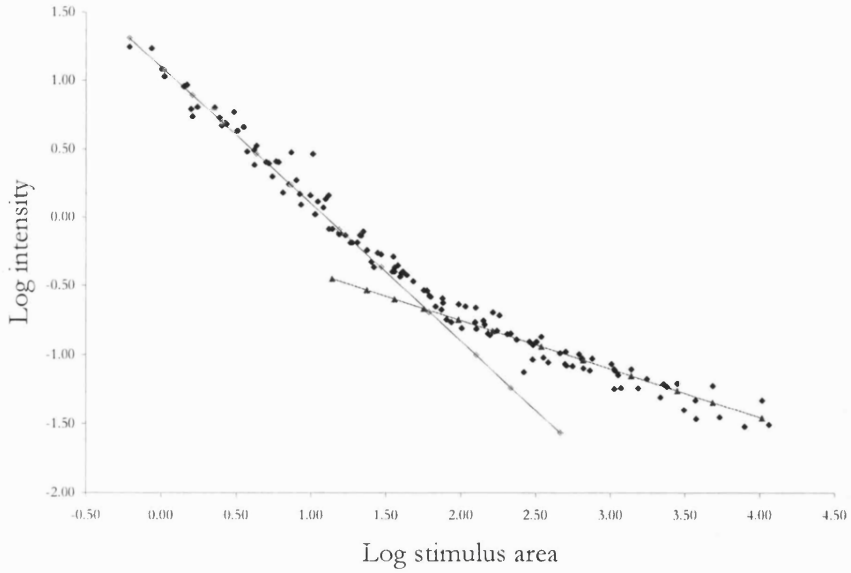


**Figure 2-3. Summation curves from different eccentricities shifted laterally along the log area axis (Wilson, 1970)**

In contrast, Inui (1981), using projection perimetry and a background illumination of 10 apostilbs, found almost no summation outside Ricco's area for eccentricities of 0 to 10°. In the fovea, the coefficient of summation (calculated from a re-plot of his data) was 0.05. The largest test spot used had a diameter of 60′, which is about the same size as the Goldmann size IV.

#### 2.5.2.1.3.3 The importance of spatial summation

The DLS threshold results from a contribution of summation within Ricco's area and summation from the area outside Ricco's area, if the test object is larger than Ricco's area. At photopic light intensities, the Goldmann size III target is larger than Ricco's area up to about 40° eccentricity (Wilson, 1970). The DLS threshold at any particular retinal location is, therefore, dependent on the size of Ricco's area and the value of the co-efficient of summation for the area outside Ricco's area. The non-linear relationship between target area (outside Ricco's area) and threshold intensity implies a non-linear relationship between the number of neural elements responsible for light detection and the threshold light intensity. Correct interpretation of the health of the underlying retina from the DLS at a specific retinal location depends on knowledge of physiologic spatial summation.

#### 2.5.2.1.3.4 Spatial summation in glaucoma

In glaucoma, the applicability of the concept of adjusting the light sensitivity at a given retinal location according to local spatial summation properties depends on what happens to spatial summation in glaucoma. This problem was addressed by Fellmann (1988) who compared the

sensitivity increases with increasing target size in normal and glaucomatous patients. In addition, sites of depressed sensitivity were tested with a size V target and a cluster of size III targets, to cover the same area. He found that the differences between the sensitivities to size III and V targets could be explained 73% of the time by recruitment of 'undamaged units' (into the size V area) and normal spatial summation. 'Pathologic summation' (greater than expected) explained the remaining 27%. Lower than expected (for normal spatial summation) sensitivity for smaller target sizes was found in fewer than half the 16 glaucomatous eyes studied by another investigator (Dannheim and Drance, 1974). The remainder had normal summation or increased variability of DLS measurements.

#### 2.5.2.1.3.5 Spatial summation and ageing

As the prevalence of glaucoma increases with age, it is important to know whether spatial summation changes with age, in order to correctly interpret changes in summation in glaucoma patients. Dannheim and Drance (1971) studied summation in 35 normal subjects aged from 20 to 79 years. Although lower retinal sensitivity was found in older subjects, the shape of the summation curves was preserved, indicating that spatial summation is unaffected by ageing.

#### 2.5.2.1.4 Retinal location

The type and density of retinal receptor, and their neuronal connections, varies with retinal eccentricity, and is presumably the basis for differences in DLS thresholds and summation characteristics discussed above. Generally, the ovoid pattern of ganglion cell density distribution is reflected by the shape of the DLS 'hill of vision'.

### 2.5.2.2 Optical factors: refractive error, magnification and axial length

Uncorrected refractive errors have been shown to have a greater affect on central, than on peripheral, vision (Sloan, 1961; Atchison, 1987; Herse, 1992), although the finding is not universal. Others (Weinreb and Perlman, 1986; Goldstick and Weinreb, 1987; Heuer et al., 1987; Henson and Morris, 1993) have reported decreased sensitivity across the field with defocus. Retinal flux may remain unchanged in blurred conditions, but the retinal area in which the light falls will be greater in the blurred condition and local spatial summation is likely to affect threshold detection sensitivity. The effect of blur is, thus, greater on thresholds for small stimuli (< Goldmann size III) than for larger stimuli (Sloan, 1961; Atchison, 1987). The extent of retinal blur (retinal blur circle diameter) is dependent on the product of pupil diameter and defocus (Herse, 1992; Henson and Morris, 1993). Defocus has no effect on short-term fluctuation (Goldstick and Weinreb, 1987; Henson and Morris, 1993) or corrected loss variance (Goldstick and Weinreb, 1987).

Greater axial length will have the effect of increasing the size of the retinal spot size (angular size is unchanged). The change in DLS with larger or smaller spot sizes will be affected by local spatial

summation characteristics. Photoreceptor and ganglion cell spacing may vary with eye size, and this may alter summation characteristics so that spatial summation may vary with eye size.
Similarly, the retinal magnification factor changes with eccentricity, so that the same angular target size gives rise to a larger retinal spot size in the periphery. The difference in the central 30° doesn't not amount to more than 5% (Bennett et al., 1994).

### 2.5.2.3 Patient factors

Variability of responses arises from the nature of the test, in which the DLS is defined by the light intensity of a test spot that is seen 50% of the time, so that uncertainty is central to the measurement procedure.
An important test aspect influencing the quality of a visual field examination is the interaction between the patient and the task of the examination, which will be affected by factors such as motivation, anxiety, spatial attention and attention span (including fatigue) and understanding of the procedure (including learning). As a measure of the quality of an examination, various strategies have been devised, such as catch trials (testing false-positive and false negative responses and fixation losses) and estimates of short-term fluctuation.
Learning effects manifest as an improvement in visual function with time, and learning occurs at different rates in different individuals. The effect may be seen during the first examination, between the examination of the first and second eye, and between follow-up examinations (Searle et al., 1991; Heijl et al., 1989). Fatigue increases with the length of the test (Heijl and Drance, 1983; Johnson et al., 1988), is worse in the second eye tested (Hudson et al., 1994), and increases with age (Langerhorst et al., 1987).

#### 2.5.2.3.1 Fixation

Reasonably stable fixation is required. In alert, co-operative subjects, three types of fixational nystagmus have been identified (Tate and Lynn, c1977). The first is tremor with small amplitude linear (5" to 30" of arc) and torsional (45" of arc) components of 70 to 90 Hz. The second consists of slow drifts (0.8′ to 6.0′ of arc) of about 2 Hz. The third type occurs during attempted fixation consists of rapid microsaccades of 2′ to 50′ of arc magnitude. The combination of torsional and vertical movements can range over 4° of arc.
A measure of fixation stability is made during automated perimetry by plotting the blind spot at the start of the test and then presenting stimuli at this location during the course of the test. If they are seen, then the assumption is made that fixation has changed (fixation loss).

#### 2.5.2.3.2 Short-term fluctuation

This is a measure of the variability of a subject's responses during the course of a test, and is estimated from repeated threshold determination at a number of field locations.

#### 2.5.2.3.3 Long-term fluctuation

This is a measure of the variability of a subject's responses between tests, corrected for the in-test variability. It has two components: homogenous (affecting the whole field) and heterogeneous (affecting different points differently).

Short-term fluctuation and both components of long-term fluctuation are increased in glaucoma, as a manifestation of the disease (Flammer et al., 1984). Haefliger and Flammer (1991) used a form of profile perimetry (Octopus F8 program) to examine the short-term fluctuation at, and the slope of, the borders of glaucomatous scotomata and the blind spot. The slope of the borders of glaucomatous scotomata were broader and less steep than the border of the blind spot, and short-term fluctuation was much greater. This indicates that the fluctuation is a characteristic of the reduced sensitivity at the scotoma border, and not a function of testing at the edge of a scotoma per se. Boeglin et al (1992) demonstrated that long-term fluctuation in the field of glaucoma patients is related to short-term fluctuation and the DLS at the tested location.

#### 2.5.2.3.4 False positive responses

This measure of patient reliability tests whether the patient is responding in the absence of a stimulus. The automated perimeter omits a stimulus presentation, and a false positive response is recorded if the patient presses the response button.

#### 2.5.2.3.5 False-negative responses

This measure of patient reliability tests whether the patient is failing to respond in the presence of a previously-seen stimulus. The automated perimeter presents a brighter stimulus than one previously seen at the same location, and a false-negative response is recorded if the patient fails to press the response button.

### 2.5.2.4 Normative data (Inter- and intra- individual variability)

There are two main variables that affect the DLS at any retinal point: eccentricity in the retina and age of the subject.

#### 2.5.2.4.1 Eccentricity

DLS decreases with increasing distance from fixation (Katz and Sommer, 1986; Heijl et al., 1987; Zulauf, 1994), an effect more marked in the superior field (Katz and Sommer, 1986; Heijl et al., 1987). Normative data have been published (Heijl et al., 1987).

Variation in DLS increases with distance from fixation for both inter- and intra-individual variability (Katz and Sommer, 1986; Zulauf, 1994), including both intra-test and inter-test components (Heijl et al., 1987). The distribution of values about the age-corrected mean is non-Gaussian (Heijl et al., 1986; Heijl et al., 1987; Zulauf, 1994), generally demonstrating negative skew and positive kurtosis (large negative deviations are more common than large positive ones).

#### 2.5.2.4.2 Age

Measured DLS declines with age. Pointwise age slopes for the Humphrey perimeter are given by Heijl et al. (1986; 1987). The age slopes are greater further from fixation (Heijl et al., 1986; Katz and Sommer, 1986; Heijl et al., 1987; Zulauf, 1994), so that there is a steepening of the hill of vision with age (in the dB scale).

Potential causes of reduced sensitivity are reduced transmission of the ocular media and a smaller pupil (senile miosis). These effects are likely to be greater in perimeters with background illumination at the low photopic/mesopic level. A potentially important effect is the colour temperature of the background illumination, and the degree to which the background is attenuated by media opacity (Lowe et al., 1997).

There is also likely to be a neural contribution to the decreased light sensitivity with age.

Empirically-derived mean age-corrected pointwise sensitivities and distributions about the mean value have been incorporated into software analysis packages (Statpac (Heijl et al., 1986; Heijl et al., 1991)).

### 2.5.3 Summary Statistics

Summary statistics are generated to give an overview of the status of the field. These are mean deviation, pattern standard deviation, short-term fluctuation, and corrected pattern standard deviation.

#### 2.5.3.1 Mean deviation (MD)

The MD is a location-weighted average deviation from the age-corrected normal reference field. The calculation takes the variance at each measured point into account (Heijl et al., 1986).

### 2.5.3.2 Pattern standard deviation (PSD)

The perimeter calculates a normal reference field based on the subject's age. The reference field is subtracted from the measured field to give a total deviation map. The summary figure for PSD is a location-weighted standard deviation of the pointwise differences between the measured and the normal reference fields (similar to the standard deviation of deviations).
The pattern deviation map highlights points depressed below the average field performance. The measured field is elevated or depressed towards the level of the reference field (to account for the overall level of performance) so that localised loss stands out from generalised depression. The data are also displayed in the form of probability maps, in which the measured threshold is compared with the prediction intervals for normality.

### 2.5.3.3 Short-term fluctuation (SF)

SF is a weighted mean of the standard deviations at the 10 points at which the DLS is estimated twice.

### 2.5.3.4 Corrected pattern standard deviation (CPSD)

CPSD estimates that part of the PSD that is not caused by SF.

The summary parameters do not take into account spatial features within the field.
A further analysis given in the Humphrey visual field test is the Glaucoma Hemifield Test (Asman and Heijl, 1992). The central (24°) field is divided into 5 sectors, based loosely on the RNFL arrangement, in each (superior and inferior) hemifield (Figure 2-4). Measurement results in these sectors are graded according to a score assigned to the point-by-point significance in the Statpac pattern deviation probability map. Field normality is judged in terms of score differences between pairs of mirror-imaged sectors (Heijl et al., 1991).

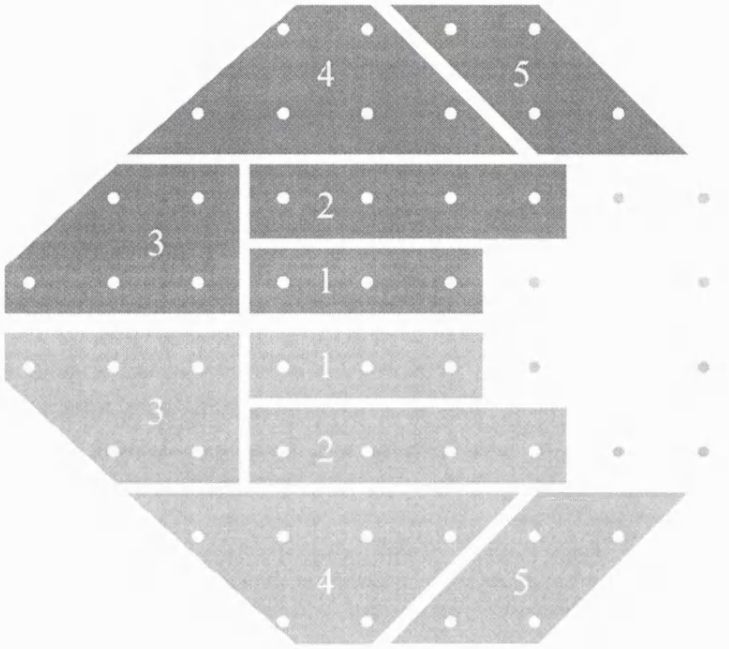


**Figure 2-4. Glaucoma hemifield test sectors (Asman and Heijl, 1992)**

### 2.5.4 Visual field changes in glaucoma

The recognition of the characteristics of early visual field changes is of great importance in the identification of glaucoma early in the course of the disease. A significant component of the early changes to the RNFL is diffuse thinning (Tuulonen and Airaksinen, 1991). One would, therefore, imagine that this would be reflected in the pattern of visual function loss. In Heijl's opinion (1989): "It is true that glaucoma usually is non-focal and that early disease therefore does not appear as extremely small, reproducible and well defined scotomas. In our experience, however, entirely diffuse loss almost never occurs in glaucoma. Some areas are always more affected than others, resulting in areas of localised loss, glaucomatous visual field defects." The identification of diffuse loss is difficult, largely because it is a non-specific sign, occurring with media opacity and miosis as well as glaucoma. Attention has consequently focused on the focal components. Where diffuse loss has been identified in glaucoma patients, it is associated with higher mean IOP than patients with focal loss (Caprioli et al., 1987; Samuelson and Spaeth, 1993) and a neuroretinal rim/optic disc area ratio that is equal in all quadrants. This compares with greater rim loss in the supero- and infero-temporal quadrants in eyes with focal field loss (Caprioli et al., 1987).

The appearance of, and ability to detect, early glaucomatous field defects may vary with the method used to test the field. The effect of examination technique (and that of patient selection and interpretation of threshold values) on the apparent frequency distribution of the location of early

glaucomatous defects was demonstrated by Henson and Hobley (1986) who compared previous reports using different equipment. Aulhorn and Karmeyer (1977) reported the greatest frequency in the inferior nasal field and just superior to the macula using kinetic perimetry on the Goldmann perimeter. Furuno and Matsuo (1979), using static perimetry on the Friedmann Mark I Visual Field Analyser, conversely reported a lower frequency of defects in the lower nasal field and a higher frequency in the superior field, particularly above the blind spot and greater than 15° from the fovea. Heijl and Lundqvist (1984), using static perimetry and the Competer perimeter (to 15° vertically and 20° horizontally), also demonstrated higher defect frequencies in the superior field, gradually increasing with eccentricity. Coughlan and Friedmann (1981), using static perimetry and the Friedmann Mark II Visual Field Analyser, also demonstrated a higher frequency in the superior field, and a reduced frequency in the inferotemporal quadrant. A feature of the Friedmann Mark II Visual Field Analyser is that the size of the visual stimuli gradually increases from the centre to the periphery in order to compensate for reduced sensitivity in the periphery. Henson and Hobley (1986) divided the visual field into areas of low, medium and high frequency, according to the prevalence of early field defects in 109 glaucomatous eyes. A low frequency was found in the inferotemporal region and around the fovea. A medium frequency was found in the arcuate areas out to about 15° vertically and 30° nasally. The highest frequency was found in the superior periphery (maximal at 22.5° above the fovea).

Gramer et al (1982), using automated static perimetry with the Octopus Program 31, found a higher frequency of defects in the upper hemifield, especially nasally, with increasing frequency from 6° to 30° from the fovea. Fewer absolute, but equally frequent relative, defects were found in the lower temporal quadrant.

Nicholas and Werner (1980) also found that the frequency of superior field defects was twice that of inferior defects in early visual field loss, tested with kinetic Goldmann perimetry.

The location of deteriorating visual field locations in initially normal fields in eyes at risk of glaucomatous field loss was investigated by Poinoosawmy et al (1995) with the Progressor program. Patients were ocular hypertensive or unilateral normal tension glaucoma (NTG) patients. In ocular hypertensive eyes, the frequency of deteriorating locations was greater in the superior hemifield, and increased with eccentricity to about 15°. In the unilateral NTG patients, the frequency was greatest in the superior paracentral and inferior nasal step regions.

Drance (1969) examined the contralateral eyes of patients with unilateral glaucomatous field defects. These contralateral eyes were normal to a 1 mm white target. He performed a detailed examination, using the Tubingen perimeter, plotting thresholds at 1° intervals along the oblique meridians. Defects discovered in the contralateral eyes were small absolute paracentral scotomas in the Bjerrum area surrounded by a zone of relative scotoma and separated from the blind spot by a completely normal, or much less disturbed, area. When interpreting this data, it should be borne in mind that defects narrow as they approach the disc, thus becoming less easy to find. In addition, the test target

becomes larger relative to the scotoma width, and thus may overlap undamaged field, giving the impression of a shallower, or absent, defect.

Hart and Becker (1982) performed a retrospective review of patient records and found 98 eyes of 72 patients that developed visual field defects while under review. Goldmann kinetic perimetry was performed every 4 months. All scotomas, when first detected, were confirmed with meridional threshold static perimetry. Field defects, repeatable on a second test (at least one by static perimetry), were defined as glaucomatous as follows:

i. nasal steps (>10° in size, or <10° in size if found in 2 or more isopters separated by 10°)

ii. paracentral scotomas (within 10° of fixation)

iii. Bjerrum scotomas (between 10 and 20° of fixation)

iv. arcuate enlargement of the blind spot (polar extension of 5° or more)

v. any other defect corresponding to the distribution of a nerve fibre bundle

The frequency of the first type of defect, in eyes developing a field defect, is given in Table 2-3.

| Defect type | Frequency |
|---|---|
| Superior nasal step | 33% |
| Inferior nasal step | 21% |
| Paracentral or Bjerrum scotoma | 41% |
| Arcuate enlargement of the blind spot | 30% |
| Bjerrum scotoma isolated from blind spot | 20% |
| Temporal defect | 3% |

**Table 2-3. The frequency of first type visual field defect by location (Hart and Becker, 1982)**

In the year before the onset of a definite glaucomatous defect, 30.6% showed central isopter constriction (> 2 s.d. beyond age corrected means from a normal population) in at least one test. 6.5% of ocular hypertensives who did not develop a field defect for at least 3 years showed central isopter constriction.

In 22 eyes (22.4%), the initial defect was found to disappear and then reappear at the same location at a later date. This effect was not related to the level of the IOP. 67 (68.4%) showed a gradual evolution of the initial defect, and 9 (9.2%) demonstrated an abrupt defect onset with rapid evolution.

Similar findings of transient occurrence of a defect or of increased variability of sensitivity have been reported by other workers.

Werner and Drance (1977) reviewed 22 eyes, of 22 patients, with initially normal visual fields that subsequently developed glaucomatous field defects. These were compared with 22 eyes with raised IOP that did not develop visual field loss ('control group'). Visual fields had been tested with kinetic

and static techniques (Goldmann and Tubingen perimeters). 45.5% of the eyes developing glaucoma had a paracentral defect as the first abnormality, 70% of which had an associated nasal step. In 54.5%, a nasal step was the first defect. Retrospective analysis of the visual fields of these eyes revealed some abnormality ('disturbance') in the region of the defect in 59% prior to the onset of a definite defect. This took the form of increased test-retest variability of DLS values or minor depressions in sensitivity. 27.3% of the 'control group' demonstrated similar abnormalities.

Stürmer (1985) examined 20 glaucomatous eyes with profile perimetry (radial profiles originating at the fovea, 1° resolution, Goldmann size III target). He found that the first perimetrically determinable sensitivity disturbance to be increased scatter, with normal and reduced values from the same location. The regions of increased scatter had poorly defined borders. Similarly, relative scotomas had poorly defined borders characterised by increased scatter.

Although the frequency of glaucomatous scotomas in the region of the fovea has been reported to be low in glaucomatous eyes using standard static perimetry, Anctil and Anderson (1984) found reduced foveal sensitivity to the Goldmann size I stimulus in 43% of the more severely glaucomatous eye of patients with asymmetric glaucoma. This foveal loss was found with generalised depression of the field, with scotomas that impinged on fixation, and with scotomas greater than 5° from fixation. In a group of glaucoma patients selected for early to moderate field loss and the presence of RNFL atrophy in the papillomacular bundle, Mizokami et al (1987) demonstrated foveal dysfunction with the Quantitative Maculometer (250 apostilb background and target size 6.37′) measurements of spatial contrast sensitivity.

The region temporal to the blind spot is rarely tested with modern automated perimeters. Pennebaker and Stewart (1992) tested the temporal field with a customised program on the Humphrey Field Analyzer in eyes with previously established glaucomatous defects on the 30-2 program. 6 contiguous defective points were required to qualify as a temporal scotoma. With these criteria, the temporal field was found to provide equivalent information to the central Bjerrum area in 47.5% of eyes, less information in 44.5% and more information in 8%.

There is some evidence that the prevailing IOP level can affect DLS. Hart and Becker (1977) demonstrated central isopter constriction in normal subjects when IOP was raised as a result a response to topical steroids. Eye cups have also been used to temporarily raise the IOP, and reduced visual function, including the manifestation of glaucomatous defects, has been demonstrated in normal and glaucomatous eyes (Drance, 1962; Scott and Morris, 1967; Trible and Anderson, 1997). There is some indication that the effect may be greater in glaucomatous eyes (Trible and Anderson, 1997). Surgical reduction of IOP in a chronic glaucoma has been shown to cause an improvement in mean sensitivity in proportion to the amount of IOP reduction (Gandolfi, 1995) or with a reduction of >40% (Tsai et al., 1991).

## 2.6 Correlation of structural and functional changes in glaucoma

Early studies investigating the relationship between structural and functional measures in glaucoma were hampered by the difficulty in quantifying both ONH structure and visual field loss, and were necessarily qualitative in nature. Automated static perimetry and advances in imaging tools have made more accurate quantification possible.

A summary of published studies will be presented here, starting with early investigations using kinetic perimetry, and then covering more recent studies that have used automated static perimetry. Studies that made whole visual field/ONH comparisons are described first (divided into sections according to the imaging instrument used), and then studies that attempted sectoral visual field/ONH comparisons are described. Lastly, studies that have made comparisons between ganglion cell numbers, determined histologically, and DLS, are presented.

Quantitative studies are difficult to compare because of the wide range of glaucoma severity included. Apparent correlations are likely to be improved by the inclusion of more severe cases. As a guide, visual field summary indices are given for each of the studies, where available. Many studies are difficult to interpret as a result of inclusion biases (Garway-Heath and Hitchings, 1998b): glaucoma patients being required to have 'typical' ONH and field changes, and normal eyes being required to have none of these. These biases are also likely to improve apparent correlations. There is also difficulty in comparing studies attempting structure/function comparisons in ONH/field sectors, because each study uses a different division of ONH and field.

### 2.6.1 Kinetic perimetry

Read and Spaeth's (1974) proposed a map, relating sectoral ONH damage with patterns of visual field loss (redrawn in Figure 2-5) derived from clinical observations. Their proposal requires the RNFL to be organised in the neuroretinal rim with respect to eccentricity. The evidence for this is controversial (see section 2.3.1).

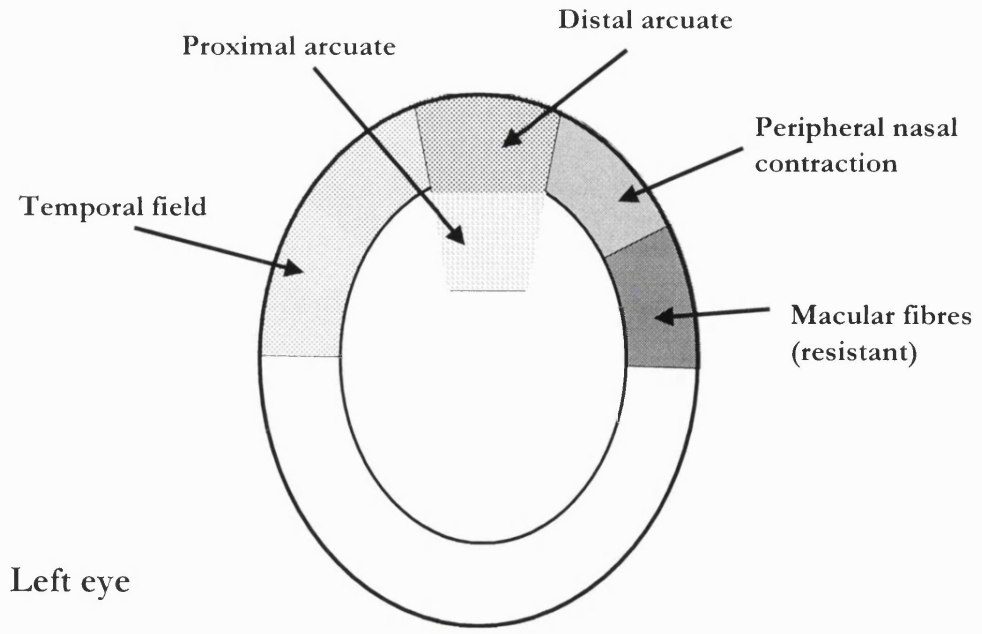


**Figure 2-5. Read and Spaeth's (1974) map relating structural changes at the disc to visual field defect type**

Hart et al. (1978) correlated the area of the $I_4e$ isopter with the cup-disc ratio (CDR), and found that change in CDR had a linear relation to change in the area of the $I_4e$ isopter in ocular hypertensive eyes that developed visual field loss. There was no relation in eyes that had no visual field loss.

## 2.6.2 Automated perimetry

### 2.6.2.1 Whole disc/field comparisons

Planimetry

Gloster (1978) correlated 4 indices derived from measurements of optic disc photographs with visual function indices derived from three methods of perimetry. The structural indices were vertical, horizontal and area cup/disc ratios and narrowest rim width/disc diameter ratio. The forms of perimetry were: 1) 74 flashes presented in fixed positions on the Globuck screen (extent of field was given as number of stimuli seen), 2) 188 flashes presented in fixed positions on the Goldmann perimeter (extent of field was given as number of stimuli seen), and 3) Goldmann kinetic perimetry (extent of field was given as the area of the field plotted on the chart). All subjects examined had a history of intraocular pressure > 20mmHg, and were classified as ocular hypertensive, glaucoma suspect or glaucomatous. 150 eyes had full visual fields, 50 had early defects, 50 moderate defects

and 50 had advanced defects. The correlations are summarised in Table 2-4. The best correlation was between the vertical cup/disc ratio and Goldmann static perimetry.

| | Globuck screen | Static Goldmann perimetry | Kinetic Goldmann perimetry |
|---|---|---|---|
| Vertical cup/disc ratio | -0.68 | -0.79 | -0.69 |
| Horizontal cup/disc ratio | -0.62 | -0.55 | -0.55 |
| Area cup/disc ratio | -0.68 | -0.67 | -0.66 |
| Rim/disc ratio | 0.60 | 0.69 | 0.56 |

(all correlations at $p<0.001$)

**Table 2-4. Correlation between structural optic disc parameters and visual function (Gloster, 1978)**

Balazsi et al. (1984a) correlated magnification-corrected neuroretinal rim area with Octopus JO visual field indices, colour vision (Farnsworth-Munsell 100 Hue Test) and contrast sensitivity, in 12 normal, 16 glaucoma suspect and 11 glaucomatous eyes. Visual field indices were not reported. The correlations are summarised in Table 2-5.

| | Correlation (r) |
|---|---|
| Mean retinal sensitivity | 0.37 * |
| Colour vision | -0.35 * |
| Log contrast sensitivity (1.5 cpd) | 0.62 † |

(cpd = cycles per degree, * $p<0.05$, † $p=0.001$)

**Table 2-5. Correlation of visual function with neuroretinal rim area (Balazsi et al., 1984a)**

Airaksinen et al. (1985a) correlated magnification-corrected neuroretinal rim area with Octopus JO visual field indices in normal, glaucoma suspect, and glaucomatous eyes. Visual field data are given in Table 2-6.

| | Mean defect, mean ± standard deviation (dB) |
|---|---|
| Normal | -0.20 ± 1.50 |
| Suspected glaucoma | -2.00 ± 2.63 |
| Glaucoma | -4.38 ± 6.02 |

(dB = decibel)

**Table 2-6. Subject visual field indices (Airaksinen et al., 1985a)**

A curvilinear relationship between neuroretinal rim area and mean defect was demonstrated by a quadratic regression fit ($R^2 = 0.41$, $p<0.01$). The quadratic fit was significantly better than a linear fit. It was evident from the scatter plot that a few eyes had field loss as advanced as –24dB.

Airaksinen et al. (1985b) also correlated the appearance of the RNFL, scored semi-quantitatively, with Octopus JO summary indices in normal, glaucoma suspect and glaucomatous eyes. There was a wide range of glaucoma severity, with some eyes having a mean defect as high as 24dB. The relationship between diffuse RNFL loss and visual field mean defect was curvilinear. Quadratic regression determined a significant correlation ($r^2= 0.60$, $p<0.0001$) between the diffuse loss RNFL score and mean defect.

Drance et al. (1986) correlated a number of psychophysical (DLS perimetry, contrast sensitivity and colour vision) and electrophysiological (cortical evoked potentials and pattern electroretinogram (PERG)) measurements with quantitative (neuroretinal rim area) and semi-quantitative (diffuse and localised RNFL score) structural measurements in normal, glaucoma suspect and glaucomatous eyes (total 131). Improvements in predicting structural measurements by combining function test results were investigated by forward stepwise multiple regression. The range of visual field MD was not stated. The best correlations for single parameters were found between visual field mean threshold and the structural parameters of diffuse RNFL score, neuroretinal rim area and horizontal cup/disc ratio ($R^2$ of 49%, 24% and 22%, respectively). The prediction of neuroretinal rim area was improved by adding ether contrast sensitivity or PERG measurements.

Guthauser et al. (1987) correlated neuroretinal rim area with visual field indices in 50 eyes with glaucomatous field loss. The mean MD and standard deviation was not stated, but 20 eyes had a MD greater than -2dB. Neuroretinal rim area was measured by planimetry, with the cup defined by pallor. No ocular magnification corrections were made. The correlation between neuroretinal rim area and MD was $r = -0.58$ ($p = 0.0001$). A correction was made for the correlation of the (glaucomatous) neuroretinal rim area and the disc area. The correlation between the corrected neuroretinal rim area and MD was $r = -0.72$ ($p = 0.0001$).

Jonas et al. (1988b) correlated several morphologic optic disc variables with visual field indices derived from the Octopus programs 32 and 34-Delta in 253 normal eyes and 158 eyes with early primary open angle glaucoma. Visual field indices are not stated for the normal subjects. The glaucoma eyes were divided into groups, depending on the appearance of the disc. The mean defect ranged from 3.3dB ± 5.0 in the 'early glaucoma' group, to maximal field loss in the 'end-stage glaucoma' group. The morphological parameter demonstrating the highest correlations with visual field mean defect was neuroretinal rim area (Table 2-7).

| | Correlation with visual field mean defect (Spearman's r) |
|---|---|
| Neuroretinal rim area | -0.68 |
| Vertical cup/disc ratio | 0.66 |
| Horizontal cup/disc ratio | 0.58 |
| Horizontal/vertical cup/disc ratio | -0.52 |
| Cup area | 0.42 |

(all p values <0.001)

**Table 2-7. Linear correlation (Spearman's r value) between structural parameters and visual field indices (Jonas et al., 1988b)**

Airaksinen et al. (1990) correlated quantitative optic disc parameters and semi-quantitative RNFL scores with the 'functional channel fraction' (FCF) or 'neural capacity' derived from high-pass resolution perimetry (HPRP). FCF is intended to be an estimation of the number of functional ganglion cells relative to average normal. 36 ocular hypertensives and 39 glaucoma patients were studied. The results may be influenced by the requirement of glaucomatous eyes to have 'typical' disc and field changes. FCF was correlated with the total RNFL score ($r = -0.63$, $p<0.0001$) and with neuroretinal rim area ($r = 0.44$, $p<0.001$). Inspection of the scatter plot suggests a linear correlation between FCF and RNFL score, but possible a curvilinear relationship with neuroretinal rim area. Jonas and Grundler (1997) correlated quantitative optic disc parameters with mean visual field loss (Octopus G1 program) in 302 eyes with primary open angle glaucoma. Study results may be biased by the inclusion of optic disc appearance in the selection criteria, and of specific patterns of visual field loss. The relationship between neuroretinal rim area and visual field was found to be curvilinear, and a (further) transformation was performed to the decibel visual field data (square root of the visual field mean defect (MD)). Thus the square root of the logarithm of the DLS was plotted against neuroretinal rim area. A linear relationship was found. Visual field indices were also plotted against 'rim defect', which is the difference between the measured neuroretinal rim area and that expected for the disc size. Results are summarised in Table 2-8.

| | Correlation with visual field MD | Correlation with square root visual field MD |
|---|---|---|
| Neuroretinal rim area | -0.66 | -0.70 |
| Neuroretinal rim area defect | 0.67 | -0.72 |
| Rim/disc area ratio | -0.63 | -0.67 |

(MD = mean deviation, p values <0.0001)

**Table 2-8. Linear correlation (r value) between structural parameters and visual field indices (Jonas and Grundler, 1997)**

The transformation (square root) of the visual field indices marginally improved the correlation with the structural parameters. Inspection of the scatter plots confirms a curvilinear relationship of neuroretinal rim area with decibel MD and a linear relationship with square root decibel MD. The analysis of neuroretinal rim area defect did not appear to improve the correlation with visual indices.

Rodenstock Optic Nerve Head Analyzer

Caprioli et al. (1989) correlated neuroretinal rim area and a parameter called the 'average polar profile', derived from RNFL thickness measurements, with visual field MD derived from Humphrey 30-2 and 24-2 and Octopus G1 and 32 programs. The average polar profile is the mean of the superior and inferior polar profiles, each of which is the difference between the mean RNFL height in the superior, or inferior, quadrant and the mean height in the temporal quadrant. 52 normal, 79 glaucoma suspect and 101 glaucomatous eyes were studied. Visual field indices are summarised in Table 2-9.

| | Mean deviation, mean ± standard error (dB) |
|---|---|
| Normal | 0.7 ± 0.3 |
| Suspected glaucoma | 0.1 ± 0.2 |
| Glaucoma | -7.3 ± 0.6 |

(dB = decibel)

**Table 2-9. Visual field summary parameters (Caprioli et al., 1989)**

The average polar profile was correlated more strongly with visual field MD than was neuroretinal rim area (Table 2-10). Data were fitted with a linear model. Inspection of the scatter plot given in the paper suggests a quadratic model may have given a better fit. Similar results were obtained in a study with slightly larger cohorts (Caprioli, 1990).

| | Correlation (r) |
|---|---|
| Neuroretinal rim area | -0.37 |
| Average polar profile | -0.44 |

(p values <0.0001)

**Table 2-10. Linear correlation (r) between structural parameters and visual field mean deviation (Caprioli et al., 1989)**

Lachenmayr et al. (1991) correlated semi-quantitative measurements of the RNFL (Airaksinen et al., 1984) and quantitative measurements of the neuroretinal rim with various psychophysical tests, including light-sense (DLS) perimetry, flicker perimetry, resolution perimetry and colour vision. The correlations were made in 61 eyes with a range of visual field loss, from advanced glaucomatous loss to normal fields. Results are summarised in Table 2-11. The best correlation was found between the RNFL scores and flicker perimetry. In general, better correlations were found with combined diffuse and localised RNFL scores than either alone.

| | DLS perimetry (mean sensitivity/dB) | Flicker perimetry (mean frequency/cps) | Resolution perimetry (mean ring score) | Colour vision (100-Hue score) |
|---|---|---|---|---|
| Total RNFL score | -0.39 † | -0.61 ‡ | 0.34 † | ns |
| Total diffuse RNFL score | -0.36 † | -0.58 ‡ | 0.29 * | ns |
| Total localized RNFL score | ns | ns | 0.26 * | ns |
| Neuroretinal rim area | ns | ns | -0.26 * | ns |

(DLS = differential light sensitivity, dB = decibel, cps = cycles per second, RNFL = retinal nerve fibre layer, * $p<0.05$, † $p<0.01$, ‡ $p<0.0001$, ns = not significant)

**Table 2-11. Correlation (r values) of structural and functional tests (Lachenmayr et al., 1991)**

Nanba and Iwata (1992) correlated quantitative measurements of the ONH with the summary indices derived from Humphrey Visual Field Analyzer 30-2 perimetry in 44 normal, 23 ocular hypertensive and 66 glaucomatous eyes. All stages of glaucomatous field loss were included, with sensitivity losses of up to –30dB. Although linear correlations were performed, the authors

considered the relationship between structural and functional measures to be curvilinear. The correlation coefficients are given in Table 2-12.

| | Correlation (r) |
|---|---|
| Global | |
| Neuroretinal rim area | 0.65 |
| Cup/disc ratio | -0.55 |
| Cup volume | -0.60 |

**Table 2-12. Correlation of structural parameters and visual field mean deviation (Nanba and Iwata, 1992)**

Tomita et al. (1993) correlated the 'functional channel fraction' (FCF) of high-pass resolution perimetry with measurements of neuroretinal rim area in 26 eyes of 18 patients with normal tension glaucoma. 14 eyes were considered to have less advanced visual field loss and 12 to have advanced loss. The results of the correlation may be affected by the requirement of the glaucomatous eyes to have 'typical' glaucomatous disc and field changes. The correlation between FCF and neuroretinal rim area was 0.54 ($p<0.05$). The relationship appeared linear from the scatter plot.

Heidelberg Retina Tomograph (HRT)

Brigatti and Caprioli (1995) correlated morphological parameters derived from the HRT (software version 1.10, reference plane at 320 microns below the reference ring) with visual field parameters in 46 patients with early to moderate glaucomatous field loss (mean MD -4.8 ± 6.2dB). The highest correlation was found with the structural measurement of 'third moment' (a measure of cup shape), but neuroretinal rim parameters were not evaluated (Table 2-13).

| | Correlation with visual field MD Pearson's r |
|---|---|
| Third moment | -0.65 * |
| Mean cup depth | -0.36 |
| Cup volume | -0.33 |
| Cup area | -0.14 |
| Mean RNFL height | -0.11 |
| Height variation in contour | 0.08 |
| Optic disc area | 0.03 |

(MD = mean deviation, RNFL = retinal nerve fibre layer, * $p < 0.0001$)

**Table 2-13. Correlation of HRT structural parameters with visual field mean deviation (Brigatti and Caprioli, 1995)**

Iester et al. (1997a) similarly correlated morphological parameters derived from the HRT, with more recent software (version 1.11S, in which the reference plane is set 50 microns below the height of the disc margin between 350° and 356°), in normal, ocular hypertensive, and high- and low-tension glaucoma eyes. Visual field indices, from the Humphrey 30-2 program, are summarised in Table 2-14.

| | MD, mean ± standard deviation (dB) |
|---|---|
| Normal | -0.74 ± 1.62 |
| Ocular hypertension | -0.44 ± 1.77 |
| Low tension glaucoma | -6.52 ± 5.89 |
| High tension glaucoma | -6.38 ± 6.34 |

(MD = mean deviation, dB = decibel)

**Table 2-14. Subject visual field indices (Iester et al., 1997a)**

The correlations between visual field MD and the various structural parameters, for all subjects together, are given in Table 2-15. The most important predictor of MD was neuroretinal rim area, followed by cup shape measure.

| | Visual field MD |
|---|---|
| Neuroretinal rim area | 0.44 |
| Cup shape measure | -0.43 |
| Neuroretinal rim volume | 0.35 |
| Cup area | -0.28 |
| Mean RNFL thickness | 0.28 |
| RNFL cross-sectional area | 0.27 |
| Cup/disc area ratio | -0.25 |
| Mean cup depth | -0.21 |
| Cup volume | -0.19 |
| Optic disc area | ns |
| Maximum cup depth | ns |
| Height variation contour | ns |

(MD = mean deviation, RNFL = retinal nerve fibre layer, p values <0.001, except ns = not significant)

**Table 2-15. Pearson's correlation coefficient between HRT parameters and visual field mean deviation (Iester et al., 1997a)**

Uchida et al. (1996) correlated various HRT parameters with the visual field indices derived from the Humphrey 30-2 and 24-2 and Octopus G1 and G2 visual field analysers in 43 normal and 53 early glaucoma eyes. Cases with field loss > 10dB were excluded. Visual field parameters are summarised in Table 2-16.

| | Mean defect, mean ± standard deviation (dB) |
|---|---|
| Normal subjects | -0.4 ± 1.6 |
| Glaucoma patients | -4.8 ± 3.4 |

(dB = decibel)

**Table 2-16. Subject visual field indices (Uchida et al., 1996)**

Linear correlations between structural parameters and visual field indices were made with Spearman's correlation coefficient, with a Bonferonni correction for multiple comparisons. The parameter demonstrating the best correlation with visual function was the cup shape measure. The results of the correlations are shown in Table 2-17.

| | Correlation coefficients (Spearman's r) |
|---|---|
| Cup shape measure | -0.61 † |
| Mean retinal thickness | 0.46 * |
| Neuroretinal rim volume | 0.44 † |
| Cup/disc area ratio | -0.43 † |
| Height variation contour | 0.43 † |
| Cup area | -0.34 * |
| Neuroretinal rim area | ns |
| Cup volume | ns |
| Retinal cross-sectional area | ns |

(† $p<0.01$, * $p<0.05$, ns = not significant)

**Table 2-17. Spearman's correlation coefficient between HRT parameters and visual field mean defect (Uchida et al., 1996)**

Salgarello et al. (1999) correlated HRT structural parameters with visual function, as measured by the pattern electroretinogram (PERG) in 34 eyes with ocular hypertension (OHT). The eyes with OHT had (undefined) normal 30-2 Humphrey fields. Although a relationship between structural measures and visual function was being sought, eyes with subjective optic disc abnormalities, such as a vertical cup/disc ratio >0.5, were excluded. The PERG was measured at 6 different spatial frequencies and 8 standard HRT parameters were considered for the whole disc and each of the predefined segments,

giving a total of 56 structural parameters. Despite the very large number of correlations being made, a p value of <0.01 was considered significant. The only correlation that reached this level of significance was that between inferotemporal cup shape measure and the PERG at the 2.6 cycles per degree frequency.

OCT

Parisi et al. (1999) correlated RNFL thickness measured with the OCT with visual function as measured by the pattern electroretinogram (PERG), visual evoked potentials (VEP) and spatial contrast sensitivity (SCS) in 32 untreated eyes with ocular hypertension (OHT). The eyes with OHT had (undefined) normal 24-2 Humphrey fields. Although a relationship between structural measures and visual function was being sought, eyes with (poorly defined) subjective optic disc abnormalities, such as an increased vertical-to-horizontal cup/disc ratio, were excluded. Despite this, significant correlations with the measures of visual function were found (Table 2-18).

| | Correlation coefficients | Significance (p) |
|---|---|---|
| PERG latency | -0.47 | 0.007 |
| PERG amplitude | 0.52 | 0.002 |
| VEP latency | -0.42 | 0.016 |
| VEP amplitude | 0.46 | 0.008 |
| SCS (3 cpd) | -0.36 | 0.044 |

(PERG = pattern electroretinogram, VEP = visual evoked potential, SCS = spatial contrast sensitivity, cpd = cycles per degree. Pearson's correlation for PERG and VEP, Spearman's correlation for SCS)

**Table 2-18. Correlation coefficient between OCT RNFL thickness and tests of visual function (Parisi et al., 1999)**

### 2.6.2.2 Correlations of optic nerve head/visual field sectors

Caprioli and Miller (1988) correlated quantitative measurements of the ONH, derived from the Rodenstock Optic Nerve Head Analyzer, with the summary indices derived from Octopus Program 32 perimetry in 50 glaucoma suspects and 37 glaucoma patients. Correlations were made for the whole disc, and for disc segments: the inferior disc quadrant with the superior hemifield and the superior disc quadrant with the inferior hemifield. Visual field data are given in Table 2-19.

| | Mean defect, mean ± standard error (dB) |
|---|---|
| Suspected glaucoma | -0.4 ± 0.2 |
| Glaucoma | -7.2 ± 1.0 |

(dB = decibel)

**Table 2-19. Subject visual field indices (Caprioli and Miller, 1988)**

The best correlation was found with the neuroretinal rim area and a better correlation was found for global neuroretinal rim area than hemifield comparisons. Results are summarised in Table 2-20.

| | Correlation (r) |
|---|---|
| Global | |
| Neuroretinal rim area | -0.49 * |
| Cup/disc ratio | 0.42 * |
| Cup volume | 0.42 * |
| Inferior quadrant rim area | -0.46 |
| Superior quadrant rim area | -0.28 |

(* p = 0.000, p value not stated for hemifield correlations)

**Table 2-20. Correlation of structural and visual field measurements (Caprioli and Miller, 1988)**

Tsai et al. (1995) measured the height of the of the peripapillary retina with the HRT (using the 320μm reference plane). The difference between the mean height in 4 pre-defined segments (supero-temporal and supero-nasal, and infero-temporal and infero-nasal, Figure 2-6) and the mean height in the temporal sector (-25° to +25°) was correlated with the mean deviation in regions of the visual field (Figure 2-6), derived from the Humphrey perimeter hemifield divisions. The mean deviation for each sector, in normal and glaucomatous subjects, is given Table 2-21. The visual field was tested with both achromatic and short wavelength perimetry.

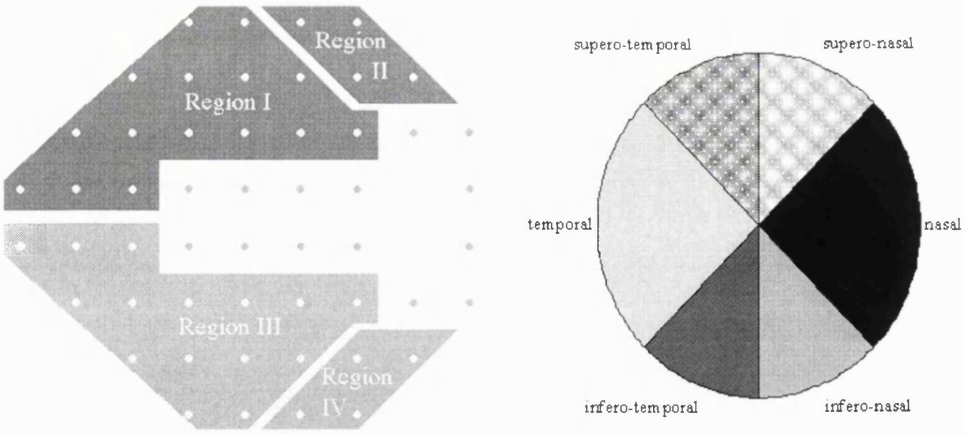


**Figure 2-6. Visual field and optic disc divisions (Tsai et al., 1995)**

| Region | Normal subjects<br>Mean MD ± standard deviation | Glaucoma subjects<br>mean MD ± standard deviation |
|---|---|---|
| Global (dB) | -0.13 ± 1.28 | -3.97 ± 4.70 |
| Region I (dB) | 0.07 ± 1.21 | -6.19 ± 8.44 |
| Region II (dB) | -0.41 ± 2.41 | -5.19 ± 7.73 |
| Region III (dB) | 0.20 ± 1.11 | -2.41 ± 4.26 |
| Region IV (dB) | 0.15 ± 1.61 | -2.35 ± 4.49 |

(MD = mean deviation, dB = decibel)

**Table 2-21. Mean deviation for each region of the visual field (Tsai et al., 1995)**

The linear correlation was examined between dB DLS and neuroretinal rim area and peripapillary retinal height (Table 2-22). However, a plot of achromatic Region I mean deviation against infero-temporal retinal height gave the impression of a curvilinear relationship between the two. The apparent correlation may have been artificially improved by the large range of dB defect values (two extreme values of a mean deviation < -25 dB and mean height < 0.00 mm).

| | Visual field area | W-on-W perimetry Rho | SWAP perimetry Rho |
|---|---|---|---|
| Neuroretinal rim area | Global | 0.47 | 0.56 |
| Rim/disc area ratio | Global | 0.45 | 0.51 |
| Retinal height: | | | |
| Global | Global | 0.61 | 0.45 |
| Inferotemporal | Region I | 0.66 | 0.49 |
| Inferonasal | Region II | 0.43 | 0.37 |
| Superotemporal | Region III | 0.67 | 0.55 |
| Superonasal | Region IV | 0.41 | 0.38 |

(W-on-W = white-on-white, SWAP = short wavelength automated perimetry)

**Table 2-22. Spearman rank-order correlation coefficient (rho) for correlations between visual field region mean deviation and optic nerve head structural parameters (Tsai et al., 1995)**

Weinreb et al. (1995) compared global and regional structural measures obtained with the HRT and the Nerve Fiber Analyzer with achromatic visual field indices in 53 glaucomatous eyes. The visual field was divided into two regions (Figure 2-7, Table 2-23): superior (upper 5 Glaucoma Hemifield divisions) and inferior (lower 5 Glaucoma Hemifield divisions).

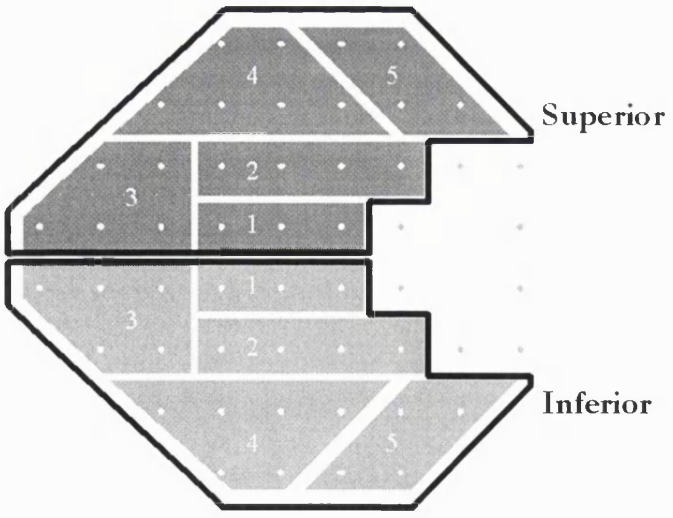


**Figure 2-7. Visual field regions (Weinreb et al., 1995)**

| Region: | Glaucoma subjects mean deviation mean (95% C.I.) |
|---|---|
| Global (dB) | -5.4 (-4.5 – -6.3) |
| Superior (dB) | -5.9 (-4.8 – -7.0) |
| Inferior (dB) | -4.9 (-3.9 – 5.9) |
| Hemifield difference (dB) | 1.0 (0.0 – 2.0) |

(dB = decibel)

**Table 2-23. Mean deviation for each region of the visual field (Weinreb et al., 1995)**

The nerve fibre layer thickness measurements from the two imaging devices were made in 3 ONH regions (0° is at the temporal horizontal meridian, and degrees are counted anticlock-wise): superior (45° to 134°), inferior (225° to 314°), and global (0° to 359°). For the HRT, RNFL thickness measurements were derived from the difference between the height on a 1.5 disc diameter circle and a reference plane 50 microns below the temporal edge (350 to 356°) of the same measurement circle. For the Nerve Fiber Analyzer, RNFL measurements were derived from the ratio of retardation measurements in the 3 regions to mean temporal retardation (at 350 to 356°). Global, regional and hemifield comparisons of RNFL measures and visual field MD were used in analyses (Table 2-24).

| | HRT RNFL cross-sectional area $R^2$ | GDx Retardation ratio $R^2$ |
|---|---|---|
| Global | ns | 0.13 † |
| Superior hemifield | ns | 0.08 * |
| Inferior hemifield | 0.13 † | 0.21 ‡ |
| Hemifield difference | 0.20 ‡ | ns |

(HRT = Heidelberg retina tomograph, RNFL = retinal nerve fibre layer, * $p<0.05$, †$p<0.01$, ‡ $p<0.001$, ns = not significant)

**Table 2-24. Correlation of structural parameters with (regional) visual field mean deviation (Weinreb et al., 1995)**

Kono et al. (1997) correlated global and sectoral HRT parameters with Humphrey 30-2 visual field indices and 'neural capacity' (NC) of high-pass resolution perimetry (HPRP) in 37 normal tension glaucoma patients. HRT images were analysed with software version 1.09 (reference plane 320μm below the reference ring). The study results are likely to be biased by the requirement of glaucomatous eyes to have both recognisable glaucomatous disc changes and 'typical' glaucomatous visual field defects. The HRT parameters were analysed for the whole disc (global) and in quadrants.

The Humphrey and HPRP fields were divided into corresponding sectors, according to the visual field divisions proposed by Wirtschafter et al. (1982) (Humphrey field divisions shown in Figure 2-8)

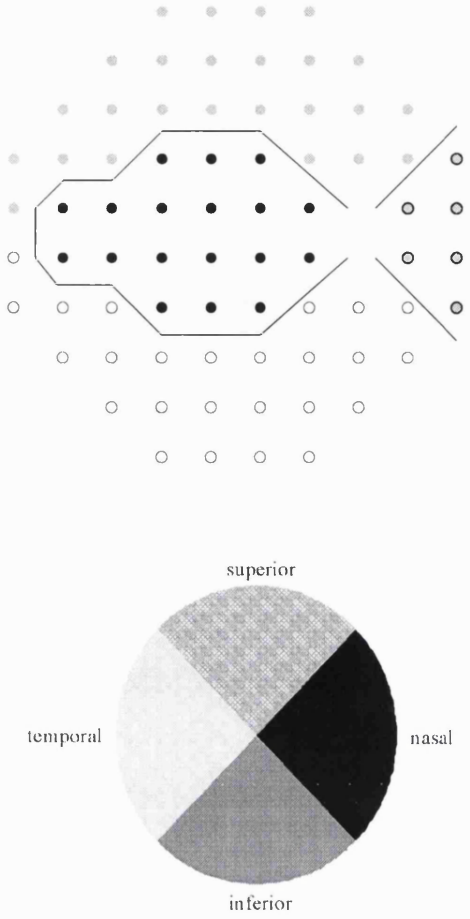


**Figure 2-8. Humphrey visual field and optic disc sectors (Kono et al., 1997)**

Visual field indices were not stated. 21 eyes were classified as having early field loss and 16 as having moderate or advanced field loss. The correlations between neuroretinal rim area and functional indices are summarised in Table 2-25. In general, correlations were slightly better between neuroretinal rim area and NC than neuroretinal rim area and MD. The only segment correlation that improved on the global correlation was that for the inferior segment. Scatter in the plots of NC and MD against neuroretinal rim area was too great to assess a pattern for the global parameters. However, the plots for the inferior quadrant were suggestive a curvilinear relationship for both NC and MD. NC is intended to be an estimation of the number of functional ganglion cells relative to average normal, and one might expect a linear relationship with neuroretinal rim area (as a cross-section of the retinal nerve fibres as they exit the eye, the area should be proportional to the number of axons).

| | Correlation with DLS MD | Correlation with HPRP NC |
|---|---|---|
| Global | 0.34 * | 0.38 * |
| Superior | ns | ns |
| Inferior | 0.43 † | 0.58 † |
| Temporal | ns | ns |
| Nasal | ns | ns |

(DLS = differential light sensitivity, MD = mean deviation, HPRP = high-pass resolution perimetry, NC = neural capacity, * = $p<0.05$, † = $p<0.01$, ns = not significant)

**Table 2-25. Spearman's rank correlation coefficients for correlations between neuroretinal rim area and mean deviation and neural capacity (Kono et al., 1997)**

Eid et al. (1997) correlated global and sectoral HRT parameters with Humphrey visual field indices in 125 subjects. HRT images were analysed with software version 1.11 and the standard reference plane (50 microns below the temporal disc margin at 350° to 356°). The study results are likely to be biased by the requirement of glaucomatous eyes to have recognisable glaucomatous disc changes, and normal eyes to have subjectively normal discs. The optic disc and peripapillary area were analysed in regions: global, superior (40° to 110°) and inferior (250° to 320°). The visual field was similarly analysed in regions: global, superior (upper hemifield regions 2 to 5) and inferior (lower hemifield regions 2 to 5). The visual field indices are summarised in Table 2-26.

| | Normal subjects<br>mean MD ± standard deviation | Glaucoma patients<br>mean MD ± standard deviation |
|---|---|---|
| Global | 0.4 ± 1.8 | -9.1 ± 7.3 |
| Superior region | -0.4 ± 1.9 | -10.3 ± 8.4 |
| Inferior region | -0.5 ± 1.7 | -9.0 ± 8.0 |

(MD = mean deviation)

**Table 2-26. Mean deviation for each region of the visual field (Eid et al., 1997)**

The correlations between the various structural parameters and visual field (sector) MD, for all subjects, are given in Table 2-27. Mean deviation was as great as –25dB in some eyes, and this would increase the apparent correlation. The scatter in the data was such that the pattern of correlation (linear or otherwise) could not be assessed.

| | Correlation (r) |
|---|---|
| Cup/disc area ratio | 0.41 ‡ |
| Neuroretinal rim volume | 0.37 ‡ |
| Neuroretinal rim area | 0.36 ‡ |
| Cup area | 0.36 † |
| Cup volume | 0.27 * |
| Disc area | ns |
| RNFL height | |
| Global | 0.49 ‡ |
| Superior | 0.49 ‡ |
| Inferior | 0.44 ‡ |
| RNFL cross-sectional area | |
| Global | 0.47 ‡ |
| Superior | 0.46 ‡ |
| Inferior | 0.41 ‡ |

(RNFL = retinal nerve fibre layer, * P=0.002, † P=0.001, ‡ P<0.001, ns = not significant)

**Table 2-27. Correlation of structural parameters with (regional) visual field mean deviation (Eid et al., 1997)**

Iester et al. (1997c) correlated HRT structural measures with the visual field (global MD, and superior and inferior MD) in three disc sectors (global, superior 45° - 135° and inferior 225° - 315°) in normal and glaucomatous individuals. Sectoral visual field indices are given in Table 2-28.

| Region | Normal subjects (mean ± standard deviation) | Glaucoma subjects (mean ± standard deviation) |
|---|---|---|
| Global (dB) | 0.05 ± 1.34 | -7.41 ± 7.12 |
| Inferior (dB) | 0.06 ± 1.29 | -6.91 ± 7.78 |
| Superior (dB) | 0.72 ± 1.68 | -9.35 ± 8.10 |

(dB = decibel)

**Table 2-28. Mean deviation for each region of the visual field (Iester et al., 1997c)**

The correlation coefficients (Table 2-29) are generally higher than those reported by Weinreb et al. (1995) (Table 2-24), and similar to those reported by Tsai et al. (1995) (Table 2-22). The higher values may, in part, be attributed to the inclusion of subjects with more damaged fields.

| | Global disc Pearson's r | Inferior disc sector Pearson's r | Superior disc sector Pearson's r |
|---|---|---|---|
| Third moment | -0.49 ‡ | -0.52 ‡ | -0.46 ‡ |
| Cup area | -0.35 ‡ | -0.39 ‡ | -0.44 ‡ |
| Neuroretinal rim volume | 0.32 ‡ | 0.47 ‡ | 0.24 † |
| Mean height contour | -0.29 † | -0.53 ‡ | -0.31 ‡ |
| Cup volume | -0.26 † | -0.31 ‡ | -0.24 † |
| Optic disc area | ns | ns | ns |

(† $p<0.01$, ‡ $p<0.001$, ns = not significant)

**Table 2-29. Correlation of structural parameters with (regional) visual field mean deviation (Iester et al., 1997c)**

Niessen et al. (1996) correlated RNFL cross-sectional area, derived from retardation measurements measured with the Nerve Fiber Analyzer I, with Humphrey 30-2 visual field indices in 24 normal eyes and 6 ocular hypertensive, nine glaucoma suspect, 3 early glaucoma, 7 moderate glaucoma and 27 severe glaucoma eyes. The peripapillary RNFL was divided into quadrants. The superior quadrant was correlated with the inferior hemifield MD and the inferior quadrant with the superior hemifield MD. A major problem with the analysis lies with the fact that visual fields were only performed in 4 of the normal subjects. In the remaining 20, a MD of 0dB was assumed and entered into the correlation with RNFL cross-sectional area. The results are summarised Table 2-30.

| RNFL cross-sectional area | Spearman's r |
|---|---|
| 360° | -0.34 |
| Inferior quadrant | -0.44 |
| Superior quadrant | -0.53 |

(RNFL = retinal nerve fibre layer)

**Table 2-30. Correlation of structural parameters with (regional) visual field mean deviation (Niessen et al., 1996)**

Tjon-Fo-Sang and Lemij (1997) correlated RNFL thickness values, derived from retardation measurements measured with the Nerve Fiber Analyzer I, with Humphrey 30-2 visual field indices in 200 eyes of 155 patients with glaucoma. The mean visual field MD was -10.33dB (range -31.5 to 0.76dB). The Peripapillary RNFL was divided into 4 segments: superior and inferior of 120° each, temporal of 70° and nasal of 50°. The superior sector was correlated with the inferior hemifield MD and the inferior sector with the superior hemifield MD. $R^2$ values were only 0.07 for each correlation (p value not stated).

Iester et al. (1998) correlated the RNFL height, as measured by the HRT software version 1.11 (reference plane 350° to 356° at the temporal margin), with visual field MD (global MD, and superior and inferior MD, (Table 2-31). The disc was divided into a 100° superior (25° to 125°), 100° nasal (130° to 230°), 100° inferior (235° to 335°), 40° temporal (340° to 20°), and a polar (superior plus inferior) sector. The correlations are given in Table 2-32.

| Visual Field Region | Normal subjects<br>MD (dB)<br>(mean ± standard deviation) | Glaucoma subjects<br>MD (dB)<br>(mean ± standard deviation) |
|---|---|---|
| Global | 0.20 ± 1.34 | -10.12 ± 6.93 |
| Inferior | -0.74 ± 3.96 | -8.02 ± 7.18 |
| Superior | 0.42 ± 2.26 | -11.43 ± 7.01 |

(MD = mean deviation, dB = decibel)

**Table 2-31. Mean deviation for each region of the visual field (Iester et al., 1998)**

| RNFL height | Correlation with (sector) visual field MD<br>Pearson's r |
|---|---|
| Global | -0.36 ‡ |
| Superior | -0.26 † |
| Inferior | -0.44 ‡ |
| Polar | -0.44 ‡ |

(RNFL = retinal nerve fibre layer,† $p<0.01$, ‡ $p<0.001$)

**Table 2-32. Correlation of structural parameters with (regional) visual field mean deviation (Iester et al., 1998)**

Chen et al. (1998) correlated parameters derived from the Nerve Fiber Analyzer (NFA) II in 4 quadrants (superior 50° to 139°, nasal 140° to 229°, inferior 230 to 319°, and temporal 320° to 49°) with visual field indices (global and superior and inferior hemifields) in subjects with varying degrees of glaucoma. Mean MD was –6.3 ± 6.7dB. NFA parameters most highly correlated with visual function were those 'corrected' for baseline retardation in the temporal/nasal part of the peripapillary ellipse.

### 2.6.3 Histological studies

Ganglion cell numbers, counted histologically, have been correlated with visual function as measured by automated perimetry in human (Quigley et al., 1989) and primate eyes (Harwerth et al., 1999). The study of human eyes included glaucoma 3 cases and 5 normal controls. Ganglion cells were counted in areas of the retina considered to correspond to the Humphrey 24-2 visual field test

points. The conversion factor used, of 250°/mm, is probably about 12.5% too small (Garway-Heath et al., 1998b), and sampled retinal areas, therefore, may not have corresponded well with the visual field data. No correction for the lateral displacement of ganglion cells from the fovea was made. This would have affected the results for the central 4 points in the Humphrey 24-2 grid (Garway-Heath et al., 2000). The percentage of the expected number of ganglion cells was plotted against the dB sensitivity loss, and linear regression was performed to assess the relationship between the two, with all points considered together, and a sub-analysis for the central 12° of the field. The slope of the regression line for the whole field suggested a 20% ganglion cell loss was associated with a 5dB sensitivity loss. That for the central 12° suggested a 50% ganglion cell loss for a 5dB sensitivity loss. The scatter of points was too great to evaluate whether the relationship was truly linear, and the confidence intervals for the slope of the regression were not stated.

Harwerth et al. (1999) studied 10 rhesus monkeys, in whom experimental glaucoma had been induced in one eye and the other eye acted as a control. Visual function was quantified by behavioural perimetry with the Humphrey 24-2 perimetry. The results demonstrated that the relationship between percentage ganglion cell loss and dB sensitivity loss was curvilinear. Points at which sensitivity loss for a given percentage ganglion cell loss appeared to be less than the overall trend most frequently were points near the fovea. This would be consistent with lower spatial summation near the fovea. An important feature of the plots was an apparent offset, so that the sensitivity loss curve was shifted upward and sensitivity losses were apparent before ganglion cell losses. A possible explanation for this is that the visual fields were performed at a time that IOP in the glaucoma eyes was very high. It has been demonstrated that acutely raised IOP can precipitate visual field defects in both normal and glaucomatous eyes (Drance, 1962; Scott and Morris, 1967; Trible and Anderson, 1997), and that IOP reduction in the situation of chronically raised IOP may result in an improvement in visual function (Gandolfi, 1995).

# 3 SECTION III: Investigations

## 3.1 Aims and plan of research

The aims of the research are as follows:

1. Various methods of imaging that make measurements of ONH structure are in use. In making measurements, the relationship between image size and actual size of fundal structures is of great importance, and is dependent on the characteristics of the optics of the imaging system and of the eye. In the first section (3.2.1.1) of the investigations the aim is to establish the relationship between the various optical components of the eye and image magnification, and to compare existing methods to correct for ocular magnification to establish their equivalence. Sources of error of the methods will be identified. Magnification of the fundus imaging equipment will also be established (3.2.1.2).
2. Modern imaging equipment, such as the HRT, makes measurements of a large number of morphological parameters. The aim of this section (3.2.2) of the investigations is to establish which of the ONH structural measurements best identifies glaucomatous optic neuropathy, and to ascertain the optimum statistical treatment of the measurement data to distinguish between normal and glaucomatous optic nerve heads.
3. Visual function is typically quantified by automated perimetry, with DLS given in decibels. The relationship between DLS and ganglion cell numbers is not well characterised. The aim of this section (3.3) of the investigations is to establish the physiological relationship between DLS and ganglion cell numbers.
4. In order to know how the DLS at a certain point in the retina relates to a structural measurement at the ONH it is necessary to establish the anatomical relationship between the two. The aim of this section (3.4) of the investigation is to establish an anatomical basis for the sub-division of the ONH and visual field into corresponding sectors.
5. The relationship between structural measurements of the ONH and DLS in the visual field is not well characterised. It is not known whether there is a linear or non-linear relationship between neuroretinal rim area and decibel DLS, or whether the relationship differs in different ONH/visual field sectors. The aim of this section (3.5) of the investigations is to characterise the actual structure/function relationship from imaging and visual field measurements in a group of normal subjects and patients with early glaucoma.

## 3.2 Measurement of optic nerve head structure

### 3.2.1 Magnification corrections

Since the 1970's it has been recognised that the size of the optic cup is related to the size of the optic disc in the normal population (Teal et al., 1972; Bengtsson, 1976), and similarly, the area of the neuroretinal rim is related to optic disc size (Britton et al., 1987; Caprioli and Miller, 1987; Jonas et al., 1988g). For this reason, it is necessary to make actual measurements of the size of ONH features, rather than relative measurements that vary with optic disc size (such as the cup/disc ratio), in order to distinguish pathological from physiological states. It is not possible to measure the dimensions of the ONH directly in vivo, except during vitreo-retinal surgery (Bartz-Schmidt et al., 1994), and so clinicians have to rely on measurements made on images of the ONH. The size of an image of a feature in the fundus of the eye is dependent on magnification due to the camera and magnification due to the eye, as well as factors such as the position of the feature of interest in the fundus (eccentricity) (Holden and Fitzke, 1988; Bennett et al., 1994) and the position of the camera with respect to the eye (Behrendt and Doyle, 1965; Pach et al., 1989; Arnold et al., 1993; Lotmar, 1984).

#### 3.2.1.1 Ocular magnification corrections

##### 3.2.1.1.1 Background

Various methods to correct for eye-camera (Bengtsson and Krakau, 1977; Bengtsson and Krakau, 1992) and eye (Bennett et al., 1994; Littmann, 1982; Littmann, 1988; Wilms, 1986) magnification have been published, and all make assumptions about the optics of the eye to a greater or lesser extent (see section 2.4.2.1). The estimate of the ocular component ('q') by calculation from axial length, anterior chamber depth, lens thickness, refractive error and corneal curvature (Bennett et al., 1994) utilises more information, and makes fewer assumptions, about the optical dimensions of the eye than other published methods.

##### 3.2.1.1.2 Purpose

The purpose of this study is to compare the available methods for equivalence, identify errors where they occur and establish whether these errors are systematic or random in nature.

##### 3.2.1.1.3 Methods

Data of the ocular biometry from three independent cohorts of patients was collected:
Set 1) comprised 90 consecutive subjects from the Ocular Hypertension Clinic at Moorfields Eye Hospital. Each underwent keratometry, measurement of spectacle refraction and ultrasound biometry. All measurements were made by one clinician (DFG-H). Keratometry was performed using a calibrated Javal-Schiotz (Haag-Streit) keratometer, the mean of 2 meridians being taken. Ultrasound biometry was performed with a calibrated Allergan Humphrey Ultrasound Biometer

(Model 820) using a tonometer-mounted, hard-tipped probe, and operated in the semi-automatic mode. The median of 5 good quality measurements was taken.

Set 2) comprised 59 consecutive glaucoma patients from the Medical Research Council 5FU Trabeculectomy Trial at Moorfields Eye Hospital. Each underwent keratometry, refraction by an optometrist, measurement of the optical anterior chamber depth and ultrasound biometry. All measurements were made by one of two experienced optometrists. Keratometry was performed using a calibrated Javal-Schiotz (Haag-Streit) keratometer, the mean of 2 meridians being taken. Optical pachymetry was performed with the Haag Streit Depth Measuring Device II, taking the median of three readings. Ultrasound biometry was performed with a calibrated Allergan Humphrey Ultrasound Biometer (Model 820) using a tonometer mounted, hard-tipped probe, and operated in the semi-automatic mode. The median of 3 good quality measurements was taken.

Set 3) 60 consecutive glaucoma patients from The National Medical Research Council (Singapore) 5FU Trabeculectomy Trial at the Singapore National Eye Centre. Each underwent keratometry, refraction by a trained optometrist, measurement of the optical anterior chamber depth and ultrasound biometry. Refraction and keratometry was carried out in a routine refraction clinic by the duty optometrist. All ultrasound biometry and optical pachymetry was carried out by a single ophthalmologist. Keratometry was performed using a calibrated Topcon KR 3000, averaging five readings, the mean of 2 meridians being taken. Optical pachymetry was performed with Haag Streit Depth Measuring Devices I & II, taking the median of three readings. Ultrasound biometry was performed with a calibrated Storz "Compuscan" using a tonometer mounted, hard-tipped probe, taking the mean of 16 high quality readings, having a standard deviation of less than or equal to 0.12mm.

Keratometry readings are given as the anterior radius of curvature of the cornea ($r_1$) in millimeters. Subject characteristics are summarised in Table 3-1.

| | | Data set 1 | Data set 2 | Data set 3 |
|---|---|---|---|---|
| Age / years | | 54.1 ± 15.1 | 68.3 ± 9.4 | 61.8 ± 10.8 |
| Sex / % | Male | 52.2 | 66.1 | 70.0 |
| Ethnicity / % | Caucasian | 80.0 | 86.4 | - |
| | Chinese Asian | 1.1 | - | 81.6 |
| | Indian Asian | 10.0 | 5.1 | 6.7 |
| | Malay | - | - | 11.7 |
| | Afro-Caribbean | 8.9 | 8.5 | - |
| Diagnosis / % | POAG* | 20.0 | 94.9 | 51.7 |
| | Ocular Hypertension | 65.6 | - | - |
| | CACG† | - | 5.1 | 46.7 |
| | Normal | 14.4 | - | - |
| | SOAG‡ | - | - | 1.7 |

(age: mean ± standard deviation, * Primary open angle glaucoma , † Chronic angle closure glaucoma, ‡ Secondary open angle glaucoma)

**Table 3-1. Subject demographic data**

The study design followed the tenets of the Declaration of Helsinki and informed consent was obtained from each subject after the nature of the procedures was fully explained.
The data collected was used to calculate the ocular factor 'q' by 11 different methods (Table 3-2).

| References | Number of methods | Abbreviations |
|---|---|---|
| Bengtsson and Krakau (1992) | 3 | BK1, BK2, BK3 |
| Littmann (1982); Littmann (1988) | 2 | L1, L2 |
| Bennett et al. (1994) | 2 | BRE1, BRE2 |
| Wilms (1986) | 2 | W1, W2 |
| personal communication – Gerhard Zinser | 1 | HRT |
| derivation appended | 1 | |

**Table 3-2. Sources of methods to derive the ocular magnification factor**

Calculations were performed for each data set using, firstly, the anterior chamber depth (ACD) and axial length as measured by ultrasound, and, secondly, the ACD as measured optically and the modified axial length (ultrasound axial length plus the difference between the optical and ultrasound ACD). For data set 1, the optical ACD was taken to be the ultrasonic depth plus 0.25mm (mean correction from the literature (Schelenz and Kammann, 1989; Shammas, 1984; Olsen and Nielsen, 1989; Foster et al., 1997)). For data set 2, optical ACD was measured, and a constant 0.55mm

corneal thickness was added. For data set 3, optical ACD was measured from anterior corneal epithelium to anterior lens capsule and optical corneal thickness was measured from anterior epithelial to posterior endothelial surface.

Calculations were made using the following assumptions: the refractive index of aqueous and vitreous humour were taken as 1.336 (Bennett and Rabbetts, 1989), the equivalent power of the cornea as 331.5/ $r_1$ (Olsen, 1986) and the ametropia, A, as $A = F_{sp} / (1 - 0.001v F_{sp})$, where $F_{sp}$ is the spectacle refraction and 'v' is the vertex distance (a value of 14mm was assumed).
The calculation of 'q' by method BRE1 is regarded as nearest to the 'true' value. The other methods, divided into those that use axial length (BK1, BRE2, L2 and W2), keratometry and ametropia only (L1, BK3, W1, HRT and the New method) and ametropia only (BK2), were compared. In addition to calculated values for 'q', an arbitrary (constant) value was also compared. The difference between method BRE1 and the various methods is expressed as the 'error' of the method.

Statistics

Methods were compared by plotting the difference between two methods against the mean of the methods (Bland and Altman, 1986). Where the difference between the methods was not related to the magnitude of the result, methods were compared using a paired t-test. The mean 'error' (difference between BRE1 and other methods) is a measure of systematic bias of a method, and the standard deviation of 'errors' is a measure of the random error (consistency of estimations). The relationship between the 'error' and the axial length, keratometry and ametropia was explored by linear regression analysis.

#### 3.2.1.1.4 Results

Biometric data for the data sets are summarised in Table 3-3.
The mean 'error' of each method is displayed in Table 3-4. The standard deviation of 'errors' is given in Table 3-5.
Linear regression analysis was performed with the 'error' of the 'keratometry and ametropia' methods (L1, BK3, W1, HRT and New) as the dependent variable and (modified) axial length as independent variable. The regression lines for data set 2 are shown in Figure 3-1.

| Measurement | Ultrasound | | | Optical/ultrasound | | |
|---|---|---|---|---|---|---|
| Data set | (1) | (2) | (3) | (1) | (2) | (3) |
| Axial length / mm | 23.26 +/- 0.97 | 24.04 +/- 1.58 | 23.39 +/- 1.32 | 23.51 +/- 0.97 | 24.39 +/- 1.62 | 23.7 +/- 1.26 |
| Anterior chamber depth / mm | 3.10 +/- 0.38 | 2.81 +/- 0.40 | 2.60 +/- 0.56 | *3.35 +/- 0.38 | †3.16 +/- 0.41 | ‡3.03 +/- 0.45 |
| Lens thickness / mm | 4.44 +/- 0.45 | 4.85 +/- 0.41 | 5.01 +/- 0.49 | - | - | - |
| Keratometry / mm | 7.77 +/- 0.24 | 7.73 +/- 0.25 | 7.61 +/- 0.26 | - | - | - |
| Refraction / D | -0.01 +/- 2.13 | -0.15 +/- 1.58 | -0.82 +/- 2.05 | - | - | - |
| Equivalent power of cornea / D | 42.7 +/- 1.3 | 42.9 +/- 1.4 | 43.6 +/- 1.51 | - | - | - |
| Equivalent power of lens / D | 25.0 +/- 2.1 | 21.7 +/- 2.7 | 24.3 +/- 3.0 | 24.4 +/- 2.1 | 21.0 +/- 3.0 | 23.5 +/- 3.0 |
| Equivalent power of eye / D | 63.1 +/- 2.2 | 60.6 +/- 2.9 | 63.5 +/- 3.2 | 62.4 +/- 2.2 | 59.8 +/- 3.0 | 62.5 +/- 3.1 |

(mm = millimetres, D = dioptres, * = ultrasonic ACD plus 0.25mm, † = optical ACD plus 0.55mm (corneal thickness), ‡ = optical ACD plus optical corneal thickness)

**Table 3-3. Summary of ocular biometry**

| | Mean 'error' / % | | | | | |
|---|---|---|---|---|---|---|
| Measurement | Ultrasound | | | Optical/ultrasound | | |
| Data set | (1) | (2) | (3) | (1) | (2) | (3) |
| L (1) | +8.1 | +3.6 | +7.6 | +7.1 | +2.2 | +6.0 |
| BK (3) | +8.1 | +3.6 | +7.5 | +7.1 | +2.2 | +5.9 |
| W (1) | +6.5 | +2.0 | +5.8 | +5.5 | +0.6 | +4.2 |
| HRT | +4.3 | -0.1 | +3.6 | +3.3 | -1.4 | +2.1 |
| New | +4.4 | -0.1 | +3.7 | +3.4 | -1.4 | +2.1 |
| BRE (2) | +1.1 | +0.3 | +0.7 | +1.3 | +0.5 | +0.9 |
| BK (1) | +2.2 | +1.3 | +1.7 | +2.3 | +1.4 | +1.9 |
| W (2) | +2.3 | +1.4 | +1.8 | +2.5 | +1.6 | +2.1 |
| L (2) | +2.5 | +1.4 | +2.3 | +2.6 | +1.5 | +2.4 |
| BK (2) | +5.1 | +1.0 | +5.9 | +4.1 | -0.4 | +4.3 |
| Constant | +1.3 | -2.8 | +0.6 | +0.3 | -4.1 | -0.9 |

**Table 3-4. Mean 'error' for each method**

| | standard deviation of 'errors' / % | | |
|---|---|---|---|
| Data set | (1) | (2) | (3) |
| L (1) | 3.2 | 4.2 | 4.6 |
| BK (3) | 3.0 | 4.3 | 4.5 |
| W (1) | 3.0 | 4.2 | 4.4 |
| HRT | 2.9 | 4.2 | 4.3 |
| New | 2.9 | 4.2 | 4.3 |
| BRE (2) | 0.6 | 0.7 | 0.9 |
| BK (1) | 0.6 | 0.8 | 0.9 |
| W (2) | 0.6 | 0.8 | 0.9 |
| L (2) | 0.9 | 1.1 | 1.2 |
| BK (2) | 3.6 | 5.0 | 5.3 |
| Constant | 4.4 | 6.8 | 5.6 |

**Table 3-5. Standard deviation of the 'error' for each method**

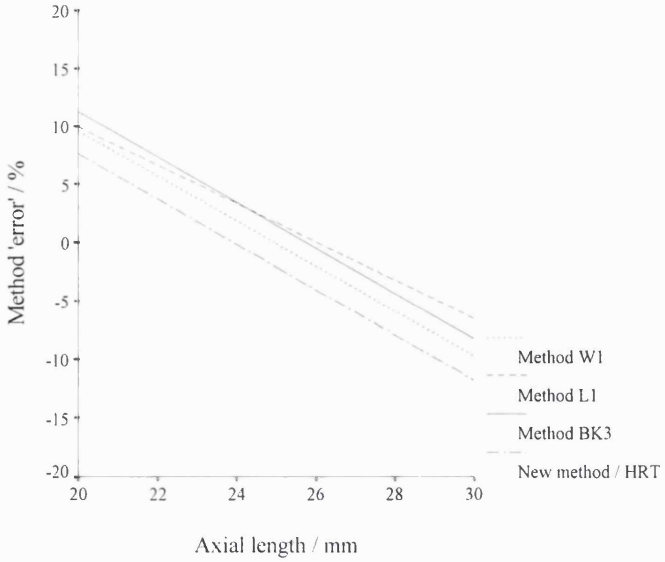


**Figure 3-1 Relationship between (modified) axial length and the 'error' of the 'keratometry and ametropia' methods to determine 'q' (regression lines shown). The analysis was significant for all methods and all data sets ($r^2$ = 0.09 to 0.46 and p = 0.003 to < 0.000).**

Linear regression analysis was performed with the 'error' of the 'spectacle refraction' method (BK2) and the 'error' from assuming a constant as the dependent variables and (modified) axial length as independent variable. The regression lines for data set 2 are shown in Figure 3-2. The analysis was significant for all data sets ($r^2 = 0.35$ to 0.56 and $p < 0.000$).

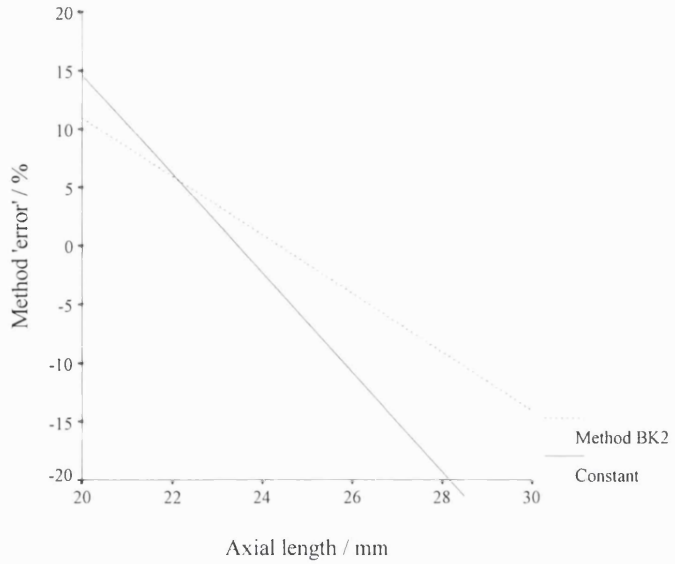


**Figure 3-2. Relationship between (modified) axial length and the 'error' of the 'ametropia only' method and the 'error' resulting from using a constant value for 'q' (regression lines shown)**

Linear regression analysis was performed with the 'error' of the 'axial length' methods (BK1, BRE2, L2 and W2) as the dependent variables and (modified) axial length as independent variable. The regression lines for data set 2 are shown in Figure 3-3. The analysis was significant for all methods in data set 2 ($r^2 = 0.07$ to 0.39, $p = 0.045$ to $< 0.000$). The analysis was not significant for any method in data sets 1 and 3.

The 'error' of method L2 was related to the ametropia ($r^2$ = 0.12 to 0.29, $p < 0.000$) and the 'error' of method BK2 was related to the keratometry ($r^2$ = 0.26 to 0.35, $p < 0.000$). No other consistent relationships were found.

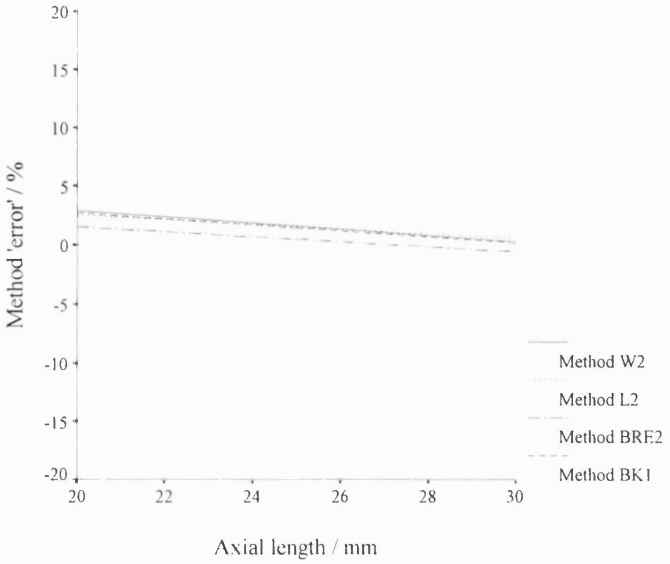


**Figure 3-3. Relationship between (modified) axial length and the 'error' of the 'axial length' methods to determine 'q' (regression lines shown)**

Comparisons with Littmann's method (L1):

L1 demonstrated the largest mean difference from BRE1 of any 'keratometry and ametropia' method (+2.2 to +7.1%).

L1 was significantly larger than L2 in all data sets by 1.1% to 4.3% ($p = 0.017$ to $< 0.000$).

There was no significant mean difference between L1 and BK3 for any data set.

L1 was significantly larger than BK2 in all data sets by 1.7 to 2.8% ($p < 0.000$).

L1 was significantly larger than HRT in all data sets by 3.5 to 3.7% ($p < 0.000$).

L1 was significantly larger than the New method in all data sets by 3.5 to 3.7% ($p < 0.000$).

Comparisons with the New method:

The difference between the New method and HRT was 0.03% in each data set ($p < 0.000$).

These methods demonstrated the smallest mean difference from BRE1 of any 'keratometry and ametropia' method (-1.4 to +3.4%). They also demonstrated the smallest mean difference from the 'abbreviated axial length' method (BRE2), using the modified axial length (-1.3 to +2.0%).

Comparisons with the constant:

The standard deviation of the calculation 'error' was reduced by 84 to 90% using the 'abbreviated axial length' method (BRE2), by 23 to 38% using the 'keratometry and ametropia' methods (New and HRT) and by 5 to 26% using the 'ametropia' method (BK2).

#### 3.2.1.1.5 Discussion

In their paper, Bengtsson and Krakau (1977) described the nature of camera- and ocular-magnification for the purpose of measuring the size of an optic disc from a photographic image. In this paper, they presented a method to correct for ocular magnification based on the spectacle refraction of the eye. Since then other authors have presented methods based on ametropia and keratometry (Bengtsson and Krakau, 1992; Littmann, 1982; Wilms, 1986), axial length only (Bennett et al., 1994; Bengtsson and Krakau, 1992), axial length and ametropia (Littmann, 1988; Wilms, 1986), and axial length, anterior chamber depth, crystalline lens thickness, keratometry and ametropia (Bennett et al., 1994). All these different methods make certain assumptions about the optics of the eye, and it is important to establish how the results of these methods compare and identify potential errors, in order to interpret studies that have used theses different methods.

##### 3.2.1.1.5.1 Errors of the methods

###### *3.2.1.1.5.1.1 Axial length methods*

For those methods assuming a constant value for $A_1P'$, the error is small (Figure 3-3). The distance $A_1P'$ varies little in the population so that the maximum error in calculating 'q', from the assumption of a constant 1.82 mm (method BRE2), is unlikely to exceed +/- 2.5% (Bennett et al., 1994). 95% of estimations using this method were within 1.8% of the more detailed method, BRE1, in this study.

###### *3.2.1.1.5.1.2 Keratometry and ametropia methods*

The mean off-set error associated with these methods (Table 3-4) varies, with Littmann's correction exhibiting the greatest bias and the HRT and New methods the least. The magnitude of error arises from the assumptions made about the equivalent power of the crystalline lens (or refractive power of the eye). The value used by Littmann of 19.11 D for the crystalline lens (and 58.64 D for the eye) is lower than the mean value of all three data sets in this study. It was suspected by Bengtsson and Krakau (1992) that this value was too low and the assumption explains the overestimation of 'q' when compared with axial length methods. Figure 3-1 illustrates the error in estimating 'q', using the 'keratometry and ametropia' methods, with respect to axial length. All make a relative underestimation of 'q' in long eyes compared with short eyes. This arises from the assumption of a constant value for the equivalent power of the crystalline lens for all eyes, whereas, in reality, the equivalent power of the crystalline lens declines with increasing axial length of the eye (Sorsby et al.,

1957; van Alphen, 1961). Assuming a constant lens power results in over-estimation of K′ in long eyes (as lens power is overestimated) and consequent under-estimation of 'q'. Analysis of our data demonstrates that it is not possible to predict the power of the lens from the keratometry and ametropia, in agreement with previous reports (van Alphen, 1961), so that it is not possible to correct for this error if axial length is unknown.

The relatively smaller errors of the keratometry and ametropia methods in data set 2, when compared with sets 1 and 3, may be attributed to the longer (mean) axial length in this group, which is nearer to the values assumed in the schematic eyes.

The improvement in the accuracy of determining 'q' (23 to 38%) using these methods over the use of a constant value is moderate. The variability of lens power in the data sets in this study is greater than that of corneal power (Table 3-3), and this prevents more accurate estimation of 'q'.

#### *3.2.1.1.5.1.3 Spectacle refraction method*

The off-set bias of this method is relatively small, because the assumed 'normal' value of the refractive power of the eye in this method (60 D) approximates the values found by calculation (Table 3-3). There remains a systematic underestimation of 'q' in long eyes (Figure 3-2) because only part of the variation in axial length is manifest by ametropia, the remainder being masked by the 'emmetropising' effects of changes in corneal and crystalline lens power.

### 3.2.1.1.5.2 Measurement/observation error

However accurate the theoretical calculations, measurements have to be made of various optical components of the eye, and these are all subject to measurement error. The principle measurements that are made for subsequent calculations are: refraction, keratometry, axial length, ACD and lens thickness (LT). The repeatability of these measurements has been assessed, and the 95% confidence interval for measurements repeated on two (Rudnicka et al., 1992b; Zadnik et al., 1992) to five (Butcher and O'Brien, 1991) occasions were found to be: subjective refraction +/- 0.63D (Zadnik et al., 1992), keratometry +/- 0.93D (Zadnik et al., 1992) and +/- 0.48 D (Butcher and O'Brien, 1991), axial length +/- 0.18 mm (Rudnicka et al., 1992b) and +/- 0.35 (Butcher and O'Brien, 1991), ACD (contact probe) +/- 0.29 mm (Zadnik et al., 1992) and +/- 0.12 mm (Rudnicka et al., 1992b), and LT +/- 0.20 mm (Zadnik et al., 1992) and +/- 0.12 mm (Rudnicka et al., 1992b). However, estimations of repeatability tell us nothing of accuracy, and it is possible for 'off-set' errors to occur. The keratometer is simply calibrated with a sphere of known curvature. Off-set errors are unlikely to occur, provided the equipment has been correctly calibrated for the user, though subsequent calculation of equivalent corneal power varies from instrument to instrument (Olsen, 1986). Off-set errors are also unlikely to occur in measurement of subjective refraction in the presbyopic age group. Refraction measurement error is minimised by the HRT because refraction does not have to be measured separately (it is taken from the divergence of the laser beam required to obtain the image).

The measurement is also in the plane of the optic disc, rather than the fovea, as in subjective refraction.

Ultrasound measurements of the ACD, LT and axial length are more difficult to validate. Comparison of ACD measurements with a contact ultrasound probe with those using an immersion technique (Schelenz and Kammann, 1989) found the contact technique to measure an average of about 0.3 mm shorter than the immersion, which in turn has been found to give very similar measurements to optical methods (Jansson, 1963). Contact ultrasound measurements of ACD have recently been shown to underestimate optical measurements by a mean 0.16mm (Foster et al., 1997). This is in broad agreement with the findings in this study. Similarly, contact methods give shorter axial length measurements than immersion methods by 0.14 mm to 0.28 mm (Schelenz and Kammann, 1989; Shammas, 1984; Olsen and Nielsen, 1989).

The accuracy of ultrasound biometry and keratometry, and the optical assumptions made, are tested in everyday clinical practice, in the form of predicting intra-ocular lens power for cataract surgery. A theoretical model (Olsen, 1987) has been evaluated. This model makes the same assumptions for corneal power calculation as are made in this study and assumes the same refractive index of aqueous and vitreous humour. It was found that, once corrections were made for the position of the intraocular implant (postoperative ACD), the mean error in postoperative refraction could be accounted for by underestimation of the axial length using a contact ultrasound probe (Olsen et al., 1989; Olsen et al., 1990). The underestimation, of 0.16 mm to about 0.30 mm, is consistent with anterior chamber shallowing, caused by the contact ultrasound probe. We therefore recalculated the ocular magnification for the data sets using the optical ACD (with an equivalent adjustment to the axial length). Results are shown in Table 3-3 and Table 3-4.

The overall accuracy of the method can be deduced from the postoperative refraction results of cataract surgery, once the axial length off-set error (contact probe) correction has been made (Olsen et al., 1989; Olsen, 1992; Olsen et al., 1995). The standard deviation of postoperative refractions is up to 0.87 D, so that 95% of results should fall within 1.70 D. This represents about 2.8% of the average refractive power of the eye.

#### 3.2.1.1.5.3 Comparison with previous reports

Mansour (1990) and Jonas et al. (1988d) found Littmann's method L1 to overestimate method L2 by a mean 3.6% and 3% respectively. This compares with 1.1 to 4.2% in the same direction for our data sets. Barr (1995) made a theoretical assessment of the accuracy of the Littmann method (L2). He found that, within the range of +/- 4 D ametropia, the mean error was +3.3% and the error increased with hypermetropia. The result is similar to that found in the real eyes of our data sets with a mean error of +1.5 to 2.7%, and with larger errors in eyes with shorter axial lengths.

Mansour (1990) found measurements by method L1 to be larger than those by BK2 by 0.9 % +/- 2.2%, which compares to a mean difference in this study of 2.6 to 2.9% in the same direction. The explanation for this is the difference in the assumed 'normal' power of the eye in the methods, 58.64

D for L1 and 60.00 D for BK2 (a difference of 2.3%). Like Bengtsson and Krakau (1992) we found no mean difference between the methods L1 and BK3.

### 3.2.1.1.6 Appendix

Derivation of the New Method

$K' = F_e + A$ ($F_e$ = refractive power of the eye, A = ametropia /principal point refraction)

$q = 17.455/K'$, and $K' = 17.455/q$

therefore, $17.455 /q = F_e + A$

$F_e = F_1 + F_L - [(w/n).F_1.F_L]$ ($F_1$ = refractive power of the cornea, $F_L$ = equivalent power of the crystalline lens) (Bennett, 1988)

$F_1 = 331.5/ r_1$ ($r_1$= radius of curvature of the anterior surface of the cornea)(Olsen, 1986)

$F_L = 21.76$ dioptres (constant taken from the Gullstrand-Emsley schematic eye)

$w/n = 0.0043$ (constant taken from the Gullstrand-Emsley schematic eye)

substituting $F_L$ and w/n,

$F_e = F_1 + 21.76 - [(0.0043).F_1.(21.76)] = F_1 + 21.76 - (0.094.F_1) = (0.906).F_1 + 21.76$

substituting $F_1$,

$F_e = (0.906).( 331.5/ r_1) + 21.76 = (300.3/ r_1) + 21.76$

Therefore, $K' = (300.3/ r_1) + 21.76 + A$

and $17.455/q = (300.3/ r_1) + 21.76 + A$

$1/q = (17.21 / r_1) + 1.247 + (A / 17.455)$

#### 3.2.1.1.6.1 Comment

Bengtsson (1999) commented that the new method described assumes that the refraction, the power of the lens, and the power of the cornea are all independent (uncorrelated) variables. He suggested that, because the variance of the lens power was almost the same as the variance of the total power of the eye, the power of the lens and the power of the cornea must be negatively correlated.

The new method does make this assumption. Linear regression analysis of data pooled from our 3 patient groups (209 eyes) confirms this (Figure 3-4, significance of regression p = 0.21) and the finding is consistent with previous reports (van Alphen, 1961). The power of the lens and the power of the cornea are also unrelated to refractive error.

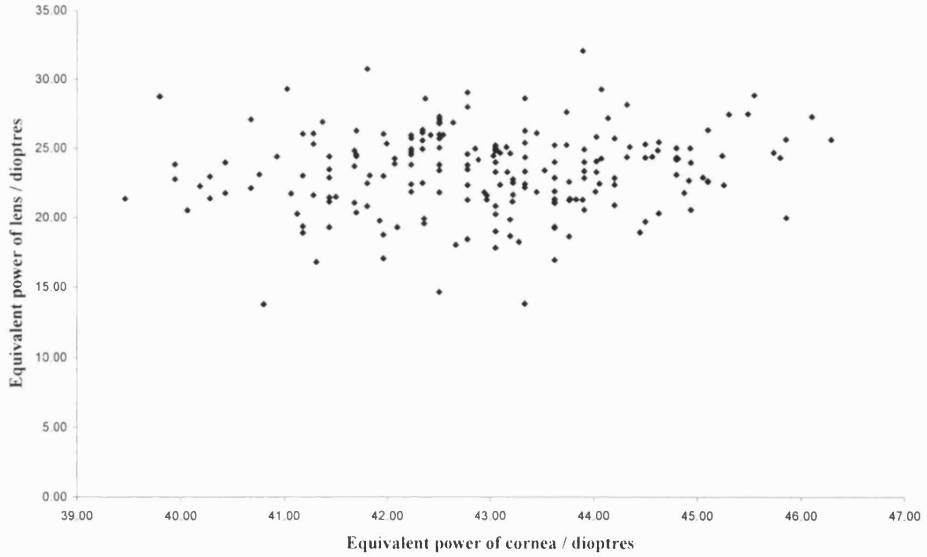


**Figure 3-4. Plot of the equivalent power of the lens against equivalent power of the cornea (all eyes)**

The refractive power of the eye depends on the refractive power of the cornea, the equivalent power of the crystalline lens, and the distance between the two ($F_e = F_1 + F_L - [(w/n).F_1.F_L]$, where $F_e$ = refractive power of the eye, $F_1$ = refractive power of the cornea, $F_L$ = equivalent power of the crystalline lens, and w/n is a function of the distance of the crystalline lens from the cornea) (Bennett, 1988). If 2 random variables are added to produce an outcome, then the variance of the outcome is the sum of the variance of those variables if they are independent (if there is a degree of positive correlation, the variance is higher than the sum, and if there is a degree of negative correlation, the variance is lower than the sum) (Bland, 1995c). Bengtsson pointed out that the variance of the lens power is almost the same as the variance of the total power of the eye, and concludes that the power of the lens and cornea must be negatively correlated. There are, however, three variables that contribute to the equivalent power of the eye, the third variable being the term $[(w/n).F_1.F_L]$. Table 3-6 summarises the means and standard deviations for each variable in the pooled data.

| | Mean (dioptres) | Standard deviation (dioptres) |
|---|---|---|
| Refractive power of cornea | 43.00 | 1.41 |
| Equivalent power of lens | 23.33 | 2.94 |
| $[(w/n).F_1.F_L]$ | 4.49 | 0.58 |
| Refractive power of the eye | 61.84 | 2.87 |

**Table 3-6. Means and standard deviation for the variables in the equation to calculate ocular magnification (new method).**

The term $[(w/n).F_1.F_L]$ is highly positively correlated with the power of the lens ($r^2 = 0.73$, $p < 0.000$) and less so with the power of the cornea ($r^2 = 0.32$, $p < 0.000$). Since this term is subtracted from the other two, it will tend to decrease the overall variance. This partly explains why the variance of the refractive power of the eye is lower than the sum of the variance of lens and corneal powers.

In order to maintain emmetropia in an eye, variables such as corneal power, lens power, and axial length have to be balanced. The relationship between corneal power and lens power is modified by axial length.

Both corneal power and lens power are negatively correlated with axial length ($r^2 = 0.17$, $p < 0.000$ and $r^2 = 0.36$, $p < 0.000$ respectively), so that both corneal power and lens power decrease with increasing axial length. One might therefore expect corneal power and lens power to be positively correlated. However, if axial length is constant, corneal power and lens power have to be negatively correlated to maintain emmetropia. Figure 3-5 plots lens power against corneal power for the 48 eyes from our combined data set that have an axial length between 23.0 and 23.5mm.

There is a significant negative correlation ($r^2 = 0.26$, $p < 0.000$) between lens and corneal power in this group with relatively constant axial length.

This modifying effect of axial length accounts for the lack of correlation between corneal power and lens power in the pooled data (all axial lengths).

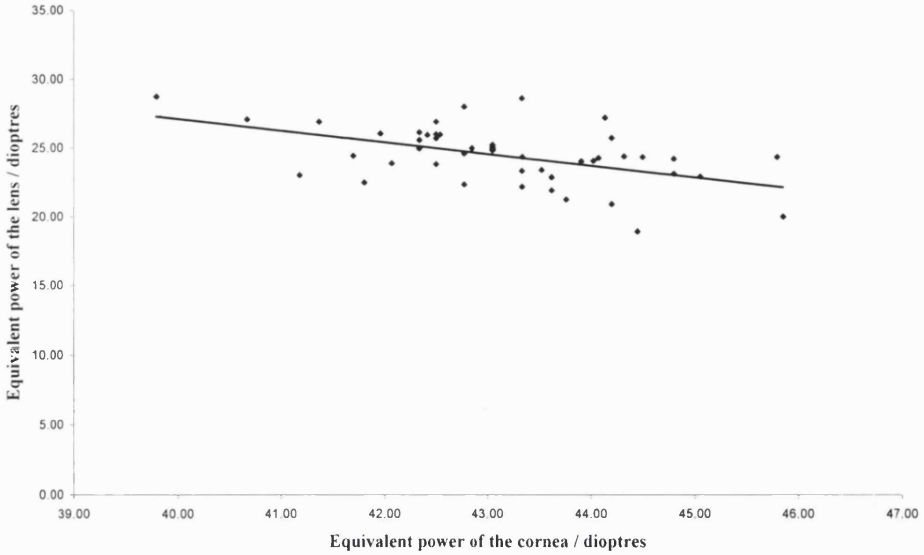


Figure 3-5. Plot of equivalent power of the lens against equivalent power of the cornea in eyes with an axial length of 23.0 to 23.5mm.

### 3.2.1.2 Camera magnification corrections

Canon CF60-U and Heidelberg retina tomograph (HRT)

#### 3.2.1.2.1 Background

The magnification characteristics of fundus imaging instruments need to be established in order to convert the image size of a fundus feature (on film or digital) to the real size (Bengtsson and Krakau, 1977; Rudnicka et al., 1998). The principles of ocular and camera magnification are covered in section 2.4.2. Camera magnification (°/mm on film, or °/pixel) can be established by imaging a target of known size at the 'fundus' of a model eye, the dimensions and optics of which are known (Rudnicka et al., 1992a).

#### 3.2.1.2.2 Purpose

The purpose of this study was to confirm the magnification characteristics of the camera (Canon CF60-U) and HRT used in the studies in this thesis.

#### 3.2.1.2.3 Methods

A model eye was constructed in the workshop of the Institute of Ophthalmology (London) according to the dimensions given by Rudnicka et al. (1992a). Briefly, the refractive system of this eye consists of a 'cornea' and a 'lens' of 43.90D and 20.81D power respectively. The object that is imaged at the 'fundus' is 1.78mm diameter circular target. The 'fundus' is curved with a radius of curvature 11.5mm. The space between the 'cornea' and the 'fundus' is filled with water. The 'fundus' is attached to the barrel of a screw gauge micrometer and so that the axial length of the eye (and refractive error) can be changed by rotating the micrometer screw (the 'fundus' and the target rotate with the micrometer). The micrometer readings that correspond to the different refractive states of the model eye are known.

The target was imaged with the Canon camera and HRT (10° field of view) with the model eye set at refractive errors ranging from –10D to +10D. The imaging distance (model eye 'cornea' to camera objective lens) was set according to the manufacturers' recommendations.

The camera/HRT magnification was calculated in the following ways:

Camera – photographs were digitised and analysed by computer-assisted planimetry using image analysis software (Lucida 2.0, Kinetic Imaging Ltd, U.K.). The size of the target on the film, in millimetres, was calculated. The camera magnification 'p' may be calculated from the equation $t = p.q.s$ (see section 2.4.2). 't' is the true size of the target (1.78mm), 'q' is the magnification of the model eye (known for each axial length/refractive error setting) and 's' is the size of the image (measured in this study). 'p' is then plotted against the refractive error of the model eye, for each determination of 'p', to examine the telecentricity of the camera.

HRT – the HRT software (version 1.11) 'distance measure' tool in the 'interactive measurement' menu was used to measure the horizontal and vertical target diameter at each axial length/refractive error setting. The value for 'q' calculated by the HRT software, at each axial length/refractive error setting, was determined from the equation given in section 3.2.1.1.6. The value for 't' given by the HRT software (by the 'distance measure' tool) was then corrected for the difference between the value for 'q' calculated by the HRT software and the known value of 'q' for the model eye at each axial length/refractive error setting, i.e. 't' multiplied by (model eye 'q'/HRT 'q').

#### 3.2.1.2.4 Results

##### 3.2.1.2.4.1 Canon CF60-U

The calculated value for 'p' was 0.971 + (0.012 * ametropia), where ametropia refers to the refractive error of the eye photographed.

##### 3.2.1.2.4.2 HRT

The corrected measurements of 't' averaged 1.78mm. The average (horizontal/vertical) corrected measurements did not vary with the refractive error of the model eye. The ratio of vertical to horizontal measurements varied from 1.03 to 1.07 across the range of measurements, with a mean 1.05.

#### 3.2.1.2.5 Discussion

The results confirm that the Canon camera is not telecentric. The camera magnification (and field of view) varies slightly (1.2% per dioptre) with the refractive error of the eye being photographed.
The results confirm that the HRT is telecentric, and the HRT 'camera' magnification assumed by the HRT software was verified. This is consistent with 0.039°/pixel (256 pixels at a field of view of 10°). However, there was a slight distortion of the image in this particular instrument, such that the vertical measurements were 5% greater than horizontal measurements. As the mean of the two was correct (the same as the known target size), the distortion has no effect on the measurements of area. These findings are consistent with recently published data (Rudnicka et al., 1998).

### 3.2.2 Distinguishing between normal and glaucomatous eyes – scanning laser ophthalmoscopy

#### 3.2.2.1 Background

The advent of scanning laser ophthalmoscopes as optic disc imaging tools has brought the prospect of greater objectivity in the description of disc topography. The Heidelberg Retina Tomograph (HRT) (Rohrschneider et al., 1994; Chauhan et al., 1994; Janknecht and Funk, 1994; Zangwill et al., 1995) and its predecessor, the Laser Tomographic Scanner (Weinreb et al., 1989; Kruse et al., 1989; Weinreb and Dreher, 1990; Dreher et al., 1991; Rohrschneider et al., 1993), are confocal scanning laser ophthalmoscopes, which enable highly reproducible measurement of the three-dimensional ONH structure. The theoretical basis for the tomographic reconstruction of the ONH surface, and the software algorithms employed to derive parameters such as neuroretinal rim areas and volumes, are described in section 2.4.1.

#### 3.2.2.2 Purpose

The aim of this study was to define the HRT parameters that best separate patients with early glaucomatous visual field loss from normal subjects. A previous study, using planimetry as the method to quantify the optic disc morphometry, identified that the measurement of the neuroretinal rim area in several disc sectors, and allowing for the size of the optic disc, enabled discrimination between normal and glaucomatous eyes with a sensitivity and specificity greater than any previously published study (Garway-Heath and Hitchings, 1998a). The aim of this study was also to evaluate the applicability of this method of data analysis to ONH measurements with the HRT.

#### 3.2.2.3 Methods

##### 3.2.2.3.1 Subjects

Two groups of subjects, normal controls and patients with early glaucomatous field defects, were recruited prospectively as part of a study on the early detection of glaucoma. All subjects gave informed consent to the investigations performed, and each had the following: medical and ocular history, slit-lamp biomicroscopy, tonometry, fundus examination, visual field testing, optic disc photography and imaging with the HRT.

.

Normal subjects. Normal subjects were recruited prospectively as part of a study on the treatment of ocular hypertensive patients and the early detection of glaucoma. Subjects recruited were friends or spouses of patients attending the Ocular Hypertension Clinic at Moorfields Eye Hospital (n = 38), Hospital staff (n = 16), or volunteers responding to advertisements on the Hospital notice boards and in a pensioners' magazine (n = 26). Restriction criteria were: Caucasian ethnic group, ametropia < 6 dioptres, visual acuity of 20/30 or better, normal visual fields, intraocular pressure of < 21

mmHg, no previous ocular history involving the posterior segment, and no family history of glaucoma involving a first degree relative. All subjects performing a normal field test were included irrespective of optic disc appearance. One eye was included in the study, chosen at random if both were eligible.

Glaucoma patients. Subjects were taken from the hospital's general glaucoma clinic (n = 37) and from the ocular hypertension clinic (n = 14 ). The former group was referred to the study on the basis of visual field defect and ocular hypertension only and the latter group were patients with ocular hypertension who developed reproducible visual field defects while under review. Restriction criteria were: Caucasian ethnic group, ametropia < 6 dioptres, visual acuity of 20/30 or better, a visual field defect reproduced on at least three successive occasions, open anterior chamber angle, intraocular pressure > 21 mmHg at diagnosis and no other posterior segment eye disease. One eye was included in the study, chosen at random if both were eligible.

The optic disc appearance did not form part of the inclusion criteria in either group (Garway-Heath and Hitchings, 1998b).

#### 3.2.2.3.2 Visual Field Testing

All visual field testing was performed with the Humphrey Field Analyser 24-2 program. Reliability criteria applied were: fixation losses < 30%, false positive responses < 15%, and false negative responses < 30%.

A normal visual field was taken to be one in which the retinal sensitivity at all locations was better than the eccentricity-related thresholds given in the Advanced Glaucoma Intervention Study (AGIS) protocol (Gaasterland et al., 1994).

A glaucomatous visual field was taken to be one in which a defect was reproduced on three successive occasions at the same location. Only patients scoring 1 - 5 (early glaucoma) were included (Gaasterland et al., 1994).

Visual fields were assessed by an independent glaucoma expert without access to clinical information, so that optic disc assessment did not form part of the diagnostic criteria.

#### 3.2.2.3.3 Imaging with the scanning laser ophthalmoscope

All the participants were imaged with the HRT (software version 1.11) in the 10 * 10 degree frame. All images were obtained by one of two trained technicians. Imaging was performed at the 1.5 cm imaging head/eye distance recommended in the instruction manual as the subject viewed a distant fixation target. Each patient had 3 high quality scan series recorded at one sitting. The quality of images was assessed with the aid of the HRT software, and by the experience of the technician. The HRT software is able to correct for small eye movements by aligning consecutive images within a scan series. Scan series with movements occurring within a single image in the series, that caused

distortion of the image which could not be corrected, were excluded from the study. The mean topography of the 3 scan series was used for the analysis.
The contour line of the optic disc edge was drawn by consensus between two observers (Wollstein, Garway-Heath). The standard reference plane was employed and the following parameters were analysed: optic disc area, cup area, cup volume, cup/disc area ratio, rim area, rim volume, cup shape measure, height variation contour, mean RNFL thickness, and RNFL cross-sectional area. Each parameter was calculated for the whole disc (global) and in the 6 pre-defined segments: temporal, temporal superior, temporal inferior, nasal, nasal superior and nasal inferior.

#### 3.2.2.3.4 Statistical analysis

The software SPSS for Windows, version 6.1, was used to perform the statistical analysis. Histogram plots were used to evaluate the distribution of the data and if they were normally distributed a student t-test was used for hypothesis testing. Defining the upper and lower limits of normal by mean $\pm$ 1.96 * standard deviation (SD), for each of the parameters, we calculated the sensitivity as the percentage of the patients lying outside the normal limits. If data distribution was not normal, the non-parametric Mann-Whitney U-test was employed. For those parameters, the normal limits were defined using the 2.5 and 97.5 percentiles as the cut-off points.
In order to determine which of the parameters measured by the HRT were related to disc size, linear regression was performed between the optic disc area (as independent variable) and each of the parameters (as dependent variables) from the data derived from the normal control subjects. Where the variability (scatter) of the dependent variable about the regression line is related to the size of that variable, log transformation of the dependent variable has been performed (Bland, 1995a).
A significant relationship was taken to be one in which the $p < 0.05$ and the R square value $> 0.1$. For those parameters found to vary with disc size, the normal ranges for each was defined by the 99% prediction intervals from the regression analysis. The 99% prediction interval was chosen to enable us to develop an analysis method that is of the greatest use clinically for the detection of glaucoma cases, and given that glaucoma is considerably less common than non-glaucoma, it is desirable to have a high test specificity.
Each parameter was also evaluated in relation to age. For those parameters found to be significantly dependent on age ($p < 0.05$), the age was included in the equation of the prediction intervals.
Regression analysis was performed as follows. Linear, quadratic and cubic regression equations were fitted. Non-linearity was tested by the difference between the sum of squares due to the quadratic or cubic equation and the sum of squares due to the linear equation (Bland, 1995b). No evidence for non-linearity for any of the relationships was found. Multiple linear regression was then performed. Univariate models were fitted first. Factors found to be statistically significant (at the 5% level) associated with the output variable and which accounted for greater than 10% of the variability in the output variable (i.e. R square $> 0.1$) were then fitted in the multivariate model.

Optic discs of controls and patients were labelled as abnormal if a parameter for the whole disc or any one of the predefined segments was found to be outside the defined normal range. With these results, specificity and sensitivity for each parameter was calculated.

### 3.2.2.4 Results

Eighty normal subjects and 51 early glaucoma patients were enrolled in the study.
The characteristics of the study population are summarised in Table 3-7.

| | Control subjects (mean ± standard deviation) | Glaucoma patients (mean ± standard deviation) | Difference (p value[1]) |
|---|---|---|---|
| Age / years | 57.2 ± 12.2 | 65.1 ± 10.1 | 0.04 |
| Male sex / % | 50 | 69 | 0.01 |
| Right eyes / % | 49 | 43 | 0.25 |
| Refraction / D | -0.05 ± 1.93 | 0.40 ± 1.63 | 0.89 |
| Keratometry / mm | 7.80 ± 0.29 | 7.77 ± 0.23 | 0.13 |
| Visual field MD / dB | 0.08 ± 1.00 | -3.62 ± 1.69 | 0.00 |

(D = dioptres, mm = millimetres, MD = mean deviation, dB = decibels, [1] = Student t-test)

**Table 3-7. Characteristics of the study population**

The mean standard deviation for the height values of the 3 HRT images, comprising the mean topographic image, were 28.3 microns for the normal group and 31.3 for the early glaucoma group ($p = 0.32$).
The group means for the global disc parameters are summarised Table 3-8. All the parameters were found to be significantly different ($p < 0.05$) between the two groups except the optic disc area.

| Parameter | Normal subjects (mean ± standard deviation) | Glaucoma patients (mean ± standard deviation) | Difference (p value[1]) |
|---|---|---|---|
| Optic disc area | 1.98 ± 0.35 | 1.89 ± 0.34 | 0.16 |
| Neuroretinal rim area | 1.55 ± 0.30 | 0.98 ± 0.23 | <0.00 |
| Neuroretinal rim volume | 0.40 ± 0.14 | 0.19 ± 0.08 | <0.00 |
| Cup area | 0.44 ± 0.29 | 0.91 ± 0.37 | <0.00 |
| Cup volume | 0.09 ± 0.09 | 0.29 ± 0.20 | <0.00[2] |
| Cup/disc area ratio | 0.21 ± 0.12 | 0.47 ± 0.14 | <0.00 |
| Mean RNFL thickness | 0.24 ± 0.06 | 0.17 ± 0.06 | <0.00 |
| RNFL cross sectional area | 1.17 ± 0.29 | 0.82 ± 0.28 | <0.00 |
| Height variation contour | 0.37 ± 0.08 | 0.31 ± 0.08 | <0.00 |
| Cup shape measure | -0.19 ± 0.07 | -0.10 ± 0.07 | <0.00 |

(RNFL = retinal nerve fibre layer, [1]Student T-test, [2]Mann-Whitney U-test)

**Table 3-8. Mean and standard deviations of the ONH parameters for normal subjects and early glaucoma patients**

The range of values of neuroretinal rim area increases as the value of the rim area itself increases, for the whole disc and for the predefined segments, thus log transformation was employed for this parameter.

Using multiple linear regression, we calculated the relationship between the total neuroretinal rim area and the following parameters: sex ($p = 0.24$), eye side ($p = 0.79$), refractive error ($p = 0.65$), keratometry ($p = 0.48$) and disc area ($p < 0.000$). The neuroretinal rim area, log of neuroretinal rim area and cup area in the global disc measures, the temporal segment and the temporal superior segment were found to be dependent on age ($p < 0.05$). No age affect was demonstrated for other parameters. Linear regression analyses between the optic disc area and each parameter are summarised in Table 3-9.

| Parameter | $R^2$ value | p value |
|---|---|---|
| Cup area | 0.36 | <0.01 |
| Neuroretinal rim area | 0.30 | <0.01 |
| Cup volume | 0.27 | <0.01 |
| Cup/disc area ratio | 0.18 | <0.01 |
| Cup shape measure | 0.10 | <0.01 |

**Table 3-9. Coefficient of determination for HRT parameters dependent on the optic disc area**

The regression equation for the rim area was: rim area = 1.021 + 0.443 * disc area - 0.006 * age.
The sensitivity and specificity to identify glaucomatous discs, using the global parameters only, was calculated using the disc size specific (linear regression) and the non disc size specific (mean ± 1.96 * SD) cut-offs.
The specificity and sensitivity for the global disc parameters was calculated for the following: log rim area, cup/disc area ratio, cup volume, cup area and cup shape measure. A parameter value lying outside the 99% prediction interval derived from the normal group labels the eye as abnormal. The specificity and the sensitivity were then calculated. The highest specificity and sensitivity were for the log of the neuroretinal rim area (98.8% and 47.1%, respectively) followed by the cup/disc area ratio (98.8%, 43.1%) and the cup volume (98.9%, 41.2%).
By defining the cut-off point as mean global result ± 1.96 * SD, the highest sensitivity values were for the log of the neuroretinal rim area (66.7%), cup/disc area ratio (52.9%) and the cup area (37.3%).
The same statistical analysis was used for each of the predefined segments. The cut-off defined by the 99% prediction interval from the linear regression between the segmental optic disc area and the various parameters gave the following results. The best separation between groups was given by the log of the neuroretinal rim area in the temporal inferior segment (specificity 100%, sensitivity 62.7%), the nasal inferior segment (specificity 98.8% sensitivity 54.9%), and cup/disc area ratio in the temporal inferior segment (specificity 100%, sensitivity 51.0%). The segment with the lowest sensitivity to detect the glaucomatous changes is the nasal segment (23.5%) followed by the temporal segment (27.5%).
Figure 3-6 illustrates the method of using linear regression between the optic disc area and log of the rim area in the temporal inferior segment.

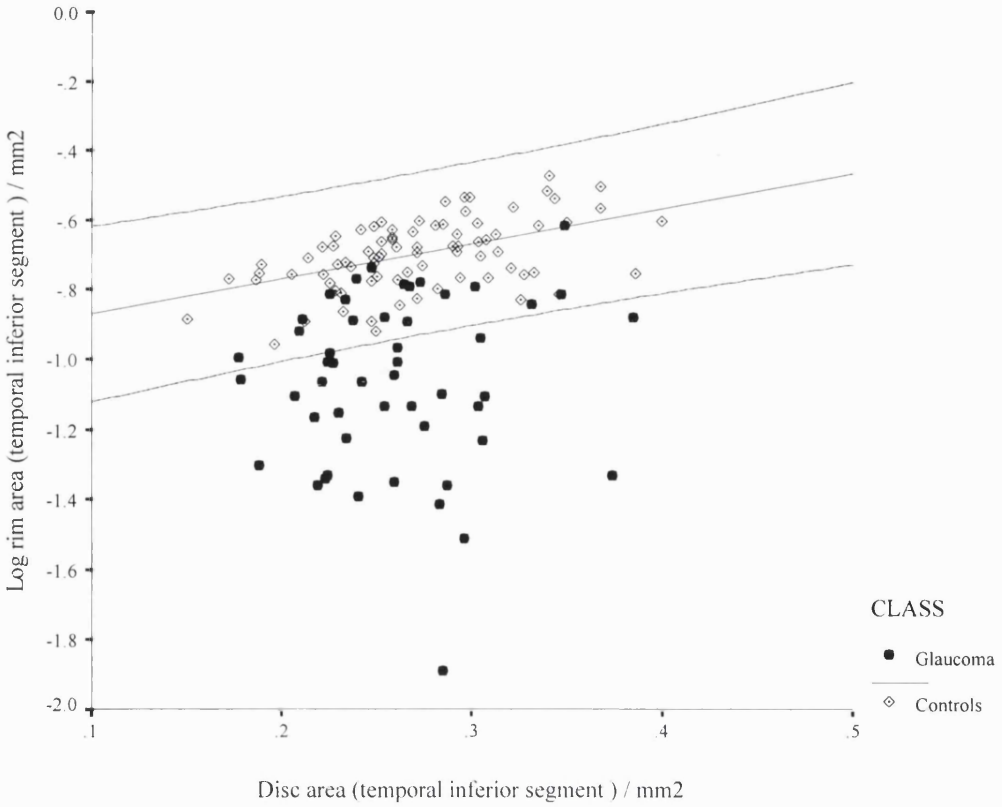


**Figure 3-6. Scatter plot between optic disc area and log neuroretinal rim area in the temporal inferior segment. The lines represent the 99% prediction interval of the normal group. Patients and normal subjects lying outside the 99% prediction interval were labelled as 'abnormal'.**

We reassessed the sensitivity of each parameter to detect the glaucomatous changes after dividing the glaucoma group into those taken from the glaucoma clinic and those who were originally diagnosed as OHT patients (converters). The pattern of abnormal segments for the clinic and 'converter' groups, respectively, was: global 45.9% and 50.0%, temporal inferior 67.6% and 50.0%, temporal superior 35.1% and 50.0%, and nasal inferior 54.1% and 57.1%. The differences between the glaucoma sub-groups were not found to be statistically significant.

The cut-off defined by the mean segmental results ± 1.96 * SD gave the following results. The highest sensitivity was found for cup/disc area ratio in the temporal inferior segment (66.7%), log of the rim area in the temporal inferior segment (66.7%) and cup/disc area ratio in the nasal inferior segment (54.9%).

Labelling the optic discs of the normal subjects and the early glaucoma patients as 'abnormal' if the global parameter or any one of the predefined segments was found to be outside the normal range (99% prediction interval), the highest specificity and sensitivity was found for the log of the rim area and the cup/disc area ratio. The results are summarised in Table 3-10.

| Parameter | Linear regression | | Mean ± 1.96 SD | |
|---|---|---|---|---|
| | Sensitivity (%) | Specificity (%) | Sensitivity (%) | Specificity (%) |
| Log neuroretinal rim area | 96.3 | 84.3 | 77.5 | 86.3 |
| Cup/disc area ratio | 97.5 | 74.5 | 83.8 | 82.4 |
| Cup area | 97.5 | 58.8 | 86.3 | 58.8 |
| Cup volume | 92.5 | 58.8 | 95.0[1] | 52.9[1] |
| Cup shape measure | 96.3 | 41.2 | 70.0 | 68.6 |

(SD = standard deviation, [1]cut-off point percentile 97.5, Linear regression method: cut-off is the lower 99% prediction interval of the regression between optic disc area and the parameter. Mean ± 1.96 SD method: cut-off is the mean parameter value minus 1.96 * SD)

**Table 3-10. Specificity and sensitivity of various parameters to distinguish between normal and glaucomatous eyes.**

### 3.2.2.5 Discussion

The HRT generates a large number of measurement parameters. Several authors have looked at these parameters in detail to determine which are of use to distinguish between normal and glaucomatous optic discs. Various approaches to data analysis have been taken, such as the generation a discriminant function from the normal and glaucomatous groups (Mikelberg et al., 1995; Iester et al., 1997b; Bathija et al., 1998; Uchida et al., 1996) and a comparison of the contour of the peripapillary surface (Caprioli et al., 1998). In such studies, it is important to take account of the severity of disease in the glaucoma group, and also the method by which the normal and glaucomatous eyes were selected. Some studies required the appearance of the ONH to be consistent with the diagnosis (normal or glaucoma) (Uchida et al., 1996; Bathija et al., 1998), whereas others specifically exclude ONH appearance as a restriction criterion (Mikelberg et al., 1995; Iester et al., 1997b). Requiring a certain appearance of the ONH at the outset of a study will obviously bias the outcome (Garway-Heath and Hitchings, 1998b). The studies that differentiate between normal and glaucoma subjects by means of a discriminant function are particularly vulnerable to this type of bias. Table 3-11 summarises the results of the studies that have reported sensitivity and specificity values.

| | Specificity (%) | Sensitivity (%) | Visual field MD (dB) |
|---|---|---|---|
| Mikelberg et al (1995) | 84 | 87 | -5.53 |
| Iester et al (1997b) | 88 | 74 | -8.33 |
| Bathija et al (1998) | 94 | 62 | <-10.00 |
| Uchida et al (1996) | 92 | 91 | -4.80 |
| Caprioli et al (1998) | 85 | 83 | -4.80 |

(MD = mean deviation, dB = decibel)

**Table 3-11. Reported sensitivity and specificity to distinguish normal from glaucomatous optic discs in several studies.**

In this study, we applied to the HRT data the method of analysis developed for planimetry (Garway-Heath and Hitchings, 1998a). If the global value alone is considered for any one parameter the sensitivity to identify a disc as abnormal is relatively low (47.1%, with a specificity of 98.8%). However, if disc segments are considered, the specificity and sensitivity (96.3% and 84.3%, respectively) is better than that reported in the other studies, despite the lesser degree of visual field loss (-3.62dB). Because the early glaucomatous changes in the optic disc can appear as a global change or as a localised defect in the various segments, the sensitivity of the assessment of either the whole disc or any individual segment alone is relatively low and it is not useful for clinical purposes. In defining the optic disc as 'abnormal' if the global parameter or any one of the predefined segments were outside the normal limits, we took into account the different modes of the early glaucomatous change and thus the sensitivity to detect early glaucomatous change was improved. Figure 3-7 and Figure 3-8 demonstrate the usefulness of this method to distinguish between normal discs and those with early glaucomatous changes.

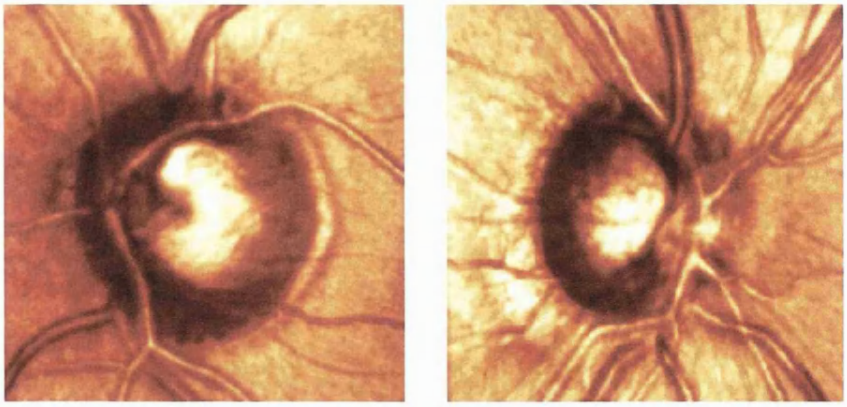

**Figure 3-7. HRT images of two participants of the study with similar cupping of the optic nerve head.**

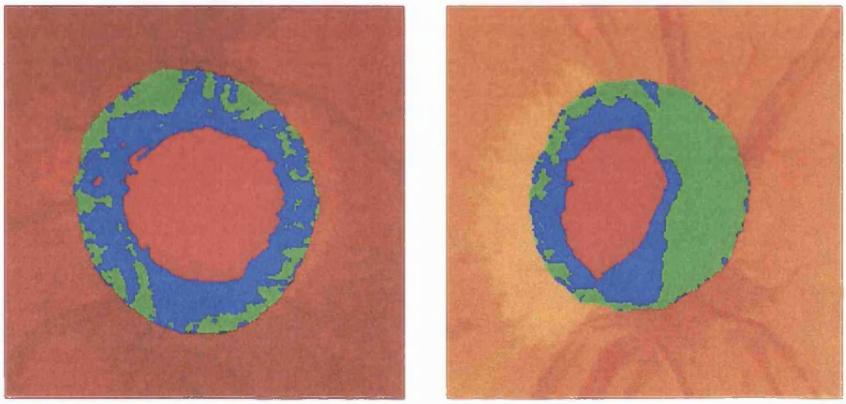

**Figure 3-8. HRT images from the same participants as in Figure 3-7, after analysis. The central coloured areas represent the optic cup (red) and NRR (blue and green). The linear regression technique correctly identifies the left image as a normal optic nerve head and the right image as an optic nerve head with early glaucomatous changes.**

Table 3-10 demonstrates the improvement in the specificity and sensitivity when disc size is taken into account, compared to a technique using mean parameter value ± 1.96 * SD as the cut-off point. It is interesting to note in the study of Uchida et al. (1996), in which a specificity of 93% and sensitivity of 77% was reported for the global cup/disc area ratio, that the disc area of the glaucoma group was larger than that of the control group. We have demonstrated in this study that cup/disc area ratio varies with disc size in the control group. Similarly, the cup shape measure, found by Uchida to have the greatest diagnostic precision of any single parameter, is likewise related to disc size. The relationship between parameter and disc size may account for Uchida's findings. The study by Mikelberg et al. (1995), in which field loss in the glaucoma group was slightly more advanced than in this study, reported a specificity of 78% and a sensitivity of 89% using the cup shape measure and the maximal depth parameters.

In this study, the segment with the highest sensitivity to detect early glaucomatous change, in each of the parameters, was the temporal inferior segment followed by the nasal inferior. Glaucomatous changes in the optic nerve head have been said to occur earliest in the infero-temporal segment (Tuulonen and Airaksinen, 1991; Jonas et al., 1993) though the nasal inferior segment has not previously been found to be the next most sensitive. This may be due to differences in the definition of the segments. The finding of preferential loss in the infero-temporal segment may arise by bias in the selection of the patients studied (Garway-Heath and Hitchings, 1998b).

The slope of the regression line between the neuroretinal rim area and disc area in the control group in this study was 0.44 (SE = 0.079). This slope represents the increase of the rim area with the increase of the disc area and is similar to previous data (range of 0.30-0.58) obtained using other imaging and measurement techniques (Britton et al., 1987; Jonas et al., 1988g; Montgomery, 1993). The finding that there is a reduction in neuroretinal rim area with increasing age in the control group is discussed fully elsewhere (Garway-Heath et al., 1997).

The normal data from this study appears similar to those from other studies (Mikelberg et al., 1995; Zangwill et al., 1996; Uchida et al., 1996) so it might be expected that the results of this study may be applicable to other clinical populations. However, this needs formal study.

The normal ranges were derived from the control group only, and this approach may, therefore, be more robust than a function derived from a discriminant analysis. The control group in this study comprised a relatively small number of Caucasian volunteers. Further validation on a larger, population based study group, and including other ethnic groups, is planned.

The normal data have been derived from a single, well-defined, population and tested on a patient group from a similar population. In addition, the images were analysed (ONH margin drawn) by the same clinicians. The ability of the normal ranges from this study to distinguish between normal subjects and glaucoma patients from other populations may be less good, and needs to be established. A preliminary study of data from another centre (Heidelberg, Germany – personal communication, Gerhard Zinser) suggests that the method may be applicable to Caucasian populations elsewhere. The method of analysis (and normal ranges derived from the Moorfields data set) was applied to 33 normal eyes and 48 eyes with visual field loss <10dB (mean 5.3dB). The specificity and sensitivity was 93.9% and 85.4% respectively.

## 3.3 Measurement of ganglion cell function: the physiological relationship between light sensitivity and ganglion cell numbers

### 3.3.1 Background

Differential light sensitivity (DLS) is the ratio of background luminance ($L_b$) to target luminance (L) at threshold (i.e. DLS = $L_b/L$). The process underlying the loss in DLS in glaucoma is retinal ganglion cell loss (Quigley et al., 1982; Kendell et al., 1995). In most clinical practices, perimetry is the only method available to objectively quantify the amount of optic nerve damage. The relationship between ganglion cell numbers and DLS is, therefore, of fundamental importance in assessment of the severity of the neuropathy and of disease progression. Summary indices derived from perimetry are used to quantify the extent of glaucomatous optic neuropathy (Asman et al., 1992; Gaasterland et al., 1994) and inferences about the pathogenesis of the condition are made from the observed pattern of visual field defects (Quigley and Addicks, 1981; Caprioli et al., 1987; Heijl and Lundqvist, 1984; Emdadi et al., 1998). Disease progression may be estimated from analyses of serial field tests, either by clinical impression, or by more quantitative means (Viswanathan et al., 1997; Wild et al., 1997; Nouri-Mahdavi et al., 1997).

Direct measurement of ganglion cell numbers during life is not yet possible, and surrogates, such as the area of the neuroretinal rim at the optic nerve head, are used. The neuroretinal rim area is a measurement of a cross-section, of variable obliquity, of the retinal nerve fibres, supporting glia and blood vessels in the ONH, and as such is proportional to the numbers of retinal nerve fibres (Yucel et al., 1998). Studies relating structural to functional measures in glaucoma frequently demonstrate a non-linear relationship between neuroretinal rim area and dB DLS (Airaksinen and Drance, 1985; Jonas and Grundler, 1997). This observation is supported by a recent study of experimental glaucoma in rhesus monkeys in which ganglion cell loss, measured histologically, was correlated with DLS, measured by behavioral perimetry. The relationship between percentage ganglion cell loss and dB DLS sensitivity loss was shown to be curvilinear (Harwerth et al., 1999). A post mortem study of human glaucomatous eyes compared the number of remaining ganglion cells to dB sensitivity loss in three eyes (Quigley et al., 1989). The results suggested that more ganglion cells have to be lost in the central field than in the peripheral field for equivalent sensitivity loss. These observations suggest that the relationship between ganglion cell numbers and DLS may not be linear.

Within a small retinal area ('Ricco's area' or 'critical area'), the visual system summates brightness information (spatial summation) so that DLS (the reciprocal of light intensity for threshold detection) is linearly related to the area of the stimulus (Glezer, 1965; Wilson, 1970; Matin, 1975; Scholtes and Bouman, 1977):

$A \sim 1/L$

or, $A = C/L$

(L = luminance, 1/L = differential light sensitivity, A = stimulus area, C = constant)

DLS (1/L) should, therefore, be linearly related to the number of ganglion cell receptive fields in the illuminated area (with a curvilinear relationship between dB DLS [which is 10*log(1/L)] and ganglion cell receptive field numbers). When the retinal area illuminated is larger than the 'critical area', spatial summation is incomplete, and is governed by the relationship (Wilson, 1970; Sloan, 1961; Dannheim and Drance, 1971; Kasai et al., 1992):

$A^k \sim 1/L$

or, $A^k = C/L$

(k = coefficient of summation)

The Goldmann size III target, used in conventional automated perimetry, is larger than the 'critical area' throughout the central 40° (Wilson, 1970), so that there is incomplete spatial summation at all visual field test points. In order to relate the DLS to ganglion cell receptive field numbers, when tested with the size III target, a correction for incomplete spatial summation is needed.

### 3.3.2 Purpose

The aim of this study is to evaluate the relationship between ganglion cell receptive field numbers and DLS for white-on white perimetry with the Goldmann size III target and to test the hypothesis that the target area (A) in the equation $A^k = C/L$ can be represented by the number of underlying ganglion cell receptive fields (G) to give $G^k = C/L$.

### 3.3.3 Methods

In order to test the hypothesis that $G^k = C/L$, the following were established for each Humphrey 30-2 visual field test point for a Goldmann size III target: ganglion cell receptive field numbers (G), average DLS (1/L), and coefficient of summation (k). From these, a value for C was calculated.

Ganglion cell receptive field numbers

This was derived from the ganglion cell density at each test point, after a correction for lateral displacement of ganglion cells from the fovea, and the area of a Goldmann size III target at each test point.

The ganglion cell density was calculated from normative data taken from the literature. Curcio and Allen (1990) reported a topographic ganglion cell density map of the human retina derived from dense sampling of 6 young (mean age 34 years) human retinae of 5 individuals. The paper includes profiles of the ganglion cell density along the vertical and horizontal meridia, in graphical format. A topographic map was reconstructed from these profiles assuming a linear change in density between meridia along lines of equal eccentricity.

Ganglion cell bodies are displaced laterally from their receptive fields in the central 2 to 3mm of retina as a result of the elongated cone fibers of Henle and oblique connection of bipolar cells (Schein, 1988; Curcio and Allen, 1990). The average lateral displacement at a series of eccentricities was calculated by Curcio and Allen (1990), assuming a central ganglion cell to cone ratio of 3 to 1

that gradually declines with eccentricity. This assumption is consistent with other reports (Wassle et al., 1990; Sjostrand et al., 1994).

In order to make a correction for lateral displacement, the number of ganglion cells in concentric annuli around the fovea was calculated from the raw ganglion cell density data. The receptive field positions were determined from the average lateral displacement values given by Curcio, and the ganglion cell receptive field density calculated.

Target stimulus area (A) was calculated with a conversion factor (q) to transform the target size from degrees of visual angle to millimeters on the retina. At the fovea, q = 0.286mm/° (Garway-Heath et al., 1998b). This conversion factor changes with eccentricity (Holden and Fitzke, 1988; Bennett et al., 1994), so that

$q_P < q_0$

(where $q_P$ = conversion factor in the periphery and $q_0$ = conversion factor at the fovea)

Target size in the periphery was calculated according to the following relationship (Bennett et al., 1994):

$q_P = q_0 - 0.000014U^2$

(where U = the angle of retinal eccentricity, in degrees)

Conventional white-on-white automated perimetry is performed using the Goldmann size III target, the diameter of which subtends 0.431° of visual angle. At the fovea, this represents 0.123 mm (0.431° * 0.286mm/°) on the retina, and an area of 0.012mm$^2$.

The ganglion cell receptive field count for each visual field test point was calculated in the following way:

$G = A * g$

(G = ganglion cell receptive field count, A = stimulus area, g = ganglion cell receptive field density).

Differential light sensitivity (DLS)

Normative data for the DLS at each Humphrey 30-2 test point were taken from the literature (Heijl et al., 1987).

Heijl et al (1987) give pointwise dB DLS for the average 50-year-old, and pointwise age slopes. The age slopes were used to derive average pointwise sensitivity values for a 34-year-old, for equivalence with the ganglion cell data.

The units of DLS are conventionally given in dB. In the Humphrey perimeter, the dB is 10 times the log of the reciprocal of stimulus intensity as measured in Lamberts (10,000 apostilbs), i.e. dB = 10* log (1/L).

Spatial summation

The relationship between increase in threshold DLS with increase in test spot size is given by (Wilson, 1970; Sloan, 1961; Dannheim and Drance, 1971; Kasai et al., 1992):

$A^k = C/L$

(L = luminance, 1/L = differential light sensitivity, A = stimulus area, C = constant, k = co-efficient of summation)

Alternatively, this can be written:

$k * \log A = \log C - \log L$ or

$\log L = \log C - k * \log A$

the slope of the line of a plot of log L against log A will, therefore, give k.

To obtain estimates of spatial summation at each visual field test point, DLS was measured in 8 normal subjects with 5 target sizes (Goldmann I to V). Perimetry was performed with the Humphrey type II 750 perimeter and the 30-2 and 'macula' full threshold programs after informed consent was obtained. The study conformed to the tenets of the declaration of Helsinki. Each subject performed one test at each test spot size in a randomised order, in one eye, chosen at random. All tests were performed within one week for each subject, with no more than 2 tests performed in one session. Subjects adapted to the perimeter illumination for 10 minutes before each session, and a near addition, calculated according to the subject's age, was used. Restriction criteria for the subjects were: corrected visual acuity ≥ 20/20, ametropia <5D sphere and <2D cylinder, no known ocular disease, and visual field test reliability indices of fixation losses (excluding the size V target) <15%, and false positive and false negative responses <15%.

Log L was plotted against log A for each subject. Visual inspection suggested a curvilinear relationship at all eccentricities. A quadratic regression line was fitted to each plot, and the slope of the tangent to the curve at the point corresponding to the size III stimulus was used to determine k for this stimulus size.

The mean subject k for each test point was calculated. These were compared with available data in the literature.

<u>Comparison of DLS and ganglion cell numbers</u>

In the relationship $A^k = C/L$, A refers to the test spot area. At any point on the retina, there will be a certain number of ganglion cell receptive fields ($G = A * g$, above) within the stimulus area.

Substitution of G for A gives

$G^k = C/L$

$G^k$ may be defined as the 'effective ganglion cell receptive field number', which is the number of ganglion cell receptive fields that would have the same sensational effect in the case of complete spatial summation (where k = 1). In the central 30° of the visual field, $0 < k < 1$.

Two comparisons between DLS and ganglion cell numbers were made:

1) DLS in dBs was plotted against the ganglion cell receptive field numbers per size III target (G).
2) DLS in 1/L (1/Lambert) was plotted against the effective ganglion cell receptive field numbers per size III target ($G^k$).

Extrapolation to glaucomatous ganglion cell loss

The relationship (equation of the regression line) between DLS (1/L) and effective ganglion cell receptive field numbers ($G^k$), derived from the second comparison, was used to calculate theoretical ganglion cell losses for 3- and 6-dB sensitivity losses at each visual field test point. A 3dB loss represents a doubling of the test spot intensity, and a 6dB loss a quadrupling.

In addition, theoretical ganglion cell losses were calculated for a dB sensitivity loss at the $p < 5\%$ level for each point.

### 3.3.4 Results

The topographic map reconstructed from the ganglion cell density data, without correction for foveal ganglion cell lateral displacement, is shown in Figure 3-9a. The topographic map following correction for foveal ganglion cell lateral displacement is shown in Figure 3-9b.

The calculated receptive field density reached about 350 000 units per $mm^2$ at 0.05mm from the foveal centre.

The mean age of subjects (for the spatial summation measurements) was 33.3 years (range 24 to 40 years). Mean refractive error was –1.75D (range 0 to -4.25D).

A typical curve for the plot of log test spot intensity against log test spot area, for the point at 9°,9° in the superonasal field in one subject, is shown in Figure 3-10.

The mean $R^2$ (± standard deviation) for the quadratic regression fits (log L against log A), for all subjects and test points, was 0.96 (±0.05), with a mean p value of 0.04.

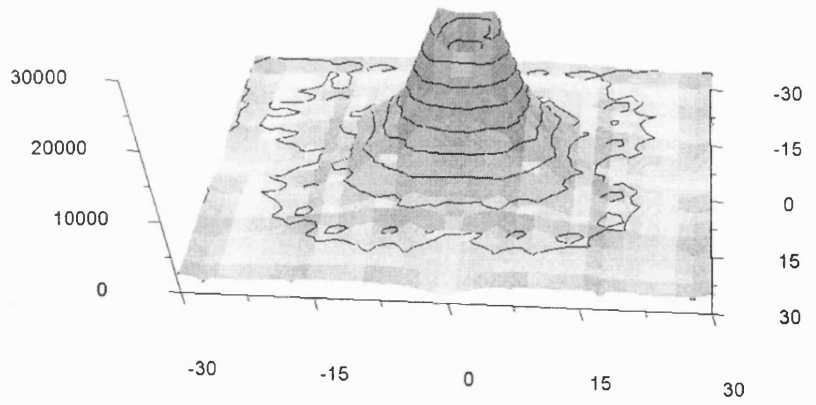


a)

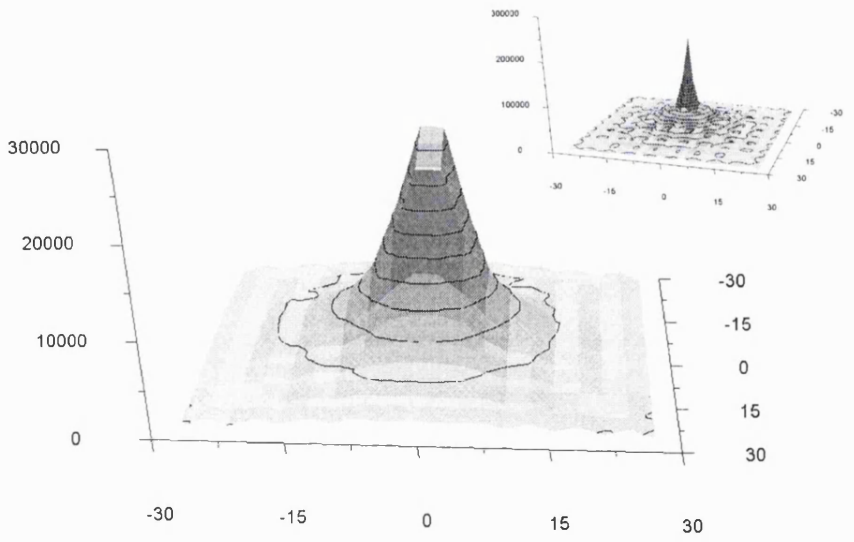


b)

Figure 3-9. 3-dimensional plots of retinal ganglion cell density/mm$^2$ (z axis) against retinal location in degrees (x and y axes). a) The central depression reflects the lateral displacement of ganglion cells away from the fovea. b) same plot as in a) following correction for lateral displacement of ganglion cells from the fovea. The main graph has the same scale as that in a), and the central peak has been truncated. The inset has a re-scaled z-axis (10 times the range) to show the peak receptive field density.

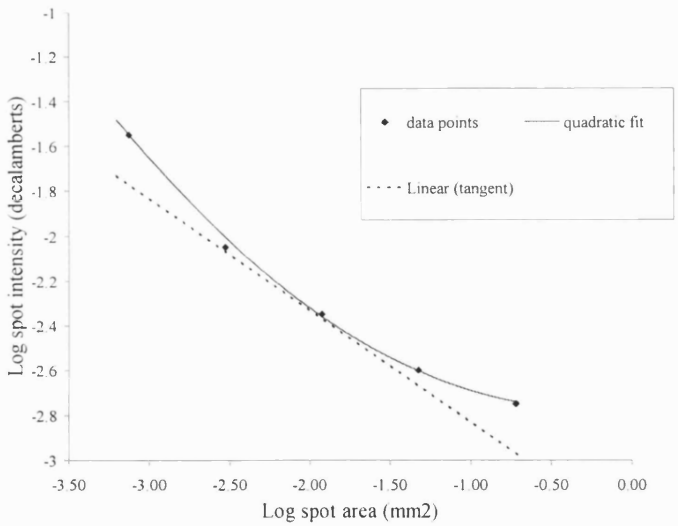


**Figure 3-10. Plot of log test spot intensity against log test spot area ($mm^2$) for a point at 9°, 9° in the superonasal field in one subject. The curve represents a quadratic regression fit to the data points. The straight line represents the tangent to the curve at the location of the size III test spot.**

The mean coefficients of summation are plotted against eccentricity, together with curves derived from data taken from the literature, in Figure 3-11. The mean pointwise standard deviation for estimations of k was 0.09.

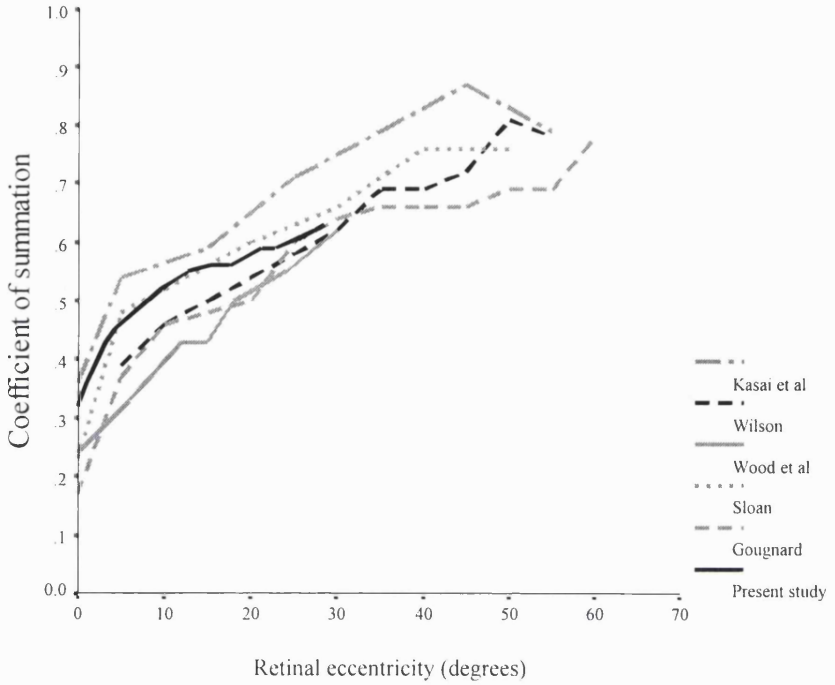


**Figure 3-11. Mean coefficient of summation for each retinal eccentricity in the Humphrey 30-2 and 'macula' grids plotted against retinal eccentricity. Curves derived from published data are shown for comparison: Gougnard (1961), Sloan (1961), Wood et al. (1986), Wilson (1970) and Kasai et al. (1992).**

The plot of dB DLS against ganglion cell receptive field numbers (G) is shown in Figure 3-12.

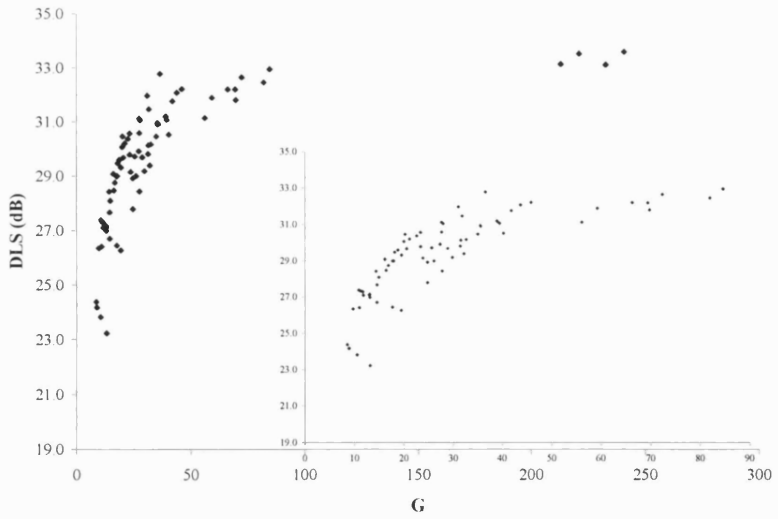


**Figure 3-12. Plot of decibel (dB) differential light sensitivity (DLS) against the ganglion cell receptive field count per Goldmann size III target (G). The inset is the same plot excluding the 4 points with the highest number of ganglion cells per target. This confirms a curvilinear relationship between variables over the entire range.**

The plot of DLS in 1/L against effective ganglion cell receptive field numbers ($G^k$) is shown in Figure 3-13. The equation of the regression line ($r^2 = 0.73$, $p < 0.000$) is: $1/L = -392 + (208 * G^k)$

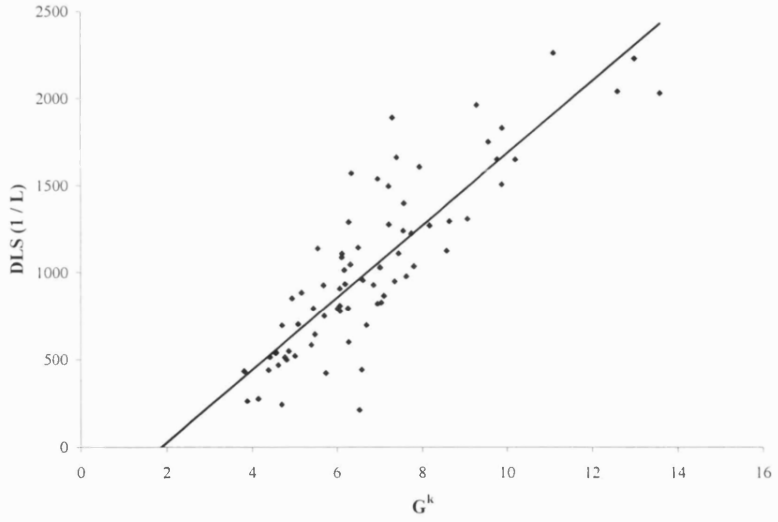


**Figure 3-13. Plot of differential light sensitivity (DLS), given as 1/Lambert, against the effective ganglion cell receptive field count per Goldmann size III target ($G^k$). The straight line represents the linear regression line through the data points.**

The predicted ganglion cell losses for selected points, at several eccentricities, for a 3 dB and a 6 dB sensitivity loss are given in Figure 3-14a and Figure 3-14b. The predicted ganglion cell losses for a sensitivity loss of 2 standard deviations from average sensitivity are given in Figure 3-14c.
The (whole field) average ganglion cell loss for a pointwise 3dB sensitivity loss is 52%, for 6dB 71%, and for 10dB 80%.

. 30 . .

. . 42 . . .

. 48 . 54 . . . .

. . . 61 66 . . . . .

42 . . . 68 . . . . .

42 . . . 69 . . . . .

. . . 62 61 . . . . .

. 52 . 55 . . . .

. . 50 . . .

. 43 . .

a)

. 44 . .

. . 59 . . .

. 67 . 74 . . . .

. . . 82 85 . . . . .

60 . . . 88 . . . . .

60 . . . 88 . . . . .

. . . 83 82 . . . . .

. 72 . 76 . . . .

. . 70 . . .

. 61 . .

b)

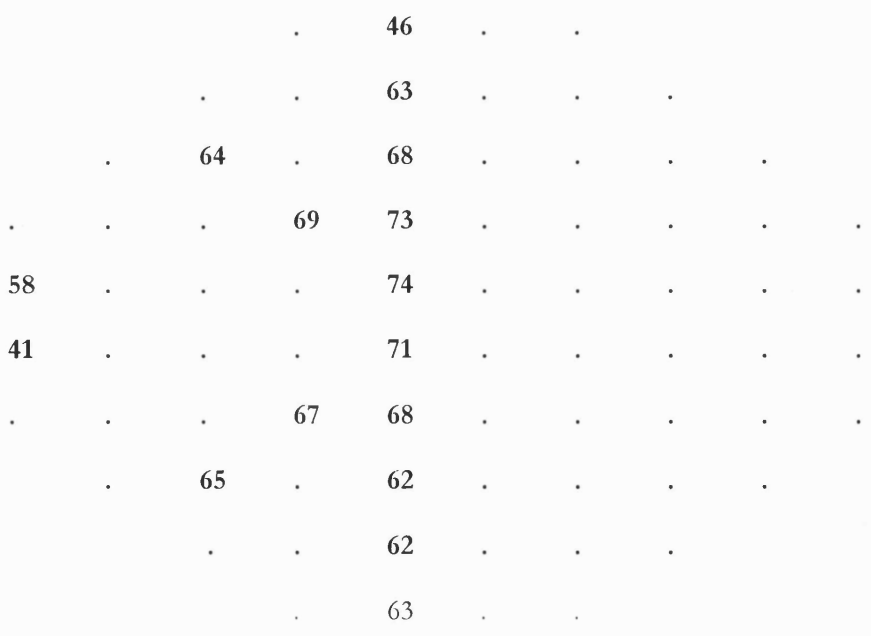


c)

**Figure 3-14. Predicted percentage ganglion cell losses (for selected visual field test points of a right eye) corresponding to: a) 3 dB light sensitivity loss, b) 6 dB light sensitivity loss, and c) the sensitivity loss that represents two standard deviations from the population mean.**

### 3.3.5 Discussion

In assessing the degree of glaucomatous damage in an eye, clinicians take into account the appearance of the optic nerve head and nerve fibre layer and the function of the nerve, usually measured by white-on-white perimetry. In most clinical practices, the pattern and dB 'depth' of scotomas, and summary indices, such as mean deviation (MD), are the only objectively quantifiable measure of the amount of nerve damage. For this reason, perimetric indices are frequently used to stage glaucomatous disease and evaluate progression, and scoring systems have been developed to formalise this (Gaasterland et al., 1994). Despite this, the relationship between such indices and the amount of structural damage has been unclear. It is not known whether there is a linear correspondence, so that a MD of -6dB represents twice as much damage as a MD of -3dB. The results of this study indicate that this is not the case. The dB scale is logarithmic, and there is a curvilinear relationship between dB DLS and underlying ganglion cell numbers (Figure 3-12). When DLS is appropriately scaled, as the reciprocal of test spot intensity, there is a linear relationship with underlying ganglion cell numbers adjusted for spatial summation (Figure 3-13). The curvilinear relationship between dB DLS and structural measures is supported by studies comparing visual field MD and neuroretinal rim area (Airaksinen and Drance, 1985; Jonas and Grundler, 1997), and by recent primate work comparing visual field MD and ganglion cell numbers counted histologically (Harwerth et al., 1999).

Additional supportive evidence comes from the comparison of the detection thresholds in acuity (high pass resolution) perimetry and conventional (DLS) perimetry. Acuity perimetry measures spatial resolution, which is, theoretically, related to the density of intact sensory units (Frisen, 1988). The spatial threshold units are the logarithm of spatial extent, in the same way that dB DLS threshold units are the logarithm of test spot intensity. Spatial thresholds and dB DLS thresholds have been found to be linearly related (Bartz Schmidt and Weber, 1993; Chauhan et al., 1993). One would, therefore, expect spatial extent and test spot intensity, and their reciprocals, sensory unit density and DLS (1/Lambert), to be linearly related. Bartz Schmidt and Weber (1993) compared pointwise sensitivity in the two tests, and calculated that a 6 dB DLS loss equated with a 50% loss of sensory units (and 12 dB with a 75% loss). This is consistent with the model proposed in this paper only for test points at about 27° eccentricity, with a 6 dB loss representing, on average, greater ganglion cell loss (mean 71%). Differences at other points may in part be explained by location-specific differences in spatial summation, which were not taken into account in Bartz Schmidt's calculations.

The values obtained for spatial summation in this study are very similar to those of previous studies (Figure 3-11) (Gougnard, 1961; Sloan, 1961; Wood et al., 1986; Wilson, 1970; Kasai et al., 1992; Dannheim and Drance, 1971). The mean standard deviation of pointwise estimates for the coefficient of summation, at 0.09, is very similar in magnitude to the findings of Gougnard (1961). It can be appreciated from Figure 3-10 that the coefficient of summation at a particular location changes with the size of stimulus target. This means that value of the coefficient of summation itself changes over the range of target sizes used to measure it (Dannheim and Drance, 1971). This is in addition to variation according to retinal location (Figure 3-11). This suggests that it may be the number a ganglions cells stimulated that determines summation. The summation characteristics of a particular location also vary with the level of background luminance (Glezer, 1965). The analysis in this paper, therefore, applies to the specific experimental conditions in this study. That is Humphrey/Goldmann perimetry (background luminance 31.5 apostilbs) and the Goldmann size III target.

The equation that relates DLS (1/Lambert) to effective ganglion cell receptive field count, can be used to predict the expected ganglion cell number, as a proportion of normal, at any point for various sensitivity losses.

The equation derived from the linear regression of DLS against 'effective' ganglion cell numbers (Figure 3-13) is:

$DLS = (208 * G^k) - 392$

from this

$(DLS + 392)/208 = G^k$ (k = location-specific coefficient of summation)

and

$((DLS + 392)/208)^{1/k} = G$

For a given field test point, substitution in the equation of the population average DLS (in 1/Lambert) for the term 'DLS', and the location-specific spatial summation value for 'k', yields the population average ganglion cell numbers at that point. Substitution of the measured DLS yields the actual number of ganglion cells at the test point.

The hypothesis tested in the study was that $G^k = C/L$. If true, the relationship between $G^k$ and L should be linear and proportional, with the regression line passing through zero. In this study, a small off-set was found. Possible explanations for this include an underestimation of the coefficient of summation at more peripheral points, an underestimation of DLS, or an overestimation of the number of ganglion cells, at these points. An underestimation of DLS might occur in the case of refractive blur in areas of incomplete summation. Refractive errors are corrected for foveal vision, and it is known that refraction in the periphery can deviate substantially from that at the fovea, and that defocus affects detection acuity (Wang et al., 1997b). The off-set accounts for the predicted loss of < 50% for a 3dB loss seen at peripheral points (Figure 3-14a).

Extrapolation of the physiological relationship between DLS and ganglion cell numbers to the pathological condition of glaucoma presupposes that spatial summation remains unchanged as ganglion cells are lost. This topic is dealt with in section 2.5.2.1.3.4. There is limited data in the literature, but the studies suggest that spatial summation is either unchanged, or a little increased, in glaucoma. Increasing spatial summation with ganglion cell loss would have the effect of overestimating the number of ganglion cells (if normal summation is assumed) in the model proposed here.

As the prevalence of glaucoma increases with age, it is important to know whether spatial summation changes with age. This is dealt with in section 2.5.2.1.3.5. The evidence suggests that spatial summation does not change with ageing. Therefore, in applying this model to older age groups, no extra assumptions need to be made when relating actual sensitivity to the age-matched average.

If a specific value of dB DLS loss is taken to indicate that a certain level of glaucomatous damage is present, this study demonstrates that the sensitivity of the visual field test to detect damage varies with eccentricity. Figure 3-14a demonstrates the case for 3 dB loss (a doubling of test spot intensity). At this level, around 70% of ganglion cells have to be lost at 4° eccentricity, but only 50% at 21°. The data of Quigley et al. (1989) lend support to this observation. Although a linear regression fit was made to the plot of dB sensitivity loss against percentage of normal ganglion cells, the analysis suggested that a greater proportion of ganglion cells had to be lost in the central, compared to more peripheral, field for equivalent dB sensitivity losses.

Figure 3-14c illustrates the projected ganglion cell losses required to produce a test point sensitivity lower than two standard deviation from the average, for selected points in a 30° field. By this measure, the sensitivity of the visual field test does not change much with eccentricity, only slightly greater ganglion cell losses are required centrally. This pattern, however, cannot be explained by inter-individual variation in ganglion cell numbers, which is lower centrally and increases with eccentricity (Curcio and Allen, 1990). Factors other than inter-individual variation in ganglion cell

numbers, such as the greater susceptibility of central thresholds to uncorrected refractive errors (Sloan, 1961; Herse, 1992), may play a role.

If dB sensitivity loss means different things in terms of ganglion cell loss in different parts of the visual field, it follows that simply averaging the defect values for each test point, to provide a summary measure, will not necessarily reflect the true underlying ganglion cell loss across the retina. A more appropriate scale for DLS would overcome this problem.

The shape of the curve relating dB DLS to underlying anatomy has often been interpreted as demonstrating a built-in redundancy of neural units in the retina, so that a certain proportion of ganglion cells has to be lost before function is compromised. This study suggests that this is an impression given by the logarithmic nature of the scale for DLS. In fact, there is a continuous, linear, relationship between DLS and underlying neural units. The difficulty in detecting early anatomical damage by tests of function may be a reflection of the wide inter-individual range in the number ganglion cell in the retina (Curcio and Allen, 1990), and the wide inter-individual range of psychophysical measurements (Heijl et al., 1987).

Perimetric indices and pointwise DLS measurements have been used to quantify disease progression (Viswanathan et al., 1997; Wild et al., 1997; Nouri-Mahdavi et al., 1997). The true pattern of progression in glaucoma is unknown, and is likely to vary from patient to patient, and within a patient according to prevailing risk factors. The simplest model to describe progression, which might represent an 'average' pattern, is a linear model. Comparison of Figure 3-14a and Figure 3-14b shows that dB loss is not linear with respect to underlying ganglion cell numbers. At 21° eccentricity, a 3dB sensitivity loss represents 50% ganglion cell loss. A further 3 dB loss, however, represents only a further 20% ganglion cell loss. The assumption of linear progression of dB DLS would underestimate 'true' (anatomical) progression when sensitivity values are near normal, and overestimate progression when sensitivity loss is already advanced. There is a need to re-evaluate models of progression in the context of the new DLS scale proposed here.

There are several implications for clinical practice of the non-linear relationship between dB DLS and ganglion cell numbers, with small dB changes representing a large reduction in ganglion cell numbers when sensitivity is near normal and a small reduction in ganglion cell numbers when sensitivity is low. Appreciation of this relationship reinforces the widely-held belief that structural changes at the optic disc and nerve fibre layer frequently occur earlier than recognisable changes in the visual field. It suggests a reappraisal of 'staging' disease by perimetric indices. The loss of the first 5dB, often regarded as early disease, in fact represents moderately advanced disease. And the difference between a MD of -10 and -15dB represents a far lesser change. Detection of disease before these levels of functional loss is, therefore, of great importance, so that appropriate treatment can be instigated. Recognition of progression of functional loss in early disease requires an understanding of the non-linear relationship between dB DLS and ganglion cell numbers, and of fluctuation of sensitivity measurements at near-normal levels. A linear model applied to dB DLS values is likely to be less sensitive in early disease. It may be possible to detect change earlier in the

disease process with a linear (1/L) model. Recognition of the presence, and patterns, of field loss will be aided by the knowledge that similar dB losses in different parts of the field imply different levels of structural damage, and that the 'probability symbols' are a much better guide than the raw sensitivity values.

## 3.4 Anatomical correlation between the visual field and optic disc

### 3.4.1 Background

The relationship between localised visual field defects and discrete RNFL loss has been investigated by means of high resolution perimetry, and the topography of the RNFL defect and the functional abnormality has been shown to be closely related (Okubo and Mizokami, 1985; Westcott et al., 1997; Orzalesi et al., 1998). However, the correspondence between ONH changes and functional deficits is less well established.

Structural damage in glaucoma is frequently quantified by measurements of the neuroretinal rim area. It has been demonstrated in experimental primate glaucoma that the area of the neuroretinal rim, measured in vivo from stereoscopic photographs and scanning laser tomographic images, is related to axon numbers measured histologically (Varma et al., 1992a; Yucel et al., 1998).

It is desirable to establish the topographical correspondence between ONH and visual field regions. This correspondence may shed light on the relationship between structural and functional changes in POAG, and possible differences in the relationship between the two in different parts of the visual field or ONH. In addition, concordance between structural and functional findings will be of use in clinical practice.

The precise relationship between visual field locations and corresponding regions of the ONH is poorly documented. Wirtschafter et al. (1982) published a 'profile of nerve fibre function in optic disc sectors', in which regions of the visual field were related to optic disc sectors. The boundaries of the visual field regions were derived from illustrations of the primate nerve fibre layer. Weber et al. (1990), Yamagishi et al. (1997) and Anton et al. (1998) have reported incomplete maps relating damaged parts of the visual field to the ONH in glaucomatous eyes.

### 3.4.2 Purpose

The purpose of this study was to establish the anatomical relationship between regions of the visual field and corresponding regions of the ONH by superimposing a visual field test pattern on RNFL photographs.

### 3.4.3 Methods

#### 3.4.3.1 Retinal nerve fibre layer (RNFL) photography

The archive of RNFL photographs from the Normal Tension Glaucoma Clinic at Moorfields Eye Hospital was searched for examples of photographs with discrete (focal and wedge) RNFL defects, and/or prominent nerve fibre bundles, the course of which could easily be traced. 69 photographs of 69 eyes satisfied these criteria.

NFL photography had been performed as part of the routine evaluation of glaucoma patients and suspects. Photographs were taken with the Canon CF60U camera at the 60° field of view, using low

sensitivity, high resolution, black-and-white film and a blue narrow-band interference filter. The Canon CF60U is not telecentric: the camera field of view (degrees of field per millimeter on the camera film) varies slightly with the refractive error of the eye photographed. The change in image size is approximately 1.2% to 1.6% per dioptre of ametropia for the Canon CF60U ((Rudnicka et al., 1998) and section 3.2.1.2.5).

The photographs were digitized at a resolution of 1552 by 1164 pixels, giving a linear scaling of 26 pixels per degree (Figure 3-15). The 'mirror' image (about the vertical meridian) of left eyes was taken, so that all eyes in the subsequent analyses were 'right eyes'.

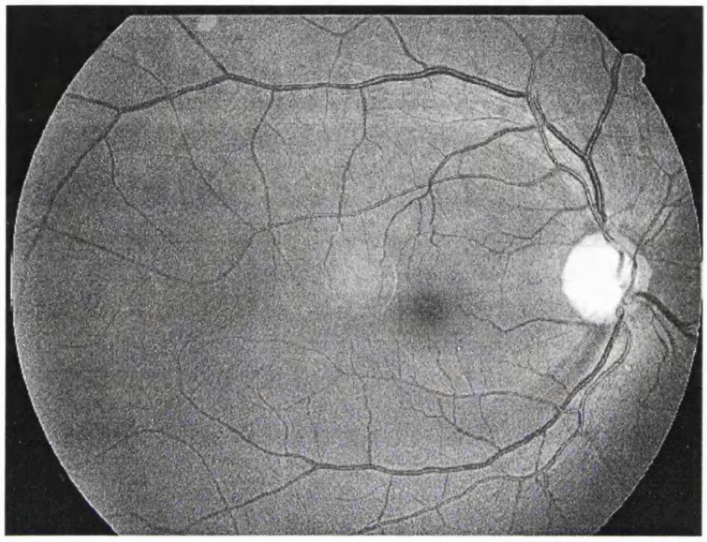

**Figure 3-15. Digitised 60° retinal nerve fibre layer photograph**

### 3.4.3.2 Generation of visual field test grid and optic disc reference circle

A Humphrey 24-2 test pattern (test points in a grid 6° apart) was generated digitally in Paint Shop Pro, version 5.01 (Jasc Software, Inc), with the same scaling of 26 pixels per degree. The size of the test spot approximates that of a Goldmann size III target (0.43°). A circle, 152 pixels in diameter (approximately 6° - the size of an average ONH) was also generated. This was divided into 30° reference sectors.

### 3.4.3.3 Generation of compound images

The Humphrey 24-2 test pattern and the RNFL photograph each cover a constant field (24° from the fovea and 60° respectively), irrespective of differences in ocular magnification between eyes, and are, therefore, appropriately scaled with respect to each other. The centre of the test pattern grid was aligned to the fovea on the RNFL images, and the two images were digitally added. The edge of the reference circle was then aligned as closely as possible to the margins of the ONH (Elschnig's ring), and was digitally added (Figure 3-16). The centre of the ONH was taken to be the centre of the reference circle.

**Figure 3-16. Retinal nerve fibre layer photograph with the Humphrey 24-2 visual field test pattern and optic nerve head reference circle superimposed**

### 3.4.3.4 Estimating the relationship between test points and the optic disc

The relationship between a test point and the ONH was determined by identifying points adjacent to the edge of a RNFL defect, or prominent bundle, and tracing the defect, or bundle, back to the ONH. The point of entry into the ONH, at the inner margin of the scleral ring of Elschnig, was determined by its relationship to the reference circle (Figure 3-17).

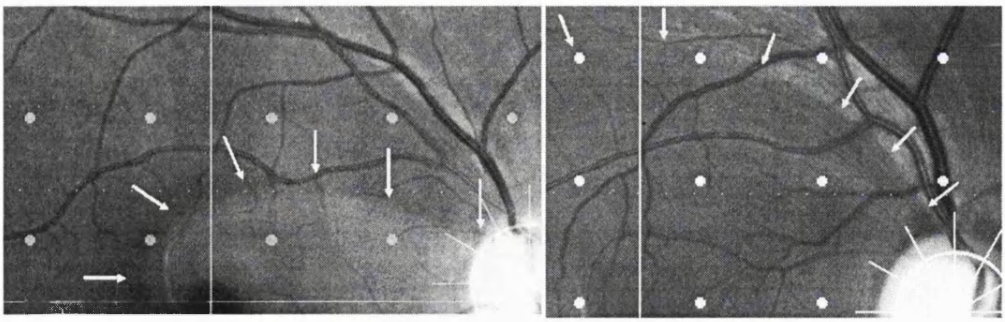

**Figure 3-17. Examples of the method for estimating the corresponding optic nerve head location of visual field test points by their proximity to retinal nerve fibre layer defects**

The temporal margin (9 o'clock, right eye) was designated 0°, and degrees were counted in a clockwise direction. The visual field grid point was then assigned a value in degrees according to the site of entry of the defect/bundle into the ONH. To account for the inverse relationship between retinal location and visual field location, the mirror image, about the horizontal meridian, of the test

point location was recorded with the degree value of its corresponding point of entry at the ONH. The points immediately above and below the ONH were not assigned positions.

The position of the centre of the ONH with respect to the fovea was recorded for each photograph. The effect of the position of the ONH on the site of entry of defects was evaluated with stepwise multiple linear regression, with site of entry as dependent variable and vertical and horizontal positions of the disc as independent variables, and a probability for F to enter of 0.05 and to remove of 0.10.

For comparison with previously published maps, the optic disc was divided into sectors as designated by Wirtschafter et al. (1982). Corresponding locations in the visual field were given the number of the disc sector for: a) Wirtschafter's map, b) map corresponding to the results of this study, and c) partial map of Weber et al. (1990).

A new map, relating visual field regions to optic disc sectors was generated from the findings of this study.

### 3.4.4 Results

52 field test points were assigned values, representing all points in the 24-2 test grid, except those immediately above and below the ONH.

A median of 22, of a possible 69, values were assigned to each point (range 4 to 58). The mean value for each point is shown in Figure 3-18.

| | | | | | | | | |
|---|---|---|---|---|---|---|---|---|
| | | | 268 | 262 | 252 | 245 | | |
| | | 264 | 274 | 281 | 275 | 260 | 246 | |
| | 271 | 285 | 291 | 296 | 298 | 283 | 253 | 229 |
| 278 | 287 | 291 | 298 | 312 | 329 | 318 | . | 218 |
| 83 | 76 | 68 | 55 | 34 | 11 | 13 | . | 167 |
| | 85 | 78 | 66 | 56 | 48 | 60 | 95 | 136 |
| | | 88 | 81 | 77 | 80 | 93 | 112 | |
| | | | 93 | 95 | 100 | 108 | | |

**Figure 3-18. The optic nerve head location, in degrees, for each visual field test point. The temporal margin (9 o'clock, right eye) was designated 0°, and degrees were counted in a clockwise direction.**

In general, central points and points in the arcuate bundles were assigned more values than peripheral points. The median standard deviation of assigned values was 7.2° (range 2.6° to 10.3°). There were no locations in particular that showed greater than average variability in assigned values. The location in the retina of the ONH was a mean 15.5° (standard deviation 0.9°) nasal to, and 1.9° (standard deviation 1.0°) above, the fovea. Figure 3-19 illustrates the position of the ONH in relation to the fovea.

a) b)

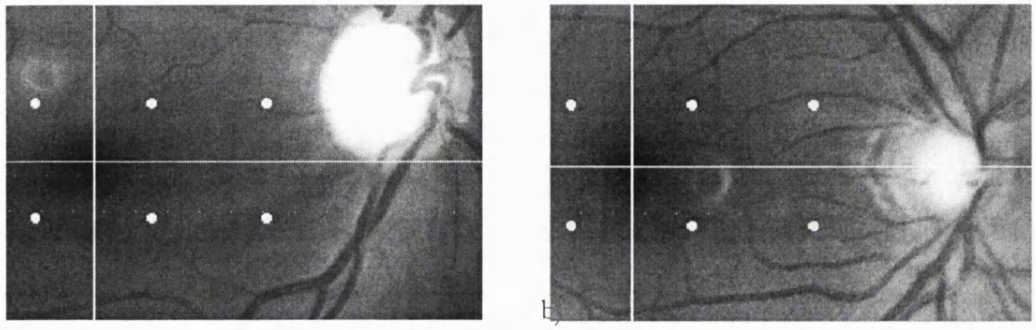

**Figure 3-19. Examples of the position of the optic nerve head in relation to the fovea**

For 28 points the site of entry into the ONH was significantly correlated with the position of the ONH in relation to the fovea. The site of entry was related to the horizontal position of the ONH in 8 field points, to the vertical position in 10, and to both the horizontal and vertical position in 10. The median $r^2$, for points with a significant relationship, was 0.44 (range 0.22 to 0.96).
Figure 3-20 shows Wirtschafter's divisions of the ONH into sectors. Figure 3-21, Figure 3-22 and Figure 3-23 illustrate the corresponding visual field divisions derived from Wirtschafter's, this, and Weber's studies.

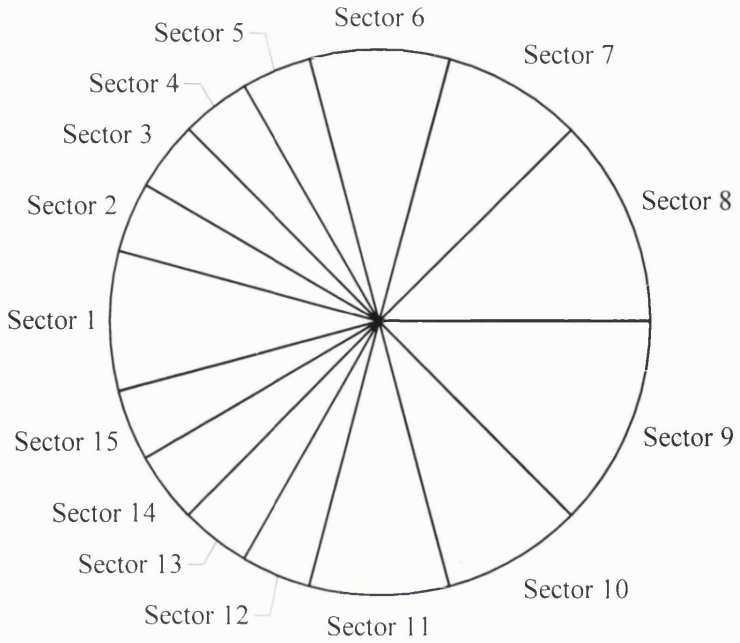


**Figure 3-20. The optic nerve head divisions of Wirtschafter et al. (1982)**

| | | | | | | | | |
|---|---|---|---|---|---|---|---|---|
| | | | 12 | 12 | 11 | 11 | | |
| | | 12 | 12 | 12 | 12 | 11 | 10 | |
| | 13 | 13 | 14 | 15 | 15 | 13 | 11 | 10 |
| 13 | 14 | 14 | 15 | 15 | 1 | 1 | 0 | 9 |
| 4 | 3 | 3 | 2 | 2 | 1 | 1 | 0 | 8 |
| | 4 | 4 | 3 | 2 | 2 | 4 | 6 | 7 |
| | | 5 | 5 | 5 | 5 | 6 | 7 | |
| | | | 5 | 5 | 6 | 6 | | |

**Figure 3-21. The number of the correspond disc sectors for visual field test points according to Wirtschafter et al. (1982)**

| | | | | | | | | |
|---|---|---|---|---|---|---|---|---|
| | | | 11 | 11 | 10 | 10 | | |
| | | 11 | 11 | 11 | 11 | 11 | 10 | |
| | 11 | 12 | 12 | 12 | 12 | 11 | 10 | 10 |
| 11 | 12 | 12 | 12 | 13 | 14 | 14 | 0 | 9 |
| 6 | 6 | 5 | 4 | 3 | 1 | 1 | 0 | 8 |
| | 6 | 6 | 5 | 4 | 4 | 5 | 6 | 8 |
| | | 6 | 6 | 6 | 6 | 6 | 7 | |
| | | | 6 | 6 | 6 | 7 | | |

Figure 3-22. The number of the correspond disc sectors for visual field test points according to the results of this study

| | | | | | | | | |
|---|---|---|---|---|---|---|---|---|
| | | | 11 | 11 | 11 | . | | |
| | | 11 | 11 | 11 | 11 | . | . | |
| | 12 | 12 | 12 | 12 | 13 | 11 | . | . |
| 13 | 13 | 13 | 13 | . | . | . | 0 | . |
| 5 | 5 | 5 | 5 | . | . | . | 0 | . |
| | 6 | 6 | 6 | 6 | 5 | 6 | . | . |
| | | . | . | . | . | . | . | |
| | | | . | . | . | . | | |

Figure 3-23. The number of the correspond disc sectors for visual field test points according to the results of the study of Weber et al. (1990)

Figure 3-24 is a map generated from the findings of this study. It takes into account the relative positions of the optic disc and fovea: the centre of the temporal optic disc segment is rotated 5° anticlockwise (downward).

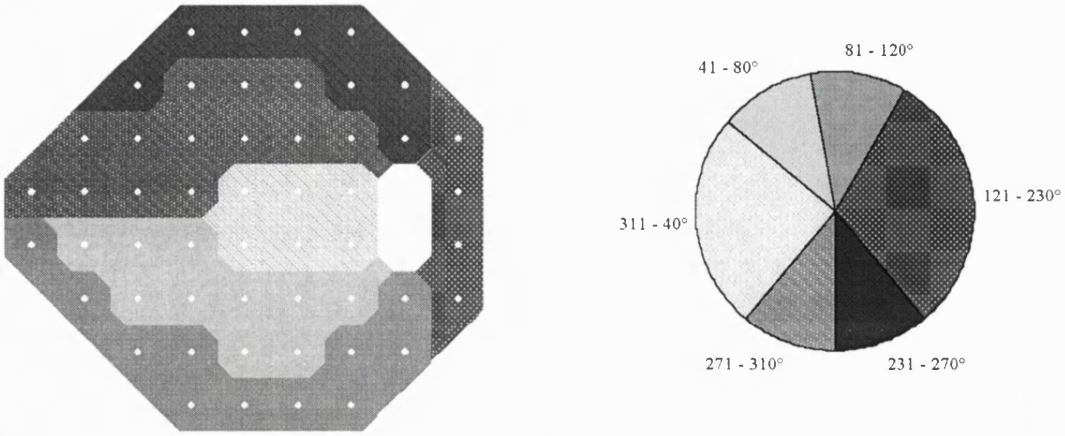


**Figure 3-24. A division of the visual field a) and optic nerve head b) into sectors according to the results of this study**

### 3.4.5 Discussion

The map relating visual field test points to positions at the ONH (Figure 3-24) is, to our knowledge, the first complete map to be derived from human RNFL images. It is compared with Wirtschafter's map in figure Figure 3-21. The maps differ in two significant respects. The first is that paracentral and arcuate areas of the visual field are represented by sectors nearer the poles of the ONH in the map derived from this study, and by sectors nearer the temporal horizontal meridian in Wirtschafter's map. The second is that Wirtschafter's map is symmetrical about the horizontal meridian, whereas the map in this study is slightly asymmetrical, reflecting the position of the ONH above the horizontal meridian. The differences between the maps probably arise from the differences in the methodology, and objectives, of the studies. In Wirtschafter's, the boundary lines in the visual field, which are related to sectors in the optic disc, were obtained by projecting illustrations of the primate RNFL onto an appropriately scaled visual field. The border of the 'optic disc' was defined as the 'physiologic blind spot', covering 13° by 9° (Hills et al., 1983). The map was not constructed for the purpose of relating visual field sectors to ONH sectors, but to justify an anatomical basis for the subdivision of the visual field. The authors stated that the ONH sectors should be regarded as arbitrary, and not exactly related to the actual point where specific nerve fibres cross the margin of the optic disc. Despite this restriction, the map has been used as the basis for studies relating visual field test results to sectors of the optic disc (Kono et al., 1997; Reyes et al., 1998).

The map derived from this study is also compared to the partial map of Weber in Figure 3-23. The two maps show good agreement. The upper visual field test points are represented by ONH sectors

slightly nearer the temporal horizontal in the map derived from this study. The two maps demonstrate a very similar asymmetry about horizontal meridian. This asymmetry has also been demonstrated in visual field maps identifying functional clusters (Mandava et al., 1993).

In relating visual function in sectors of the visual field to structure in sectors of the ONH, some decision has to be made about the size of sectors. The mean variability in assigned ONH positions to visual field test points can be a guide to appropriate sector size. The mean standard deviation of assigned values was 7.2°. This means that 95% of the time a visual field test point will be associated with a position at the ONH within approximately 14° either side of a mean. In other words, the range of possible positions at the ONH covers almost 30° for each visual field test point. When clusters of field test points are considered (sectors of the visual field), ONH sector size should probably be larger than 30°, to take account of this variability. The map illustrated in this paper (Figure 3-24) consists of four 40° sectors, one 90° sector and one 110° sector. The different sector sizes represent a compromise between minimal practical sector size and the number of visual field test points for each ONH sector.

In this study the course of RNFL defects is used to identify the region of origin of nerve fibres. An assumption is that the ganglion cell axons travel in bundles towards the ONH without any tendency to move to adjacent bundles or disperse, thereby preserving a retinotopic organisation. This assumption is probably justified (see section 2.3.1).

Sources of variability

A major source of between-eye variability in the correspondence of visual field test points to ONH sectors is the position of the ONH in relation to the fovea. In more than half the test points, ONH position accounted for nearly half the inter-individual variability. It is possible that some of the apparent vertical variation in the position of the ONH arises from torsion of the eye during photography, as a result of incorrect positioning of the head. This effect is likely to be small, and is not likely to be greater than similar incorrect positioning of the head during perimetry. Any variability that this introduces will thus reflect the clinical situation.

Retinal magnification varies between eyes. Variation in the retinal magnification, that results from inter-individual variation in the size of the eye (the number of millimetres on the retina per degree of visual angle, section 3.2.1.1), will result in differences in the absolute position (in millimetres) of the visual field test points on the retina. A change in axial length of ± 1mm results in a change in magnification of about ± 5% (section 3.2.1.1). This means that in larger eyes the visual field test points are spaced further apart. This effect is likely to result in variation in the part of the ONH that corresponds to a given visual field test point. Application of a generalised map to eyes that may be substantially longer or shorter than average should, therefore, be done with caution.

A small source of error arises from the fact that the Canon camera is not telecentric. Refractive error data was not available for the photographs in the archive, and corrections for ametropia, therefore, could not be made. The change in image size is approximately 1.6% per dioptre of ametropia for the

Canon CF60U (section 3.2.1.2.4 and Rudnicka et al., 1998). For a typical population of glaucoma patients the standard deviation of refractive error is about 2 dioptres (Table 3-3). The standard deviation of change in image size is, therefore, about ± 3.2%. It is estimated that up to 1.2° (of the mean 7.2°) of the variability in the assignation of a disc position to field test points may be accounted for by the methodology (as opposed to inter-individual anatomical variation), with no systematic error (bias).

In addition to variation resulting from the size of an eye, other morphological variables, such as the shape, rotation and tilt of the ONH, are likely to lead to variation in the relationship between visual field test points and ONH sectors. It was not possible to quantify these variables in this study.

## 3.5 Correlation between visual field light sensitivity and optic disc morphometry

### 3.5.1 Background

It has been widely reported that, in primary open angle glaucoma (POAG), visual field loss as measured by conventional automated perimetry is preceded by neuroretinal rim loss (Sommer et al., 1979b; Motolko and Drance, 1981; Pederson and Anderson, 1980; Airaksinen et al., 1992). It is not clear whether this arises because of difficulty in detecting functional damage early in the course of the disease, or because there is a 'functional reserve' in the system, so that functional loss is only recognised once the reserve has been lost. Several studies that have plotted neuroretinal rim area against differential light sensitivity (DLS), measured in decibels (Airaksinen et al., 1985a; Funk et al., 1988; Nanba and Iwata, 1992; Jonas and Grundler, 1997) demonstrate a curvilinear relationship, with large changes in neuroretinal rim area and corresponding small changes in decibel values when the rim area is large, and small changes in neuroretinal rim area and corresponding large changes in decibel values when the rim area is small. The conclusions drawn have been that there is a changing relationship between structural and functional measures as the disease progresses. However, given the likely physiological relationship between DLS and retinal ganglion cell numbers (and neuroretinal rim area) (section 3.3), the appearance may simply reflect the logarithmic DLS scale.

The neuroretinal rim area is a measure of ganglion cell axon cross-sectional area, of varying obliquity depending on the course of fibres through the disc, together with other elements, such as supporting glia and blood vessels. The rim area is, as such, a surrogate for ganglion cell numbers, though the exact relationship between the two has not been established. A linear relationship between neuroretinal rim area and axon numbers has been demonstrated (Varma et al., 1992a; Yucel et al., 1998). Similarly, a linear relationship between neuroretinal rim area and the reciprocal of light intensity, and log neuroretinal rim area and dB, would be expected.

### 3.5.2 Purpose

The purpose of this study was to evaluate the relationship between DLS and neuroretinal rim area, and to compare the conventional decibel scale with the scale of the reciprocal of light intensity.

### 3.5.3 Methods

Subjects

Two groups of subjects, normal controls and patients with early glaucomatous field defects, were recruited prospectively as part of a study on the early detection of glaucoma.

Normal subjects

These are described in section 3.2.2.3.1. Data from 102 subjects were used for this study.

Glaucoma patients

These are described in section 3.2.2.3.1. Data from 78 subjects were used for this study.

Visual Field Testing

This is described in section 3.2.2.3.2.

Imaging

Heidelberg Retina Tomograph (HRT)

This is described in section 3.2.2.3.3. Both the standard reference plane (50μ below the ONH margin between 350° and 356°) and the reference plane from the 1.10 software version (320μ below the peripheral reference ring) were employed. The following parameters were analysed: optic disc area, neuroretinal rim area, neuroretinal rim volume, cup shape measure (CSM), mean height of contour (HCM) and RNFL cross-sectional area. Each parameter was calculated for the whole disc (global) and in the 6 pre-defined segments: temporal (90°), temporal superior (45°), temporal inferior (45°), nasal (90°), nasal superior (45°) and nasal inferior (45°).

The mean time (± standard deviation) between the visual field test and imaging was 2.5 (± 4.8) months for the normal subjects and 3.4 (± 4.4) months for the glaucoma patients.

Statistical analysis

Correlations between structural measures and visual field indices were sought by linear or quadratic regression analysis. A quadratic ($y = ax + b x^2 + c$) fit was taken to be significantly better than a linear fit if the coefficient (b) for the $x^2$ term was significant at the $p<0.05$ level.

The visual field was divided into sectors corresponding to the predefined HRT disc sectors according to the field/disc relationships established in section 3.4. Sector field defect (sector MD) is the average of the dB defect values in the given sector.

The theoretical structure/function relationship assumed in section 3.3 was:

$G^k = C/L$ and

$k * \log G = \log C - \log L$

(where k = coefficient of summation, G = ganglion cell numbers, C = constant and L = luminance).

The decibel in Humphrey perimetry is $- \log L*10$.

This theoretical relationship was extended for the purposes of this analysis, and neuroretinal rim area (NRR) was the structural measure used in place of ganglion cell numbers:

$k * \log NRR = \log C - \log L$

(The slope of a regression line in a plot of log NRR against log L will give 'k').

Pointwise DLS in the visual field is given as a raw dB sensitivity value and as a dB 'deviation' value (the difference between the age-matched normal value and the measured sensitivity). The 'log sensitivty defect' value (calculated from the from the decibel values) is $- \log L_{normal}$ minus $- \log L_{measured}$ and is the same as the logarithm of the ratio of measured sensitivities, $- \log (L_{normal} / L_{measured})$.

A similar analysis can be made for the structural measure of neuroretinal rim area. The 'log rim defect' parameter is given as log $NRR_{normal}$ minus log $NRR_{measured}$ ( $NRR_{normal}$ is the age- and disc size-matched average value). This is equivalent to log ($NRR_{normal}$ / $NRR_{measured}$).

Plots of sector 'log rim defect' against sector mean deviation were compared for the standard HRT reference plane and the 320μ reference plane.

The software SPSS for Windows, version 9.0, and Microsoft Excel 97, were used to perform the statistical analyses. Where regression analyses were performed, significance was assumed at $r^2 \geq 0.10$ and $p \leq 0.01$.

### 3.5.4 Results

The characteristics of the study population are summarised in Table 3-12, and the sectoral visual field indices in Table 3-13.

| | Normal subjects<br>Mean ± standard deviation | Glaucoma patients<br>Mean ± standard deviation |
|---|---|---|
| Age (years) | 57.5 ± 12.6 | 67.7 ± 9.1 |
| Refraction (D) | 0.7 ± 1.8 | 0.8 ± 1.8 |
| Mean deviation (dB) | -0.01 ± 1.26 | -3.92 ± 2.32 |
| Mean optic disc area ($mm^2$) | 2.01 ± 0.34 | 1.90 ± 0.36 |
| Mean neuroretinal rim area ($mm^2$) | 1.54 ± 0.31 | 0.98 ± 0.26 |

(D = dioptres, dB = decibels, $mm^2$ = square millimetres)

**Table 3-12. Study population characteristics.**

| | Normal subjects | | | Glaucoma patients | | |
|---|---|---|---|---|---|---|
| | Mean | Minimum | Maximum | Mean | Minimum | Maximum |
| Global | 0.0 | -4.2 | 2.6 | -3.9 | -12.2 | 1.1 |
| Temporal | -0.2 | -4.4 | 2.3 | -2.5 | -25.4 | 1.9 |
| Sup. Temp | 0.0 | -4.0 | 2.5 | -3.7 | -14.1 | 2.6 |
| Sup. Nasal | 0.1 | -4.5 | 2.7 | -2.5 | -13.9 | 4.8 |
| Nasal | 0.1 | -5.4 | 4.3 | -2.7 | -20.5 | 3.6 |
| Inf. Nasal | 0.2 | -6.1 | 3.9 | -4.8 | -19.0 | 3.7 |
| Inf. Temp. | -0.1 | -4.1 | 2.7 | -5.3 | -17.1 | 1.3 |

**Table 3-13. Sectoral visual field mean deviation in decibels**

The plots of structural parameter against sector MD for the following parameters suggested a curvilinear relationship: neuroretinal rim area, neuroretinal rim volume and RNFL cross-sectional area. Quadratic regression fits were significantly better than linear fits for these parameters, with the

exception of neuroretinal rim area and RNFL cross-sectional area in the infero-nasal sector. The coefficient of determination ($R^2$) for the regression analyses are given in Table 3-14.
The plot of global neuroretinal rim area against MD is illustrated in Figure 3-25.

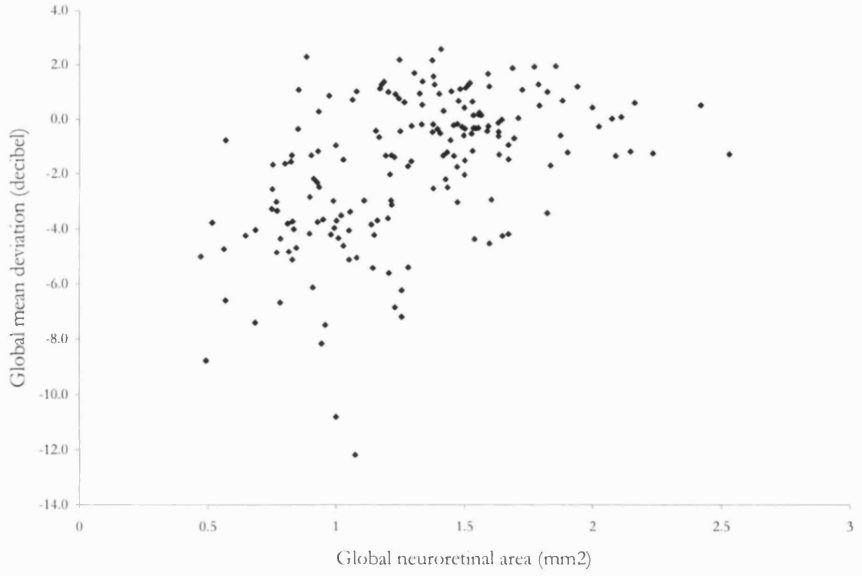


**Figure 3-25. Plot of global neuroretinal rim area against decibel mean deviation**

| | G | T | ST | SN | N | IN | IT |
|---|---|---|---|---|---|---|---|
| NRR area | 0.28 | ns | 0.26 | ns | ns | 0.14 * | 0.38 |
| NRR volume | 0.29 | ns | 0.21 | ns | ns | 0.19 | 0.35 |
| RNFL cross-sectional area | 0.17 | ns | ns | ns | ns | 0.12 * | 0.24 |

(G = global, T = temporal, ST = supero-temporal, SN = supero-nasal, N = nasal, IN = infero-nasal, IT = infero-temporal; all regressions were significant at $p < 0.0001$, ns = $R^2 < 0.1$)

**Table 3-14. Coefficient of determination ($R^2$) for quadratic (or * linear) regressions of sector structural parameter against sector mean deviation.**

Linear fits were the best model to describe cup area, cup volume, mean height of contour and cup shape measure, with the exception of cup area in the infero-temporal sector and mean height of contour in the global and infero-temporal sectors. The coefficient of determination ($R^2$) for the regression analyses are given in Table 3-15.

| | G | T | ST | SN | N | IN | IT |
|---|---|---|---|---|---|---|---|
| Cup area | 0.20 | ns | 0.17 | ns | ns | 0.13 | 0.31 * |
| Cup volume | 0.15 | ns | 0.14 | ns | ns | ns | 0.15 |
| Mean height of contour | 0.22 * | ns | 0.14 | ns | ns | 0.15 | 0.29 * |
| Cup shape measure | 0.19 | ns | ns | ns | ns | ns | 0.21 |

(G = global, T = temporal, ST = supero-temporal, SN = supero-nasal, N = nasal, IN = infero-nasal, IT = infero-temporal; all regressions were significant at $p < 0.0001$, ns = $R^2 < 0.1$)

**Table 3-15. Coefficient of determination ($R^2$) for linear (or * quadratic) regressions of sector structural parameter against sector mean deviation.**

Regression analysis of sector log neuroretinal rim area against sector mean deviaition, and sector 'log rim defect' and sector 'log sensitivity defect', demonstrated a linear relationship. The plot of global log neuroretinal rim area against global mean deviation (decibel) is shown in Figure 3-26, and of global 'log rim defect' against global 'log sensitivity defect' in Figure 3-27.

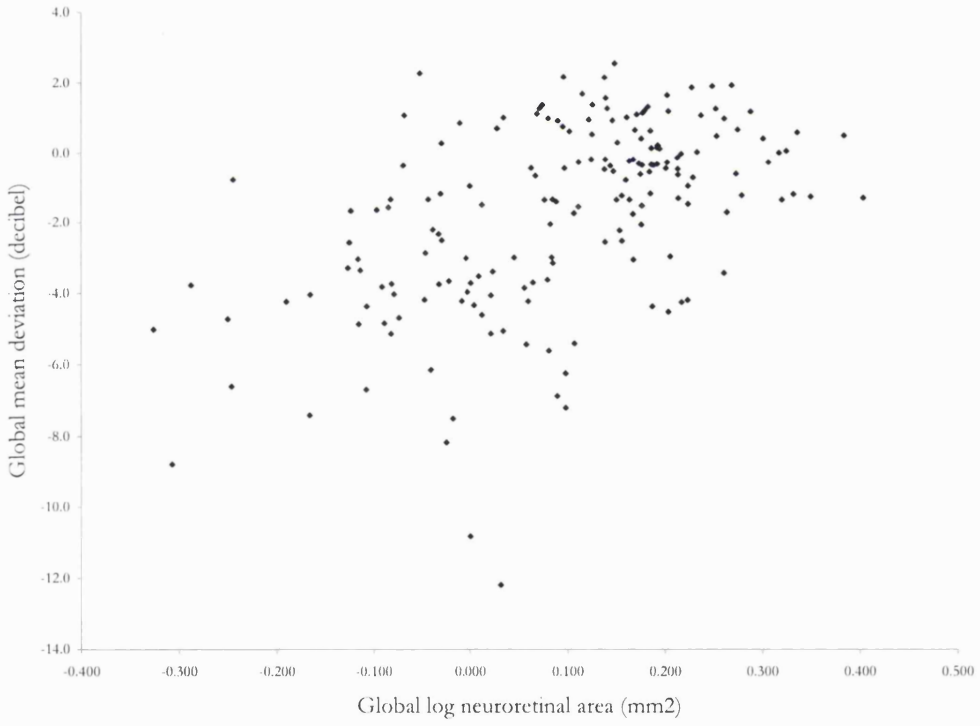


**Figure 3-26. Plot of global log neuroretinal rim area against decibel global mean deviation**

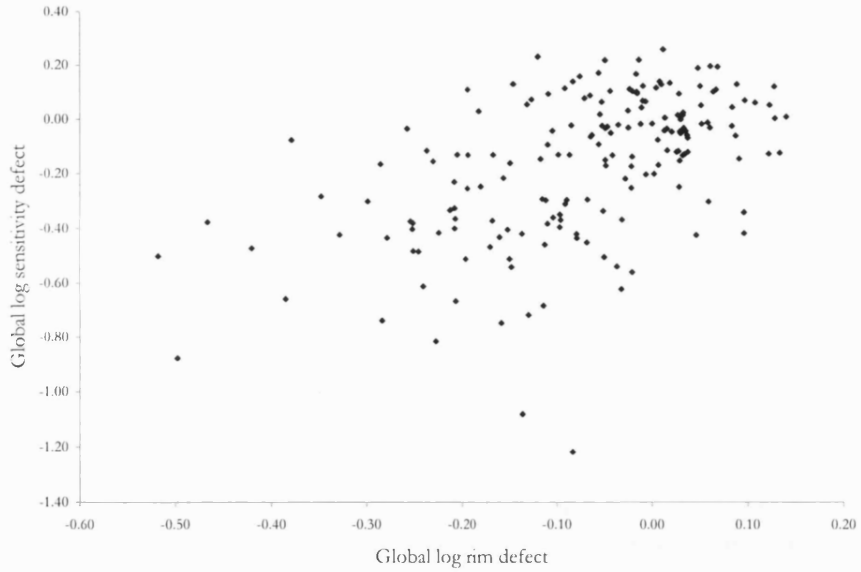


**Figure 3-27. Plot of global log rim defect against global log sensitivity defect.**

The coefficients of determination for the linear regression of 'log rim defect' (standard reference plane) and of log neuroretinal rim area (standard and 320μ reference planes) against log sensitivity defect and decibel mean deviation, respectively, are given in Table 3-16.

| | Log rim defect (standard reference plane) | Log NRR area (standard reference plane) | Log NRR area (320μ reference plane) |
|---|---|---|---|
| Global | 0.27 | 0.27 | 0.22 |
| Temporal | ns | ns | ns |
| Supero-temporal | 0.25 | 0.26 | 0.24 |
| Supero-nasal | ns | ns | 0.15 |
| Nasal | ns | ns | ns |
| Infero-nasal | 0.15 | 0.14 | 0.11 |
| Infero-temporal | 0.41 | 0.38 | 0.33 |

(All regressions were significant at $p < 0.0001$, ns = $R^2 < 0.1$)

**Table 3-16. Coefficient of determination ($R^2$) for linear regressions of sector structural parameter against sector visual field sensitivity.**

The gradient, and confidence intervals for the gradient, of the regressions of sector log rim defect against sector log sensitivity defect that were statistically significant are given in Table 3-17.

| | Constant | Gradient | Confidence intervals |
|---|---|---|---|
| Global | -0.1 | 1.1 | 0.8 - 1.3 |
| Temporal | - | - | - |
| Supero-temporal | -0.9 | 0.8 | 0.6 - 1.1 |
| Supero-nasal | - | - | - |
| Nasal | - | - | - |
| Infero-nasal | -1.0 | 1.4 | 0.9 - 1.8 |
| Infero-temporal | -0.9 | 1.0 | 0.8 - 1.2 |

**Table 3-17. Constant, gradient and 95% confidence intervals for the gradient, for regressions of sector log rim defect against sector field defect**

A plot of the anti-log of the parameters 'log rim defect' and 'log sensitivity defect' (ie the ratio of measured to expected neuroretinal rim area and the ratio of measured to expected DLS) is given in Figure 3-28.

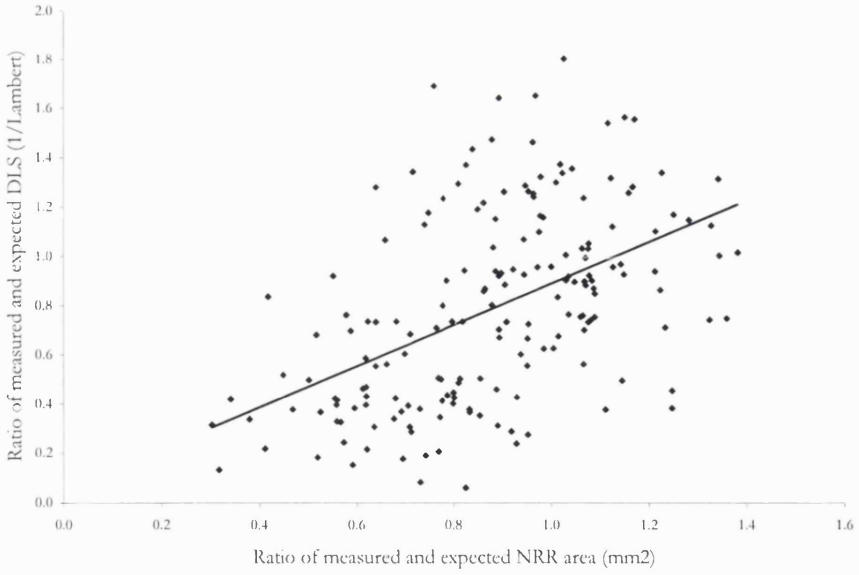


**Figure 3-28. Plot of the ratio of measured to expected neuroretinal rim (NRR) area (mm2) against the ratio of measured to expected differential light sensitivity (DLS) (1/Lambert) (equation for the regression line $y = 0.84x + 0.05$, $R^2 = 0.25$, $p<0.0000$)**

Linear regression analysis between the ratio of measured to expected DLS and the ratio of measured to expected neuroretinal rim area was significant for the whole disc (Figure 3-28) and the temporal inferior, temporal superior, and nasal inferior segments, with $r^2$ values of 0.25, 0.30, 0.20 and 0.14 respectively. At the point representing 50% expected neuroretinal rim, the percentage expected DLS was: whole disc 47% (≡ -3.3dB), temporal inferior sector 53% (≡ -2.8dB), temporal superior 59% (≡ -2.3dB) and nasal inferior 47% (≡ -3.3dB).

### 3.5.5 Discussion

The results of the study are consistent with the hypothesis that there is a curvilinear relationship between neuroretinal rim and dB DLS, and a linear relationship between neuroretinal rim area and the reciprocal of light intensity. Few studies comment on the curvilinear relationship between neuroretinal rim and dB DLS, even when apparent in plots of the data (Airaksinen et al., 1985a; Nanba and Iwata, 1992; Jonas and Grundler, 1997). In only one was a transformation attempted obtain a linear relationship (Jonas and Grundler, 1997). This transformation was to plot the square root of the visual field mean defect against neuroretinal rim area. The physiological basis for this transformation is not clear.

The relationship between sensitivity loss and neuroretinal rim loss found in this study suggests that a 50% loss of neuroretinal tissue corresponds to a 50% loss in DLS (1/Lambert scale). A 50% loss is equivalent to 3dB. For a further 50% loss of neuroretinal tissue, from this reduced level, another 3dB reduction in sensitivity would be expected. This linear relationship suggests that there is no functional reserve, but a continuous loss of DLS across the range of neuroretinal rim values. The explanation for the observation of structural changes occurring before measurable functional changes lies in the relative variability in the methods of measurement. The normal range (98% prediction intervals) for planimetric neuroretinal rim area was ± 27% to ±40% (depending on the disc segment) around the average value (Garway-Heath and Hitchings, 1998a). In other words, rim loss can be detected when between 27% and 40% has been lost. In the visual field, for a central point of mean sensitivity 32.2dB, the inter-individual standard deviation of sensitivities is about 1.9dB (Heijl et al., 1987). The 95% confidence interval will therefore be approximately 3.7dB, giving a lower limit of 28.5dB. 32.2dB represents a light intensity of 6.03 apostilbs, and 28.5dB represents 14.13 apostilbs. In other words, the lower limit of normal variability represents a light intensity a little over doubled (or DLS over halved in the scale used in this study) before a point can be identified as abnormal.

The correlations between the structural and functional measures are relatively weak, with $r^2$ values between 0.15 and 0.41 for the global, supero-temporal, infero-temporal and infero-nasal sectors. $r^2$ values were <0.10 for the temporal, nasal and supero-nasal sectors. The principal causes of the poor correlations (scatter in the data) include variations in the slope of the neuroretinal rim and optic disc tilting, inclusion of blood vessels in neuroretinal rim estimation by the HRT software algorithm,

poor sampling of the visual field (especially in the temporal and nasal sectors) and psychophysical variability. Newer testing algorithms, such as the SITA (Bengtsson and Heijl, 1998), may improve the ability to detect abnormal points in the field by reducing inter-individual variability.

There was a stronger relationship between the DLS and neuroretinal rim area in some parts of the disc than in others. The probable explanation for this is that there is a greater number of visual field test points in some field segments than in others (section 3.4). As a result, there is greater sampling, and noise is averaged out. The temporal and nasal sectors occupy the largest extent of the optic disc (each 90° for the HRT 'predefined' sectors), and have fewest corresponding field test points, resulting in poorer measurement precision.

The confidence intervals of the slopes of the regression analysis between log rim defect and field defect all included 1.0 (Table 3-17), for those regressions that were significant. This would suggest that the value for 'k' approximated 1.0 in the theoretical relationship:

$k * \log NRR = \log C - \log L$

One might expect a value of <1.0, as physiological spatial summation in the central field is <1.0. This could indicate that spatial summation increases in glaucoma. Alternatively, it may reflect changes in the configuration of the neuroretinal rim with advancing disease, such as the average slope of axons as they enter the lamina cribrosa, and the proportion of glial tissue and capillaries in the neuroretinal rim.

There was no apparent difference in the strength of correlation with the two reference plane options in the HRT (Table 3-16), although the correlation in the supero-nasal segment became significant when the 320μ reference plane was used.

The strength of correlation between neuroretinal rim area and sector field defect was not improved by taking the 'log rim defect' parameter. This is in agreement with a previous finding (Jonas and Grundler, 1997). It may be that it is the actual neuroretinal rim area that determines DLS, rather than the neuroretinal rim in relation to that expected for the disc size.

# 4 SECTION IV: Discussion and Summary

## 4.1 Ocular magnification corrections

### 4.1.1 Summary

This study confirms that the abbreviated axial length method (BRE2) differs little from the more detailed calculations that use keratometry, ametropia, ACD and lens thickness in addition (method BRE1), and is appreciably more accurate than the methods that use keratometry and ametropia alone. Therefore, if axial length is known, method BRE2 should be used in preference to methods that rely on only keratometry and ametropia.

Axial length measured using a contact ultrasound probe probably underestimates true axial length by around 0.25mm, and a correction for this should be made.

If axial length is not known, then the 'keratometry and ametropia' methods that have greatest equivalence (least off-set bias) to the axial length methods are the New method, described in section 3.2.1.1.6, and the HRT method.

'Keratometry and ametropia' methods underestimate magnification in long eyes.

The study sheds light on the inter-relation of the refractive components of the eye. In order to maintain emmetropia in an eye, variables such as corneal power, lens power, and axial length have to be balanced. Corneal and lens power are negatively correlated with axial length, so that both corneal power and lens power decrease with increasing axial length. One might therefore expect corneal power and lens power to be positively correlated. However, if axial length is constant, corneal and lens power have to be negatively correlated to maintain emmetropia. Axial length modifies the relationship between corneal and lens power.

### 4.1.2 Implications

More accurate estimation of the size of ONH features is possible if ocular magnification corrections are made on the basis of axial length. The correlation between structural and functional measurements may be improved by these more accurate measurements.

### 4.1.3 Further work

A preliminary study of magnification corrections in 43 normal eyes indicates that the correlation between neuroretinal rim area and optic disc area is greater when correction is made on the basis of axial length than when made on the basis of keratometry and ametropia. Further study is planned to evaluate the correlations with visual function.

## 4.2 Distinguishing between normal and glaucomatous eyes

### 4.2.1 Summary

These studies (section 3.2.2 and (Garway-Heath and Hitchings, 1998a)) identify that the neuroretinal rim area is the most useful morphological parameter to distinguish between normal and glaucomatous optic discs. They indicate that the facility to distinguish between normal and glaucomatous optic discs is improved by taking into account the physiological relationship between optic disc size and neuroretinal rim area and by quantifying the neuroretinal rim area in optic disc segments, thereby allowing the identification of focal neuroretinal rim loss.
Potential sources of bias in the study populations were identified, which cast doubt on the validity of studies examining the pattern of glaucomatous neuroretinal rim loss in clinic-based populations.

### 4.2.2 Implications – clinical application

The method of data analysis developed in this thesis has now been incorporated into the HRT software.

#### 4.2.2.1 Case-finding

Currently, case finding is on the basis of intra-ocular pressure (IOP) tests, visual field testing (usually suprathreshold perimetry) and optic disc examination. Table 4-1 summarises the sensitivity and specificity of each method, used alone, for case detection.

| | Specificity (%) | Sensitivity (%) |
|---|---|---|
| IOP (> 21 mmHg) (Katz et al., 1993) | 92 | 47 |
| Suprathreshold perimetry (Katz et al., 1993) | 90 | 52 |
| ONH structure (HRT) (Wollstein et al., 1998) | 96 | 84 |

**Table 4-1. Sensitivity and specificity of tests that may be used for case-finding**

On the basis of these figures, ONH analysis is the best single test, although the HRT has yet to be tested on a population basis. Even at these high levels of sensitivity and specificity, because the prevalence of glaucoma is low, large numbers of false-positive cases will be 'detected', and 16% of glaucoma cases will be missed. At a prevalence of about 2.5% in the over 50 age group (Mitchell et al., 1996), for every 1000 subjects tested, there would be 21 cases detected, 39 false-positive cases, and 4 cases would be missed.

The sensitivity and specificity of a test depends on the cut-off selected. When a cut-off is varied, as sensitivity rises, specificity falls, and vice versa. Different cut-offs can therefore be applied, depending on the disease prevalence in a given population. It is known that glaucoma becomes more

prevalent as IOP rises (Mitchell et al., 1996). A cut-off with higher sensitivity can, therefore, be applied to individuals in a population with a high IOP, and a cut-off with higher specificity to individuals with a low IOP. In this way, the number of false-positive cases can be reduced to around 29 per 1000, without affecting the numbers of cases detected and missed.

#### 4.2.2.2 Categorising individual patients

A single cut-off, together with the disease prevalence, will only give the probability of an individual being normal or glaucomatous. To take the example above, with 96% specificity, 84% sensitivity, and a glaucoma prevalence of 2.5%, and given a positive test result, the probability of the individual having glaucoma is about 35%.

The glaucoma prevalence in a population referred from the Optometrist is typically higher, and usually at least 30% (Vernon, 1998). The probability that a positive test result represents glaucoma is 90% in this population.

However, for a test result to be clinically useful, the clinician needs to know, with a high degree of certainty, whether the result indicates that an individual patient is normal or abnormal. For this purpose, 2 cut-off levels can be used, one with very high specificity, and one with very high sensitivity. If a subject lies below the high-specificity cut-off, then the clinician can be reasonably sure that the individual has glaucoma. Similarly, if a subject lies above the high-sensitivity cut-off, then the clinician can be reasonably sure that the individual is normal. Subjects lying between the cut-offs are 'borderline' individuals. This analysis has been incorporated into the HRT software (version 2.01S) and the HRTII software.

To illustrate this approach, the following two cut-offs have been selected: a) specificity 99.1%, sensitivity 70.1% and b) specificity 88.4%, sensitivity 93.5%. If these are applied to a population with a 30% glaucoma prevalence (such as that referred from an optometrist), then 85.5% of subjects will be categorised (63.8% as 'normal' and 21.7% as 'glaucomatous') and 14.5% will be 'borderline'. Of those categorised, the probability that the classification is correct is 97% (for both categories). Of those labelled 'borderline', the probability that they are glaucomatous is 48%.

This approach to diagnosis may be applied to patients referred to the hospital eye service as glaucoma suspects. Figure 4-1 is an illustrative protocol.

85.5% of patients in this population are classified by the HRT as either 'normal' or 'glaucomatous' and require no visual field testing in the Primary Care Clinic (PCC). 14.5% are classified as 'borderline', and require visual field testing. The level of ocular hypertension that requires onward referral will depend on unit policy, and the results of the HRT analysis. The numbers referred on to the glaucoma clinics under this protocol would be:

1) 21.7% with an HRT classification of 'glaucoma'
2) 7.0% with an HRT classification of 'borderline' and an abnormal visual field (that is, glaucoma cases classified as 'borderline' by the HRT)
3) the percentage of individuals with an HRT classification of 'normal' and significant ocular hypertension
4) normal individuals with an HRT classification of 'borderline' and a suspicious visual field.

6.5% of early glaucoma patients have a 'normal' HRT classification (1.6% of the population referred to PCC), so the number of glaucoma patients discharged would be the fraction of this number that do not have significant ocular hypertension. 0.9% of normal individuals (0.7% of the population referred to PCC) would be referred on with an HRT classification of 'glaucoma'.

### 4.2.3 Further work

The reference plane options in the HRT software are not optimal. The software version 1.10 reference plane is set at the outer part of the image and the absolute height may be affected by loss of axons in glaucoma and poor centration of the ONH in the image. The orientation of the plane may not be appropriate if the ONH is tilted. The software version 1.11 reference plane is set at the temporal margin of the ONH and the absolute height may be affected by loss of axons in glaucoma and imaging artefact over the scleral ring. The orientation of the plane also may not be appropriate if the ONH is tilted, although the effect is likely to be less than with the version 1.10 reference plane. Improved accuracy in the quantification of ONH anatomy, such as the neuroretinal rim, may be possible if the reference plane can be set from the scleral ring itself. A study has been initiated to assess the feasibility of identifying the contribution of the sclera to the depth reflectance (z-) profile by image deconvolution and curve-fitting.

The database, established in the studies reported in this thesis, is derived from a Caucasian population. It is well established that ONH morphology is related to ethnicity. It is, therefore, desirable to developed databases from other populations to identify differences, where they occur, and the impact of the differences on the method of data analysis presented in this thesis. Data derived from planimetry and HRT analysis from population studies in Thailand, Singapore and South Africa will shortly be available for analysis.

The clinical application of the method of classification by disc morphology is being tested in the Primary Care Clinic at Moorfields Eye Hospital. However, validation is needed in other centres as normal and patient populations may vary, as may the drawing of the ONH margin in the analysis of HRT images. Such a validation study is under way.

**Numbers per 1000 referred to PCC (assuming a 30% glaucoma prevalence in the referred population)**

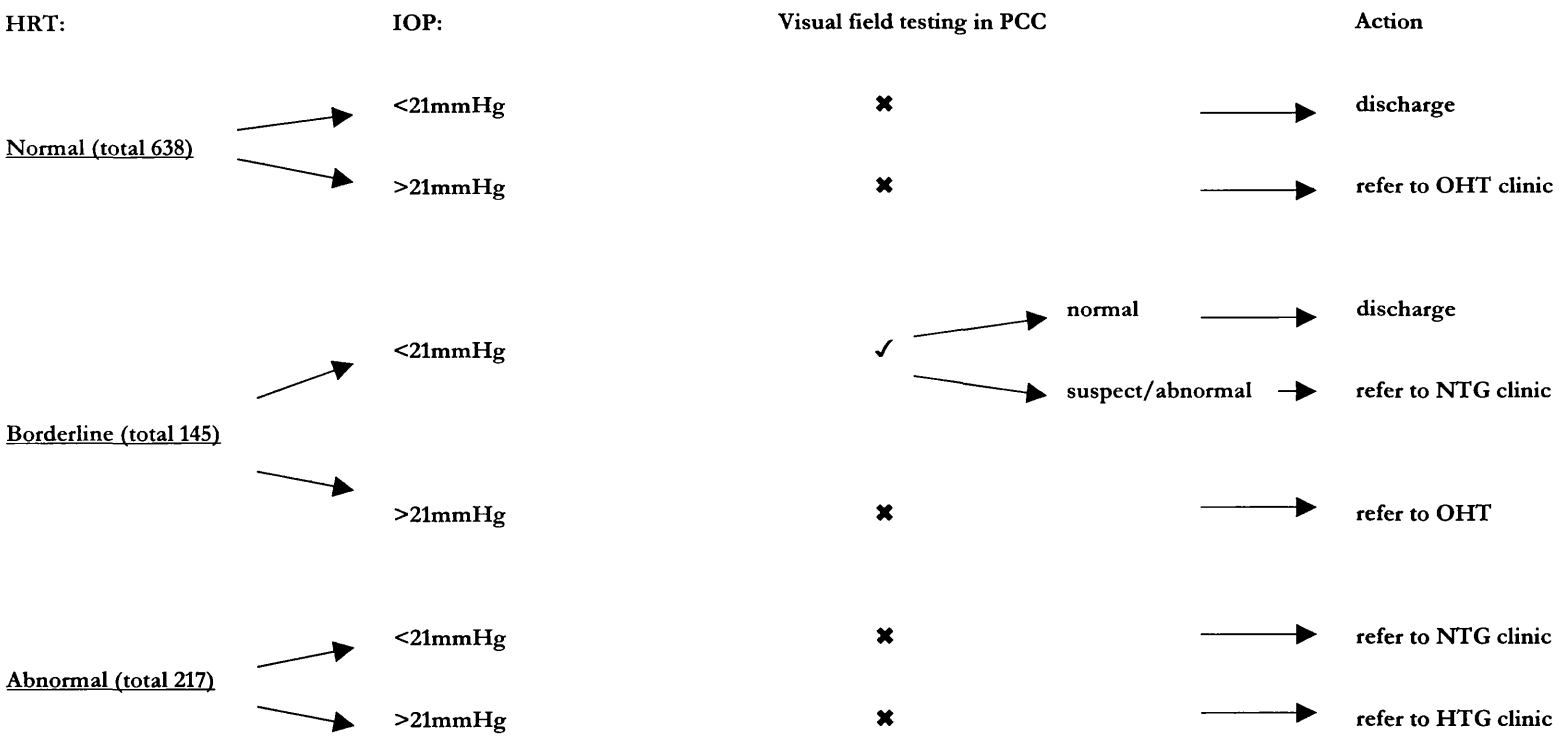


**Figure 4-1. Projected breakdown of the HRT classification of 1000 'glaucoma suspect' referrals and indications for visual field testing in the PCC.**

PCC = primary care clinic, OHT = ocular hypertension, NTG = normal tension glaucoma, HTG = high tension glaucoma

## 4.3 Measurement of ganglion cell function

### 4.3.1 Summary

The results of this study indicate that the physiological relationship between dB DLS and underlying ganglion cell number is curvilinear. When DLS is appropriately scaled, as the reciprocal of test spot intensity, there is a linear relationship with underlying ganglion cell numbers adjusted for spatial summation.

If the physiological relationship is extrapolated to glaucomatous ganglion cell loss, equal dB sensitivity losses equate with differing ganglion cell losses, depending on the location in the visual field. The probability symbols give a better indication of the severity of damage.

### 4.3.2 Implications

The model suggests a reappraisal of 'staging' disease by perimetric indices. The loss of the first 5dB, often regarded as early disease, in fact represents moderately advanced disease. And the difference between a MD of -10 and -15dB represents a far lesser change. It also suggests that the impression of an anatomical 'functional reserve', the loss of which is required before function is compromised, is a reflection of the logarithmic nature of the scale for DLS. In fact, there is a continuous, linear, relationship between DLS and underlying neural units. The difficulty in detecting early anatomical damage by tests of function may be a reflection of the wide inter-individual range in the number ganglion cell in the retina, and the wide inter-individual range of psychophysical measurements.

A linear model applied to dB DLS values is likely to be less sensitive in early disease. There is a need to re-evaluate models of progression in the context of the new DLS scale proposed in this thesis.

### 4.3.3 Further work

Extrapolation of the physiological relationship between DLS and ganglion cell numbers to the pathological condition of glaucoma presupposes that spatial summation remains unchanged as ganglion cells are lost. There is limited data in the literature, and further studies are planned.

Similarly, there is little data on the relationship between spatial summation and age. Further studies are planned to clarify this relationship.

Ganglion cell numbers cannot yet be quantified in vivo. However, there is published histological data relating ganglion cell numbers to visual function (Quigley et al., 1989; Kerrigan-Baumrind et al., 2000). Preliminary results from a collaborative study, with Professor Quigley, reanalysing his data with respect to spatial summation and a linear scale, confirm a linear relationship between ganglion cell numbers and DLS (1/Lambert).

## 4.4 Anatomical correlation between the visual field and optic disc

### 4.4.1 Summary

This study has produced a clinically useful map that relates visual field test points to regions of the ONH. The map will aid clinical evaluation of glaucoma patients and suspects, as well as forming the basis for investigations of the relationship between retinal light sensitivity and ONH structure.

### 4.4.2 Implications

A significant feature of the visual field test is the variability across the field in the density of test points in relation to ONH sectors. The poles of the ONH are much more densely sampled (arcuate areas of the field) than the temporal and nasal parts of the ONH (central and temporal areas of the field). This is likely to have a marked effect on the ease with which glaucomatous damage at the ONH is identified by the visual field. Criteria for glaucomatous visual field loss typically require a cluster of points with abnormal sensitivity (Asman and Heijl, 1992; Asman et al., 1992; Gaasterland et al., 1994). If neuroretinal rim loss is focal, or uneven, the chances of obtaining a cluster of abnormal points will be greatest where the sampling is densest, that is in field regions corresponding to the poles of the disc. It is, therefore, hardly surprising that thinning at the poles is frequently the earliest identified sign in early perimetric glaucoma (Pederson and Anderson, 1980; Jonas et al., 1993). Focal loss elsewhere is less likely to result in a cluster of depressed field points, and the eyes remain categorised as 'ocular hypertensive' or 'glaucoma suspect'.

### 4.4.3 Further work

The map derived in the study represents an 'average map'. However, the study identified systematic variations in the relationship between visual field and optic disc location. The position of the ONH in relation to the fovea had a major effect. It should be possible to refine the map on an individual basis by taking the ONH/fovea position into account. Other factors, such rotation and tilting of the ONH, need further investigation.

Visual field test locations are known to be functionally inter-dependent (Crabb et al., 1997). The map may form the basis for 'anatomical filters' for the processing ('smoothing') of visual field data on the basis of the anatomical proximity at the ONH of visual field test points (Figure 4-2).

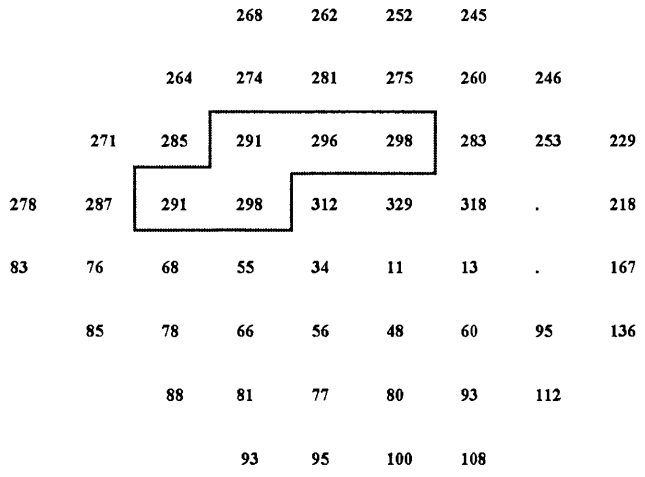


**Figure 4-2. Example of the construction of an 'anatomical filter' for the analysis of visual field data. The figures for each visual field point represents its associated position at the ONH.**

## 4.5 Correlation between visual field light sensitivity and optic disc morphometry

### 4.5.1 Summary

The results of the study are consistent with the hypothesis that there is a curvilinear relationship between neuroretinal rim and dB DLS, and a linear relationship between neuroretinal rim area and the reciprocal of light intensity.

### 4.5.2 Implications

The linear nature of the neuroretinal rim/DLS relationship reinforces the findings of the study investigating the physiological relationship between ganglion cell numbers and DLS (section 3.3). A 3dB loss represents, on average, a 50% neuroretinal rim loss, and moderately advanced disease. The curvilinear relationship between neuroretinal rim and dB DLS suggests the need for a reappraisal of models of progression.

There is less variability in measurements of structure than of function, so that imaging tools are likely to be more useful in diagnosis and management of early disease.

### 4.5.3 Further work

The relationship between sensitivity loss and neuroretinal rim loss found in this study suggests that a 50% loss of neuroretinal tissue corresponds to a 50% loss in DLS (1/Lambert scale). This suggests either a change in spatial summation or a changing relationship between neuroretinal rim area and DLS in disease. Further work will be needed to clarify this.

The correlations between the structural and functional measures are relatively weak, and better methods to quantify both ONH structure and function are needed. Further work will be directed towards improving the interpretation of measurement data derived from confocal scanning laser ophthalmoscopy, scanning laser polarimetry, optical coherence tomography and stereophotogrammetry. Measures of ONH function may be improved with alternative testing strategies (more even sampling of the visual field), better data processing (anatomical/functional filters), or new psychophysical or electrophysiological tests (for example, motion detection and the multifocal electroretinogram).

# 5 SECTION V: Supporting publications

## 5.1 Published papers and chapters


Garway-Heath, D. F., Wollstein, G. and Hitchings, R. A. (1997) Aging changes of the optic nerve head in relation to open angle glaucoma, *Br J Ophthalmol,* 81, 840-5.

Garway-Heath, D. F., Ruben, S. T., Viswanathan, A. and Hitchings, R. A. (1998) Vertical cup/disc ratio in relation to optic disc size: its value in the assessment of the glaucoma suspect, *Br J Ophthalmol,* 82, 1118-24.

Garway-Heath, D. F., Rudnicka, A. R., Lowe, T., Foster, P. J., Fitzke, F. W. and Hitchings, R. A. (1998) Measurement of optic disc size: equivalence of methods to correct for ocular magnification, *Br J Ophthalmol,* 82, 643-9.

Wollstein, G., Garway-Heath, D. F. and Hitchings, R. A. (1998) Identification of early glaucoma cases with the scanning laser ophthalmoscope, *Ophthalmology,* 105, 1557-63.

Garway-Heath, D. F. and Hitchings, R. A. (1998) Quantitative evaluation of the optic nerve head in early glaucoma, *Br J Ophthalmol,* 82, 352-61.

Garway-Heath, D. F. and Hitchings, R. A. (1998) Sources of bias in studies of optic disc and retinal nerve fibre layer morphology, *Br J Ophthalmol,* 82, 986.

Garway-Heath, D. F. (1999) Discs in practice. In *Key advances in glaucoma* RSM Publishing, London.

Garway-Heath, D. F., Poinoosawmy, D., Wollstein, G., Viswanathan, A., Kamal, D., Fontana, L. and Hitchings, R. A. (1999) Inter- and intraobserver variation in the analysis of optic disc images: comparison of the Heidelberg retina tomograph and computer assisted planimetry, *Br J Ophthalmol,* 83, 664-9.

Garway-Heath, D. F., Viswanathan, A., Westcott, M., Kamal, D., Fitzke, F. W. and Hitchings, R. A. (1999) Relationship between perimetric light sensitivity and optic disc neuroretinal rim area. In *Perimetry Update 1998/1999* (Eds, Wall, M. and Wild, J. M.) Kugler Publications, The Hague, The Netherlands, pp. 381-89.

Garway-Heath, D. F., Caprioli, J., Fitzke, F. W. and Hitchings, R. A. (2000) Scaling the hill of vision: The physiological relationship between ganglion cell numbers and light sensitivity, *Invest Ophthalmol Vis Sci,* 41, 1774-82.

Garway-Heath, D. F., Poinoosawmy, D., Fitzke, F. W. and Hitchings, R. A. (2000) Mapping the visual field to the optic disc in normal tension glaucoma eyes, *Ophthalmology,* 107, 1809-15.

# 6 SECTION V: References


Airaksinen, P. J., Mustonen, E. and Alanko, H. I. (1981) Optic disc haemorrhages precede retinal nerve fibre layer defects in ocular hypertension, *Arch Ophthalmol,* 99, 1795-801.

Airaksinen, P. J., Drance, S. M., Douglas, G. R., Mawson, D. K. and Nieminen, H. (1984) Diffuse and localized nerve fiber loss in glaucoma, *Am J Ophthalmol,* 98, 566-71.

Airaksinen, P. J. and Drance, S. M. (1985) Neuroretinal rim area and retinal nerve fiber layer in glaucoma, *Arch Ophthalmol,* 103, 203-4.

Airaksinen, P. J., Drance, S. M., Douglas, G. R. and Schulzer, M. (1985a) Neuroretinal rim areas and visual field indices in glaucoma, *Am J Ophthalmol,* 99, 107-10.

Airaksinen, P. J., Drance, S. M., Douglas, G. R., Schulzer, M. and Wijsman, K. (1985b) Visual field and retinal nerve fiber layer comparisons in glaucoma, *Arch Ophthalmol,* 103, 205-7.

Airaksinen, P. J., Tuulonen, A., Valimaki, J. and Alanko, H. I. (1990) Retinal nerve fiber layer abnormalities and high-pass resolution perimetry, *Acta Ophthalmol Copenh,* 68, 687-9.

Airaksinen, P. J., Tuulonen, A. and Alanko, H. I. (1992) Rate and pattern of neuroretinal rim area decrease in ocular hypertension and glaucoma, *Arch Ophthalmol,* 110, 206-10.

Allingham, R. R., Wiggs, J. L., De La Paz, M. A., Vollrath, D., Tallett, D. A., Broomer, B., Jones, K. H., Del Bono, E. A., Kern, J., Patterson, K., Haines, J. L. and Pericak-Vance, M. A. (1998) Gln368STOP myocilin mutation in families with late-onset primary open- angle glaucoma, *Invest Ophthalmol Vis Sci,* 39, 2288-95.

Anctil, J. L. and Anderson, D. R. (1984) Early foveal involvement and generalized depression of the visual field in glaucoma, *Arch Ophthalmol,* 102, 363-70.

Anderson, D. R. (1969) Ultrastructure of human and monkey lamina cribrosa and optic nerve head, *Arch Ophthalmol,* 82, 800-14.

Anton, A., Yamagishi, N., Zangwill, L., Sample, P. A. and Weinreb, R. N. (1998) Mapping structural to functional damage in glaucoma with standard automated perimetry and confocal scanning laser ophthalmoscopy, *Am J Ophthalmol,* 125, 436-46.

Armaly, M. E. (1969a) The correlation between the appearence of the optic cup and visual function, *Trans Amer Acad Ophth and Otolaryngology,* 73, 898-913.

Armaly, M. F. (1969b) The optic cup in the normal eye, *Am J Ophthalmol,* 68, 405-7.

Armaly, M. F. and Sayegh, R. E. (1969) The Cup/Disc Ratio. The findings of tonometry and tomography in the normal eye, *Arch Ophthalmol,* 82, 191-6.

Armaly, M. F., Krueger, E. D., Maunder, L., Becker, B., Hetherington, J., Kolker, A. E., Levene, R. Z., Maumenee, E., Pollack, I. P. and Shaffer, R. N. (1980) Biostatistical analysis of the collaborative glaucoma study: I. Summary report of the risk factors for glaucomatous visual-field defects, *Arch Ophthalmol,* 98, 2163-73.

Arnold, J. V., Gates, J. W. C. and Taylor, K. M. (1993) Possible errors in the measurement of retinal lesions, *Invest Ophth Vis Sci,* 34, 2576-80.

Asman, P. and Heijl, A. (1992) Glaucoma Hemifield Test. Automated visual field evaluation, *Arch Ophthalmol,* 110, 812-9.

Asman, P., Heijl, A., Olsson, J. and Rootzen, H. (1992) Spatial analyses of glaucomatous visual fields; a comparison with traditional visual field indices, *Acta Ophthalmol Copenh,* 70, 679-86.

Atchison, D. A. (1987) Effect of defocus on visual field measurement, *Ophthalmic Physiol Opt,* 7, 259-65.

Aulhorn, E. and Harms, H. (1972) In *Handbook of sensory physiology*, Vol. 7 (Ed, Autrum, J.) Springer-Verlag, New York.

Aulhorn, E. and Karmeyer, H. (1977) Frequency distribution in early glaucomatous visual field defects, *Docum Ophthalmol Proc Series,* 14, 75-83.

Balazsi, A. G., Drance, S. M., Schulzer, M. and Douglas, G. R. (1984a) Neuroretinal rim area in suspected glaucoma and early chronic open-angle glaucoma. Correlation with parameters of visual function, *Arch Ophthalmol,* 102, 1011-4.

Balazsi, A. G., Rootman, J., Drance, S. M., Schulzer, M. and Douglas, G. R. (1984b) The effect of age on the nerve fiber population of the human optic nerve, *Am J Ophthalmol,* 97, 760-6.

Bankes, J. L. K., Perkins, E. S., Tsolakis, S. and Wright, J. E. (1968) Bedford Glaucoma Survey, *Br Med J,* 1, 791-6.

Barr, D. B. (1995) An appraisal of the accuracy of Littmann's method of determining the real dimension of a retinal object., *Acta Ophthalmologica Scandinavica Supplement,* 216, 1-12.

Bartsch, D. U. and Freeman, W. R. (1993) Laser-Tissue Interaction and Artifacts in Confocal Scanning Laser Ophthalmoscopy and Tomography, *Neuroscience & Biobehavioral Reviews,* 17, 459-67.

Bartsch, D. U. and Freeman, W. R. (1994) Axial intensity distribution analysis of the human retina with a confocal scanning laser tomograph, *Exp Eye Res,* 58, 161-73.

Bartz Schmidt, K. U. and Weber, J. (1993) Comparison of spatial thresholds and intensity thresholds in glaucoma, *Int Ophthalmol,* 17, 171-8.

Bartz-Schmidt, K. U., Weber, J. and Heimann, K. (1994) Validity of Two-Dimensional Data Obtained with the Heidelberg Retina Tomograph as Verified by Direct Measurements in Normal Optic Nerve Heads, *German Journal of Ophthalmology,* 3, 400-5.

Bathija, R., Zangwill, L., Berry, C. C., Sample, P. A. and Weinreb, R. N. (1998) Detection of early glaucomatous structural damage with confocal scanning laser tomography, *J Glaucoma,* 7, 121-7.

Bedwell, C. H. (1982) In *Visual Fields. A basis for efficient investigation* Butterworth Scientific, London, pp. 122-70.

Behrendt, T. and Doyle, K. E. (1965) Reliability of image size measurements in the new Zeiss fundus camera, *Am J Ophthalmol,* 59, 896-9.

Bengtsson, B. (1976) The variation and covariation of cup and disc diameters, *Acta Ophthalmologica,* 54, 804-18.

Bengtsson, B. and Krakau, C. E. T. (1977) Some essential optical features of the Zeiss fundus camera, *Acta Ophthalmol (Kbh.),* 55, 123-31.

Bengtsson, B. (1980) The alteration and asymmetry of cup and disc diameters, *Acta Ophthalmol,* 58, 726-32.

Bengtsson, B. (1981a) The prevalence of glaucoma, *Br J Ophthalmol,* 65, 46-9.

Bengtsson, B. (1981b) Aspects of the epidemiology of chronic glaucoma, *Acta Ophthalmol Suppl (Copenh),* 146, 1.

Bengtsson, B. (1989) Incidence of manifest glaucoma, *Br J Ophthalmol,* 73, 483-7.

Bengtsson, B. and Krakau, C. E. T. (1992) Correction of optic disc measurements on fundus photographs, *Graefes Arch Clin Exp Ophthalmol,* 230, 24-8.

Bengtsson, B. and Heijl, A. (1998) SITA Fast, a new rapid perimetric threshold test. Description of methods and evaluation in patients with manifest and suspect glaucoma [In Process Citation], *Acta Ophthalmol Scand,* 76, 431-7.

Bengtsson, B. (1999) Measurement of optic disc size (letter), *Br J Ophthalmol,* 83, 252.

Bennett, A. G. (1988) A method of determining the equivalent powers of the eye and its crystalline lens without resort to phakometry, *Ophthal Physiol Opt,* 8, 53-9.

Bennett, A. G. and Rabbetts, R. B. (1989) In *Clinical Visual Optics* Butterworths, Second London, pp. 249-74.

Bennett, A. G., Rudnicka, A. R. and Edgar, D. F. (1994) Improvements on Littmann's method of determining the size of retinal features by fundus photography, *Graefes Arch Clin Exp Ophthalmol,* 232, 361-7.

Betz, P., Camps, F., Collignon-Brach, C. and Weekers, R. (1981) Stereophotography and photogrammetry of the physiological cup of the disc (author's transl), *J Fr Ophtalmol,* 4, 193-203.

Bhandari, A., Fontana, L., Fitzke, F. W. and Hitchings, R. A. (1997) Quantitative analysis of the lamina cribrosa in vivo using a scanning laser opthalmoscope, *Curr Eye Res,* 16, 1-8.

Bland, J. M. and Altman, D. G. (1986) Statistical methods for assessing agreement between two methods of clinical measurement, *Lancet,* 1, 307-10.

Bland, M. (1995a) In *An Introduction to Medical Statistics* Oxford Medical Publications, 2nd Oxford, U.K., pp. 191-2.

Bland, M. (1995b) In *An introduction to medical statistics* Oxford Medical Publications, Oxford, U.K., pp. 313-4.

Bland, M. (1995c) In *An Introduction to Medical Statistics* Oxford Medical Publications, 2nd Oxford, UK, pp. 93-4.

Boeglin, R. J., Caprioli, J. and Zulauf, M. (1992) Long-term fluctuation of the visual field in glaucoma, *Am J Ophthalmol,* 113, 396-400.

Brigatti, L. and Caprioli, J. (1995) Correlation of visual field with scanning confocal laser optic disc measurements in glaucoma [published erratum appears in Arch Ophthalmol 1996 Apr;114(4):424], *Arch Ophthalmol,* 113, 1191-4.

Britton, R. J., Drance, S. M., Schulzer, M., Douglas, G. R. and Morrison, D. K. (1987) The area of the neuroretinal rim of the optic nerve in normal eyes, *Am J Ophthalmol,* 103, 497-504.

Broadway, D. C. and Drance, S. M. (1998) Glaucoma and vasospasm [see comments], *Br J Ophthalmol,* 82, 862-70.

Broadway, D. C., Nicolela, M. T. and Drance, S. M. (1999) Optic disk appearances in primary open-angle glaucoma, *Surv Ophthalmol,* 43 Suppl 1, S223-43.

Bunce, C., Evans, J., Fraser, S. and Wormald, R. (1998) BD8 certification of visually impaired people, *Br J Ophthalmol,* 82, 72-6.

Butcher, J. M. and O'Brien, C. (1991) The reproducibility of biometry and keratometry measurements, *Eye,* 5, 708-11.

Butt, Z., McKillop, G., O'Brien, C., Allan, P. and Aspinall, P. (1995) Measurement of ocular blood flow velocity using colour Doppler imaging in low tension glaucoma, *Eye,* 9, 29-33.

Butt, Z., C, O. B., McKillop, G., Aspinall, P. and Allan, P. (1997) Color Doppler imaging in untreated high- and normal-pressure open-angle glaucoma, *Invest Ophthalmol Vis Sci,* 38, 690-6.

Calkins, D. J., Tsukamoto, Y. and Sterling, P. (1998) Microcircuitry and mosaic of a blue-yellow ganglion cell in the primate retina, *J Neurosci,* 18, 3373-85.

Caprioli, J., Klingbeil, U., Sears, M. and Pope, B. (1986) Reproducibility of optic disc measurements with computerized analysis of stereoscopic video images, *Arch Ophthalmol,* 104, 1035-9.

Caprioli, J. and Miller, J. M. (1987) Optic disc rim area is related to disc size in normal subjects, *Arch Ophthalmol,* 105, 1683-5.

Caprioli, J., Sears, M. and Miller, J. M. (1987) Patterns of early visual field loss in open-angle glaucoma [published erratum appears in Am J Ophthalmol 1987 Jul 15;104(1): 98], *Am J Ophthalmol,* 103, 512-7.

Caprioli, J. and Miller, J. M. (1988) Correlation of structure and function in glaucoma. Quantitative measurements of disc and field, *Ophthalmology,* 95, 723-7.

Caprioli, J. (1989) Correlation of visual function with optic nerve and nerve fiber layer structure in glaucoma, *Surv Ophthalmol,* 33, 319-30.

Caprioli, J., Ortiz Colberg, R., Miller, J. M. and Tressler, C. (1989) Measurements of peripapillary nerve fiber layer contour in glaucoma, *Am J Ophthalmol,* 108, 404-13.

Caprioli, J. (1990) The contour of the juxtapapillary nerve fiber layer in glaucoma, *Ophthalmology,* 97, 358-65.

Caprioli, J. (1994) Clinical evaluation of the optic nerve in glaucoma, *Trans Am Ophthamol Soc,* 92, 589-641.

Caprioli, J., Park, H. J., Ugurlu, S. and Hoffman, D. (1998) Slope of the peripapillary nerve fiber layer surface in glaucoma, *Invest Ophthalmol Vis Sci,* 39, 2321-8.

Carpel, E. F. and Engstrom, P. F. (1981) The normal cup-disk ratio, *Am J Ophthalmol,* 91, 588-97.

Cartwright, M. J. and Anderson, D. R. (1988) Correlation of asymmetric damage with asymmetric intraocular pressure in normal-tension glaucoma (low-tension glaucoma), *Arch Ophthalmol,* 106, 898-900.

Casagrande, V. A. (1994) A third parallel visual pathway to primate area V1, *Trends Neurosci,* 17, 305-10.

Chandler, P. A. and Grant, W. M. (1965) In *Lectures on Glaucoma* Lea and Febiger, Philadelphia, pp. 14-6, 112-3.

Charliat, G., Jolly, D. and Blanchard, F. (1994) Genetic risk factor in primary open-angle glaucoma: a case-control study, *Ophthalmic Epidemiol,* 1, 131-8.

Chauhan, B. C., LeBlanc, R. P., McCormick, T. A. and Rogers, J. B. (1993) Comparison of high-pass resolution perimetry and pattern discrimination perimetry to conventional perimetry in glaucoma, *Can J Ophthalmol,* 28, 306-11.

Chauhan, B. C., LeBlanc, R. P., McCormick, T. A. and Rogers, J. B. (1994) Test-retest variability of topographic measurements with confocal scanning laser tomography in patients with glaucoma and control subjects, *Am J Ophthalmol,* 118, 9-15.

Chen, Y. F., Wang, T. H., Lin, L. L. and Hung, P. T. (1997) Influence of axial length on visual field defects in primary open-angle glaucoma, *J Formos Med Assoc,* 96, 968-71.

Chen, Y. Y., Chen, P. P., Xu, L., Ernst, P. K., Wang, L. and Mills, R. P. (1998) Correlation of peripapillary nerve fiber layer thickness by scanning laser polarimetry with visual field defects in patients with glaucoma, *J Glaucoma,* 7, 312-6.

Chi, T., Ritch, R., Stickler, D., Pitman, B., Tsai, C. and Hsieh, F. Y. (1989) Racial differences in optic nerve head parameters, *Arch Ophthalmol,* 107, 836-9.

Coffey, M., Reidy, A., Wormald, R. P. L., Wu, J. X., Wright, L. A. and Courtney, P. (1993) Prevalence of glaucoma in the west of Ireland, *Br J Ophthalmol,* 77, 17-21.

Colenbrander, M. C. (1960) Measurement of optic disc excavation, *Ophthalmologica,* 139, 491.

Coughlan, M. and Friedmann, A. I. (1981) The frequency distribution of early visual field defects in glaucoma, *Doc Ophthalmol Proc Ser,* 26, 345-9.

Crabb, D. P., Fitzke, F. W., McNaught, A. I. and Hitchings, R. A. (1997) In *Perimetry Update 96/97* Kugler Publications, Amsterdam.

Craig, J. E. and Mackey, D. A. (1999) Glaucoma genetics: where are we? Where will we go?, *Curr Opin Ophthalmol,* 10, 126-34.

Crichton, A., Drance, S. M., Douglas, G. R. and Schulzer, M. (1989) Unequal intraocular pressure and its relation to asymmetric visual field defects in low-tension glaucoma, *Ophthalmology,* 96, 1312-4.

Curcio, C. A., Sloan, K. R., Jr., Packer, O., Hendrickson, A. E. and Kalina, R. E. (1987) Distribution of cones in human and monkey retina: individual variability and radial asymmetry, *Science,* 236, 579-82.

Curcio, C. A. and Allen, K. A. (1990) Topography of ganglion cells in human retina, *J Comp Neurol,* 300, 5-25.

Curcio, C. A., Allen, K. A., Sloan, K. R., Lerea, C. L., Hurley, J. B., Klock, I. B. and Milam, A. H. (1991) Distribution and morphology of human cone photoreceptors stained with anti-blue opsin, *J Comp Neurol,* 312, 610-24.

Dacey, D. M. and Brace, S. (1992) A coupled network for parasol but not midget ganglion cells in the primate retina, *: Vis Neurosci,* 9, 279-90.

Dacey, D. M. and Petersen, M. R. (1992) Dendritic field size and morphology of midget and parasol ganglion cells of the human retina, *Proc Natl Acad Sci U S A,* 89, 9666-70.

Dacey, D. M. (1993a) Morphology of a small-field bistratified ganglion cell type in the macaque and human retina, *Vis Neurosci,* 10, 1081-98.

Dacey, D. M. (1993b) The mosaic of midget ganglion cells in the human retina, *J Neurosci,* 13, 5334-55.

Dacey, D. M. (1994) Physiology, morphology and spatial densities of identified ganglion cell types in primate retina, *Ciba Found Symp,* 184, 12-28.

Dacey, D. M. and Lee, B. B. (1994) The 'blue-on' opponent pathway in primate retina originates from a distinct bistratified ganglion cell type, *Nature,* 367, 731-5.

Dacey, D. M. (1996) Circuitry for color coding in the primate retina, *Proc Natl Acad Sci U S A,* 93, 582-8.

Dandona, L., Quigley, H. A., Brown, A. E. and Enger, C. (1990) Quantitative regional structure of the normal human lamina cribrosa. A racial comparison, *Arch Ophthalmol,* 108, 393-8.

Dannheim, F. and Drance, S. M. (1971) Studies of spatial summation of central retinal areas in normal people of all ages, *Can J Ophthalmol,* 6, 311-9.

Dannheim, F. and Drance, S. M. (1974) Psychovisual disturbances in glaucoma. A study of temporal and spatial summation, *Arch Ophthalmol,* 91, 463-8.

Daubs, J. G. and Crick, R. P. (1981) Effect of refractive error on the risk of ocular hypertension and open angle glaucoma, *Trans Ophthalmol Soc U K,* 101, 121-6.

Dichtl, A., Jonas, J. B. and Naumann, G. O. (1996) Course of the optic nerve fibers through the lamina cibrosa in human eyes, *Graefes Arch Clin Exp Ophthalmol,* 234, 581-5.

Dichtl, A., Jonas, J. B. and Naumann, G. O. (1999) Retinal nerve fiber layer thickness in human eyes, *Graefes Arch Clin Exp Ophthalmol,* 237, 474-9.

Diehl, D. L., Quigley, H. A., Miller, N. R., Sommer, A. and Burney, E. N. (1990) Prevalence and significance of optic disc hemorrhage in a longitudinal study of glaucoma, *Arch Ophthalmol,* 108, 545-50.

Dielemans, I., Vingerling, J. R., Wolfs, R. C., Hofman, A., Grobbee, D. E. and de Jong, P. T. (1994) The prevalence of primary open-angle glaucoma in a population-based study in The Netherlands. The Rotterdam Study, *Ophthalmology,* 101, 1851-5.

Dielemans, I., Vingerling, J. R., Algra, D., Hofman, A., Grobbee, D. E. and de Jong, P. T. (1995) Primary open-angle glaucoma, intraocular pressure, and systemic blood pressure in the general elderly population. The Rotterdam Study, *Ophthalmology,* 102, 54-60.

Dielemans, I., de Jong, P. T., Stolk, R., Vingerling, J. R., Grobbee, D. E. and Hofman, A. (1996) Primary open-angle glaucoma, intraocular pressure, and diabetes mellitus in the general elderly population. The Rotterdam Study, *Ophthalmology,* 103, 1271-5.

Drance, S. M. (1962) Studies in the susceptibility of the eye to raised intraocular pressure, *Arch Ophth,* 68, 76-83.

Drance, S. M. (1969) The early field defects in glaucoma, *Invest Ophthalmol Vis Sci,* 8, 84.

Drance, S. M., Fairclough, M., Butler, D. and Kottler, M. S. (1977) The importance of disc haemorrhage in the prognosis of chronic open angle glaucoma, *Arch Ophthalmol,* 95, 226-8.

Drance, S. M., Airaksinen, P. J., Price, M., Schulzer, M., Douglas, G. R. and Tansley, B. W. (1986) The correlation of functional and structural measurements in glaucoma patients and normal subjects, *Am J Ophthalmol,* 102, 612-6.

Drance, S. M., Douglas, G. R., Wijsman, K., Schulzer, M. and Britton, R. J. (1988) Response of blood flow to warm and cold in normal and low-tension glaucoma patients, *Am J Ophthalmol,* 105, 35-9.

Drasdo, N. (1977) The neural representation of visual space, *Nature,* 266, 554-6.

Dreher, A. W., Tso, P. C. and Weinreb, R. N. (1991) Reproducibility of topographic measurements of the normal and glaucomatous optic nerve head with the laser tomographic scanner, *Am J Ophthalmol,* 111, 221-9.

Eid, T. M., Spaeth, G. L., Katz, L. J., Azuara-Blanco, A., Agusburger, J. and Nicholl, J. (1997) Quantitative estimation of retinal nerve fiber layer height in glaucoma and the relationship with optic nerve head topography and visual field, *J Glaucoma,* 6, 221-30.

Elliot, R. H. (1921) The yielding of the optic nerve-head in glaucoma, *Br J Ophthalmol,* 307-15.

Elsner, A. E., Burns, S. A., Hughes, G. W. and Webb, R. H. (1992) Reflectometry with a scanning laser ophthalmoscope, *Appl Opt,* 31, 3697-710.

Emdadi, A., Zangwill, L., Sample, P. A., Kono, Y., Anton, A. and Weinreb, R. N. (1998) Patterns of optic disk damage in patients with early focal visual field loss, *Am J Ophthalmol,* 126, 763-71.

Emery, J. M., Landis, D., Paton, D., Boniuk, M. and Craig, J. M. (1974) The Lamina Cribrosa in Normal and Glaucomatous Human Eyes, *Tr Am Acad Ophth Otol,* 78, 290-300.

Felius, J., De Jong, L. A., van den Berg, T. J. and Greve, E. L. (1995) Functional characteristics of blue-on-yellow perimetric thresholds in glaucoma, *Invest Ophthalmol Vis Sci,* 36, 1665-74.

Felius, J., Swanson, W. H., Fellman, R. L., Lynn, J. R. and Starita, R. J. (1996) In *XIIth International Perimetric Society Meeting* (Eds, Wall, M. and Heijl, A.) Kugler Publications, Amsterdam/New York, Wurzburg, Germany.

Fellmann, R. L., Lynn, J. R., Starita, R. J. and Swanson, W. H. (1988) In *VIII International Perimetric Society Meeting* (Ed, Heijl, A.) Kugler & Ghedini Publications, Amsterdam, Berkeley, Milano, pp. 313-24.

Fine, B. and Yanoff, M. (1979) *Ocular histology*, 2nd Hagerstown. Harper & Row,

Fishman, R. S. (1970) Optic disc asymmetry. A sign of ocular hypertension, *Arch Ophthalmol,* 84, 590-4.

Fitzgibbon, T. and Taylor, S. F. (1996) Retinotopy of the human retinal nerve fibre layer and optic nerve head, *J Comp Neurol,* 375, 238-51.

Fitzgibbon, T. (1997) The human fetal retinal nerve fiber layer and optic nerve head: a DiI and DiA tracing study, *Vis Neurosci,* 14, 433-47.

Flammer, J., Drance, S. M. and Zulauf, M. (1984) Differential light threshold. Short- and long-term fluctuation in patients with glaucoma, normal controls, and patients with suspected glaucoma, *Arch Ophthalmol,* 102, 704-6.

Fontana, L., Bhandari, A., Fitzke, F. W. and Hitchings, R. A. (1998a) In vivo morphometry of the lamina cribrosa and its relation to visual field loss in glaucoma, *Curr Eye Res,* 17, 363-9.

Fontana, L., Poinoosawmy, D., Bunce, C. V., C, O. B. and Hitchings, R. A. (1998b) Pulsatile ocular blood flow investigation in asymmetric normal tension glaucoma and normal subjects, *Br J Ophthalmol,* 82, 731-6.

Ford, M. and Sarwar, M. (1963) Features of the clinically normal optic disc, *Br J Ophthalmol,* 47, 50-3.

Foster, P. J., Alsbirk, P. H., Baasanhu, J., Munkhbayar, D., Uranchimeg, D. and Johnson, G. J. (1997) Anterior chamber depth in Mongolians. Variation with age, sex and method of measurement., *Am J Ophthalmol,* 124, 53-60.

Frisen, L. (1988) Acuity perimetry: estimation of neural channels, *Int Ophthalmol,* 12, 169-74.

Funk, J., Bornscheuer, C. and Grehn, F. (1988) Neuroretinal rim area and visual field in glaucoma, *Graefes Arch Clin Exp Ophthalmol,* 226, 431-4.

Funk, J., Dieringer, T. and Grehn, F. (1989) Correlation between neuroretinal rim area and age in normal subjects, *Graefes Arch Clin Exp Ophthalmol,* 227, 544-8.

Furuno, F. and Matsuo, H. (1979) Early stage progression in glaucomatous visual field changes, *Doc Ophthalmol Proc Ser,* 19, 247-53.

Gaasterland, D. E., Ederer, F., Sullivan, E. K., Caprioli, J. and Cyrlin, M. N. (1994) Advanced Glaucoma Intervention Study. 2. Visual Field Test Scoring and Reliability, *Ophthalmology,* 101, 1445-55.

Gandolfi, S. A. (1995) Improvement of visual field indices after surgical reduction of intraocular pressure, *Ophthalmic Surg,* 26, 121-6.

Garway-Heath, D. F., Wollstein, G. and Hitchings, R. A. (1997) Aging changes of the optic nerve head in relation to open angle glaucoma, *Br J Ophthalmol,* 81, 840-5.

Garway-Heath, D. F. and Hitchings, R. A. (1998a) Quantitative evaluation of the optic nerve head in early glaucoma, *Br J Ophthalmol,* 82, 352-61.

Garway-Heath, D. F. and Hitchings, R. A. (1998b) Sources of bias in studies of optic disc and retinal nerve fibre layer morphology, *Br J Ophthalmol,* 82, 986.

Garway-Heath, D. F., Ruben, S. T., Viswanathan, A. and Hitchings, R. A. (1998a) Vertical cup/disc ratio in relation to optic disc size: its value in the assessment of the glaucoma suspect, *Br J Ophthalmol,* 82, 1118-24.

Garway-Heath, D. F., Rudnicka, A. R., Lowe, T., Foster, P. J., Fitzke, F. W. and Hitchings, R. A. (1998b) Measurement of optic disc size: equivalence of methods to correct for ocular magnification, *Br J Ophthalmol,* 82, 643-9.

Garway-Heath, D. F., Caprioli, J., Fitzke, F. W. and Hitchings, R. A. (2000) Scaling the hill of vision: The physiological relationship between ganglion cell numbers and light sensitivity, *Invest Ophthalmol Vis Sci,* 41, 1774-82.

Geijssen, H. C. and Greve, E. L. (1987) The spectrum of primary open angle glaucoma. I: Senile sclerotic glaucoma versus high tension glaucoma, *Ophthalmic Surg,* 18, 207-13.

Geijssen, H. C. and Greve, E. L. (1990) Focal ischaemic normal pressure glaucoma versus high pressure glaucoma, *Doc Ophthalmol,* 75, 291-301.

Geijssen, H. C. (1991) *Studies on normal pressure glaucoma,* MD ThesisUniversity of Amsterdam

Georgopoulos, G., Andreanos, D., Liokis, N., Papakonstantinou, D., Vergados, J. and Theodossiadis, G. (1997) Risk factors in ocular hypertension, *Eur J Ophthalmol,* 7, 357-63.

Ghosh, K. K., Martin, P. R. and Grunert, U. (1997) Morphological analysis of the blue cone pathway in the retina of a New World monkey, the marmoset Callithrix jacchus, *J Comp Neurol,* 379, 211-25.

Glezer, V. D. (1965) The receptive fields of the retina, *Vision Res,* 5, 497-525.

Gloster, J. (1975) Vertical ovalness and glaucomatous cupping, *Br J Ophthalmol,* 59, 721-4.

Gloster, J. (1978) Quantitative relationship between cupping of the optic disc and visual field loss in chronic simple glaucoma, *Br J Ophthalmol,* 62, 665-9.

Goldberg, I., Hollows, F. C., Kass, M. A. and Becker, B. (1981) Systemic factors in patients with low-tension glaucoma, *Br J Ophthalmol,* 65, 56-62.

Goldstick, B. J. and Weinreb, R. N. (1987) The effect of refractive error on automated global analysis program G-1, *Am J Ophthalmol,* 104, 229-32.

Goodchild, A. K., Ghosh, K. K. and Martin, P. R. (1996) Comparison of photoreceptor spatial density and ganglion cell morphology in the retina of human, macaque monkey, cat, and the marmoset Callithrix jacchus, *J Comp Neurol,* 366, 55-75.

Gougnard, L. (1961) Etudes des sommations spatiales chez le sujet normal par la perimetrie statique, *Ophthalmologica,* 142, 469-86.

Gramer, E., Gerlach, R., Krieglstein, G. K. and Leydhecker, W. (1982) [Topography of early glaucomatous visual field defects in computerized perimetry], *Klin Monatsbl Augenheilkd,* 180, 515-23.

Greve, E. L. (1973) *Single and multiple stimulus static perimetry in glaucoma; the two phases of perimetry (Thesis),* The Hague. Dr W. Junk B.V.,

Guthauser, U., Flammer, J. and Niesel, P. (1987) The relationship between the visual field and the optic nerve head in glaucomas, *Graefes Arch Clin Exp Ophthalmol,* 225, 129-32.

Haeffliger, I. O., Meyer, P., Flammer, J. and Luscher, T. F. (1994) The vascular endothelium as a regulator of the ocular circulation: a new concept in ophthalmology?, *Surv Ophthalmol,* 39, 123-32.

Haefliger, I. O. and Flammer, J. (1991) Fluctuation of the differential light threshold at the border of absolute scotomas. Comparison between glaucomatous visual field defects and blind spots, *Ophthalmology,* 98, 1529-32.

Hallett, P. E. (1963) Spatial Summation, *Vision Res,* 3, 9-24.

Hart, W. M., Yablonski, M., Kass, M. A. and Becker, B. (1978) Quantitative Visual Field and Optic Disc Correlates Early in Glaucoma, *Archives of Ophthalmology,* 96, 2209-11.

Hart, W. M., Jr. and Becker, B. (1977) Visual field changes in ocular hypertension. A computer-based analysis, *Arch Ophthalmol,* 95, 1176-9.

Hart, W. M., Jr. and Becker, B. (1982) The onset and evolution of glaucomatous visual field defects, *Ophthalmology,* 89, 268-79.

Harwerth, R. S., Smith, E. L. d. and DeSantis, L. (1993) Mechanisms mediating visual detection in static perimetry, *Invest Ophthalmol Vis Sci,* 34, 3011-23.

Harwerth, R. S., Carter-Dawson, L., Shen, F., Smith, E. L., 3rd and Crawford, M. L. (1999) Ganglion cell losses underlying visual field defects from experimental glaucoma, *Invest Ophthalmol Vis Sci,* 40, 2242-50.

Hayreh, S. S. (1974) Anterior ischaemic optic neuropathy. I. Terminology and pathogenesis, *Br J Ophthalmol,* 58, 955-63.

Hayreh, S. S., Zimmerman, M. B., Podhajsky, P. and Alward, W. L. (1994) Nocturnal arterial hypotension and its role in optic nerve head and ocular ischemic disorders, *Am J Ophthalmol,* 117, 603-24.

Hayreh, S. S. (1995) The 1994 Von Sallman Lecture. The optic nerve head circulation in health and disease, *Exp Eye Res,* 61, 259-72.

Hayreh, S. S. (1996a) Blood supply of the optic nerve head, *Ophthalmologica,* 210, 285-95.

Hayreh, S. S. (1996b) Duke-elder lecture. Systemic arterial blood pressure and the eye, *Eye,* 10, 5-28.

Healey, P. R., Mitchell, P., Smith, W. and Wang, J. J. (1997) The influence of age and intraocular pressure on the optic cup in a normal population, *J Glaucoma,* 6, 274-8.

Healey, P. R., Mitchell, P., Smith, W. and Wang, J. J. (1998) Optic disc hemorrhages in a population with and without signs of glaucoma, *Ophthalmology,* 105, 216-23.

Heegaard, S. (1997) Morphology of the vitreoretinal border region, *Acta Ophthalmol Scand Suppl,* 222, 1-31.

Heijl, A. and Drance, S. M. (1983) Changes in differential threshold in patients with glaucoma during prolonged perimetry, *Br J Ophthalmol,* 67, 512-6.

Heijl, A. and Lundqvist, L. (1984) The frequency distribution of earliest glaucomatous visual field defects documented by automatic perimetry, *Acta Ophthalmol Copenh,* 62, 658-64.

Heijl, A., Lindgren, A. and Olsson, J. (1986) In *Seventh International Visual Field Symposium*, Vol. 49 (Eds, Greve, E. L. and Heijl, A.) Martinus Nijhoff/Dr W. Junk Publishers, Amsterdam, pp. 153-68.

Heijl, A., Lindgren, G. and Olsson, J. (1987) Normal variability of static perimetric threshold values across the central visual field, *Arch Ophthalmol,* 105, 1544-9.

Heijl, A. (1989) Computerized perimetry in glaucoma management, *Acta Ophthalmol Copenh,* 67, 1-12.

Heijl, A., Lindgren, G. and Olsson, J. (1989) The effect of perimetric experience in normal subjects, *Arch Ophthalmol,* 107, 81-7.

Heijl, A., Lindgren, G., Lindgren, A., Olsson, J., Asman, P., Myers, S. and Patella, M. (1991) In *Perimetry Update 1990/91* (Eds, Mills, R. P. and Heijl, A.) Kugler & Ghedini, Amsterdam, pp. 303-15.

Henson, D. B. and Hobley, A. J. (1986) Frequency distribution of early glaucomatous visual field defects, *: Am J Optom Physiol Opt,* 63, 455-61.

Henson, D. B. and Morris, E. J. (1993) Effect of uncorrected refractive errors upon central visual field testing, *Ophthalmic Physiol Opt,* 13, 339-43.

Hernandez, M. R., Igoe, F. and Neufeld, A. H. (1986) Extracellular matrix of the human optic nerve head, *Am J Ophthalmol,* 102, 139-48.

Hernandez, M. R., Luo, X. X., Igoe, F. and Neufeld, A. H. (1987) Extracellular matrix of the human lamina cribrosa, *Am J Ophthalmol,* 104, 567-76.

Hernandez, M. R., Luo, X. X., Andrzejewska, W. and Neufeld, A. H. (1989) Age-related changes in the extracellular matrix of the human optic nerve head, *Am J Ophthalmol,* 107, 476-84.

Hernandez, M. R., Andrzejewska, W. M. and Neufeld, A. H. (1990) Changes in the extracellular matrix of the human optic nerve head in primary open-angle glaucoma, *Am J Ophthalmol,* 109, 180-8.

Hernandez, M. R. and Neufeld, A. H. (1991) In *Glaucoma Update IV* (Ed, Kriegelstein, G. K.) Springer-Verlag, Berlin, pp. 74-9.

Hernandez, M. R. (1992) Ultrastructural immunocytochemical analysis of elastin in the human lamina cribrosa. Changes in elastic fibers in primary open-angle glaucoma, *Invest Ophthalmol Vis Sci,* 33, 2891-903.

Hernandez, M. R. and Ye, H. (1993) Glaucoma: changes in extracellular matrix in the optic nerve head, *Ann Med,* 25, 309-15.

Herschler, J. and Osler, R. H. (1980) Baring of the circulinear vessel, an early sign of optic nerve damage, *Arch Ophthalmol,* 98, 865-9.

Herse, P. R. (1992) Factors influencing normal perimetric thresholds obtained using the Humphrey Field Analyzer, *Invest Ophthalmol Vis Sci,* 33, 611-7.

Heuer, D. K., Anderson, D. R., Feuer, W. J. and Gressel, M. G. (1987) The influence of refraction accuracy on automated perimetric threshold measurements, *: Ophthalmology,* 94, 1550-3.

Hills, J. F., Wirtschafter, J. D. and Maeder, P. (1983) In *Fifth International Visual field Symposium* (Eds, Greve, E. L. and Heijl, A.) Dr W. Junk Publishers, The Hague, pp. 459-64.

Hitchings, R. A. and Spaeth, G. L. (1976) The optic disc in glaucoma. I: Classification, *Br J Ophthalmol,* 60, 778-85.

Hitchings, R. A. and Spaeth, G. L. (1977) The optic disc in glaucoma II: correlation of the appearance of the optic disc with the visual field, *Br J Ophthalmol,* 61, 107-13.

Hitchings, R. A. (1996) Glaucoma: current thinking, *Br J Hosp Med,* 55, 312-4.

Hogan, M. J., Alvarado, J. A. and Esperson Weddell, J. (1971) *Histology of the human eye: an atlas and textbook*, Philadelphia. W. B. Saunders Company,

Holden, A. L. and Fitzke, F. W. (1988) Image size in the fundus: structural evidence for wide-field retinal magnification factor, *Brit J Ophthalmol,* 72, 228-30.

Hollows, F. C. and Graham, P. A. (1966) Intraocular pressure, glaucoma and glaucoma suspects in a defined population, *Br J Ophthalmol,* 50, 570-86.

Hollows, F. C. and McGuiness, R. (1966) The size of the optic cup, *Trans Ophthalmol Soc Aust,* 25, 33-8.

Hoyt, W. F. and Newman, N. M. (1972) The earliest defect in glaucoma?, *Lancet,* 1, 692-3.

Hoyt, W. F., Frisen, L. and Newman, N. M. (1973) Fundoscopy of Nerve Fiber layer defects in glaucoma, *Investigative Ophthalmology,* 12, 814-29.

Hudson, C., Wild, J. M. and EC, O. N. (1994) Fatigue effects during a single session of automated static threshold perimetry, *Invest Ophthalmol Vis Sci,* 35, 268-80.

Iester, M., Mikelberg, F. S., Courtright, P. and Drance, S. M. (1997a) Correlation between the visual field indices and Heidelberg retina tomograph parameters, *J Glaucoma,* 6, 78-82.

Iester, M., Mikelberg, F. S. and Drance, S. M. (1997b) The effect of optic disc size on diagnostic precision with the Heidelberg retina tomograph, *Ophthalmology,* 104, 545-8.

Iester, M., Swindale, N. V. and Mikelberg, F. S. (1997c) Sector-based analysis of optic nerve head shape parameters and visual field indices in healthy and glaucomatous eyes, *J Glaucoma,* 6, 370-6.

Iester, M., Courtright, P. and Mikelberg, F. S. (1998) Retinal nerve fiber layer height in high-tension glaucoma and healthy eyes, *J Glaucoma,* 7, 1-7.

Inui, T., Mimura, O. and Kani, K. (1981) Retinal sensitivity and spatial summation in the foveal and parafoveal regions, *J Opt Soc Am,* 71, 151-63.

James, C. B. and Smith, S. E. (1991) Pulsatile ocular blood flow in patients with low tension glaucoma, *Br J Ophthalmol,* 75, 466-70.

Janknecht, P. and Funk, J. (1994) Optic nerve head analyser and Heidelberg retina tomograph: accuracy and reproducibility of topographic measurements in a model eye and in volunteers, *Br J Ophthalmol,* 78, 760-8.

Jansson, F. (1963) Measurement of intraocular distances by ultrasound and comparison between optical and ultrasonic determinations of the depth of the anterior chamber, *Acta Ophthalmol,* 41, 25-61.

Javitt, J. C., Spaeth, G. L., Katz, L. J., Poryzees, E. and Addiego, R. (1990) Acquired pits of the optic nerve. Increased prevalence in patients with low-tension glaucoma, *Ophthalmology,* 97, 1038-43.

Jay, J. L. and Murdoch, J. R. (1993) The rate of visual field loss in untreated primary open angle glaucoma, *Br J Ophthalmol,* 77, 176-8.

Jensen, J. E. (1984) Glaucoma screening a 16-year follow-up of ocular normotensives, *Acta Ophthalmol Copenh,* 62, 203-9.

Johnson, B. M., Miao, M. and Sadun, A. A. (1987) Age-related decline of human optic nerve axon populations, *Age,* 10, 5-9.

Johnson, C. A., Adams, C. W. and Lewis, R. A. (1988) Fatigue effects in automated perimetry, *Applied Optics,* 27, 1030-7.

Johnson, D. H. (2000) Myocilin and glaucoma: A TIGR by the tail?, *Arch Ophthalmol,* 118, 974-8.

Jonas, J. B., Gusek, G. C., Guggenmoos-Holzmann, I. and Naumann, G. O. (1987) Optic nerve head drusen associated with abnormally small optic discs, *Int Ophthalmol,* 11, 79-82.

Jonas, J. B., Guggenmoos-Holzmann, I. and Naumann, G. O. H. (1988a) Cilioretinal arteries in large optic discs, *Ophthalmic Research,* 20, 269-74.

Jonas, J. B., Gusek, G. and Naumann, G. O. H. (1988b) Optic disc morphometry in chronic primary open angle glaucoma II Correlation of the intrapapillary morphometric data to visual field indices, *Graefe's Arch Ophthalmol,* 226, 531-8.

Jonas, J. B., Gusek, G. C., Guggenmoos-Holzmann, I. and Naumann, G. O. (1988c) Size of the optic nerve scleral canal and comparison with intravital determination of optic disc dimensions, *Graefes Arch Clin Exp Ophthalmol,* 226, 213-5.

Jonas, J. B., Gusek, G. C., Guggenmoos-Holzmann, I. and Naumann, G. O. H. (1988d) Variability in the real dimensions of human optic discs, *Graefes Arch Clin Exp Ophthalmol,* 226, 332-6.

Jonas, J. B., Gusek, G. C. and Naumann, G. O. (1988e) Optic disk morphometry in high myopia, *Graefes Arch Clin Exp Ophthalmol,* 226, 587-90.

Jonas, J. B., Gusek, G. C. and Naumann, G. O. (1988f) Optic disc morphometry in chronic primary open-angle glaucoma. I. Morphometric intrapapillary characteristics, *Graefes Arch Clin Exp Ophthalmol,* 226, 522-30.

Jonas, J. B., Gusek, G. C. and Naumann, G. O. (1988g) Optic disc, cup and neuroretinal rim size, configuration and correlations in normal eyes [published errata appear in Invest Ophthalmol Vis Sci 1991 May;32(6) 1893 and 1992 Feb;32(2) 474-5], *Invest Ophthalmol Vis Sci,* 29, 1151-8.

Jonas, J. B. and Naumann, G. O. (1989) Parapapillary retinal vessel diameter in normal and glaucoma eyes. II. Correlations, *Invest Ophthalmol Vis Sci,* 30, 1604-11.

Jonas, J. B., Nguyen, N. X. and Naumann, G. O. (1989a) The retinal nerve fiber layer in normal eyes, *Ophthalmology,* 96, 627-32.

Jonas, J. B., Nguyen, X. N., Gusek, G. C. and Naumann, G. O. (1989b) Parapapillary chorioretinal atrophy in normal and glaucoma eyes. I. Morphometric data, *Invest Ophthalmol Vis Sci,* 30, 908-18.

Jonas, J. B., Zach, F. M., Gusek, G. C. and Naumann, G. O. (1989c) Pseudoglaucomatous physiologic large cups, *Am J Ophthalmol,* 107, 137-44.

Jonas, J. B., Muller Bergh, J. A., Schlotzer Schrehardt, U. M. and Naumann, G. O. (1990) Histomorphometry of the human optic nerve, *Invest Ophthalmol Vis Sci,* 31, 736-44.

Jonas, J. B., Mardin, C. Y., Schlotzer Schrehardt, U. and Naumann, G. O. (1991) Morphometry of the human lamina cribrosa surface, *Invest Ophthalmol Vis Sci,* 32, 401-5.

Jonas, J. B., Schmidt, A. M., Muller Bergh, J. A., Schlotzer Schrehardt, U. M. and Naumann, G. O. (1992) Human optic nerve fiber count and optic disc size, *Invest Ophthalmol Vis Sci,* 33, 2012-8.

Jonas, J. B., Fernandez, M. C. and Sturmer, J. (1993) Pattern of glaucomatous neuroretinal rim loss, *Ophthalmology,* 100, 63-8.

Jonas, J. B. and Konigsreuther, K. A. (1994) Optic disk appearance in ocular hypertensive eyes, *Am J Ophthalmol,* 117, 732-40.

Jonas, J. B. and Schiro, D. (1994) Localised wedge shaped defects of the retinal nerve fibre layer in glaucoma, *Br J Ophthalmol,* 78, 285-90.

Jonas, J. B. and Xu, L. (1994) Optic disk hemorrhages in glaucoma, *Am J Ophthalmol,* 118, 1-8.

Jonas, J. B. and Grundler, A. E. (1997) Correlation between mean visual field loss and morphometric optic disk variables in the open-angle glaucomas, *Am J Ophthalmol,* 124, 488-97.

Kahn, H. A., Leibowitz, H. M., Ganley, J. P., Kini, M. M., Colton, T., Nickerson, R. S. and Dawber, T. R. (1977) The Framingham Eye Study. II. Association of ophthalmic pathology with single variables previously measured in the Framingham Heart Study, *Am J Epidemiol,* 106, 33-41.

Kaiser, H. J., Flammer, J., Graf, T. and Stumpfig, D. (1993) Systemic blood pressure in glaucoma patients, *Graefes Arch Clin Exp Ophthalmol,* 231, 677-80.

Kaiser, H. J., Flammer, J., Wenk, M. and Luscher, T. (1995) Endothelin-1 plasma levels in normal-tension glaucoma: abnormal response to postural changes, *Graefes Arch Clin Exp Ophthalmol,* 233, 484-8.

Kaiser, H. J., Schoetzau, A., Stumpfig, D. and Flammer, J. (1997) Blood-flow velocities of the extraocular vessels in patients with high- tension and normal-tension primary open-angle glaucoma, *Am J Ophthalmol,* 123, 320-7.

Kasai, N., Takahashi, G., Koyama, N. and Kitahara, K. (1992) In *Xth International Perimetric Society Meeting* (Ed, Mills, R. P.) Kugler Publications, Kyoto, Japan, pp. 557-62.

Katz, J. and Sommer, A. (1986) Asymmetry and variation in the normal hill of vision, *Arch Ophthalmol,* 104, 65-8.

Katz, J., Tielsch, J. M., Quigley, H. A., Javitt, J., Witt, K. and Sommer, A. (1993) Automated suprathreshold screening for glaucoma: the Baltimore Eye Survey, *Invest Ophthalmol Vis Sci,* 34, 3271-7.

Kendell, K. R., Quigley, H. A., Kerrigan, L. A., Pease, M. E. and Quigley, E. N. (1995) Primary open-angle glaucoma is not associated with photoreceptor loss, *Invest Ophthalmol Vis Sci,* 36, 200-5.

Kerrigan, L. A., Zack, D. J., Quigley, H. A., Smith, S. D. and Pease, M. E. (1997) TUNEL-positive ganglion cells in human primary open-angle glaucoma, *Arch Ophthalmol,* 115, 1031-5.

Kerrigan-Baumrind, L. A., Quigley, H. A., Pease, M. E., Kerrigan, D. F. and Mitchell, R. S. (2000) Number of ganglion cells in glaucoma eyes compared with threshold visual field tests in the same persons, *Invest Ophthalmol Vis Sci,* 41, 741-8.

Kirsch, R. F. and Anderson, D. R. (1973a) Clinical recognitionof glaucomatous cupping, *Am J Ophthalmol,* 75, 442-54.

Kirsch, R. F. and Anderson, D. R. (1973b) Identification of the glaucomatous disc, *Trans Amer Acad Ophthalmol Otolaryngol,* 77, 143-56.

Kitazawa, Y., Horie, T., Aoki, S. and et al. (1977) Untreated Ocular Hypertension : a long term prospective study, *Arch Ophthalmol,* 95, 1180-4.

Kitazawa, Y., Shirato, S. and Yamamoto, T. (1986) Optic disc hemorrhage in low-tension glaucoma, *Ophthalmology,* 93, 853-7.

Klaver, J. H., Greve, E. L., Goslinga, H., Geijssen, H. C. and Heuvelmans, J. H. (1985) Blood and plasma viscosity measurements in patients with glaucoma, *Br J Ophthalmol,* 69, 765-70.

Klein, B. E., Klein, R., Sponsel, W. E., Franke, T., Cantor, L. B., Martone, J. and Menage, M. J. (1992) Prevalence of glaucoma. The Beaver Dam Eye Study, *Ophthalmology,* 99, 1499-504.

Klein, B. E., Klein, R. and Jensen, S. C. (1994) Open-angle glaucoma and older-onset diabetes. The Beaver Dam Eye Study, *Ophthalmology,* 101, 1173-7.

Knighton, R. W. (1995) Quantitative Reflectometry of the Ocular Fundus, *IEEE Engineering in Medicine & Biology,* 43-51.

Kono, Y., Chi, Q. M., Tomita, G., Yamamoto, T. and Kitazawa, Y. (1997) High-pass resolution perimetry and a Humphrey Field Analyzer as indicators of glaucomatous optic disc abnormalities. A comparative study, *Ophthalmology,* 104, 1496-502.

Kouyama, N. and Marshak, D. W. (1997) The topographical relationship between two neuronal mosaics in the short wavelength-sensitive system of the primate retina, *Vis Neurosci,* 14, 159-67.

Kronfeld, P. C. (1967) In *Symposium on Glaucoma. Transactions of the New Orleans Academy of Ophthalmology* (Eds, Armaly, M. F., Becker, B. and Haas, J. S.) C.V. Mosby Co., St. Louis, pp. 62-73.

Kruse, F. E., Burk, R. O., Volcker, H. E., Zinser, G. and Harbarth, U. (1989) Reproducibility of topographic measurements of the optic nerve head with laser tomographic scanning, *Ophthalmology,* 96, 1320-4.

Lachenmayr, B. J., Airaksinen, P. J., Drance, S. M. and Wijsman, K. (1991) Correlation of retinal nerve-fiber-layer loss, changes at the optic nerve head and various psychophysical criteria in glaucoma, *Graefes Arch Clin Exp Ophthalmol,* 229, 133-8.

Lampert, P. W., Vogel, M. H. and Zimmerman, L. E. (1968) Pathology of the optic nerve in experimental acute glaucoma. Electron microscopic studies, *Invest Ophthalmol,* 7, 199-213.

Langerhorst, C. T., van den Berg, T. J. T. P., Veldman, E. and Greve, E. L. (1987) Population study of global and local fatigue with prolonged threshold testing in automated perimetry, *Doc Ophthalmol Proc Series,* 49, 657-62.

Lee, B. B. (1996) Receptive field structure in the primate retina, *Vision Res,* 36, 631-44.

Leske, M. C. and Podgor, M. J. (1983) Intraocular pressure, cardiovascular risk variables, and visual field defects, *Am J Epidemiol,* 118, 280-7.

Leske, M. C., Connell, A. M., Schachat, A. P. and Hyman, L. (1994) The Barbados Eye Study. Prevalence of open angle glaucoma, *Arch Ophthalmol,* 112, 821-9.

Leske, M. C., Connell, A. M., Wu, S. Y., Hyman, L. G. and Schachat, A. P. (1995) Risk factors for open-angle glaucoma. The Barbados Eye Study, *Arch Ophthalmol,* 113, 918-24.

Leske, M. C. and Wu, S.-Y. (1996) Risk factors for open-angle glaucoma: The Barbados Eye Study (letter - reply), *Arch Ophthalmol,* 114, 235.

Levene, R. (1980) Low tension glaucoma: a critical review and new material, *Surv Ophthalmol,* 61, 621-64.

Leventhal, A. G., Rodieck, R. W. and Dreher, B. (1981) Retinal ganglion cell classes in the old world monkey: morphology and central projection, *Science,* 213, 1139-42.

Leydhecker, W., Akiyama, K. and Newman, H. G. (1959) Der intraokulare Durck gesunder Menschlicher, *Augen Klin Monatsbl Augenheilkd,* 133, 662-70.

Lichter, P. R. (1976) Variability of expert observers in evaluating the optic disc, *Trans Am Ophthalmol Soc,* 74, 532-72.

Lie, I. (1980) Visual detection and resolution as a function of retinal locus, *Vision Res,* 20, 967-74.

Littmann, H. (1982) Zur Bestimmung der wahren Grosse eines Objektes auf dem Hintergrund des lebenden Auges, *Klin Monatsbl Augenheilkd,* 180, 286-9.

Littmann, H. (1988) Zur Bestimmung der wahren Grosse eines Objektes auf dem Hintergrund des lebenden Auges, *Klin Monatsbl Augenheilkd,* 192, 66-7.

Littmann, H. (1992) Determination of the true size of an object on the fundus of the living eye. By H. Littmann from the original article, "Zur Bestimmung der wahren Grosse eines Objektes auf dem Hintergrund des lebenden Auges," which originally appeared in Klinisches Monatsblatter fur Augenheilkunde 1982; 180:286-9. Translated by TD Williams [classical article], *Optometry & Vision Science,* 69, 717-20.

Lotmar, W. (1984) Dependence of magnification upon the camera-to-eye distance in the Zeiss fundus camera, *Acta Ophthalmol,* 62, 131-4.

Lowe, T., Fitzke, F., McCune, K., Khaw, P. T. and Hitchings, R. A. (1997) Differences between the Humphrey field analyser (HFA) models 640 and 750 in normals, glaucomatous, cataract and aphakic subject groups, *Invest Ophthalmol Vis Sci,* 38, S572. Abstract number 2669.

Lundberg, L., Wettrell, K. and Linner, E. (1987) Ocular hypertension. A prospective twenty-year follow-up study, *Acta Ophthalmol Copenh,* 65, 705-8.

Lutjen-Drecoll, E. (1999) Functional morphology of the trabecular meshwork in primate eyes, *Prog Retin Eye Res,* 18, 91-119.

Maisel, J. M., Pearlstein, C. S., Adams, W. H. and Heotis, P. M. (1989) Large optic disks in the Marshallese population, *Am J Ophthalmol,* 107, 145-50.

Mandava, S., Zulauf, M., Zeyen, T. and Caprioli, J. (1993) An evaluation of clusters in the glaucomatous visual field, *Am J Ophthalmol,* 116, 684-91.

Mansour, A. M., Shoch, D. and Logani, S. (1988) Optic disk size in ischemic optic neuropathy [see comments], *Am J Ophthalmol,* 106, 587-9.

Mansour, A. M. (1990) Measuring fundus landmarks, *Invest Ophthalmol Vis Sci,* 31, 41-2.

Martin, P. R., White, A. J., Goodchild, A. K., Wilder, H. D. and Sefton, A. E. (1997) Evidence that blue-on cells are part of the third geniculocortical pathway in primates, *Eur J Neurosci,* 9, 1536-41.

Mason, R. P., Kosoko, O., Wilson, M. R., Martone, J. F., Cowan, C. L., Jr., Gear, J. C. and Ross Degnan, D. (1989) National survey of the prevalence and risk factors of glaucoma in St. Lucia, West Indies. Part I. Prevalence findings, *Ophthalmology,* 96, 1363-8.

Matin, L. (1975) Ricco's law: response as a power function of stimulus luminance and distance from target center, *Vision Res,* 15, 1381-4.

Michelson, G., Langhans, M. J. and Groh, M. J. (1996) Perfusion of the juxtapapillary retina and the neuroretinal rim area in primary open angle glaucoma, *J Glaucoma,* 5, 91-8.

Mikelberg, F. S., Drance, S. M., Schulzer, M., Yidegiligne, H. M. and Weis, M. M. (1989) The normal human optic nerve. Axon count and axon diameter distribution, *Ophthalmology,* 96, 1325-8.

Mikelberg, F. S., Parfitt, C. M., Swindale, N. V., Graham, S. L., Drance, S. M. and Gosine, R. (1995) Ability of the Heidelberg Retina Tomograph to detect early glaucomatous visual field loss, *J Glaucoma,* 4, 242-7.

Minckler, D. S., Tso, M. O. and Zimmerman, L. E. (1976) A light microscopic, autoradiographic study of axoplasmic transport in the optic nerve head during ocular hypotony, increased intraocular pressure, and papilledema, *Am J Ophthalmol,* 82, 741-57.

Minckler, D. S., Bunt, A. H. and Klock, I. B. (1978) Radioautographic and cytochemical ultrastructural studies of axoplasmic transport in the monkey optic nerve head, *Invest Ophthalmol Vis Sci,* 17, 33-50.

Minckler, D. S. (1980) The organization of nerve fiber bundles in the primate optic nerve head, *Arch Ophthalmol,* 98, 1630-6.

Minckler, D. S. and Spaeth, G. L. (1981) Optic nerve damage in glaucoma, *Surv Ophthalmol,* 26, 128-48.

Minckler, D. S. (1989) Histology of optic nerve damage in ocular hypertension and early glaucoma, *Surv Ophthalmol,* 33, 401-2.

Mitchell, P., Smith, W., Attebo, K. and Healey, P. R. (1996) Prevalence of open-angle glaucoma in Australia. The Blue Mountains Eye Study, *Ophthalmology,* 103, 1661-9.

Mitchell, P., Smith, W., Chey, T. and Healey, P. R. (1997) Open-angle glaucoma and diabetes: the Blue Mountains eye study, Australia, *Ophthalmology,* 104, 712-8.

Mizokami, K., Katsumori, N. and Miyazawa, H. (1987) In *Seventh International Visual Field Symposium,* Vol. 49 (Eds, Greve, E. L. and Heijl, A.) Martinus Nijhoff/Dr W. Junk Publishers, Dordrecht, pp. 469-74.

Montgomery, D. M. (1993) Clinical disc biometry in early glaucoma, *Ophthalmology,* 100, 52-6.

Morgan, J. E., Jeffery, G. and Foss, A. J. (1998) Axon deviation in the human lamina cribrosa [see comments], *Br J Ophthalmol,* 82, 680-3.

Motolko, M. and Drance, S. M. (1981) Features of the optic disc in preglaucomatous eyes, *Arch Ophthalmol,* 99, 1992-5.

Moya, F. J., Brigatti, L. and Caprioli, J. (1999) Effect of aging on optic nerve appearance: a longitudinal study, *Br J Ophthalmol,* 83, 567-72.

Mullie, M. A. and Sanders, M. D. (1985) Scleral canal size and optic nerve head drusen, *Am J Ophthalmol,* 99, 356-9.

Murdoch, I. (1996) Epidemiology and primary open angle glaucoma, *Community Eye Health,* 9, 19-22.

Nanba, K. and Iwata, K. (1992) In *Perimetry Update 1992/93* (Ed, Mills, R. P.) Kugler Publications, Amsterdam/New York, pp. 165-9.

Nicholas, S. P. and Werner, E. B. (1980) Location of early glaucomatous visual field defects, *Can J Ophthalmol,* 15, 131-3.

Nickells, R. W. (1996) Retinal ganglion cell death in glaucoma: the how, the why, and the maybe, *J Glaucoma,* 5, 345-56.

Nicolela, M. T. and Drance, S. M. (1996) Various glaucomatous optic nerve appearances: clinical correlations, *Ophthalmology,* 103, 640-9.

Nicolela, M. T., Drance, S. M., Rankin, S. J., Buckley, A. R. and Walman, B. E. (1996a) Color Doppler imaging in patients with asymmetric glaucoma and unilateral visual field loss, *Am J Ophthalmol,* 121, 502-10.

Nicolela, M. T., Hnik, P. and Drance, S. M. (1996b) Scanning laser Doppler flowmeter study of retinal and optic disk blood flow in glaucomatous patients, *American Journal of Ophthalmology,* 122, 775-83.

Niessen, A. G., van den Berg, T. J., Langerhorst, C. T. and Greve, E. L. (1996) Retinal nerve fiber layer assessment by scanning laser polarimetry and standardized photography, *Am J Ophthalmol,* 121, 484-93.

Nouri-Mahdavi, K., Brigatti, L., Weitzman, M. and Caprioli, J. (1997) Comparison of methods to detect visual field progression in glaucoma [published erratum appears in Ophthalmology 1998 Jan;105(1):7], *Ophthalmology,* 104, 1228-36.

O' Brien, C., Butt, Z., Ludlam, C. and Detkova, P. (1997) Activation of the coagulation cascade in untreated primary open-angle glaucoma, *Ophthalmology,* 104, 725-9.

Odberg, T. and Riise, D. (1985) Early diagnosis of glaucoma. The value of successive stereophotography of the optic disc, *Acta Ophthalmol (Copenh),* 63, 257-63.

Ogden, T. E. (1974) The nerve-fiber layer of the primate retina: an autoradiographic study, *Invest Ophthalmol,* 13, 95-100.

Ogden, T. E. (1983a) Nerve fiber layer of the owl monkey retina: retinotopic organization, *Invest Ophthalmol Vis Sci,* 24, 265-9.

Ogden, T. E. (1983b) Nerve fiber layer of the macaque retina: retinotopic organization, *Invest Ophthalmol Vis Sci,* 24, 85-98.

Ogden, T. E. (1983c) Nerve fiber layer of the primate retina: thickness and glial content, *Vision Res,* 23, 581-7.

Ogden, T. E. (1984) Nerve fiber layer of the primate retina: morphometric analysis, *Invest Ophthalmol Vis Sci,* 25, 19-29.

Ogden, T. E., Duggan, J., Danley, K., Wilcox, M. and Minckler, D. S. (1988) Morphometry of nerve fiber bundle pores in the optic nerve head of the human, *Exp Eye Res,* 46, 559-68.

Okubo, K. and Mizokami, K. (1985) In *Procedings of the 6th International Visual Field Symposium* (Eds, Heijl, A. and Greve, E. L.) Dr W. Junk Publishers, Dordrecht, The Netherlands, pp. 457-66.

Olsen, T. (1986) On the calculation of power from curvature of the cornea, *Br J Ophthalmol,* 70, 152-4.

Olsen, T. (1987) Theoretical approach to intraocular lens calculation using Gaussian optics, *J Cataract Refract Surg,* 13, 141-5.

Olsen, T., Andersen, C. U. and Plesner, H. J. (1989) Computerised intraocular lens calculation: clinical results and predictability, *Br J Ophthalmol,* 73, 220-4.

Olsen, T. and Nielsen, P. J. (1989) Immersion versus contact technique in the measurement of axial length by ultrasound, *Acta Ophthalmologica,* 101-2.

Olsen, T., Thim, K. and Corydon, L. (1990) Theoretical versus SRK I and SRK II calculation of intraocular lens power, *J Cataract Refract Surg,* 16, 217-25.

Olsen, T. (1992) Sources of error in intraocular lens power calculation, *J Cataract Refract Surg,* 18, 125-9.

Olsen, T., Corydon, L. and Gimbel, H. (1995) Intraocular lens power calculation with an improved anterior chamber depth prediction algorithm, *Journal of Cataract & Refractive Surgery,* 21, 313-9.

Olver, J. M., Spalton, D. J. and McCartney, A. C. (1994) Quantitative morphology of human retrolaminar optic nerve vasculature, *Invest Ophthalmol Vis Sci,* 35, 3858-66.

Orzalesi, N., Miglior, S., Lonati, C. and Rosetti, L. (1998) Microperimetry of localized retinal nerve fiber layer defects, *Vision Res,* 38, 763-71.

Pach, J., Pennell, D. O. and Romano, P. E. (1989) Optic disc photogrammetry: magnification factors for eye position, centration, and ametropias, refractive and axial; and their application in the diagnosis of optic nerve hypoplasia, *Ann Ophthalmol,* 21, 454-62.

Parisi, V., Manni, G., Gandolfi, S. A., Centofanti, M., Colacino, G. and Bucci, M. G. (1999) Visual function correlates with nerve fiber layer thickness in eyes affected by ocular hypertension, *Invest Ophthalmol Vis Sci,* 40, 1828-33.

Pederson, J. E. and Anderson, D. R. (1980) The mode of progressive disc cupping in ocular hypertension and glaucoma, *Arch Ophthalmol,* 98, 490-5.

Pena, J. D., Netland, P. A., Vidal, I., Dorr, D. A., Rasky, A. and Hernandez, M. R. (1998) Elastosis of the lamina cribrosa in glaucomatous optic neuropathy, *Exp Eye Res,* 67, 517-24.

Pennebaker, G. E. and Stewart, W. C. (1992) Temporal visual field in glaucoma: a re-evaluation in the automated perimetry era, *Graefes Arch Clin Exp Ophthalmol,* 230, 111-4.

Perkins, E. S. (1973a) The Bedford glaucoma survery. II. Rescreening of normal population, *Br J Ophthalmol,* 57, 186-92.

Perkins, E. S. (1973b) The Bedford glaucoma survey. I. Long-term follow-up of borderline cases, *Br J Ophthalmol,* 57, 179-85.

Perkins, E. S. and Phelps, C. D. (1982) Open angle glaucoma, ocular hypertension, low tension glaucoma and refraction, *Arch Ophthalmol,* 100, 1464-7.

Phelps, C. D. and Corbett, J. J. (1985) Migraine and low-tension glaucoma. A case-control study, *Invest Ophthalmol Vis Sci,* 26, 1105-8.

Pickard, R. (1948) The alteration in size of the normal optic disc cup, *Br J Ophthalmol,* 32, 355-61.

Plesch, A., Klingbeil, U. and Bille, J. (1987) Digital laser scanning fundus camera, *Appl Opt,* 26, 1480-86.

Podgor, M. J., Leske, M. C. and Ederer, F. (1983) Incidence estimates for lens changes, macular changes, open-angle glaucoma and diabetic retinopathy, *Am J Epidemiol,* 118, 206-12.

Poinoosawmy, D., McNaught, A. I., Fitzke, F. W. and Hitchings, R. A. (1995) In *Perimetry Update 1994/95* (Eds, Mills, R. P. and Wall, M.) Kugler Publications, Amsterdam, pp. 289-97.

Portney, G. L. (1973) Qualitative parameters of the normal optic nerve head, *Am J Ophthalmol,* 76, 655-9.

Portney, G. L. (1974) Photogrammetric categorical analysis of the optic nerve head, *Tr Am Acad Ophth & Otol,* 78, 275-89.

Portney, G. L. (1976) Photogrammetric analysis of the three-dimensional geometry of normal and glaucomatous optic cups, *Tr Am Acad Ophth & Otol,* 81, 239-46.

Primrose, J. (1971) Early signs of the glaucomatous disc, *Brit J Ophthalmol,* 55, 820-5.

Quigley, E. N., Quigley, H. A., Pease, M. E. and Kerrigan, L. A. (1996a) Quantitative studies of elastin in the optic nerve heads of persons with primary open-angle glaucoma, *Ophthalmology,* 103, 1680-5.

Quigley, H. and Anderson, D. R. (1976) The dynamics and location of axonal transport blockade by acute intraocular pressure elevation in primate optic nerve, *Invest Ophthalmol,* 15, 606-16.

Quigley, H., Pease, M. E. and Thibault, D. (1994) Change in the appearance of elastin in the lamina cribrosa of glaucomatous optic nerve heads, *Graefe's Arch Clin Exp Ophthalmol,* 232, 257-61.

Quigley, H. A. and Green, W. R. (1979) The histology of human glaucoma cupping and optic nerve damage : clinicopathologic correlation in 21 eyes, *Ophthalmology,* 86, 1803-27.

Quigley, H. A., Miller, N. R. and George, T. (1980) Clinical evaluation of nerve fiber layer atrophy as an indicator of glaucomatous optic nerve damage, *Arch Ophthalmol,* 98, 1564-71.

Quigley, H. A. and Addicks, E. M. (1981) Regional differences in the structure of the lamina cribrosa and their relation to glaucomatous optic nerve damage, *Arch Ophthalmol,* 99, 137-43.

Quigley, H. A., Addicks, E. M., Green, W. R. and Maumenee, A. E. (1981) Optic nerve damage in human glaucoma. II. The site of injury and susceptibility to damage, *Arch Ophthalmol,* 99, 635-49.

Quigley, H. A., Addicks, E. M. and Green, W. R. (1982) Optic Nerve Damage in Human Glaucoma - III. Quantitative Correlation of Nerve Fiber Loss and Visual Field Defect in Glaucoma, Ischemic Neuropathy, Papilledema, and Toxic Neuropathy, *Arch Ophthalmol,* 100, 135-46.

Quigley, H. A., Hohman, R. M., Addicks, E. M., Massof, R. W. and Green, W. R. (1983) Morphologic changes in the lamina cribrosa correlated with neural loss in open-angle glaucoma, *Am J Ophthalmol,* 95, 673-91.

Quigley, H. A., Dunkelberger, G. R. and Green, W. R. (1989) Retinal ganglion cell atrophy correlated with automated perimetry in human eyes with glaucoma, *Am J Ophthalmol,* 107, 453-64.

Quigley, H. A., Brown, A. E., Morrison, J. D. and Drance, S. M. (1990) The size and shape of the optic disc in normal human eyes, *Arch Ophthalmol,* 108, 51-7.

Quigley, H. A., Brown, A. and Dorman Pease, M. E. (1991) Alterations in elastin of the optic nerve head in human and experimental glaucoma, *Br J Ophthalmol,* 75, 552-7.

Quigley, H. A., Katz, J., Derick, R. J., Gilbert, D. and Sommer, A. (1992) An evaluation of optic disc and nerve fiber layer examinations in monitoring progression of early glaucoma damage, *Ophthalmology,* 99, 19-28.

Quigley, H. A. (1995) Ganglion cell death in glaucoma: pathology recapitulates ontogeny, *Aust N Z J Ophthalmol,* 23, 85-91.

Quigley, H. A., Nickells, R. W., Kerrigan, L. A., Pease, M. E., Thibault, D. J. and Zack, D. J. (1995) Retinal ganglion cell death in experimental glaucoma and after axotomy occurs by apoptosis, *Invest Ophthalmol Vis Sci,* 36, 774-86.

Quigley, H. A., Tielsch, J. M., Katz, J. and Sommer, A. (1996b) Rate of progression in open-angle glaucoma estimated from cross- sectional prevalence of visual field damage [see comments], *Am J Ophthalmol,* 122, 355-63.

Quigley, H. A. and Vitale, S. (1997) Models of open-angle glaucoma prevalence and incidence in the United States, *Invest Ophth Vis Sci,* 38, 83-91.

Radius, R. L., Maumenee, A. E. and Green, W. R. (1978) Pit-like changes of the optic nerve head in open-angle glaucoma, *Br J Ophthalmol,* 62, 389-93.

Radius, R. L. and Anderson, D. R. (1979a) The histology of retinal nerve fiber layer bundles and bundle defects, *Arch Ophthalmol,* 97, 948-50.

Radius, R. L. and Anderson, D. R. (1979b) The course of axons through the retina and optic nerve head, *Arch Ophthalmol,* 97, 1154-8.

Radius, R. L. (1981a) Regional Specificity in Anatomy at the Lamina Cribrosa, *Arch Ophthalmol,* 99, 478-80.

Radius, R. L. (1981b) Distribution of pressure-induced fast axonal transport abnormalities in primate optic nerve. An autoradiographic study, *Arch Ophthalmol,* 99, 1253-7.

Radius, R. L. and Gonzales, M. (1981) Anatomy of the Lamina Cribrosa in Human Eyes, *Arch Ophthalmol,* 99, 2159-62.

Radius, R. L. (1987) Anatomy of the optic nerve head and glaucomatous optic neuropathy, *Surv Ophthalmol,* 32, 35-44.

Read, R. M. and Spaeth, G. L. (1974) The practical clinical appraisal of the optic disc in glaucoma: The natural history of cup progression and some specific disc-field correlations., *Trans Am Acad Ophthalmol Otolaryngol,* 78, 255-67.

Reidy, A., Minassian, D. C., Vafidis, G., Joseph, J., Farrow, S., Wu, J., Desai, P. and Connolly, A. (1998) Prevalence of serious eye disease and visual impairment in a north London population: population based, cross sectional study, *Bmj,* 316, 1643-6.

Reyes, R. D., Tomita, G. and Kitazawa, Y. (1998) Retinal nerve fiber layer thickness within the area of apparently normal visual field in normal-tension glaucoma with hemifield defect, *J Glaucoma,* 7, 329-35.

Richardson, D. W., Honour, A. J., Fenton, G. W., Stott, F. H. and Pickering, G. W. (1964) Variation in arterial pressure throughout the day and night, *Clin Sci,* 26, 445-60.

Robinson, R., Deutsch, J., Jones, H. S., Youngson-Reilly, S., Hamlin, D. M., Dhurjon, L. and Fielder, A. R. (1994) Unrecognised and unregistered visual impairment [see comments], *Br J Ophthalmol,* 78, 736-40.

Rohrschneider, K., Burk, R. O. and Volcker, H. E. (1993) Reproducibility of topometric data acquisition in normal and glaucomatous optic nerve heads with the laser tomographic scanner, *Graefes Arch Clin Exp Ophthalmol,* 231, 457-64.

Rohrschneider, K., Burk, R. O., Kruse, F. E. and Volcker, H. E. (1994) Reproducibility of the optic nerve head topography with a new laser tomographic scanning device, *Ophthalmology,* 101, 1044-9.

Rudnicka, A. R., Edgar, D. F. and Bennett, A. G. (1992a) Construction of a model eye and its applications, *Ophthal Physiol Opt,* 12, 485-90.

Rudnicka, A. R., Steele, C. F., Crabb, D. P. and Edgar, D. F. (1992b) Repeatability, reproducibility and intersession variability of the Allergan Humphrey ultrasonic biometer, *Acta Ophthalmologica,* 70, 327-34.

Rudnicka, A. R., Burk, R. O., Edgar, D. F. and Fitzke, F. W. (1998) Magnification characteristics of fundus imaging systems, *Ophthalmology,* 105, 2186-92.

Sakugawa, M. and Chihara, E. (1985) Blockage at two points of axonal transport in glaucomatous eyes, *Graefes Arch Clin Exp Ophthalmol,* 223, 214-8.

Salgarello, T., Colotto, A., Falsini, B., Buzzonetti, L., Cesari, L., Iarossi, G. and Scullica, L. (1999) Correlation of pattern electroretinogram with optic disc cup shape in ocular hypertension, *Invest Ophthalmol Vis Sci,* 40, 1989-97.

Samuelson, T. W. and Spaeth, G. L. (1993) Focal and diffuse visual field defects: their relationship to intraocular pressure, *Ophthalmic Surg,* 24, 519-25.

Sanchez, R. M., Dunkelberger, G. R. and Quigley, H. A. (1986) The number and diameter distribution of axons in the monkey optic nerve, *Invest Ophthalmol & Vis Sci,* 27, 1342-50.

Schein, S. J. (1988) Anatomy of macaque fovea and spatial densities of neurons in foveal representation, *J Comp Neurol,* 269, 479-505.

Schelenz, J. and Kammann, J. (1989) Comparison of contact and immersion techniques for axial length measurement and implant power calculation, *J Cataract Refract Surg,* 15, 425-8.

Schiller, P. H., Logothetis, N. K. and Charles, E. R. (1990) Role of the color-opponent and broad-band channels in vision, *Vis Neurosci,* 5, 321-46.

Scholtes, A. M. and Bouman, M. A. (1977) Psychophysical experiments on spatial summation at threshold level of the human peripheral retina, *Vision Res,* 17, 867-73.

Schwartz, B., Reinstein, N. M. and Lieberman, D. M. (1973) Pallor of the Optic Disc. Quantitative photographic evaluation, *Arch Ophthalmol,* 89, 278-87.

Schwartz, B. (1980) Optic disc changes in ocular hypertension, *Surv Ophthalmol,* 25, 148-54.

Schwartz, J. T., Reuling, F. H. and Garrison, R. J. (1975) Acquired cupping of the optic nerve head in normotensive eyes, *Brit J Ophthalmol,* 59, 216-22.

Scott, A. B. and Morris, A. (1967) Visual field changes produced by artificially elevated intraocular pressure, *Am J Ophthalmol,* 63, 308-12.

Searle, A. E., Wild, J. M., Shaw, D. E. and EC, O. N. (1991) Time-related variation in normal automated static perimetry, *Ophthalmology,* 98, 701-7.

Sekine, m., Araie, M., Suzuki, Y. and Koseki, N. (1994) [Study on risk factors for progression of visual field damage in normal-tension glaucoma], *Nippon Ganka Gakkai Zasshi,* 98, 369-73.

Shammas, H. J. (1984) A comparison of immersion and contact techniques for axial length measurement, *Journal American Intra Ocular Implant Society,* 10, 444-7.

Shapley, R. (1990) Visual sensitivity and parallel retinocortical channels, *Annu Rev Psychol,* 41, 635-58.

Sheldrick, J. H., Ng, C., Austin, D. J. and Rosenthal, A. R. (1994) An analysis of referral routes and diagnostic accuracy in cases of suspected glaucoma, *Ophthalmic Epidemiol,* 1, 31-9.

Sheldrick, J. H. and Sharp, A. J. (1994) Glaucoma screening clinic in general practice: prevalence of occult disease, and resource implications, *Br J Gen Pract,* 44, 561-5.

Shiose, Y., Kitazawa, Y., Tsukahara, S., Akamatsu, T., Mizokami, K., Futa, R., Katsushima, H. and Kosaki, H. (1991) Epidemiology of glaucoma in Japan--a nationwide glaucoma survey, *Jpn J Ophthalmol,* 35, 133-55.

Sjostrand, J., Conradi, N. and Klaren, L. (1994) How many ganglion cells are there to a foveal cone? A stereologic analysis of the quantitative relationship between cone and ganglion cells in one normal human fovea, *Graefes Arch Clin Exp Ophthalmol,* 232, 432-7.

Sloan, L. L. (1961) Area and luminance of test object as variables in examination of the visual field by projection perimetry, *Vision Res,* 1, 121-38.

Snydacker, D. (1964) The normal optic disc. Ophthalmoscopic and photographic studies, *Am J Ophthalmol,* 58, 958-64.

Sommer, A., Pollack, I. and Maumenee, A. E. (1979a) Optic disc parameters and onset of glaucomatous field loss. II. Static screening criteria, *Arch Ophthalmol,* 97, 1449-54.

Sommer, A., Pollack, I. and Maumenee, A. E. (1979b) Optic disc parameters and onset of glaucomatous field loss. I. Methods and progressive changes in disc morphology, *Arch Ophthalmol,* 97, 1444-8.

Sommer, A., Katz, J., Quigley, H. A., Miller, N. R., Robin, A. L., Richter, R. C. and Witt, K. A. (1991a) Clinically detectable nerve fiber atrophy precedes the onset of glaucomatous field loss, *Arch Ophthalmol,* 109, 77-83.

Sommer, A., Tielsch, J. M., Katz, J., Quigley, H. A., Gottsch, J. D., Javitt, J. and Singh, K. (1991b) Relationship between intraocular pressure and primary open angle glaucoma among white and black Americans. The Baltimore Eye Survey, *Arch Ophthalmol,* 109, 1090-5.

Sommer, A. (1996) Doyne Lecture. Glaucoma: facts and fancies, *Eye,* 10, 295-301.

Sorsby, A., Benjamin, B., Davey, J. B., Sheridan, M. and Tanner, J. M. (1957) Emmetropia and its aberrations, Medical Research Council, London, Report number 293

Spaeth, G. L., Hitchings, R. A. and Sivalingam, E. (1976) The optic disc in glaucoma: pathogenetic correlation of five patterns of cupping in chronic open-angle glaucoma, *Trans Am Acad Ophthalmol Otolaryngol,* 81, 217-23.

Spaeth, G. L. (1994) A new classification of glaucoma including focal glaucoma, *Surv Ophthalmol,* 38, S9-17.

Sponsel, W. E. (1989) Tonometry in question: can visual screening tests play a more decisive role in glaucoma diagnosis and management?, *Surv Ophthalmol,* 33, 291-300.

Stürmer, J. (1985) What do glaucomatous visual fields really look like in fine-grid computerized profile perimetry?, *Dev Ophthalmol,* 12, 1-47.

Tate, G. W. and Lynn, J. R. (c1977) In *Principles of quantitative perimetry: testing and interpreting the visual field* Grune & Stratton, New York, pp. 107-12.

Teal, P. K., Morin, J. D. and McCulloch, C. (1972) Assessment of the normal disc, *Trans Am Ophthalmol Soc,* 70, 164-77.

Teikari, J. M. (1987) Genetic factors in open-angle (simple and capsular) glaucoma. A population-based twin study, *Acta Ophthalmol Copenh,* 65, 715-20.

Tezel, G., Kass, M. A., Kolker, A. E., Becker, B. and Wax, M. B. (1997) Plasma and aqueous humor endothelin levels in primary open-angle glaucoma, *J Glaucoma,* 6, 83-9.

Thanos, S., Rohrbach, J. M. and Thiel, H. J. (1991) Postmortem preservation of ganglion cells in the human retina. A morphometric investigation with the carbocyanine dye DiI, *Retina,* 11, 318-27.

Thibos, L. N. (1998) Acuity perimetry and the sampling theory of visual resolution, *Optom Vis Sci,* 75, 399-406.

Thylefors, B., Negrel, A. D., Pararajasegaram, R. and Dadzie, K. Y. (1995) Global data on blindness, *Bull World Health Organ,* 73, 115-21.

Tielsch, J. M., Sommer, A., Witt, K., Katz, J. and Royall, R. M. (1990) Blindness and Visual Impairment in an American Urban Population - The Baltimore Eye Survey, *Archives of Ophthalmology,* 108, 286-90.

Tielsch, J. M., Sommer, A., Katz, J., Royall, R. M., Quigley, H. A. and Javitt, J. (1991) Racial variations in the prevalence of primary open-angle glaucoma. The Baltimore Eye Survey, *JAMA,* 266, 369-74.

Tielsch, J. M., Katz, J., Sommer, A., Quigley, H. A. and Javitt, J. C. (1994) Family history and risk of primary open angle glaucoma. The Baltimore Eye Survey, *Archives of Ophthalmology,* 112, 69-73.

Tielsch, J. M., Katz, J., Quigley, H. A., Javitt, J. C. and Sommer, A. (1995a) Diabetes, intraocular pressure, and primary open-angle glaucoma in the Baltimore Eye Survey, *Ophthalmology,* 102, 48-53.

Tielsch, J. M., Katz, J., Sommer, A., Quigley, H. A. and Javitt, J. C. (1995b) Hypertension, perfusion pressure, and primary open-angle glaucoma. A population-based assessment, *Arch Ophthalmol,* 113, 216-21.

Tjon-Fo-Sang, M. J. and Lemij, H. G. (1997) The sensitivity and specificity of nerve fiber layer measurements in glaucoma as determined with scanning laser polarimetry, *Am J Ophthalmol,* 123, 62-9.

Tomita, G., Maeda, M., Sogano, S. and Kitazawa, Y. (1993) An analysis of the relationship between high-pass resolution perimetry and neuroretinal rim area in normal-tension glaucoma, *Acta Ophthalmologica,* 71, 196-200.

Tomlinson, A. and Phillips, C. I. (1971) Emergence Point and Angulation of disc Vessels in the Normal Eye, *British journal of ophthalmology,* 55, 165-73.

Tomlinson, A. and Phillips, C. I. (1974) Ovalness of the optic cup and disc in the normal eye, *Br J Ophthalmol,* 58, 543-8.

Trew, D. R. and Smith, S. E. (1991a) Postural studies in pulsatile ocular blood flow: II. Chronic open angle glaucoma, *Br J Ophthalmol,* 75, 71-5.

Trew, D. R. and Smith, S. E. (1991b) Postural studies in pulsatile ocular blood flow: I. Ocular hypertension and normotension, *Br J Ophthalmol,* 75, 66-70.

Trible, J. R. and Anderson, D. R. (1997) Factors associated with intraocular pressure-induced acute visual field depression, *Arch Ophthalmol,* 115, 1523-7.

Tsai, C. S., Shin, D. H., Wan, J. Y. and Zeiter, J. H. (1991) Visual field global indices in patients with reversal of glaucomatous cupping after intraocular pressure reduction, *Ophthalmology,* 98, 1412-9.

Tsai, C. S., Ritch, R., Shin, D. H., Wan, J. Y. and Chi, T. (1992) Age-related decline of disc rim area in visually normal subjects, *Ophthalmology,* 99, 29-35.

Tsai, C. S., Zangwill, L., Sample, P. A., Garden, V., Bartsch, D. U. and Weinreb, R. N. (1995) Correlation of Peripapillary Retinal Height and Visual Field in Glaucoma and Normal Subjects, *Journal Of Glaucoma,* 4, 110-6.

Tuulonen, A. and Airaksinen, P. J. (1991) Initial glaucomatous optic disk and retinal nerve fiber layer abnormalities and their progression, *Am J Ophthalmol,* 111, 485-90.

Tuulonen, A., Airaksinen, J., Schwartz, B., Alanko, H. I. and Juvala, P. A. (1992) Neuroretinal Rim Area Measurements by Configuration and by Pallor in Ocular Hypertension and Glaucoma, *Ophthalmology,* 99, 1111-6.

Uchida, H., Brigatti, L. and Caprioli, J. (1996) Detection of structural damage from glaucoma with confocal laser image analysis, *Invest Ophthalmol Vis Sci,* 37, 2393-401.

Usui, T., Iwata, K., Shirakashi, M. and Abe, H. (1991) Prevalence of migraine in low-tension glaucoma and primary open-angle glaucoma in Japanese, *Br J Ophthalmol,* 75, 224-6.

van Alphen, G. W. H. M. (1961) On emmetropia and ametropia, *Ophthalmologica,* 142 (Suppl), 1-92.

Varma, R., Quigley, H. A. and Pease, M. E. (1992a) Changes in optic disk characteristics and number of nerve fibers in experimental glaucoma, *Am J Ophthalmol,* 114, 554-9.

Varma, R., Steinmann, W. C. and Scott, I. U. (1992b) Expert agreement in evaluating the optic disc for glaucoma, *Ophthalmology,* 99, 215-21.

Varma, R., Tielsch, J. M., Quigley, H. A., Hilton, S. C., Katz, J., Spaeth, G. L. and Sommer, A. (1994) Race-, age-, gender-, and refractive error-related differences in the normal optic disc, *Arch Ophthalmol,* 112, 1068-76.

Varma, R., Skaf, M. and Barron, E. (1996) Retinal nerve fiber layer thickness in normal human eyes [published erratum appears in Ophthalmology 1997 Feb;104(2):174], *Ophthalmology,* 103, 2114-9.

Vernon, S. A. (1998) The changing pattern of glaucoma referrals by optometrists, *Eye,* 12, 854-7.

Viswanathan, A. C., Fitzke, F. W. and Hitchings, R. A. (1997) Early detection of visual field progression in glaucoma: a comparison of PROGRESSOR and STATPAC 2 [see comments], *Br J Ophthalmol,* 81, 1037-42.

Vrabec, F. (1966) The temporal raphe of the human retina, *Am J Ophthalmol,* 62, 926-38.

Wang, J. J., Mitchell, P. and Smith, W. (1997a) Is there an association between migraine headache and open-angle glaucoma? Findings from the Blue Mountains Eye Study, *Ophthalmology,* 104, 1714-9.

Wang, L., Cioffi, G. A. and Van Buskirk, E. M. (1998) The vascular pattern of the optic nerve and its potential relevance in glaucoma, *Cur Opin Ophthalmol,* 9, 24-9.

Wang, Y. Z., Thibos, L. N. and Bradley, A. (1997b) Effects of refractive error on detection acuity and resolution acuity in peripheral vision, *Invest Ophthalmol Vis Sci,* 38, 2134-43.

Wassle, H., Grunert, U., Rohrenbeck, J. and Boycott, B. B. (1989) Cortical magnification factor and the ganglion cell density of the primate retina, *Letter To Nature,* 341, 643-6.

Wassle, H., Grunert, U., Rohrenbeck, J. and Boycott, B. B. (1990) Retinal ganglion cell density and cortical magnification factor in the primate, *Vision Res,* 30, 1897-911.

Wassle, H. and Boycott, B. B. (1991) Functional architecture of the mammalian retina, *Physiol Rev,* 71, 447-80.

Wassle, H., Grunert, U., Martin, P. R. and Boycott, B. B. (1994) Immunocytochemical characterization and spatial distribution of midget bipolar cells in the macaque monkey retina, *Vision Res,* 34, 561-79.

Weber, J., Dannheim, F. and Dannheim, D. (1990) The topographical relationship between optic disc and visual field in glaucoma, *Acta Ophthalmol Copenh,* 68, 568-74.

Weinreb, R. N. and Perlman, J. P. (1986) The Effect of Refractive Correction on Automated Perimetric Thresholds, *Am J Ophthalmol,* 101, 706-9.

Weinreb, R. N., Dreher, A. W. and Bille, J. F. (1989) Quantitative assessment of the optic nerve head with the laser tomographic scanner, *Int Ophthalmol,* 13, 25-9.

Weinreb, R. N. and Dreher, A. W. (1990) In *Scanning laser ophthalmoscopy and tomography* (Eds, Neasemann, J. E. and Burk, R. O. W.) Quintessenz, Munchen, Germany, pp. 177-82.

Weinreb, R. N., Shakiba, S., Sample, P. A., Shahrokni, S., van Horn, S., Garden, V. S., Asawaphureekorn, S. and Zangwill, L. (1995) Association between quantitative nerve fiber layer measurement and visual field loss in glaucoma, *Am J Ophthalmol,* 120, 732-8.

Weismann, E. L., Asiff, C. F., Phelps, C. D., Podos, S. M. and Becker, B. (1973) Vertical elongation of the optic cup in glaucoma, *Trans Am Acad Ophthalmol Otolaryngol,* 77, 157-63.

Werner, E. B. and Drance, S. M. (1977) Early visual field disturbances in glaucoma, *Arch Ophthalmol,* 95, 1173-5.

Westcott, M. C., McNaught, A. I., Crabb, D. P., Fitzke, F. W. and Hitchings, R. A. (1997) High spatial resolution automated perimetry in glaucoma, *Br J Ophthalmol,* 81, 452-9.

Wild, J. M., Hutchings, N., Hussey, M. K., Flanagan, J. G. and Trope, G. E. (1997) Pointwise univariate linear regression of perimetric sensitivity against follow-up time in glaucoma [see comments], *Ophthalmology,* 104, 808-15.

Wilder, H. D., Grunert, U., Lee, B. B. and Martin, P. R. (1996) Topography of ganglion cells and photoreceptors in the retina of a New World monkey: the marmoset Callithrix jacchus, *Vis Neurosci,* 13, 335-52.

Wilms, K. H. (1986) Zur Struktur einfacher Programme zur Berechnung von absoluten Grossen des Augenhintergrundes, *Optometrie,* 4, 204-6.

Wilson, M. E. (1970) Invariant features of spatial summation with changing locus in the visual field, *J Physiol,* 207, 611-22.

Wilson, M. R., Hertzmark, E., Walker, A. M., Childs Shaw, K. and Epstein, D. L. (1987) A case-control study of risk factors in open angle glaucoma, *Arch Ophthalmol,* 105, 1066-71.

Wirtschafter, J. D., Becker, W. L., Howe, J. B. and Younge, B. R. (1982) Glaucoma visual field analysis by computed profile of nerve fiber function in optic disc sectors, *Ophthalmology,* 89, 255-67.

Wollstein, G., Garway-Heath, D. F. and Hitchings, R. A. (1998) Identification of early glaucoma cases with the scanning laser ophthalmoscope, *Ophthalmology,* 105, 1557-63.

Wood, J. M., Wild, J. M., Drasdo, N. and Crews, S. J. (1986) Perimetric profiles and cortical representation, *Ophthalmic Res,* 18, 301-8.

Woon, W. H., Fitzke, F. W., Bird, A. C. and Marshall, J. (1992) Confocal imaging of the fundus using a scanning laser ophthalmoscope, *Br J Ophthalmol,* 76, 470-4.

Wormald, R. P., Wright, L. A., Courtney, P., Beaumont, B. and Haines, A. P. (1992) Visual problems in the elderly population and implications for services, *BMJ,* 304, 1226-9.

Wormald, R. P., Basauri, E., Wright, L. A. and Evans, J. R. (1994) The African Caribbean Eye Survey: risk factors for glaucoma in a sample of African Caribbean people living in London, *Eye,* 8, 315-20.

Yamagishi, N., Anton, A., Sample, P. A., Zangwill, L., Lopez, A. and Weinreb, R. N. (1997) Mapping structural damage of the optic disk to visual field defect in glaucoma, *Am J Ophthalmol,* 123, 667-76.

Yamazaki, S., Inoue, Y. and Yoshikawa, K. (1996) Peripapillary fluorescein angiographic findings in primary open angle glaucoma, *Br J Ophthalmol,* 80, 812-7.

Yin, Z. Q., Vaegan, Millar, T. J., Beaumont, P. and Sarks, S. (1997) Widespread choroidal insufficiency in primary open-angle glaucoma, *J Glaucoma,* 6, 23-32.

Yucel, Y. H., Gupta, N., Kalichman, M. W., Mizisin, A. P., Hare, W., de Souza Lima, M., Zangwill, L. and Weinreb, R. N. (1998) Relationship of optic disc topography to optic nerve fiber number in glaucoma, *Arch Ophthalmol,* 116, 493-7.

Zadnik, K., Mutti, D. O. and Adams, A. J. (1992) The repeatability of measurements of the ocular components, *Invest Opthalmol Vis Sci,* 33, 2325-33.

Zangwill, L., Shakiba, S., Caprioli, J. and Weinreb, R. N. (1995) Agreement between clinicians and a confocal scanning laser ophthalmoscope in estimating cup/disk ratios, *Am J Ophthalmol,* 119, 415-21.

Zangwill, L. M., van Horn, S., de Souza Lima, M., Sample, P. A. and Weinreb, R. N. (1996) Optic nerve head topography in ocular hypertensive eyes using confocal scanning laser ophthalmoscopy, *Am J Ophthalmol,* 122, 520-5.

Zulauf, M. (1994) Normal visual fields measured with Octopus Program G1. I. Differential light sensitivity at individual test locations, *Graefes Arch Clin Exp Ophthalmol,* 232, 509-15.